Non-reactive scattering of rotational quantum state selected molecular beams

A thesis submitted in partial fulfilment of
the requirement for the degree of

Doctor of Philosophy in Chemistry

at the
University of Canterbury
Christchurch
New Zealand

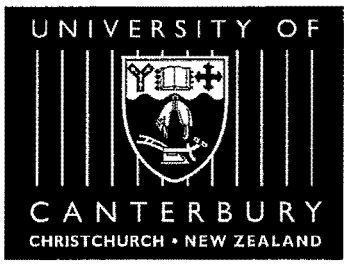

Wan-Ping Hu
January 2000

Table of content

LIST OF FIGURES

LIST OF TABLES

PUBLICATIONS

1. *Collisional Attenuation of Focused CH_3Cl Molecular Beams in a Hexapole Filter.* D. A. Blunt, S. A. Harris, Wan-ping Hu, and P. W. Harland, J. Phys. Chem. A, **102**, p. 1482, **1998.**

Abstract: The attenuation of hexapole-focused CH_3Cl molecular beams has been studied as a function of inert gas and nitrogen gas pressure in a hexapole-collision cell. Cross sections have been determined as a function of relative velocity, using seeded beams, and as a function of specific $|JKM\rangle$ states through variation of the electric field strength in the hexapole. Beam attenuation is attributed to rotationally inelastic collisions in which a beam molecule following a focusing upper Stark state ($KM < 0$) trajectory through the hexapole field is converted by a ΔM or ΔJ, ΔM transition into a non-focusing rotational state (KM = 0 or KM > 0), which then follows a modified, non-focusing trajectory and is lost from the beam. Experimental cross sections are in the range from 200 to 670 $Å^2$, consistent with collisions controlled by a long-range interaction (8 to 15 Å) involving the transfer of a few J mol^{-1} of energy. Collision cross sections estimated using a van der Waals interaction potential with dispersion and dipole-induced dipole terms suggest that cross sections of these magnitudes most probably correspond to collisions in which only the M quantum number changes.

2. *Collisional reorientation of symmetric-top molecules in Stark fields.* Wan-ping Hu, S. A. Harris, P. W. Harland, and L. F. Phillips, International Journal of Quantum Chemistry, **71**, p. 75-82, **1999**.

Abstract: Calculated cross sections for collisional defocusing of a beam of symmetric-top molecules in a hexapole field are compared with new and recent experimental values. The calculations show that collision processes involving changes in K have much smaller cross sections than those for changing M, and cross sections for changing J are smaller still. The beam defocusing produced by collisions with a background gas that is not the same species as the molecules in the beam occurs mainly as a consequence of ΔM transitions induced by a time-varying field which comprises the dipole-induced dipole potential and the anisotropic part of the London potential between the symmetric top and its collision partner. Because the dipole-dipole potential depends on $1/r^3$, its time variation is much slower, and so it is much less effective than the potentials which vary as $1/r^6$ at inducing transitions by this mechanism during long-range (~ 1 nm) collisions at moderate relative velocity (~ 500 m/s).

3. *Upper Stark State collisional relaxation cross sections for single rotational states of CH_3F.* C. Vallance, W-P. Hu, and P.W. Harland, J. Phys. Chem. A., **103**, 6, p. 665-670, **1999**.

Abstract: A radio-frequency electric resonance cell has been used to modulate individual rotational states present in a state selected molecular beam of symmetric top molecules prepared for use in a beam attenuation experiment. Tagging states in this way allows cross sections for collisionally induced ΔM transitions to be measured for single rotational states. A hexapole transmission curve attenuation method reported earlier suffered from poor rotational state resolution and the measurement of cross sections was very time consuming in comparison to the method reported here. Cross sections measured using the two different methods show remarkably good agreement.

4. *Spatial deorientation of upper-Stark-state-selected supersonic beams of CH_3F, CH_3Cl, CH_3Br, and CH_3I.* P. W. Harland, Wan-Ping Hu, C. Vallance, and P. R. Brooks, Phys. Rev. A, **60**,p.3138-3143, **1999**.

Abstract: The spatial scrambling of upper Stark state ($KM_J < 0$) selected beams of CH_3F, CH_3Cl, CH_3Br and CH_3I in field free space has been investigated. It has been proposed that the mechanism for spatial deorientation as the electric field strength is reduced to zero is the change in precessional frequency and loss of spatial direction as the total angular momentum **J** decouples from the collapsing electric field and couples with the nuclear spin. Supersonic beams were quantum state selected in a hexapole inhomogeneous electric field and directed between a pair of parallel field plates before being focused through a second hexapole field to a quadrupole mass spectrometer detector. Exposure of the beam to zero field in the parallel plate region leads to an attenuation of the beam signal relative to the non-zero field case due to defocusing of newly formed lower Stark states and $KM = 0$ states in the second hexapole field. This phenomenon can be used to determine the effect of field strength on the orientation of upper Stark states within the beam. The beam signal at the detector was shown to remain constant for uniform field strengths greater than approximately 3 Vcm^{-1}, with a signal attenuation of around 40% relative to this level at zero field. Attempts were made to measure the mean lifetime for spatial scrambling by pulsing the uniform field to ground potential for increasing intervals and observing the beam attenuation. However, these measurements were complicated by the effect of the beam velocity distribution on the signal and it was found that reproducible values could not be obtained, though the results of these experiments are consistent with lifetimes lying in the expected range from 100 to 300 μs.

5. *Collisional relaxation cross-sections for upper Stark state selected beams of methyl halides.* P. W. Harland, Wan-Ping Hu, and C. Vallance. *In preparation.*

Conference presentations:

Conference of New Zealand Institute of Chemistry, University of Otago, 1996.

1. *Poster presentation*: Cross-section measurements for the relaxation of upper Stark states of CH_3Cl using quantum state selected supersonic molecular beams, Wan-Ping (Sunny) Hu, Sean A. Harris, and Peter W. Harland, University of Canterbury.

Abstract: Relaxation cross-sections have been measured for specific |JKM> states of CH_3Cl, where KM<1, i.e., upper Stark states. The cross-sections are determined from the attenuation of rotational quantum state selected supersonic molecular beams of CH_3Cl through collisions with a range of quencher gases. A strong, 10^7 Vm^{-1}, inhomogeneous hexapole electric field is used to focus and state select the upper Stark state molecules in a molecular beam. A supersonic beam of a symmetric top molecule, such as CH_3Cl, is directed into a 0.83 m long hexapole field assembly where the individual |JKM> states in the rotationally cooled beam are selectively focused as the high voltage applied to the hexapole filter is swept. An experiment involves measuring the attenuation of the CH_3Cl beam with a quadrupole mass spectrometer detector on the beam axis as the pressure in the hexapole collision chamber is varied over the range of 10^{-7} to 10^{-5} Torr ($1.33*10^{-5}$ to $1.33*10^{-3}$ Nm^{-2}) as a function of the hexapole high voltage. In the absence of the quencher, the signal intensity of the beam increases smoothly with hexapole high voltage, called a transmission curve. When the target gas is admitted to the chamber, the overall signal intensity decreases and structure appears in the transmission curves as specific |JKM> states are lost by collisional relaxation. These curves can be used to deduce the cross-section as a function of hexapole high voltage and hence quantum states. The transmission characteristics of the

hexapole filter for CH_3Cl beam has been theoretically modelled and the voltage corresponding to the transmission of specific |JKM> rotational quantum states determined from the calculations have been used to identify the relaxation processes measured.

Australasian Conference on Optics, Lasers and Spectroscopy, ACOLS, University of Canterbury, 1998.

2. *Poster presentation* #1: Spatial de-orientation lifetimes for upper Stark state selected beams of CH_3F, CH_3Cl, and CHF_3 in field-free space. C. Vallance, Wan-Ping Hu, and P. W. Harland, Chemistry Department, University of Canterbury, Christchurch, New Zealand.

Abstract: The mean lifetimes for the spatial scrambling or de-orientation of upper Stark state, $|KM_J> < 0$, selected beams of CH_3F, CH_3Cl and CHF_3 were quantum state selected in a 53 cm long hexapole inhomogeneous electric field, the A-field, and directed through a 15 cm uniform electric field, the C-field, before focusing through a second 53 cm hexapole field, the B-field, to a quadrupole mass spectrometer detector. The beam signal at the detector was shown to remain constant for a C-field > 1 V cm^{-1}. Beam intensities were attenuated by approximately 40% under field-free conditions sue to the spatial scrambling or de-orientation of the molecular dipoles and the subsequent loss of lower Stark states, $|MK_J> > 0$, and the partial loss of $|MK_J> = 0$ states in the B-field. Mean scrambling lifetimes were measured by subjecting the effect on the beam attenuation. The mean lifetimes for CH_3F, CH_3Cl and CHF_3 were found to be 120, 120 and 135 μs, respectively. These lifetimes are consistent with the observation in experiments where the orienting field was switched off prior to electron impact ionisation (Aitken *et al*, J. Chem. Phys., **1994**, 101, 11074 and Int. J. Mass Spectrom. Ion Processes, **1995**, 149/150, 297).

3. *Poster presentation* #2: Quantum state specific upper Stark State collisional relaxation cross sections for CH_3F using a radio-frequency resonance spectrometer. Wan-Ping Hu, C. Vallance, and P. W. Harland, Chemistry Department, University of Canterbury, Christchurch, New Zealand.

Abstract: A radio-frequency electric resonance cell has been used to modulate individual rotational states present in a state selected molecular beam of symmetric top molecules prepared for use in a beam attenuation experiment. Tagging states in this way allows cross sections for collisionally induced ΔM_J transitions to be measured for single rotational states. A hexapole beam transmission curve attenuation method developed several years ago at Canterbury suffered from poor rotational state resolution and the measurement of cross sections was very time consuming in comparison to the method reported here. Cross sections measured using the two different methods showed remarkably good agreement.

Centennial Meeting of the American Physical Society, Atlanta, Georgia, 1999.

4. *Poster presentation*: Spatial de-orientation lifetimes for upper Stark state selected beams of CH_3F, CH_3Cl, CH_3Br and CH_3I in field-free space. C. Vallance, Wan-Ping Hu, and P. W. Harland, Chemistry Department, University of Canterbury, Christchurch New Zealand; P. R. Brooks, Chemistry Department, Rice University, Houston, Texas.

Abstract: The mean lifetimes for the spatial scrambling or de-orientation of upper Stark state, $|KM_J> < 0$, selected beams of CH_3F, CH_3Cl and CHF_3 in field free conditions have been measured. Supersonic neat and seeded of CH_3F, CH_3Cl and CHF_3 were quantum state selected in a 53 cm long hexapole inhomogeneous electric field, the A-field, and directed through a 15 cm uniform electric field, the C-field, before focusing through a second 53 cm hexapole field, the B-field, to a quadrupole mass spectrometer detector. The beam signal at

the detector was shown to remain constant for a C-field > 1 V cm^{-1}. Beam intensities were attenuated by approximately 40% under field-free conditions due to the spatial scrambling or de-orientation of the molecular dipoles and the subsequent loss of lower Stark states, $|KM_J> > 0$, and the partial loss of, $|KM_J> = 0$ states in the B-field. Mean scrambling lifetimes were measured by subjecting the molecular beam to field-free conditions for increasing time periods and measuring the effect on the beam attenuation. The mean lifetimes for CH_3F, CH_3Cl and CHF_3 were found to be between 100 and 300 μs. These lifetimes are consistent with the observation of asymmetry effects reported for collisions of electrons with oriented molecules in experiments where the orienting field was switched off prior to electron impact ionisation (Aitken *et al*, J. Chem. Phys., **1994**, 101, 11074 and Int. J. Mass Spectrom. Ion Processes, **1995**, 149/150, 297).

Conference of New Zealand Institute of Chemistry, Victoria University of Wellington, 1999.

5. *Poster presentation*[*]: Observation of rotational quantum state populations in supersonic molecular beams and cross-sections for M_J changing collisions of specific |JK> states of CH_3F, Peter W. Harland, Sunny W-P Hu, and Claire Vallance, University of Canterbury.

Abstract: A hexapole inhomogeneous electric field has been used to quantum state select symmetric top molecules for crossed beam studies of collisions in which the molecules are spatially oriented. The efficiency of a hexapole assembly to transmit state selected beams for orientation has been found to degrade rapidly with increasing pressure. This work focuses on the process that leads to this degradation in the performance of the hexapole filter: the collisional relaxation of upper Stark states. A radio-frequency electric resonance cell has been interposed between two hexapole filters in order to monitor individual rotational states present in a beam of symmetric top molecules prepared for use in a beam attenuation experiment, where the first hexapole filter is configured as a collision cell. The attenuation of individual rotational states as a function of pressure is measured as a difference signal from a quadrupole mass filter detector through a lock-in-amplifier as the electric field in the resonance cell is modulated. The performances of both cells are satisfactory and some results are compared on the poster. Cross sections measured for the $\Delta M = \pm 1$ collisions of |11> state in a supersonic beam of CH_3F with quencher gases He, Ar, Xe, N_2, CO_2, CH_4, CH_3F, and SF_6 are tabulated on the poster.

[*] Winner of student poster prize

ACKNOWLEDGEMENTS

Without the help and advice of many people, this work would not have gone so far. Over the past four years, I have received invaluable friendship and support from so many people that it is impossible to name them all. So all I can do is to name just a few people who have been directly involved in this work.

I would like to express my most sincere gratitude to my supervisor Professor Peter W. Harland for his guidance and friendship. He has been an excellent supervisor and has taught me many valuable lessons not only in my research but also about life and the ways of the western world.

I would also like to thank Professor Phil Brooks at Rice University, Houston, Texas, and Dr James Hudson for their advice and assistance. Thank you to my former colleagues Drs Sean Harris and Claire Vallance for their companionship, and to all those in Room 732 for putting up with me.

Special thanks to the technical staff in the Mechanical and Electronic Workshop for their assistance and co-operation; the relatively smooth operation of the molecular beam machine depended much on their diverse skills and knowledge. It has been a privilege working with **all** the staff in the Chemistry Department.

Financial support from the Chemistry Department and the Marsden fund is gratefully acknowledged.

Finally, thanks to my family and all my friends for their love and support.

ABSTRACT

Non-reactive scattering of rotational quantum state selected molecular beams of symmetric top molecules has been investigated using electrostatic methods. Cross-sections for the defocusing of upper Stark-state molecules in a hexapole electric field have been measured for neat and seeded beams of CH_3F with a range of polar and non-polar quencher gases. Calculations of the hexapole focusing voltages for specific rotational states facilitated the assignment of the defocusing cross-sections to individual rotational states in the beam.

The technique of Molecular Beam Electric Resonance (MBER) spectrometry has been employed to detect and study individual rotational states, resulting in a dramatic improvement in quantum state resolution over the use of a single hexapole filter. Cross-sections have been measured for the relaxation of selected upper Stark states in beams of methyl halides with a range of polar and non-polar scattering gases. The application of MBER spectrometry to rotational state identification in beams of symmetric top molecules has been explored in this study. Information on the velocity, temperature, and rotational state distribution of the beam can be easily obtained from experimentation using this arrangement. It has also provided insight into the focusing properties of hexapole electric filters. Individual rotational quantum states in a beam of symmetric top molecules could be tagged using an MBER spectrometer for studies of rotational state dependent properties, such as the effect of rotational states in scattering studies.

The collisional relaxation of upper Stark-state molecules in a beam could occur through several mechanisms. Cross-sections measured using the technique of MBER have been largely attributed to an M_J changing process. The effects of the long-range attractive van der Waals interaction potential, the relative velocity dependence of the collision partners and the electric field dependence of the Stark energy have been considered in order to account for the magnitude of the relaxation cross-sections measured in this study.

CHAPTER 1 INTRODUCTION

This research was initially motivated by the observation that the performance of the hexapole inhomogeneous electrostatic filter for rotational state selection is rapidly degraded as the vacuum quality declines below ultra-high vacuum standards. This has been shown in this work to be the result of the defocusing of upper Stark-state molecules in the hexapole field by collisions with background particles. One of the objectives of this project was to explain the mechanism(s) responsible for the degradation in the performance of the hexapole filter as a function of pressure. Collision cross-sections for loss of upper Stark-state symmetric top molecules in the hexapole field have been measured with a range of quencher gases. A number of questions are raised from these measurements. What do these results represent? What scattering mechanisms are involved in the defocusing of the upper Stark-state molecules? What are the relative contributions for elastic and inelastic scattering processes? What energy transfer processes are responsible for inelastic scattering? Do the cross-sections determined have contributions from all the possible mechanisms? If so, is it possible to measure cross-sections for any specific mechanism individually?

Earlier research has demonstrated the application of hexapole filters in selecting and focusing the upper Stark-state molecules in a beam of symmetric top molecules. [Beuhler 1966 and Brooks 1966] Attenuation experiments conducted for beams of symmetric top molecules in the absence of a hexapole electrostatic filter give rise to the total elastic and inelastic scattering cross-sections. Attenuation experiments conducted for rotational state selected beams in a hexapole electric field can yield the total elastic and inelastic scattering cross-sections as well as the cross-sections for the relaxation of the upper Stark-state molecules in the beams. In a theoretical evaluation of the experimental studies, the defocusing of the upper Stark-state molecules was assumed to be due to exclusively the collisional relaxation of M_J states. [Phillips 1995] Phillips reported calculated cross-sections between 20 $Å^2$ and 150 $Å^2$ for individual rotational states. A later refinement of the calculation, which included the long-range interaction, eliminated the discrepancy

between the magnitudes of the observed and calculated defocusing cross-sections. [Hu 1999]

Calculations of the rotational state dependent transmission characteristics of hexapole inhomogeneous electric field strength (DC voltage applied to the hexapole rods) showed that individual rotational states could be selected using the hexapole filter. This could be used to estimate specific $|JKM_J\rangle$ state relaxation cross-sections for a number of symmetric top molecules. Cross-sections were found to be dependent on the hexapole focusing voltage. However, the resolution of the hexapole filter in selecting individual rotational states is poor due to the beam velocity distribution, the overlapping of the rotational state transmission profiles, and degradation of the focusing condition in the hexapole as a result of elastic scattering.

A tandem hexapole arrangement was proposed, using the first hexapole filter to select specific rotational states and the second hexapole filter to analyse the resulting rotational states after collisions in the scattering cell, located between the two hexapole filters. The technique of Molecular Beam Electric Resonance spectrometry was successfully employed by Wiediger *et al* to identify rotational states in beams of symmetric top molecules. [Wiediger 1998] This technique was incorporated into the tandem hexapole arrangement, enabling the study of the collisional relaxation cross-sections of selected rotational states in beams of symmetric top molecules. This technique has also provided information to gain insight into several characteristics of the symmetric top molecular beams, such as the velocity, temperature, and rotational state distribution of the beam.

This thesis is divided into five chapters: Introduction, Theories, Experimental, Results and Discussion, and Conclusion and Future Developments.

Chapter 2 describes the theoretical aspects of the work presented in this thesis, and is divided into the following sections.

2.1. Molecular beams: describing the formations of the molecular beams.

2.2. Symmetric top molecules: describing the characteristics of symmetric top molecules.

2.3. Hexapole inhomogeneous electric field: describing the calculations of molecular trajectories in a hexapole electric field.

2.4. Resonance spectrometry: describing the principles behind Molecular Beam Electric Resonance spectrometry.

2.5. Collision cross-sections: describing the theoretical estimations of collision cross-sections.

Chapter 3 describes the experimental arrangement, and is divided into seven sections.

3.1. Vacuum system: describing the molecular beam machine and the pumping systems.

3.2. Beam production: describing three types of beam nozzles, the beam collimation arrangement, and the beam gas handling system.

3.3. Alignment system and hexapole electric field: describing the methods of aligning the components inside the molecular beam machine and the two hexapole arrangements.

3.4. Resonance electric field: describing the design and construction of the components used in MBER spectrometry.

3.5. Detection and signal processing: describing the methods of signal detection and amplification.

3.6. Computer interfacing: describing the computer interfacing media and the computer interfaced components.

3.7. Experimental methods: describing the methods and techniques employed in this research.

Chapter 4 presents the results and discussions; it is divided into two sections.

4.1. Beam characterisation: results for the characterisation of the molecular beams in single hexapole experiments, tandem hexapole experiments, and the MBER experiments.

4.2. Collision cross-sections: presenting the measurements of scattering cross-sections determined from single hexapole experiments and the MBER experiments, as well as detailed discussion and rationalisation of the findings in this research.

Chapter 5 presents the conclusion, summarising the results of the experiments and the insights gained from this project, and the future developments of this project.

Questions posed in the first paragraphs have been addressed, and answers proposed. The defocusing of the upper Stark-state molecules in a hexapole electric field by collisions with quenching gases can occur through both elastic and inelastic scattering mechanisms. Collisional relaxation cross-sections of rotational state selected symmetric top molecules measured using the technique of MBER are mainly attributed to ΔM_J transitions. Collisions leading to changes in J and K rotational states have little contribution to the experimental cross-sections. Elastic scattering processes do occur; however, their contributions to the cross-sections measured using the technique of MBER are minimised as a consequence of design features in the experiment.

CHAPTER 2 THEORIES

2.1 Molecular beams

Molecular beams, which consist of a narrow stream of molecules in a high vacuum chamber, are generally used in the experimental study of intermolecular forces. The method used for the production of molecular beams is through thermal expansion of gas molecules where the beam molecules flow from an oven source into a region of lower pressure through a narrow slit or an orifice. The properties of the resulting beam depend on the diameter of the orifice, d, relative to the mean free path, λ, of the gas in the source. The "Knudsen number" K_n is defined as the ratio of the mean free path to the orifice diameter: [Fluendy 1973]

$$K_n = \frac{\lambda}{d} \tag{2.1.1}$$

Under the condition, $K_n > 1$, effusive flow is produced, and for the condition, $K_n < 1$, hydrodynamic or supersonic flow is produced.

2.1.1 Effusive expansion, $K_n > 1$

The first molecular beams used in experiments were based on effusive flow. The behaviour of effusive beam sources has been well characterised and the beam properties can be predicted using kinetic theory. Maxwell's Law describes the velocity distribution of molecules, of mass m, in the source: [Kennard 1938]

$$f_{\text{source}}(v) = 4\pi\left(\frac{m}{2\pi k_B T}\right)^{3/2} v^2 e^{-mv^2/2k_B T} \tag{2.1.2}$$

Since the expansion is collision free, the beam molecules are in thermal equilibrium with the gas in the source. Molecules travelling at higher speed are more likely to encounter the exit aperture. The probability of a molecule passing through the orifice in a given time is therefore proportional to the velocity of the molecule, v. The velocity distribution of the beam is then:

$$f_{\text{beam}}(v) = \frac{2}{\alpha^4} v^3 e^{-v^2/\alpha^2} = \left(\frac{v}{\bar{v}}\right) f_{\text{source}}(v) \tag{2.1.3}$$

where α is the most probable velocity, $\sqrt{2k_B T/m}$, and $\bar{v}$ is the mean velocity, $\sqrt{8k_B T/\pi m}$.

Using spherical coordinates [Present 1958], the number of molecules exiting the source per second, dN, into a solid angle, dω, at an angle θ to the axis of the source orifice is:

$$dN = \frac{n\bar{v}A\cos\theta}{4\pi} d\omega \tag{2.1.4}$$

where n is the number density of the molecules in the beam source, and A is the area of the orifice. The total number of molecules, N, leaving the source per second is:

$$N = \frac{1}{4} n\bar{v}A \tag{2.1.5}$$

The beam velocity distribution depends on the temperature of the source gas, and is generally broad. The angular distribution of molecules exiting the orifice is also broad, and considerable collimation is required to produce a well-defined beam. Therefore, multiple stage pumping and/or velocity selection are required to produce a suitable beam from an effusive source for experimentation. Using a channel-like orifice with length L and radius r, rather than a thin wall orifice, can reduce the angular distribution of the beam. [Pauly 1988] However, the intensity of the beam would be comparatively low because of the requirement in maintaining low pressure in the source thereby producing sufficiently long mean free paths, $\lambda/L >> 1$. Using laser drilled multichannel arrays rather than a single aperture can increase the intensity of the beam. The interference between the flow of individual channels can usually be neglected; the equation derived for a single channel orifice may still be applied. Under optimum conditions, the intensity gained by multichannel arrays is similar to that of a single thin wall orifice because of the limit in the source pressure; however, the angular distribution of the beam is greatly reduced.

The main advantage of the effusive source is that the beam properties can be calculated from kinetic gas theory. Since, ideally, no collisions occur as molecules leave the source, the beam gas is in thermal equilibrium and maintains a well-defined distribution of vibration/rotational states. However, because the expansion is thermal, the thermal velocity distribution and angular distribution of the beam produced are generally too

broad for experimentation even with multichannel arrays. In general, experimentation requires highly directional and intense beams with narrow velocity distributions. For our experiments, a good quantum state resolution of the beam is also required. Effusive sources are usually used when beams of low vapour pressure materials are required, such as in the preparation of beams of alkali metals, for example, potassium and sodium.

2.1.2 Supersonic expansion, $K_n < 1$

The hydrodynamic beam source or supersonic source, where $K_n < 1$, is used to produce the molecular beams used in this work. These sources can typically produce beam intensities three orders of magnitude greater than an effusive source. The basic arrangement of this type of source is shown in Figure 2.1.1. [Kantrowitz 1951] The gas flow is hydrodynamic through the nozzle; that is, particles undergo a large number of collisions as they pass through the nozzle, which produces an intense jet of gas. A cone shaped skimmer allows only the core of the expanding jet to pass, forming a narrow beam, while the remaining gas particles are deflected away.

2.1.2.1 Structure of the expansion

Photographs of these free jet expansions have been taken by electron beam induced fluorescence. [Campargue 1984] As shown in Figure 2.1.2, the structure of such an expansion is rather complicated. The term *supersonic* arises because the resulting velocity of the beam exceeds the local speed of sound. The beam is extracted from the core of the expansion by a skimmer placed within the zone of silence, where molecules are travelling at a speed greater than the velocity of sound under the operating conditions, that is, the Mach number M is greater than 1.

$$M = \frac{u}{a}, \tag{2.1.6}$$

u is velocity of the particle, and a is the local velocity of sound,

$$a = \sqrt{\frac{\gamma k_B T}{m}} \tag{2.1.7}$$

where γ is the ratio of heat capacities for the source gas, $\gamma = \frac{C_p}{C_v}$.

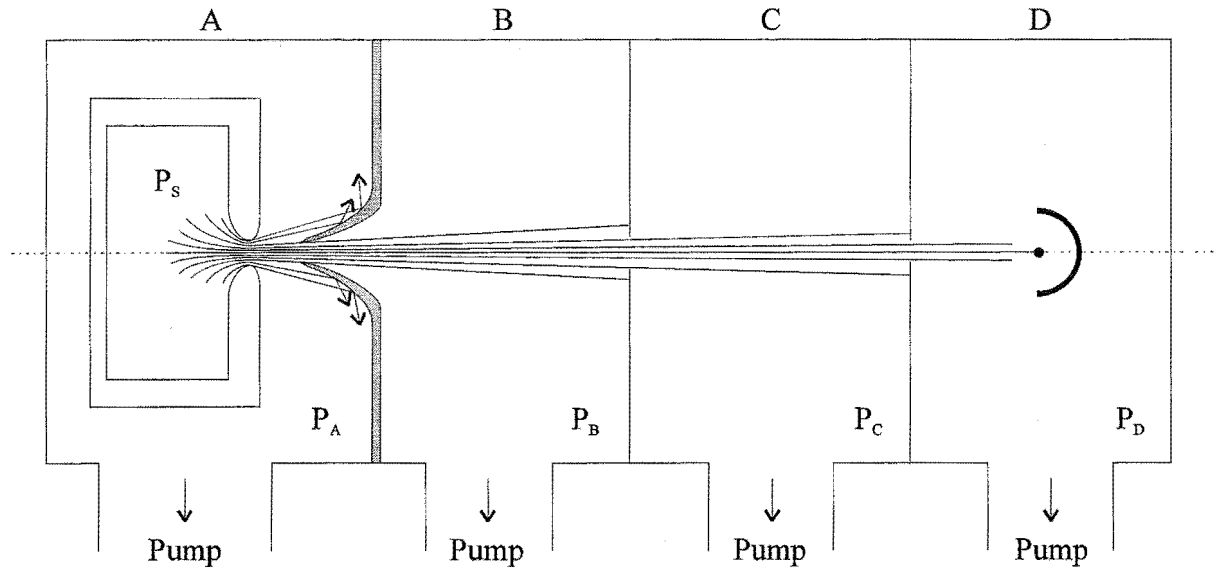

Figure 2.1.1 Schematic diagram of a supersonic beam source. A, B, C, and D are the nozzle, collimating (buffer), experimental, and detection chambers respectively.

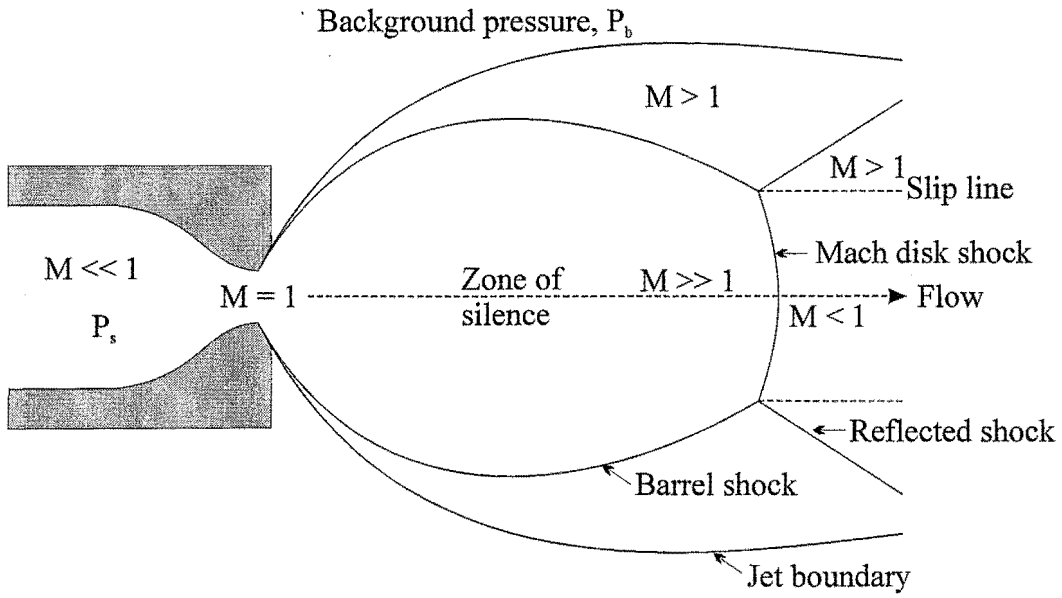

Figure 2.1.2 The supersonic expansion.

The pressure requirements for supersonic flow depend on the Mach number at the nozzle exit being equal to 1. This is achieved when the ratio of the stagnation pressure at the source, P_s, to the background pressure, P_b, exceeds a critical value G, which is less than 2.1 for all gases. [Miller 1988]

$$\frac{P_s}{P_b} > G \equiv \left(\frac{\gamma+1}{2}\right)^{\frac{\gamma}{\gamma+1}} \tag{2.1.8}$$

The pressure gradient between the source and the background causes the gas molecules to accelerate through the nozzle. If $P_s/P_b < G$, the gas molecules will exit the nozzle subsonically with the exiting pressure at the nozzle nearly equal to P_b. When $P_s/P_b \geq G$, $M = 1$ at the nozzle, the exit pressure at the nozzle is equal to P_s/G, approximately one half of P_s. Since the exit pressure is greater than P_b, the gas molecules continue to expand, and M continues to increase so that the gas molecules are moving faster than the rate of information transfer, that is the speed of sound. The gas flow cannot "sense" downstream boundary conditions and thus over-expands, which leads to the formation of a series of shock waves. The shock waves are very thin nonisentropic regions of large density, pressure, temperature, and velocity gradients.

Referring to Figure 2.1.2, the gas first expands isentropically and M continues to increase. It over-expands and must be recompressed by a system of shocks, the barrel shock at the sides and the Mach disk shock perpendicular to the centre of the beam. The location of the Mach disk, X_M (the distance from the nozzle), is relative to the nozzle diameter, d, such that

$$\frac{X_M}{d} = 0.67\left(\frac{P_s}{P_b}\right)^{\frac{1}{2}} \tag{2.1.9}$$

The core of the supersonic expansion is isentropic and its properties are independent of the background pressure, P_b, because the core flow can not "sense" any external condition (hence the term zone of silence). It is from this region that a skimmer extracts the molecular beam.

2.1.2.2 Skimmer

The shape and position of the skimmer are critical in achieving the maximum beam intensity. The maximum beam intensity is achieved when the distance of the skimmer from the nozzle, X_s, relative to the nozzle diameter, d, is: [Campargue 1984]

$$\left(\frac{X_s}{d}\right)_{\max} = 0.125\left(\frac{1}{K_n}\frac{P_s}{P_b}\right)^{\frac{1}{3}} \qquad (2.1.10)$$

The nozzle to skimmer distance must be increased as much as possible to allow cooling in the undisturbed part of the expansion and, thus, in the resulting molecular beam. Increasing the stagnation pressure will increase the effective length of the zone of silence and the effect of cooling. If the skimmer is placed too close to the nozzle, the skimmer will act as a virtual source, and the expansion may become effusive.

The geometry of the skimmer must be optimised to minimise any disturbance of the beam by background gas penetration. From the theories and experiments in continuum gas dynamics, there is a well-established relationship between the Mach number and the maximum angle of a sharp pointed cone, which can result in a so-called "attachment" of the bow of the shock wave to the cone apex or tip. [Anderson 1966] The ideal skimmer, therefore, has the following requirements: [Gentry 1974]

- an orifice with an edge as sharp as possible,
- a small exterior angle at the orifice to ensure that the shock wave is "attached", and
- a large interior angle to minimise scattering losses inside the skimmer.

The orifice should be highly symmetric and perpendicular to the beam axis. Two such skimmers were used in these experiments, the first to extract the beam from the zone of silence, and the second further downstream to collimate and define the beam. (See details in the Section 3.2.3.)

2.1.2.3 Characteristics of the beam

A simple theory explaining the action of the nozzle is based upon the assumption that the expansion is isentropic; that is, the increase in forward velocity of the beam comes from a reduction of the local enthalpy of the beam gases. The collisions, which occur in the nozzle region, convert the internal energy and the random motion of the particles into directed translational motion of the beam. Therefore, the velocity in the direction of the beam flow increases as the temperature of the beam decreases. Based on the first law of thermodynamics, velocity is related to temperature as:

$$\frac{1}{2}mu^2 = \int_{T_f}^{T_i} C_p \, dT \tag{2.1.11}$$

where $C_p = \frac{\gamma R}{\gamma - 1}$. Assuming C_p is independent of T and $T_i >> T_f$, the terminal velocity u_∞ can be expressed as:

$$u_\infty = \left[\frac{2R}{m}\left(\frac{\gamma}{\gamma - 1}\right)T_i\right]^{\frac{1}{2}} \tag{2.1.12}$$

The decrease in temperature from T_i to T_f, derived from the first law of thermodynamics above, can be expressed as: [Fluendy 1973]

$$\frac{T_f}{T_i} = \left(1 + \frac{\gamma - 1}{2}M^2\right)^{-1} \tag{2.1.13}$$

Hence, the increase in the forward velocity can be calculated in the ideal case to be:

$$\frac{u_f}{u_i} \cong M\left(\frac{\gamma}{3}\frac{T_f}{T_i}\right)^{\frac{1}{2}} \tag{2.1.14}$$

where $u_i = \sqrt{3k_B T_i / m}$. From the decrease in the internal temperature of the beam, the width of the velocity distribution can also be calculated.

$$\frac{\Delta u}{u} \sim \left(\frac{2}{\gamma}\right)^{\frac{1}{2}} / M \tag{2.1.15}$$

Accordingly, once M is known, all thermodynamic properties of the expansion can be calculated. However, the form of the velocity distribution for such an expansion is not well understood. It is assumed to be approximated by a three dimensional Maxwell-

Boltzmann distribution characterised by the parallel, $T_{//}$, and perpendicular, $T_{\perp}$, temperatures of the beam superimposed on the flow velocity, u. The parallel and perpendicular temperatures, $T_{//}$ and $T_{\perp}$, are related to the velocity distributions parallel and perpendicular to the direction of flow. The velocity distribution for the beam $f_{beam}(v)$ is then given by:

$$f_{beam}(v) = Av^2 e^{-m(v-u)^2/2k_B T_{//}} \qquad (2.1.16)$$

where A is a normalisation constant.

The advantages of the supersonic expansion far outweigh those of the effusive expansion. Supersonic beams have relatively high intensities, near monochromatic velocities, and lower vibration/rotational temperatures for polyatomic beams. The main disadvantage is that in order to satisfy the condition, $K_n << 1$, the stagnation pressure is usually between 100 to 10000 Torr. For molecules with low vapour pressure at room temperature, seeding in a gas mixture is often required to achieve a pressure high enough for the supersonic expansion. In these experiments, both continuous and pulsed supersonic beam sources, which are described in Section 3.2, have been utilised.

2.1.3 Seeded beams

If there are sufficient collisions to maintain energy and momentum equilibrium between two species when a binary gas mixture is expanded from the nozzle to form a supersonic beam, both species in the beam will have the same velocity and temperature. The properties of the supersonic expansion of one gas species can be modified by the technique of seeding. [Anderson 1966] Seeding in a heavier gas will decrease the velocity of the seed gas and in a lighter gas will increase the velocity of the seed gas. The mole fraction of the seed determines the degree of increase or decease in the resulting beam velocity. The flow velocity can be determined using the *average* mass and *average* heat capacity of the gases in the mixture in the equations described above for the supersonic expansion.

Another tendency in seeded beams is the preferential axial focusing of the heavier component in the binary mixture known as hydrodynamic focusing. The perpendicular velocity is given by:

$$v_{\perp} = \left(\frac{2kT_{\perp}}{m}\right)^{\frac{1}{2}} \tag{2.1.17}$$

The perpendicular temperature $T_{\perp}$ is the same for both species; therefore, the divergence of the lighter component will be greater than for the heavier component in the seeded beam.

2.2 *Symmetric top molecules*

The basic definition of the Stark effect is the splitting of degenerate quantum states by an electric field, due to the interaction of the field with the electric dipole moment of the molecule. Symmetric top molecules are chosen in this study as they have permanent electric dipole moments that are parallel to the rotational angular momentum and therefore the dipole moment does not average to zero over rotation. A molecule, such as, CH_3F, is a symmetric top rotor. The rotational energy levels can be obtained by solving the Schrödinger equation, using the Hamiltonian operator with the classical expression for the energy of the rotating body in terms of the angular momentum.

2.2.1 Rotational energy – Classical expression

In general, moments of inertia described by the three principal axes are represented by the following equation of an ellipsoid: [Townes 1955]

$$\frac{x^2}{I_x^2}+\frac{y^2}{I_y^2}+\frac{z^2}{I_z^2}=1 \tag{2.2.1}$$

where, I_x, I_y, and I_z are the moments of inertia along the directions of the principal axes x, y, and z. The classical expression of rotational energy is described as:

$$E=\frac{J_x^2}{2I_x}+\frac{J_y^2}{2I_y}+\frac{J_z^2}{2I_z} \tag{2.2.2}$$

where J_x, J_y, J_z are angular momenta about axes x, y, z, respectively, since the energy of a body rotating about axis x is $E = \frac{1}{2}I_x\omega_x^2$, where ω_x is the angular velocity (in rad s^{-1}), and $J_x = I_x\omega_x$, with similar expressions for the other axes.

For a symmetric top molecule, $I_x = I_y \neq I_z$. Because, CH_3F is a prolate symmetric top molecule, the perpendicular component of the total moment of inertia, $I_\perp$, is less than the parallel component, $I_{/\!/}$, where $I_x = I_y = I_\perp$ and $I_z = I_{/\!/}$. The rotational energy can be expressed as: [Atkins 1998]

$$E=\frac{J_x^2+J_y^2}{2I_\perp}+\frac{J_z^2}{2I_{/\!/}} \tag{2.2.3}$$

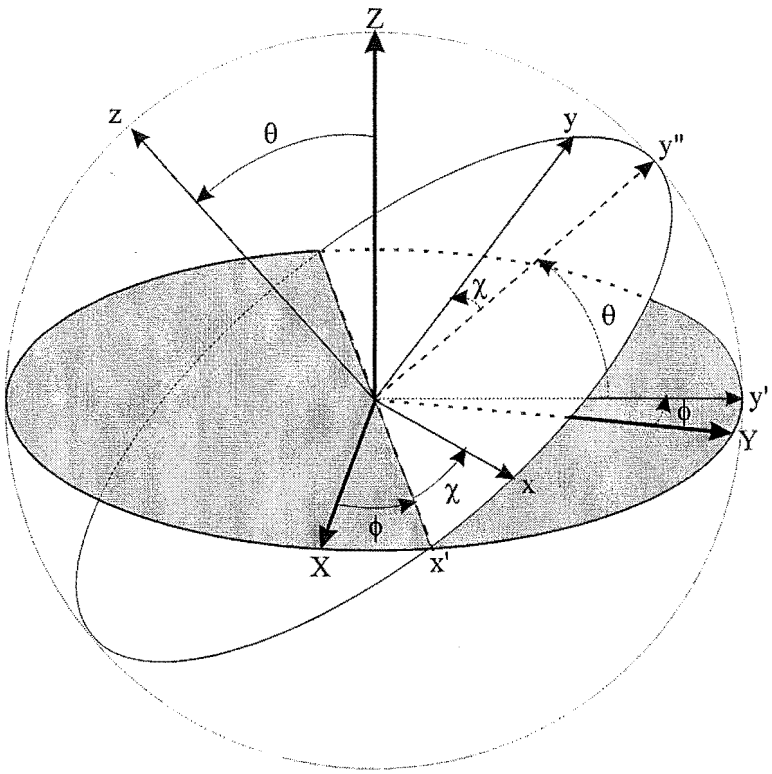

Figure 2.2.1 Euler angles ϕ, θ, and χ relating the space-fixed axes X, Y, Z and molecule-fixed axes x, y, z.

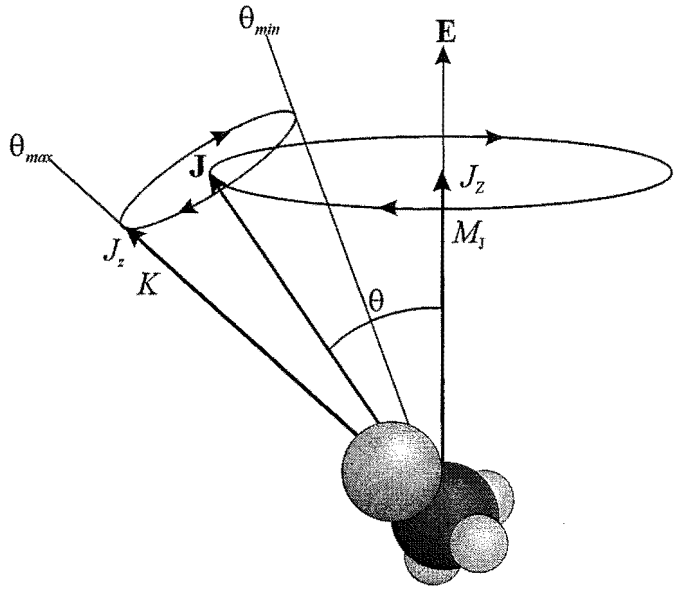

Figure 2.2.2 The classical motion of a prolate symmetric top molecule in an electric field. The total angular momentum is along the laboratory axis, i.e. the electric field direction.

We can rewrite this in terms of $J^2 = J_x^2 + J_y^2 + J_z^2$ by adding and subtracting $J_z^2/2I_\perp$

$$E = \frac{J_x^2 + J_y^2 + J_z^2}{2I_\perp} + \frac{J_z^2}{2I_{//}} - \frac{J_z^2}{2I_\perp} = \frac{J^2}{2I_\perp} + \left(\frac{1}{2I_{//}} - \frac{1}{2I_\perp}\right) J_z^2 \qquad (2.2.4)$$

When a molecule is placed in an external electric field, the motion of a symmetric top molecule is usually described in terms of Euler's angles, as illustrated in Figure 2.2.1. Axes *x*, *y*, and *z* are fixed to the molecule. The *Z*-axis is in the direction of the applied electric field. The potential energy for a symmetric top molecule in an electric field can be expressed as:

$$W_o = -\mu\varepsilon\cos\theta \qquad (2.2.5)$$

where μ is the electric dipole moment vector, ε is the electric field vector and θ is the angle between μ and ε. In terms of Euler's angles (see details in Appendix B.1.1), the total rotational energy of such a symmetric top molecule in an electric field is:

$$W = E + W_o = \frac{I_\perp}{2}(\dot{\phi}^2 \sin^2\theta + \dot{\theta}^2) + \frac{I_{//}}{2}(\dot{\phi}\cos\theta + \dot{\chi})^2 - \mu\varepsilon\cos\theta \qquad (2.2.6)$$

The solution to the above equation, showing the motion of a prolate symmetric top molecule, is illustrated in Figure 2.2.2.

2.2.2 Rotational energy – Quantum theory

The symmetric top Hamiltonian based on Equation (2.2.4) is therefore,

$$\hat{H} = \frac{\hat{J}^2}{2I_\perp} + \left(\frac{1}{2I_{//}} - \frac{1}{2I_\perp}\right)\hat{J}_z^2 \qquad (2.2.7)$$

where $\hat{J} = \hat{J}_x + \hat{J}_y + \hat{J}_z$; which are angular momentum operators and must be determined. The eigenvalues of $\hat{J}$ and $\hat{J}_z$ can be obtained:

$$\hat{J}^2\psi = J(J+1)\left(\frac{h}{2\pi}\right)^2\psi$$

$$\hat{J}_z\psi = K\frac{h}{2\pi}\psi \qquad (2.2.8)$$

where J is the angular momentum quantum number and must be an integer, $J = 0, 1, 2, ..., J$, and K is the quantum number used to describe the component of J on the molecular axis, z. For a given value of J, there can be $2J + 1$ values of K, $K = 0, \pm1, \pm2, ..., \pm J$.

Hence, the total rotational energy can be expressed as:

$$E = \frac{J(J+1)h^2}{8\pi^2 I_\perp} + \left(\frac{h^2}{8\pi^2 I_{//}} - \frac{h^2}{8\pi^2 I_\perp}\right) K^2 \qquad (2.2.9)$$

or as the rotational term value $F(J,K)$ in wave number units: [Levine 1970b]

$$F(J,K) = \frac{E}{h} = BJ(J+1) + (A - B)K^2 \qquad (2.2.10)$$

where $A = h/8\pi^2 I_{//}$ and $B = h/8\pi^2 I_\perp$. When $K = 0$, there is no component of angular momentum about the molecular axis and all energy levels depend only on $I_\perp$.

Again, when the molecule is placed in an external electric field, the Hamiltonian should be considered in terms of Euler angles. (See details in Appendix B.1.) The energy, E, can be expressed as in Equation (2.2.10)

$$\frac{E}{h} = BJ(J+1) + (A - B)K^2$$

with

$$J = n_{max} + \tfrac{1}{2}|K + M_J| + \tfrac{1}{2}|K - M_J| \qquad (2.2.11)$$

where J and K are as described in Equation (2.2.8) and M_J is the quantised component of J on a laboratory axis, the electric field axis, with permitted values, $M_J(h/2\pi)$, of $M_J = 0, \pm 1, \pm 2, \ldots, \pm J$ for a total of $2J+1$ values. The parameter n_{max} is defined in Appendix B.1.2.

A symmetric rotor is $2(2J+1)$-fold degenerate for $K \neq 0$ and $(2J+1)$-fold degenerate for $K = 0$. The M_J-degeneracy is removed when an electric field is applied to the molecule, because in the presence of the field, the energy of the molecule depends on its orientation in space. This splitting of states by an electric field is called the Stark effect. The Stark energy is given in Equation (2.2.5). As shown in Figure 2.2.2, θ is the angle between J and the electric field E. Since the projection of J on the direction of E is expressed in terms of M_J, $\varepsilon \cos\theta$ might be expected to be $\varepsilon (M_J/J)$. Similarly, the component of μ along the J direction is $\mu (K/J)$, since K is an angular component of J on the z-axis. Hence the Stark energy might be expected simply to be:[†] [Townes 1955]

$$W_0 = -\mu\varepsilon \cos\theta = -\mu\varepsilon \frac{M_J K}{J^2} = -\mu\varepsilon \frac{M_J K}{J(J+1)} \qquad (2.2.12)$$

[†] When the vector model is used J^2 should be replaced with $J(J+1)$.

Exact calculations of energies by solving the Schrödinger equation can be slow and time consuming (see Appendix B.1), however, an approximation may be made in the case of a weak field, where the Stark energy is a small correction to the total energy. The Stark energies that arise from the range of electric field strengths, considered in this thesis, are weak compared to the field free rotational energies, therefore, solutions can be found using perturbation theory.

The first-order Stark energy may be described as a perturbation over the field-free Schrödinger wave function, which is defined in Equation (B.1.21) in Appendix B.1: [Levine1970a]

$$W_1 = -\varepsilon \int \psi^* (\mu \cos\theta) \psi d\tau$$

Upon integration,

$$W_1 = -\mu\varepsilon \frac{M_J K}{J(J+1)} = -\mu\varepsilon \langle \cos\theta \rangle \qquad (2.2.13)$$

where $\langle \cos\theta \rangle$ is the average value of $\cos\theta$, which varies as the molecule precesses about its angular momentum vector J. If the product of $M_J K$ is less than zero, the molecule is said to be in an upper Stark state, where the Stark energy decreases with decreasing electric field. For molecules in lower Stark states, those with $M_J K$ greater than zero, the opposite is true. Passing through an inhomogeneous electric field, symmetric top molecules in different Stark states will follow different trajectories. As a result, a hexapole electrostatic field has been used as a state selection filter. [Kramer 1965, Brooks 1969] The characteristics of the hexapole electric field are described in Section 2.3.

Combining Equation (2.2.10) and (2.2.13), the total rotational energy of a symmetric top molecule in an electric field is,

$$W(JKM_J) = E + W_1 = BJ(J+1) + (A - B)K^2 - \mu\varepsilon \frac{M_J K}{J(J+1)}. \qquad (2.2.14)$$

where A and B from Equation (2.2.10) are re-defined in more general terms as rotational constants $\hbar^2/2I_{//}$ and $\hbar^2/2I_{\perp}$.

2.3 *Hexapole inhomogeneous electric field*

Inhomogeneous electrostatic fields, such as hexapole electric fields, have been used as state selectors for symmetric top molecules since the 1960s. [Kramer 1965 and Brooks 1969] Ideally, six rods of hyperbolic cross section should be used to generate a hexapole electric field; however, rods of such shape are difficult to fabricate. Six circular rods, positioned with the inscribed radius r_0 closely match the properties of the hyperbolic rods with inscribed radius r_0 and give a good approximation of the ideal hexapole electric field. [Anderson 1997] The hexapole rods are arranged as shown in Figure 2.3.1, with alternating positive and negative electric potentials, $\pm U_0$, applied to the rods. The electric field potential for ideal $2n$-fold hyperbolic rods in cylindrical coordinates is,

$$U_n(r,\phi) = U_0\left(\frac{r}{r_0}\right)^n \cos(n\phi) \tag{2.3.1}$$

The electric potential, U, of the hexapole field ($n = 3$) for circular rods with r_0 identical to hyperbolic rods is approximately, (the symbols are as illustrated in Figure 2.3.1.)

$$U(r,\phi) = U_0\left(\frac{r}{r_0}\right)^3 \cos(3\phi) \tag{2.3.2}$$

The electric field vector **E** is given by the negative gradient of the potential:

$$\mathbf{E} = -\nabla U(r,\phi) \tag{2.3.3}$$

where the gradient operator is the sum of unit vector partial derivatives:

$$\nabla = \frac{\partial}{\partial r}\mathbf{e}_r + \frac{\partial}{\partial \phi}\mathbf{e}_\phi + \frac{\partial}{\partial z}\mathbf{e}_z \tag{2.3.4}$$

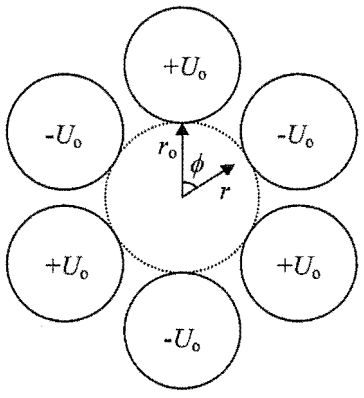

Figure 2.3.1 Hexapole electric field assembly, where ϕ is the angle between the electric field vector and the effective dipole moment of the molecule and r is the position of the molecule in radial coordinates.

Therefore the electric field becomes:

$$\mathbf{E} = 3U_0\left(\frac{r^2}{r_0^3}\right)\cos(3\phi)\mathbf{e}_r - 3U_0\left(\frac{r^2}{r_0^3}\right)\sin(3\phi)\mathbf{e}_\phi \tag{2.3.5}$$

and the electric field strength ε is:

$$\varepsilon = (\mathbf{E}\cdot\mathbf{E})^{1/2} = 3U_0\frac{r^2}{r_0^3} \tag{2.3.6}$$

In an inhomogeneous hexapole electric field, molecules with permanent dipole moments, such as symmetric top molecules, experience a force, exerted by the interaction between the electric field gradient and the molecular dipole, moving the molecules to where their interaction energies are lower. This force can be expressed in terms of the Stark energy, W, as given in Section 2.2,

$$F_r = -\nabla W = -\frac{\partial W}{\partial \varepsilon}\nabla\varepsilon = \mu_{eff}\frac{\partial \varepsilon}{\partial r} = \frac{6U_0\mu_{eff}}{r_0^3}r \tag{2.3.7}$$

where μ_{eff} is the effective dipole moment of the molecule and is dependent on the quantum state of the molecule. In terms of quantum numbers J, K, and M_J, the radial force is:

$$F_r = \frac{6U_0\mu}{r_0^3}\frac{M_JK}{J(J+1)}r = m\ddot{r} \tag{2.3.8}$$

Assuming the centrifugal component of the radial force is zero, the radial acceleration $\ddot{r} = \frac{d^2r}{dt^2}$ is expressed as,

$$\ddot{r} = \frac{6U_0\mu}{mr_0^3}\frac{M_JK}{J(J+1)}r = \omega^2 r \tag{2.3.9}$$

where ω is

$$\omega = \left(\frac{6U_0\mu}{mr_0^3}\frac{M_JK}{J(J+1)}\right)^{1/2} \tag{2.3.10}$$

Three types of trajectories are possible depending on the sign of the product M_JK.

- For $M_JK = 0$, no force is exerted on the molecule by the electric field, the electric field does not influence the molecular trajectory.

- For $M_J K < 0$, the radial displacement, r, is

$$r(t) = A\cos(\omega t) + B\sin(\omega t) \tag{2.3.11}$$

which leads to a focusing trajectory. The radial velocity, $\dot{r}$, is

$$\dot{r}(t) = \frac{dr}{dt} = -A\omega\sin(\omega t) + B\omega\cos(\omega t) \tag{2.3.12}$$

- For $M_J K > 0$, the radial displacement, r, is

$$r(t) = Ae^{\omega t} + Be^{-\omega t} \tag{2.3.13}$$

which leads to a divergent trajectory. The radial velocity, $\dot{r}$, is

$$\dot{r}(t) = \frac{dr}{dt} = -A\omega e^{\omega t} - B\omega e^{-\omega t} \tag{2.3.14}$$

A and B are constants that must be determined from the initial conditions of the molecule entering the hexapole field. The trajectories of individual states through the field can be predicted by solving Equations (2.3.11 - 2.3.14). The transmission of symmetric top molecules through a hexapole electric field is illustrated in Figure 2.3.2. For a molecule entering the hexapole electric field at t = 0, the radial displacement $r(0)$ is dependent on the distance between the point nozzle and the beginning of the hexapole field, l_1, and the angle of the divergence of the molecular trajectory, α, as illustrated in Figure 2.3.3. A beam stop is sometimes used to block off the molecules travelling in the centre of the hexapole field where the electric field is zero.

For $M_J K < 0$,

$$r(0) = A\cos(\omega 0) + B\sin(\omega 0)$$

where $\cos(\omega 0) = 1$ and $\sin(\omega 0) = 0$. Consequently, $r(0) = A = l_1\tan\alpha$. When $\alpha \ll 1$, $\tan\alpha \approx \alpha$, thus, $A = l_1\alpha$. At t = 0, the radial velocity of the molecule depends on the beam velocity, v, as well as the entrance angle, α:

$$\dot{r}(0) = \frac{dr}{dt} = -A\omega\sin(\omega 0) + B\omega\cos(\omega 0) = v\sin\alpha$$

When $\alpha \ll 1$, $\sin\alpha \approx \alpha$, thus $B\omega = v\sin\alpha = v\alpha$. $B = v\alpha/\omega$. Equation (2.3.11) can now be expressed as

$$r(t) = l_1\alpha\cos(\omega t) + \frac{v\alpha}{\omega}\sin(\omega t) \tag{2.3.15}$$

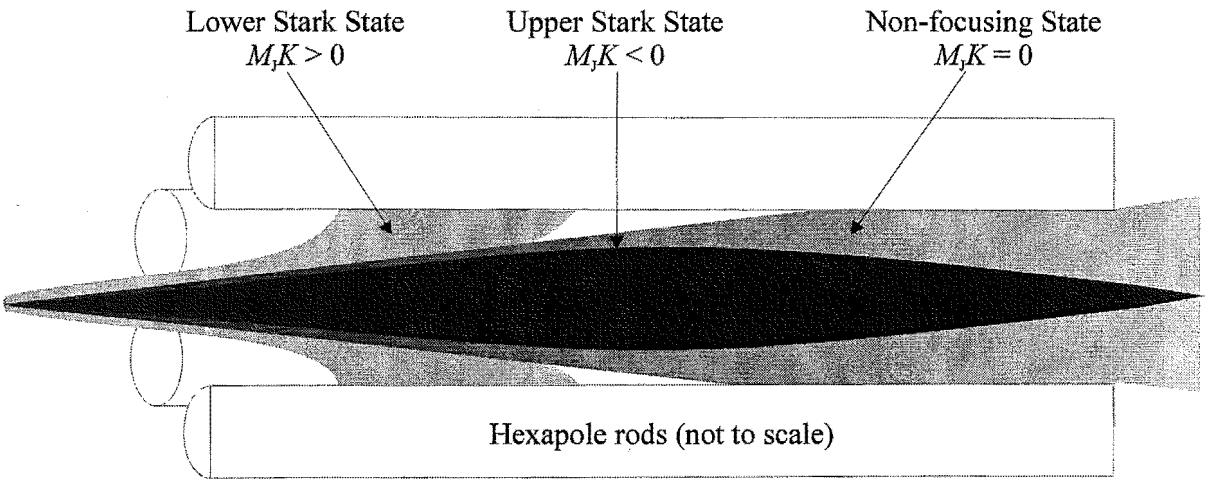

Figure 2.3.2 The trajectories for different rotational quantum states in a beam of symmetric to molecules passing through a hexapole electric field.

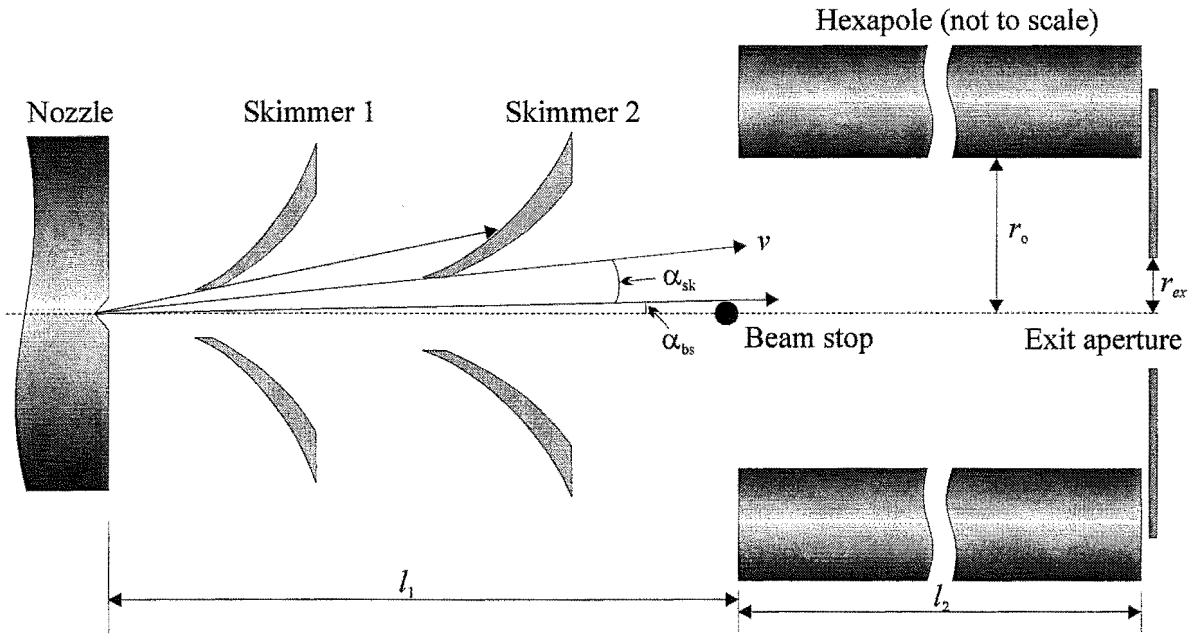

Figure 2.3.3 Conditions restricting the transmissions through the hexapole field.

and Equation (2.3.12) becomes,

$$\dot{r}(t) = \frac{dr}{dt} = -l_1\alpha\omega \sin(\omega t) + v\alpha \cos(\omega t) \tag{2.3.16}$$

Similarly for $M_J K > 0$,

$$r(0) = Ae^{\omega 0} + Be^{-\omega 0} = A + B = l_1 \tan\alpha \approx l_1\alpha$$

$$\dot{r}(0) = -A\omega\, e^{\omega 0} - B\omega\, e^{-\omega 0} = A\omega - B\omega = v \sin\alpha \approx v\alpha$$

Rearranging the above two relationships, yields:

$$A = \frac{l_1\omega\alpha + v\alpha}{2\omega} \text{ and } B = \frac{l_1\omega\alpha - v\alpha}{2\omega}$$

Substituting these into Equation (2.3.13) and (2.3.14), and using the relationships of hyperbolic functions: [Anton 1988]

$$\sinh x = \frac{e^x - e^{-x}}{2} \text{ and } \cosh x = \frac{e^x + e^{-x}}{2}$$

Equation (2.3.13) can now be expressed as

$$r(t) = l_1\alpha \cosh(\omega t) + \frac{v\alpha}{\omega} \sinh(\omega t) \tag{2.3.17}$$

and Equation (2.3.14) becomes,

$$\dot{r}(t) = l_1\alpha\omega \sinh(\omega t) + v\alpha \cosh(\omega t) \tag{2.3.18}$$

In general, equations describing the motion of symmetric top molecules can be expressed in terms of R and V, where R is the radial distance at the entrance of the hexapole field, that is $r(t_{initial}) = l_1\alpha$, and V is the radial velocity at the entrance of the hexapole field, that is $\dot{r}(t_{initial}) = v\alpha$. Therefore, the trajectories of the molecules in the hexapole field can be predicted using the following equations:

For $M_J K < 0$,

$$r(t) = R \cos(\omega t) + \frac{V}{\omega} \sin(\omega t) \tag{2.3.19}$$

$$\dot{r}(t) = -R\omega \sin(\omega t) + V \cos(\omega t) \tag{2.3.20}$$

For $M_J K > 0$,

$$r(t) = R\cosh(\omega t) + \frac{V}{\omega}\sinh(\omega t) \tag{2.3.21}$$

$$\dot{r}(t) = R\omega\sinh(\omega t) + V\cosh(\omega t) \tag{2.3.22}$$

For $M_J K = 0$,

$$r(t) = R + Vt \tag{2.3.23}$$

$$\dot{r}(t) = V \tag{2.3.24}$$

2.3.1 Hexapole transmission of $|JKM_J\rangle$ states

For successful transmission of a symmetric top molecule in rotational state $|JKM_J\rangle$ through a hexapole filter, the following experimental conditions, which are illustrated in Figure 2.3.3, must be met. (A detailed derivation of these conditions and the definition of terms are given in Appendix B.2.)

- The molecule must enter the hexapole field. The range of the molecular entrance angle α is limited by the hexapole entrance condition.

$$\alpha_{bs} < \alpha < \alpha_{sk}$$

- The maximum radial displacement of the sinusoidal trajectory must be less than the inscribed radius of the hexapole, r_o.

$$\alpha_{max} < \frac{r_o^2\omega^2}{v^2(1+\beta_1^2)}$$

- The molecule must be able to leave the hexapole through an exit aperture of radius, r_{ex}. The radial displacement of the molecule must be less than r_{ex} at the exit of the hexapole field.

$$\alpha_{ex} < \frac{r_{ex}\omega}{v}(\beta_1\cosh\beta_2 + \sinh\beta_2)^{-1}$$

where α_{bs}, α_{sk}, l_1, and l_2 are shown in Figure 2.3.3, $\beta_1 = \frac{l_1\omega}{v}$ and $\beta_2 = \frac{l_2\omega}{v}$

In summary, the divergent angle, α, for the focusing trajectories of a symmetric top molecule is physically limited by the skimmer, the nozzle-hexapole distance, l_1, the inscribed radius of the hexapole, r_0, the hexapole length, l_2, the exit aperture radius, r_{ex}, and the beam stop radius, if it is present. The divergent angle must be greater than α_{bs}, if the beam stop is present, and less than α_{sk}. For the molecules to be successfully transmitted through the hexapole field α must also be less than α_{max} and α_{ex}. A beam stop is used to block off the molecules travelling in the centre axis where the hexapole electric field is zero. Signal detected without a beam stop consists of the upper Stark-state molecules, fractions of the $M_J K = 0$ and a small fraction of the axial lower Stark-state molecules. In our experiments, the presence of the beam stop has little effect on the results, because the signal attributed to the axial molecules, which remained constant independent of the voltages applied to the hexapole rods, have been eliminated as background signals in all experiments.

2.3.2 Transmission probability

Assuming no beam stop is present and the angular distribution of the molecules from the nozzle is uniform, the fraction of molecules transmitted through the hexapole field at a particular hexapole voltage, U_0, is:

$$A(U_0, v, \rho) = \frac{\alpha_0^2}{\alpha_{sk}^2} \tag{2.3.25}$$

where $\rho = \langle\cos\theta\rangle = M_J K[J(J+1)]^{-1}$, the averaged orientation of rotational state $|JKM_J\rangle$, and α_0 is the smaller of α_{max} and α_{ex}. The probability of transmitting a particular $|JKM_J\rangle$ state is given by integrating $A(U_0, v, \rho)$ over the velocity distribution of the beam molecule $f(v)$, as in Section 2.1.

$$P_{JKM_J}(U_0) = \int_0^\infty A(U_0, v, \rho) f(v) dv \tag{2.3.26}$$

The total transmission probability over all possible states at a given hexapole voltage is,

$$T(U_0) = \sum_{JKM_J} P_{JKM_J}(U_0) f_{JK} \tag{2.3.27}$$

where f_{JK} is the fraction of molecules in rotational state $|JK\rangle$. [Townes 1955]

$$f_{JK} = \frac{S(I, K)(2J+1)e^{-E/kT_{rot}}}{\sum_{J=0}^{\infty}\sum_{K=0}^{J} S(I, K)(2J+1)e^{-E/kT_{rot}}} \qquad (2.3.28)$$

In the above equation, E is the rotational energy in the absence of the electric field, T_{rot} is the rotational temperature of the molecule, $2J + 1$ is the statistical weight due to the different orientations of J, which are the degenerate M_J states, and $S(I, K)$ are the statistical weights due to the nuclear spin for rotational levels of a symmetric top molecule with three identical nuclei of spin I. The symmetric top molecules considered in this thesis have three-fold symmetry about the axis. As a result, the statistical weights for such molecules have spin and K degeneracy, and are listed in Table 2.3.1.

Table 2.3.1 Statistical weights, $S(I, K)$, due to nuclear spin for rotational levels of a symmetric top molecule CX_3Y with three identical nuclei spin I. (A constant factor $(2I + 1)/3$ has been omitted and n is a positive integral)

Case	Statistical weights
$K = 0$	$4I^2 + 4I + 3$
$K = 3n$	$2(4I^2 + 4I + 3)$
$K \neq 3n$	$2(4I^2 + 4I)$

2.3.3 Rotational state selection

Computer programs have been written which simulate the trajectories of the symmetric top molecules transmitted through a hexapole filter under the experimental arrangements described in this thesis. (See Appendix C.2 and C.3) Examples of calculated transmission curves are shown in Figure 2.3.4. Hexapole transmission probabilities are state dependent (as shown in Figure 2.3.4) and individual rotational states could be selected using appropriate hexapole voltages.

The molecules in the lower Stark states undergo divergent trajectories through a hexapole field and are therefore lost from the beam. The molecules in the upper Stark states pass through the hexapole with sinusoidal oscillations. These molecules are focused away from the axis and back toward the axis every half period of a complete oscillation, $\pi\omega^{-1}$.

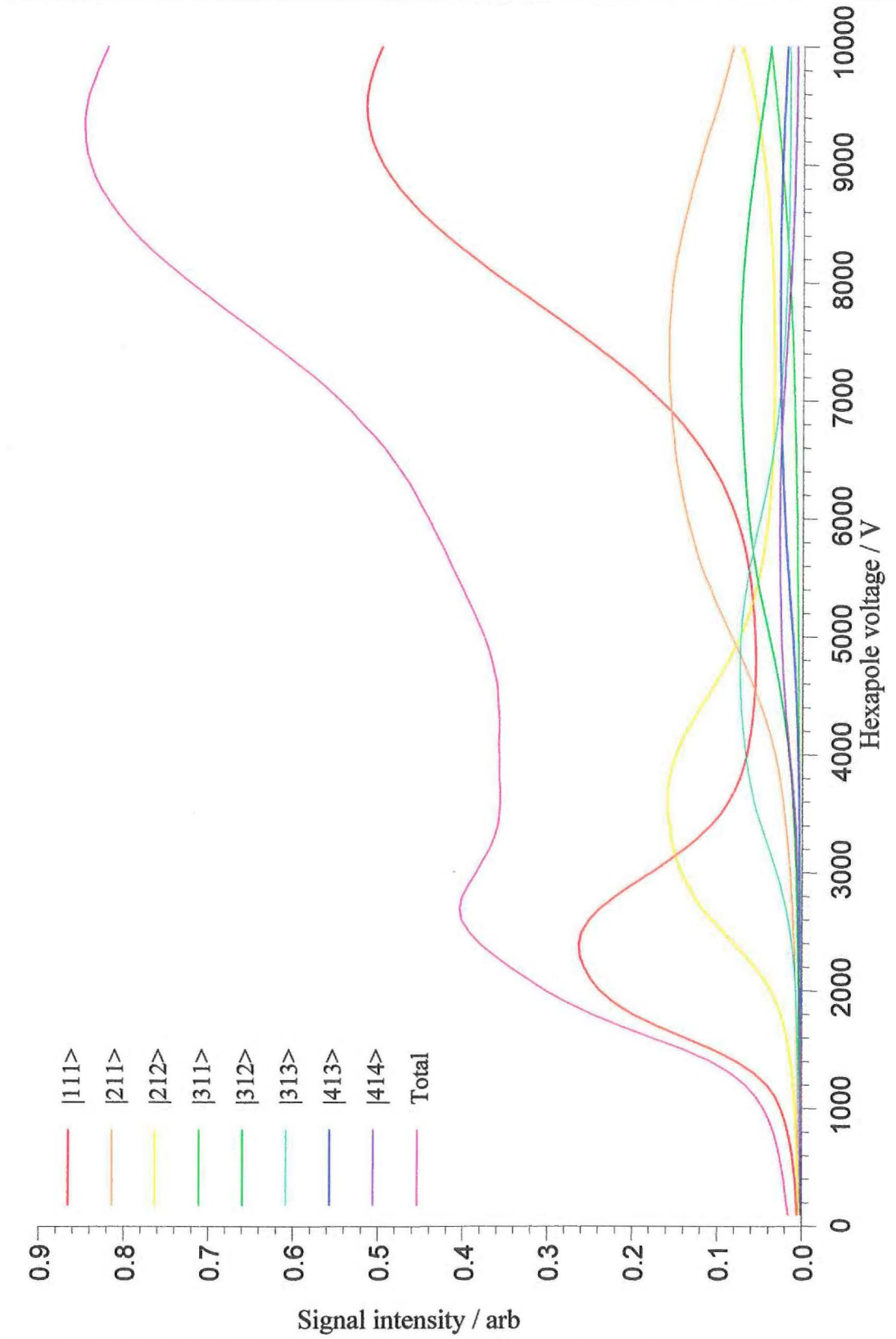

Figure 2.3.4 Calculated rotational state transmission curves for a beam of seeded CH_3Cl, assuming a beam temperature of 5 K and a beam velocity of 560 m/s.

The distance, d_f, along the hexapole field at which the molecules are focused at the axis is given by,

$$d_f = v\frac{\pi}{\omega} \tag{2.3.29}$$

Substituting Equation (2.3.10) for ω, the voltage applied to the hexapole for a particular $|JKM_J\rangle$ state to be focused at a distance, d_f, along the hexapole is, [Bernstein 1982]

$$U_{0,f}(JKM_J, d_f) = \frac{\pi^2 v^2 m r_0^3}{6\, d_f^2 \mu}\frac{J(J+1)}{M_J K} \tag{2.3.30}$$

If d_f is the length of the hexapole field, the voltage needed for the $|JKM_J\rangle$ state to be focused at the exit of the field can be calculated. This exit focusing of the individual $|JKM_J\rangle$ state is therefore accomplished by varying the hexapole voltage. Molecules in non-focusing, $M_J K = 0$, states and molecules travelling on the axis of the hexapole field will also be transmitted through the hexapole independent of the hexapole voltage. The molecules travelling on the axis of the hexapole and some of the non-focusing states can be blocked by the use of a beam stop located at the entrance of the hexapole field. In the absence of a beam stop, the ratio of state-selected molecules to non-focusing/axial molecules will increase with decreased hexapole field exit aperture. However, the overall transmission probability decreases with decreasing exit aperture radius because of the spread in the velocity distribution of the molecular beam. Therefore, the resolution of the hexapole filter has a limitation imposed upon it by an acceptable signal level. Because the population of these molecules in the non-desirable state remained constant regardless of the hexapole voltage, it is possible to eliminate such signals as background signals by subtracting off the signal measured when no electric field is applied to the hexapole rods.

There are other factors reducing the resolution of the hexapole filter in selecting rotational quantum states in a beam of symmetric top molecules. For example, molecules in more than one $|JKM_J\rangle$ state could be focused at or near the same hexapole voltage. The resolution of the hexapole filter can be improved by using a beam of low rotational temperature, thereby increasing the population of the low-lying rotational states.

Another technique is the combination of the hexapole filter with an electric resonance field, acting together as a Rabi type Molecular Beam Electric Resonance spectrometer

(MBER). This technique has been employed in this work and has proven to be a powerful tool in selecting individual rotational states in a beam of symmetric top molecules. Principles involved in this technique are discussed in the Section 2.4.

2.4 Resonance spectrometry

The rotational quantum states in a beam of symmetric top molecules can be studied individually using a Rabi type Molecular Beam Electric Resonance spectrometer, MBER. [Muenter 1992] In our experiments, three electric fields, A, B, & C are employed. Electric fields A and B are hexapole inhomogeneous electric fields, which select the upper Stark states of the symmetric top molecules in the beams. Electric field C is a resonance field, which can be tuned to induce transitions between rotational states. These transitions reflect the population of the corresponding rotational state in the beam. The populations of individual quantum states can, therefore, be experimentally obtained as a function of the electric field strength applied to the resonance field. [Wiediger 1998, Vallance 1999]

2.4.1 Resonance transitions

The spectroscopic selection rules for rotational state transitions of symmetric top molecules are $\Delta J = 0, \pm 1$, $\Delta K = 0$, and $\Delta M_J = 0, \pm 1$. The energy for a $\Delta J = 0$, $\Delta M_J = \pm 1$ transition can be supplied by the resonance field with its frequency in the radio frequency region, $h\nu = \Delta W$, where

$$\Delta W = -\mu E \frac{K}{J(J+1)} [M_J - (M_J \pm 1)] = \pm \mu E \frac{K}{J(J+1)} \qquad (2.4.1)$$

Therefore,

$$\frac{\mu E}{h\nu} = \frac{J(J+1)}{K} \qquad (2.4.2)$$

To induce the desired resonance transitions, the C-field must comprise a DC electric field, E, for dipole orientation, and an oscillating electric field, $h\nu$, to affect transitions. The transition dipole of a symmetric top molecule is orthogonal to its molecular axis. Therefore, the excitation radiation, required along the transition dipole of the molecule, must have a component at right angles to the DC field, which is along the molecular axis. Two designs of the resonance cell or C-cell have been employed to provide such electric fields. (Details of the designs are discussed in Section 3.4.)

When symmetric top molecules enter the C-cell region, the energy required for the transitions may either be absorbed or emitted by the molecules. Because the probabilities of both transitions are equal, there should be no net effect on the population of the quantum states. However, the C-cell is located between two hexapole fields, Hexapole A and Hexapole B. The hexapole filter provides a population inversion of the upper Stark states in the beam before entering the C-cell region. As a result, two net transitions can be observed in the C-field region, $M_JK = -1 \rightarrow M_JK = 0$ and $M_JK = 0 \rightarrow M_JK = 1$. As shown in Figure 2.4.1, the probabilities of **a** and **b** transitions are almost equal, therefore, there is no net effect. Because of the population inversion of the focusing states to the non-focusing states, a net transition of **a′** can be observed.

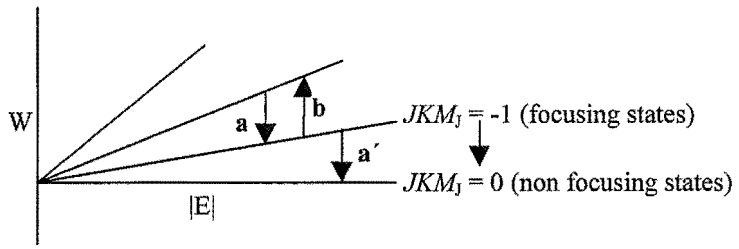

Figure 2.4.1. Stark energy against electric field strength for quantum number M_J sub-levels of a symmetric top molecule focused by a hexapole field, $M_JK < 0$. The $M_JK > 0$ are not populated due to the rejection in the first hexapole filter. A net **a′** transition, $M_JK = -1 \rightarrow M_JK = 0$, could be induced by the RF field.

2.4.2 Quantum state selection

On entering the hexapole field, molecules in the upper Stark states, following sinusoidal trajectories, are focused at the exit of the hexapole electric field, and those in the lower Stark states following divergent trajectories are lost from the beam. The static DC and oscillating RF electric fields are supplied in resonance with the transition energy for a certain rotational state, e.g. $|JK\rangle$; $M_J = \pm 1$. A fraction of the molecules originally in the upper Stark states ($M_JK < 0$) undergo transitions and become $M_JK = 0$ states, which would not be focused by the second hexapole field. The net loss of signal due to the transitions reflects the population of the transition-induced quantum state in the molecular beam.

According to equation (2.4.2), $|JK\rangle$ states in a beam of symmetric top molecules may be identified as a function of E if $h\nu$ remains constant. The relative intensities of the signal corresponding to the $|JK\rangle$ states should reflect the rotational population distribution of the beam. A computer program has been written to simulate the spectra of $|JK\rangle$ states for symmetric top molecules in our experimental arrangements. (See Appendix C.1) Because the population of the rotational quantum states is dependent on the "temperature" of the beam after expansion from the nozzle source, a comparison between the calculated and the experimental results will yield an estimation of the beam temperature.

2.5 *Collision cross-section*

Collision cross-sections can be described simply as $\sigma_{12} = \pi d^2$, where d is the distance between the centres of the two collision partners, 1 and 2. σ_{12} represents the area about molecule 1 perpendicular to the path of molecule 2, within which interaction between molecule 1 and 2 would occur. If molecule 1 and 2 are considered to be rigid spheres, d equals the sum of the two radii. In realistic cases, cross-sections depend on the relative velocities and various interaction potentials between the two collision partners. Cross-sections determined from experiments give insight into the type(s) of interactions involved in the collisions.

2.5.1 Experimental method

Numerous scattering experiments have been reported for measuring cross-sections under single collision conditions. [Buck 1988] The cross-sections measured are either differential cross-sections, based on crossed beam methods, or integral cross-sections, based on beam-gas methods.

Consider, under ideal conditions, a beam of molecules 1 with intensity $I_1 = n_1 v_1$, where n_1 is the number density and v_1 is the velocity of the beam, scattered by molecule 2, which is fixed in space. The differential cross-section is described by the number of molecules dN, per time interval dt scattered into solid angle $d\omega$ divided by the incident beam intensity I_1:

$$\frac{d\sigma}{d\omega} = \frac{d\mathrm{N}}{(d\omega\, dt) I_1} \tag{2.5.1}$$

The integral cross-section is the integral over the complete solid angle:

$$\sigma = \int \frac{d\sigma}{d\omega} d\omega \tag{2.5.2}$$

The attenuation of the beam intensity can be determined using Beer's law:

$$I = I_1 e^{-z} = I_1 e^{-n_2 l \sigma} \tag{2.5.3}$$

where the dimensionless quantity e^{-z} is the probability of a beam molecule passing through the scattering region without undergoing a collision, n_2 is the particle number

density of molecule 2 in the scattering region, and l is the path length through the scattering region. The cross-section can be obtained by:

$$\sigma = \frac{1}{n_2 l} \ln \frac{I_0}{I} = \frac{k_B T}{lP} \ln \frac{I_0}{I} \tag{2.5.4}$$

where I_0 and I are the original and resulting beam intensities, P and T are the pressure and temperature of molecule 2 in the scattering region, and k_B is Boltzmann's constant. Since l, k_B, and T are constant, cross-sections can be determined from the slope of the log of negative signal plotted against pressure.

Experimentally, several deviations from ideal conditions must be taken into consideration, such as, the beam of molecule 1 being non-monochromatic, molecule 2 being non-stationary with a collective velocity spread, and n_2 being non-homogeneous throughout the length of the scattering region. The angular resolution of the detector must also be taken into account. [Budenholzer 1975]

When scattering takes place with the velocity of molecule 2, defined as v_2, the collision frequency in the scattering region is equal to $n_2 g \sigma$, with $g = |v_1 - v_2|$, the relative velocity of the molecules. The collision probability, z, can be expressed in terms of the time for molecule 1 to pass through the scattering region, l/v_1, times the collision frequency for molecule 2. [Biesen 1988]

$$z = n_2 g \sigma \frac{l}{v_1} \tag{2.5.5}$$

Taking the non-homogeneity of n_2 and the velocity distribution of molecules 1 and 2 into account, the average value of z should be:

$$\begin{aligned} \langle z \rangle_{v_1 v_2} &= \int_{v_2} \int_{v_1} \int_{l} n_{2eff}\, l\, f(v_1) f(v_2) \frac{g}{v_1} \sigma(g)\, dl\, dv_1 dv_2 \\ &= (n_2 l)_{eff} \int_{v_2} \int_{v_1} f(v_1) f(v_2) \frac{g}{v_1} \sigma(g) dv_1 dv_2 = (n_2 l)_{eff} \sigma_{eff}(\bar{g}) \end{aligned} \tag{2.5.6}$$

Taking the angular resolution of the detector into account, the probability of a beam molecule being scattered over a detectable laboratory angle Θ is described in an angular

distribution function W(Θ). [Busch 1966] Therefore the dimensionless quantity e^{-z} in Equation (2.5.3), is given by $e^{-\langle z\rangle_{v_1v_2}}$, where $\langle z\rangle_{v_1v_2}$ is written as:

$$\begin{aligned}\langle z\rangle_{v_1v_2} &= (n_2\, l)_{eff}\int_{\Omega}\int_{v_2}\int_{v_1} f(v_1)f(v_2)\frac{g}{v_1}\frac{d\sigma}{d\omega}(g,\theta)\times(1 - W(\Theta))\frac{d\omega}{d\Omega}\,dv_1dv_2d\Omega \\ &= (n_2\, l)_{eff}\,\sigma_{expt}(\bar{g})\end{aligned} \tag{2.5.7}$$

The experimental cross-section in the form of Equation (2.5.4) can also be expressed as:

$$\sigma_{expt}(\bar{g}) = \frac{1}{(n_2 l)_{eff}}\ln\frac{I_0}{I} = \sigma_{eff}(\bar{g}) - \Delta\sigma_{eff}(\bar{g}) \tag{2.5.8}$$

Based on the correction of the angular resolution of the detector, where the effective angular resolution correction $\Delta\sigma_{eff}(\bar{g})$ is:

$$\Delta\sigma_{eff}(\bar{g}) = \int_{\Omega}\int_{v_2}\int_{v_1} f(v_1)f(v_2)\frac{g}{v_1}\frac{d\sigma}{d\omega}(g,\theta)W(\Theta)\frac{d\omega}{d\Omega}\,dv_1dv_2d\Omega \tag{2.5.9}$$

The relative velocity can be estimated using a Monte Carlo simulation computer program based on the two velocity distributions according to the experimental arrangements. In a beam-gas arrangement, such as in this study, the velocity distribution of the beam has been described in Section 2.1.2, and the velocity distribution of the scattering gas is well described by the Maxwell-Boltzmann distribution.

2.5.2 Theoretical estimation

The differential cross-sections defined in Section 2.5.1 can be described in terms of spherical coordinates: [Massey 1933]

$$\frac{d\sigma}{d\omega} = \sigma(\theta), \text{ where } d\omega = 2\pi\sin\theta\, d\theta\, d\phi \tag{2.5.10}$$

The total cross-section becomes:

$$\sigma = \int_0^{2\pi}\int_0^{\pi}\sigma(\theta)\sin\theta\, d\theta\, d\phi = 2\pi\int_0^{\pi}\sigma(\theta)\sin\theta\, d\theta \tag{2.5.11}$$

The interaction potential for the type of collision cross-sections is dominated by the attractive van der Waals interaction V(r) in the form of

$$V(r) = -\frac{C}{r^s} \tag{2.5.12}$$

where C is a constant, the value of C depends on the types of interactions between the collision partners.

The total cross-section given in quantum terms for an interaction potential of this form is: [Massey 1969]

$$\begin{aligned}\sigma &= \frac{4\pi}{k^2}\sum(2n+1)\sin^2\eta_n \\ &= \frac{8\pi}{k^2}\int_0^\infty n\sin^2\eta_n\, dn\end{aligned} \tag{2.5.13}$$

where k is the wave number of relative motion, $k = \frac{1}{2} Mv_r\hbar^{-1}$, where M is the reduced mass and v_r is the relative velocity of the collision partners, and η_n is the phase shift produced in de Broglie waves for the relative motion associated with angular momentum, $\{n(n+1)\}^{\frac{1}{2}}\hbar$. [Massey 1934] A detailed derivation of the phase shift and final results for total cross-section is shown in Appendix B.3.

Using Massey and Mohr's method, the total cross-section may finally be written as:

$$\sigma = \gamma_{MM}(s)\left(\frac{C}{\hbar v}\right)^{2/(s-1)} \tag{2.5.14}$$

A second method, derived by Landau and Lifshitz [Landau 1959], gives:

$$\sigma = \gamma_{LL}(s)\left(\frac{C}{\hbar v}\right)^{2/(s-1)} \tag{2.5.15}$$

Values of $\gamma_{MM}(s)$ and $\gamma_{LL}(s)$ for s = 4, 6, 7, 8, 12 are listed in Table 2.5.1 taken from [Massey 1971] p.1325.

Table 2.5.1 Values of γ_{MM} and γ_{LL} for s = 4, 6, 7, 8, 12. (Taken from [Massey 1971] p.1325.)

s	4	6	7	8	12
γ_{MM}	10.613	7.547	7.002	6.771	6.296
γ_{LL}	11.373	8.083	7.529	7.185	6.584

Therefore, non-reactive scattering cross-sections are expected to show velocity dependence, with v as the relative velocity of the collision partners:

$$\sigma(v) \propto v^{-2/(s-1)} \tag{2.5.16}$$

For attractive van der Waals interactions, s = 6, and C takes into account the dipole and polarisation interactions. According to Equation (2.5.16), the collision cross-sections should exhibit a $v^{-0.4}$ dependence.

For collisions between a polar molecule and an atom or a molecule, polar or non-polar, the polarisation interaction includes an induced-dipole / induced-dipole interaction, also called the dispersion interaction and the London interaction, as well as the dipole / induced-dipole interaction. [Atkins 1998]

$$C = C_{\text{disp}} + C_{\text{dip-ind dip}} \tag{2.5. 17}$$

where

$$C_{\text{disp}} = \frac{3}{2}\alpha_1'\,\alpha_2'\frac{I_1\,I_2}{I_1 + I_2} \tag{2.5. 18}$$

and

$$C_{\text{dip-ind dip}} = \frac{\mu_1^2\alpha_2'}{4\pi\varepsilon_o} \tag{2.5. 19}$$

where α' and I are polarisation volumes and ionisation potentials for molecule 1 and 2 respectively, and μ_1 is the dipole moment of molecule 1. When both the collision partners are polar molecules, $C_{\text{dip-ind dip}}$ becomes: [Massey 1971]

$$C_{\text{dip-ind dip}} = \frac{\mu_1^2\alpha_2' + \mu_2^2\alpha_1'}{4\pi\varepsilon_o} \tag{2.5. 20}$$

and a dipole-dipole interaction should also be considered.

$$C_{\text{dip-dip}} = \frac{2}{3k_B T}\left(\frac{\mu_1\mu_2}{4\pi\varepsilon_o}\right)^2 \tag{2.5. 21}$$

where T is the average temperature for the two collision partners.

$$T = \frac{2T_1T_2}{T_1 + T_2} \tag{2.5. 22}$$

Interaction potentials involving dipole-quadrupole and quadrupole-quadrupole interactions are more complicated; they exhibit r^{-8} and r^{-10} dependence and their effects on the cross-sections are negligible compared with other interactions. [Margenau 1971]

2.5.3 State-to-state interaction

Cross-sections for the type of interaction that is of particular interest in this thesis are the inelastic state-to-state cross-sections. The same equations for calculating total cross-sections can be adopted to estimate state-to-state cross-sections. The interaction potential V(r) should be equal to the difference in energy between the initial state and the final state of the beam molecule. The molecules studied in this thesis are symmetric top molecules, whose rotational energy levels have been described in Section 2.2. The spectroscopic selection rules for rotational state transitions of symmetric top molecules are $\Delta J = 0, \pm 1$; $\Delta K = 0$; and $\Delta M_J = 0, \pm 1$. [Townes 1955] The hexapole filters were used to isolate the upper Stark-state components in the beam. The attenuation of molecules in the upper Stark state, $M_J K < 0$, to a non-focusing state, $M_J K = 0$, can be carried out to determine collision cross-sections involving this type of transition.

The transitions possible for $|JKM_J\rangle$ states according to these selection rules using a hexapole filter are:

- $\Delta J = 0$, $\Delta M_J = \pm 1$, where $J > 0$, $|K| > 0$, and $M_J K < 0$.
- $\Delta J = \pm 1$, $\Delta M_J = 0, \pm 1$, where $J > 0$, $|K| > 0$, and $M_J K < 0$.

It should be noted that the Dirac notation, used to describe the upper Stark state, has omitted the negative sign which should be present for either the K or M_J quantum number so that $M_J K < 0$. Also, Oka and Phillips have suggested that $\Delta M_J > \pm 1$ are possible under some circumstances. [Oka 1973, Johns 1975, and Phillips 1995]

The rotational energy, $W(JKM_J)$, for a symmetric top molecule in an external electric field is:

$$W(JKM_J) = E + W_1 = BJ(J+1) + (A - B)K^2 - \mu\varepsilon\frac{M_J K}{J(J+1)}. \qquad (2.5.23)$$

As described in Section 2.2, the rotational constants A is $\hbar^2/2I_{//}$ and B is $\hbar^2/2I_{\perp}$.

For a $\Delta J = \pm 1$ and $\Delta M_J = 0$ transition, the transition energy is independent of the electric field, the minimum transition energy (where |K| = 1) is $4B$. For a $\Delta J = 0$ and $\Delta M_J = \pm 1$ transition (Stark state transition), the transition energy decreases with increasing J. Figure 2.5.1 illustrates the low-lying rotational states of a prolate symmetric top molecule.

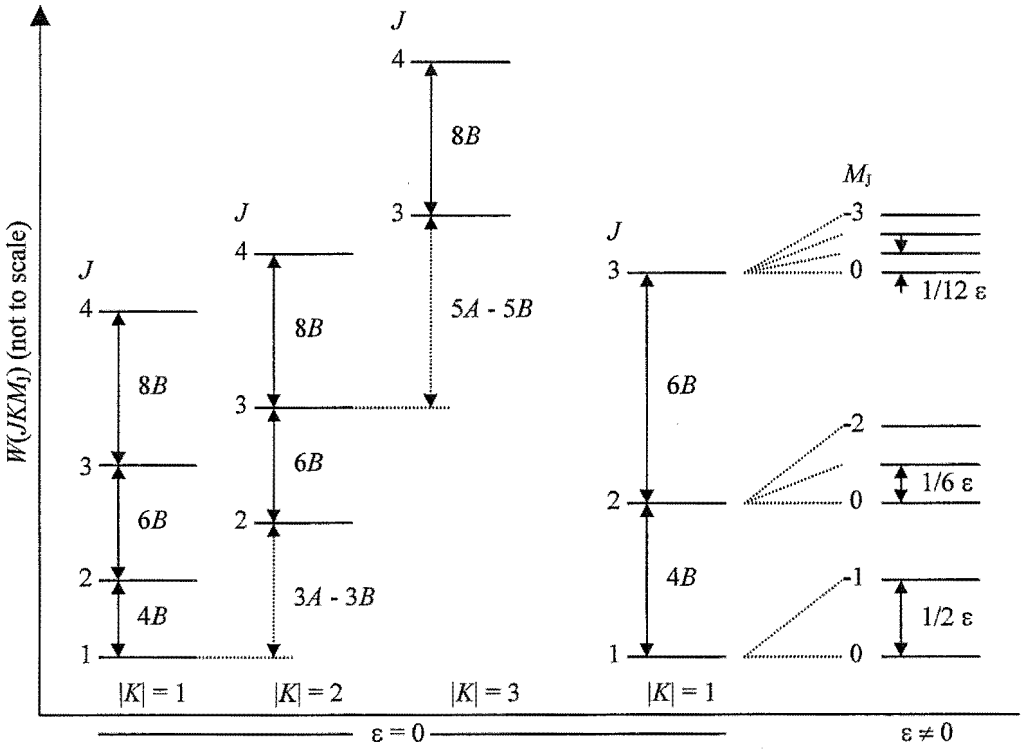

Figure 2.5.1. Low-lying rotational energy levels of a prolate symmetric top molecule.

CHAPTER 3 EXPERIMENTAL

3.1 Vacuum system

The research for this thesis has been performed using a molecular beam machine, which is illustrated in Figure 3.1.1. The molecular beam machine is assembled from sections, or chambers, that are interconnected. Each section is differentially pumped to maintain high vacuum.

3.1.1 History of the molecular beam machine

The present geometry of the molecular beam machine has resulted from modifications and refinements, which have allowed the apparatus to be used for new and different applications. Originally, the machine was constructed to study of appearance potentials of cluster ions. [Cameron 1994a]. Only two chambers were necessary for this application. Later the machine was required for the study of oriented molecules. This required the addition three chambers, two to accommodate the hexapole assembly, and another custom-made detection chamber, to be used to study scattering in crossed beam experiments. A frame was built with a rail system to support the weight of the five chambers and the pumps. [Aitken 1995, Blunt 1995, and Harris 1997]

3.1.2 Current configuration

The molecular beam machine currently comprises seven interconnected stainless steel vacuum chambers. These are the nozzle chamber, the buffer chamber, the first hexapole chamber, C-cell chamber, the second hexapole chamber, the detection/scattering chamber, and the ion source chamber. The C-cell section was added to accommodate the RF resonance cell, used for the Molecular Beam Electric Resonance Spectrometry in this research. The ion source section was added for the study of ion-molecule reactions. [Vallance 1999a] All sections are differentially pumped with either diffusion pumps or turbo-molecular pumps, and are fitted with cryogenic traps to improve the quality of the vacuum. Apart from the detection/scattering chamber all sections are mounted on

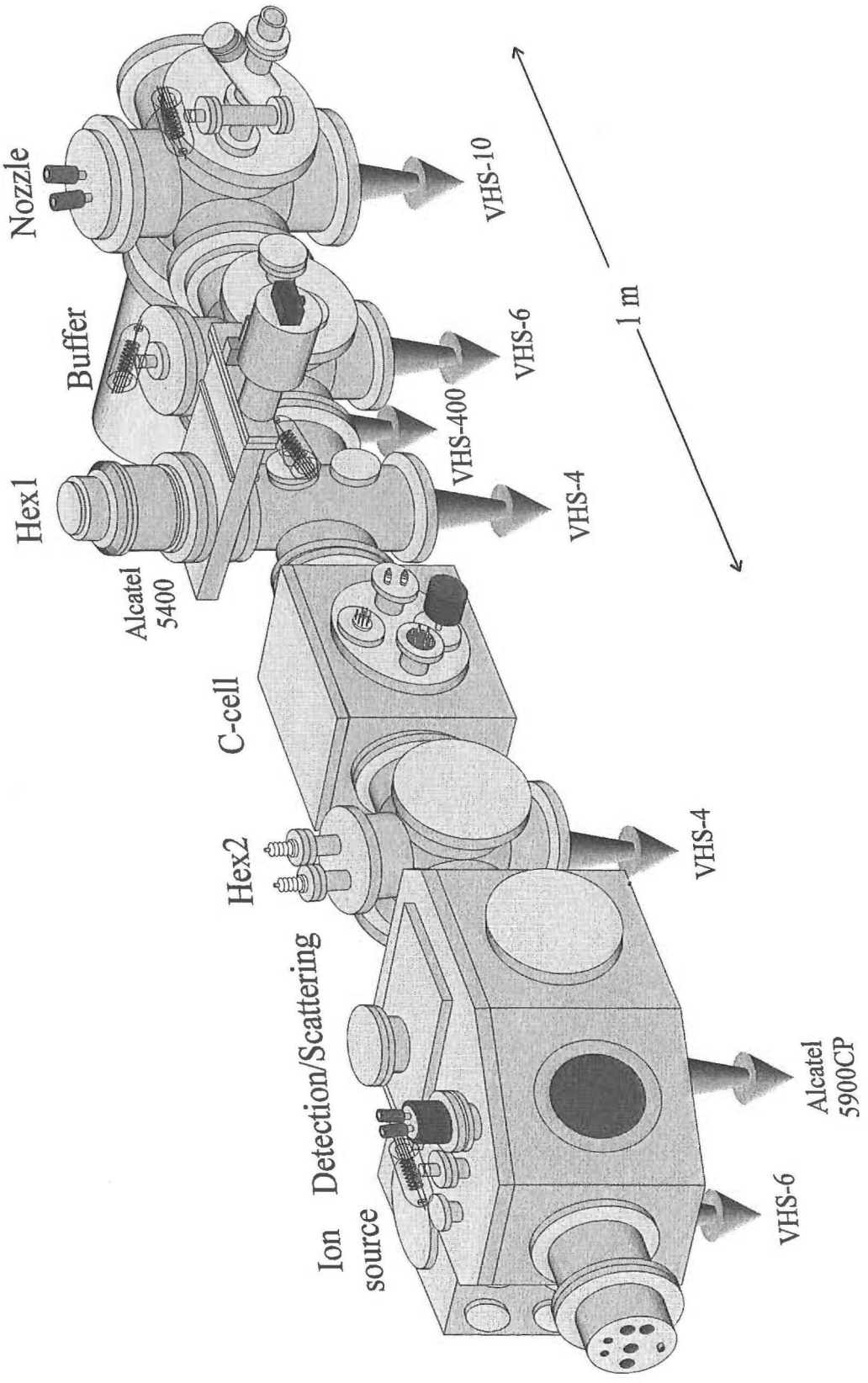

Figure 3.1.1 3-D view of the molecular beam machine.

individual *xyz*-translators, which slide along on the rail system, to eliminate stress in the joints between the chambers. The details of each section will be discussed below.

The latest major modification to the machine was the addition of a new pumping station in the nozzle chamber in order to increase pumping capacity and facilitate higher stagnation pressures in the beam source.

3.1.3 Nozzle Chamber

The supersonic molecular beam source is accommodated in the nozzle chamber. This chamber is a Huntington Laboratories 8" diameter six-way-cross chamber with 10" stainless steel ConFlat flanges at each port, see Figure 3.1.1. The beam source support is also accommodated in this chamber and is mounted on a linear translator rod axial to the chamber front flange, which is sealed with a Viton o-ring. A liquid nitrogen trap is attached to the top flange with a 10" OD to 8" OD adapter. The liquid nitrogen trap is also used to cool a copper baffle, which is positioned, using two long strips of copper, near the bottom flange of the chamber. The bottom flange is connected to a spacing spool situated above a 10" gate valve.

The nozzle chamber is pumped by a 7020 $l\ s^{-1}$ Varian VHS-10 oil diffusion pump, backed by a 1080 $l\ min^{-1}$ Alcatel 2063C mechanical pump. The chamber can be rough pumped from atmospheric pressure to the operating range of turbo-molecular pumps or oil diffusion pumps by an Alcatel mechanical pump, connected to one of the side ports of the chamber, through a high vacuum isolation valve. A Bayard-Alpert type twin-filament ion gauge is also mounted on this port to monitor the pressure in the chamber. The port connected to the buffer chamber is fitted with a skimmer, which partitions the two chambers.

As mentioned above, the latest addition to the machine was a pumping station attached to the remaining port of the nozzle chamber through a 10" tubular L-bend arrangement. (See Figure 3.1.2.) It consists of a Varian VHS-400 oil diffusion pump, backed by an Edwards M80 two-stage mechanical pump and is sealed by a pneumatic 10" OD gate valve. A 10 Litre liquid nitrogen trap is fitted between the gate valve and the diffusion

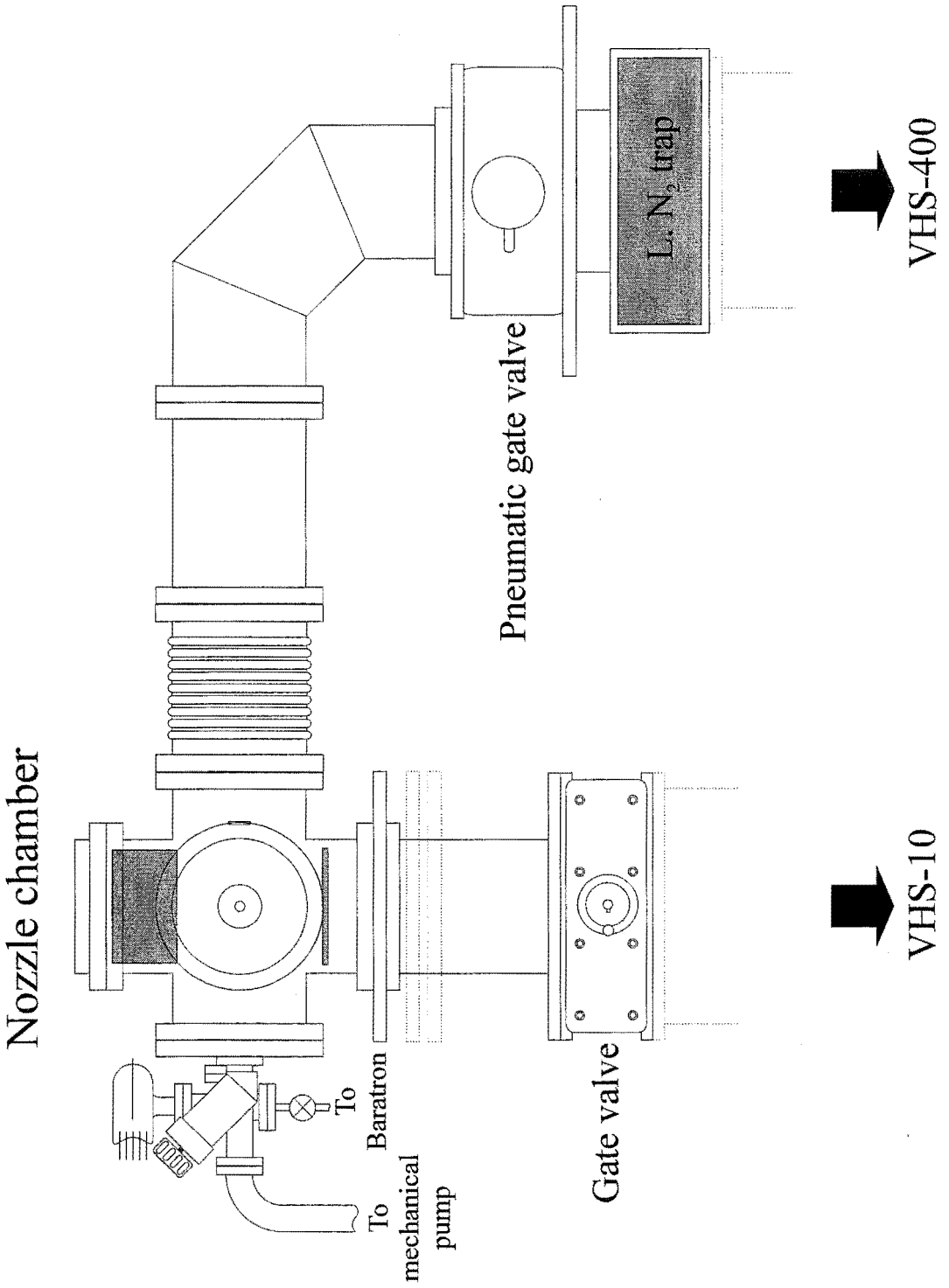

Figure 3.1.2 Front end view of the machine with the new pumping station.

pump to prevent back streaming of the diffusion pump oil into the vacuum chamber. The increase in pumping capacity in the nozzle chamber provides the potential for the production of molecular beams with higher beam intensities, by increasing the stagnation pressure in the beam sources. Consequently, rotationally cooler and more intense beams are produced, which increase experimental resolution.

3.1.4 Buffer Chamber

The buffer chamber is constructed using a Huntington Laboratories 6" six-way stainless steel cross (with 8" OD flanges), see Figure 3.1.1. Pumping of this chamber is provided by a 3000 l s^{-1} Varian VHS-6 oil diffusion pump, which is backed by a 700 l min^{-1} Edwards E2M40 mechanical pump through an isolation gate valve (NRC 77871). The pumping in this chamber helps maintain a high vacuum, typically $< 10^{-7}$ Torr, in the neighbouring hexapole chamber. The top flange of the steel cross is fitted with an ion gauge to monitor the pressure, which is typically in the 10^{-6} to 10^{-5} Torr range with the beam running. The bottom flange is attached to a spacing spool to which a baffled liquid nitrogen trap is mounted. One side port is sealed with an 8" OD Perspex window and the other with an 8" OD stainless steel flange with two 2¾" OD ports, one for a window and the other for electric feed-through. The buffer chamber in bounded by two skimmers. The first of these, which has an aperture of 1 mm diameter, is fitted on a top hat in the centre of a 6" OD stainless steel plate mounted on the alignment rods. The second skimmer has a centre hole of 1.5 mm diameter, and is fitted with a similar mounting arrangement as the first skimmer that effectively seals the buffer chamber from the nozzle chamber and the first hexapole chamber.

3.1.5 First Hexapole Chamber

The first hexapole and second hexapole chambers were originally connected together to house an 833 mm hexapole filter. [Harris 1997] The C-cell chamber was later added between the two hexapole chambers to accommodate new experimental components for MBER. The first hexapole chamber is a Varian 6" four-way stainless steel cross (with 8" OD flanges) with two 2¾" OD flanges on each side face of the cross. The top flange is

sealed with a VAT stainless steel pneumatic valve that opens to a 400 l s^{-1} Alcatel 5400 CP turbo-molecular pump operated by a CFF-450 turbo converter. The turbo-molecular pump is backed by a 373 l min^{-1} Alcatel 2020A mechanical pump through a Duniway high vacuum valve. This turbo-molecular pump is operated while the machine is in standby mode to maintain a vacuum of ~10^{-6} Torr in the machine at all times. It is sealed off during experiments when the diffusion pumps are operating to prevent oil getting into the turbo-molecular pump. The bottom flange is connected to a liquid nitrogen trap through a spacing spool. The liquid nitrogen trap is mounted to a 1500 l s^{-1} Varian VHS-4 oil diffusion pump, which is backed by a 345 l min^{-1} Alcatel 2021 mechanical pump, through an Airco Temescal 5010 gate valve.

Since this chamber is used as the collision cell, one of the 2¾" OD flanges on the side is attached to the gas supply lines through a Leybold Heraeus 283-41 DN 10KF variable leak valve. The valve is operated via a computer-controlled stepping motor, and a brass Nupro B-4HK bellows valve. The other 2¾" OD flange on the same side is also sealed off with a brass Nupro B-4HK bellows valve. The two 2¾" OD flanges on the other side are attached to pressure measuring equipment, an ion gauge and a 690 absolute MKS Baratron.

3.1.6 C-cell Chamber

The C-cell chamber is a custom-made stainless steel cube with five 8" OD conflat flange ports and an o-ring-sealed lid, see Figure 3.1.1. The bottom port is sealed with a stainless steel blank flange. One side port is sealed with a window, while the opposite port is sealed with a flange carrying four 2¾" OD flange ports. One of these is attached to a multiple electrical feed-through flange for the voltage supplies to the C-cell. Another is fitted with a flange connected to a 1000 Torr-head MKS 221B differential Baratron. A third port is used for a nude ion gauge, and the fourth port is for a high-voltage dual feed-through for the hexapole voltage supplies. A stainless steel sheet partition fits inside the cube over the port connected to the first hexapole chamber. A half-cylinder liquid nitrogen trap is fitted inside the port opening to the second hexapole chamber, and functions as a cryogenic pump.

3.1.7 Second Hexapole Chamber

The second hexapole chamber is accommodated in a Huntington Laboratories 6" six-way stainless steel cross, see Figure 3.1.1. This chamber is pumped by a 1500 l s^{-1} Varian VHS-4 oil diffusion pump, which is backed by a 75 l min^{-1} Alcatel 2004A mechanical pump through a high vacuum valve, with a configuration similar to that of the first hexapole chamber. The side ports of the chamber are sealed by 8" OD blank conflat flanges. The top flange is fitted with two 2¾" OD flanges; each flange contains a high voltage feed-through for the second hexapole voltage supply.

3.1.8 Detection/Scattering Chamber

This chamber is a large custom-made stainless steel chamber designed to accommodate a wide range of crossed beam experiments. The shape of this chamber is shown in Figure 3.1.1. There are five 8" OD ConFlat flange ports, one on each main face; and three 2¾" OD flange ports, one on each minor face. The lid and base are sealed by Viton o-rings.

The base has one 10" OD flange port, one 4½" OD flange on a 175 mm extension, and one 2¾" OD flange on a 25 mm extension. The 10" OD flange port is connected to a 540 l s^{-1} Alcatel 5900CP turbo-molecular pump through a spacing spool and a pneumatically operated Alcatel CF 150 gate valve. The turbo-molecular pump is backed by a 726 l min^{-1} Varian SD700 mechanical pump. A cylindrical liquid nitrogen trap on a 4½" OD flange is sealed to and fitted inside the 175 mm extension port.

The lid has two 2¾" OD flanges, one 4½" OD flange, and a rectangular sliding plate sealed with an o-ring, which has an 8" OD flange for mounting the ion-imaging system or a dataquad mass spectrometer. A Bayard-Alpert type ion gauge is mounted to one of the 2¾" OD flanges on the lid to monitor the pressure in this chamber.

A quadrupole mass spectrometer is mounted through an extension spool to the port on the molecular beam axis. The ion source chamber is attached to the side port perpendicular to the molecular axis. There are two additional 2¾" OD flanges, containing electrical

feed-throughs. Apart from the above-mentioned ports, all other ports are either sealed with windows or electrical feed-throughs.

3.1.9 Ion Source Chamber

This is also a custom-made stainless steel cube. Four of the faces of the cube each have an 8" OD ConFlat port, the fifth face has a 6" OD ConFlat port, and the sixth face has four 2¾" OD flanges ports. An XYZ translator is mounted on the 6" OD ConFlat port, which is opposite to the port attached to the detection/scattering chamber. This chamber is pumped through a baffled liquid Nitrogen trap and a Vacuum Research Manufacturing Company gate valve by a Varian VHS-6 diffusion pump, which is backed by the 726 l min^{-1} Varian SD700 mechanical pump shared with the 5900CP turbo-molecular pump in the detection/scattering chamber. This chamber is used to accommodate parts for crossed beam experiments. The XYZ translator usually accommodates either an electron source or an ion source. The razor blade used for the measuring of the beam profiles was also attached onto this XYZ translator.

3.1.10 Vacuum protection system

Several vital instruments used in the experiments can only be operated under high vacuum. These include the ion gauges, the hexapole filters, sensitive electronics such as the quadrupole mass spectrometer, the turbo-molecular pumps, and the diffusion pumps. In the case of a vacuum failure, various protection systems automatically switch off those instruments, which may be damaged by exposure to high pressure

The pressure in the chambers is monitored by several ion gauges (range 10^{-3} – 10^{-9} Torr), which are connected to MKS 290 controllers. At pressure in excess of 10^{-3} Torr, the ion gauge filaments automatically switch off to prevent the filaments from burning out.

However, there are several electronic components, which must be switched off at an even lower pressure than 10^{-3} Torr. To ensure that this occurs, a custom-made protection system, built by the Electronics Workshop in the Chemistry Department, has also been

installed. Output from the ion gauge controller for the ion gauge in the detection/scattering chamber, is connected to this protection unit. If the pressure in this chamber reaches a set pressure (currently 5×10^{-5} Torr), the protection unit switches off the protected electronics and activates the pneumatic valves to seal off the turbo-molecular pumps.

This custom-built protection system also safeguards the diffusion pumps from increases in pressure and temperature. The foreline pressure in the outlet of every diffusion pump is monitored by a thermocouple gauge (DST-531 Duniway Stockroom), which is connected to a MKS 286 controller. In the case of an excessive rise in the foreline pressure in any particular chamber, the protection unit will switch off power to the appropriate diffusion pump until the pressure decreases to below the set point. A rise in foreline pressure may occur if the gas load in the nozzle chamber becomes too heavy for the pump. Another common cause for a sudden rise in pressure is volatile gas molecules being released from the surface of the liquid nitrogen cold traps during the refilling process.

The diffusion pumps are water-cooled and temperature sensors are attached to the side of every diffusion pump to monitor the water temperature. The water-cooling system is connected in series to all the pumps. In the case of a cooling water failure, the temperature in any one of the pumps may exceed its set point. In such an event the protection system causes power to all the pumps to be switched off. In this case the protection unit must be reset manually.

3.2 Beam production

Molecular beams were produced in the nozzle chamber, and were collimated by two skimmers in the buffer chamber. This chamber also provides an intermediate stage of pumping to cope with the pressure difference between the nozzle and the hexapole chambers. The following aspects of the beam production are considered in this section: the molecular beam nozzles, beam gas handling system, and beam collimation.

3.2.1 Molecular beam nozzles

Three types of nozzles have been used for the production of the supersonic molecular beam, a solenoid valve, a piezoelectric valve, and a continuous flow nozzle combined with a gas-flow controller. Cross sectional views of the three nozzles are shown in Figure 3.2.1. To produce a continuous beam, either the continuous nozzle or the piezoelectric valve was used. To produce a pulsed beam, any of the three nozzles can be used, however, a rotating chopper must be used to regulate the continuous beam.

3.2.1.1 Solenoid valve

The solenoid valve (General Valve Corporation 9-181) was the original beam nozzle used in this research. This valve is shown in Figure 3.2.1 (a). The nozzle orifice is sealed by a Teflon poppet, which is fitted inside a spring-loaded plunger driven by an electromagnetic solenoid. A molybdenum disc, with a laser drilled 70 μm orifice, is held to the body of the valve by the front plate which has an orifice of 300 μm in diameter. The solenoid is operated by a custom-made Beam Source Driver (BSD), which controls the beam pulse delay, length, height, and frequency. [Blunt 1995] Typical operating parameters for the valve are 2 ms opening time at 10 Hz frequency.

A number of problems plague valves of this type. One major problem is that flakes of Teflon, produced by the action of the nozzle poppet, often cause blockage of the molybdenum disc aperture. Another problem is that the two springs used to hold the plunger might rebound, creating double beam pulses.

(a) Solenoid valve (scale 1:1)

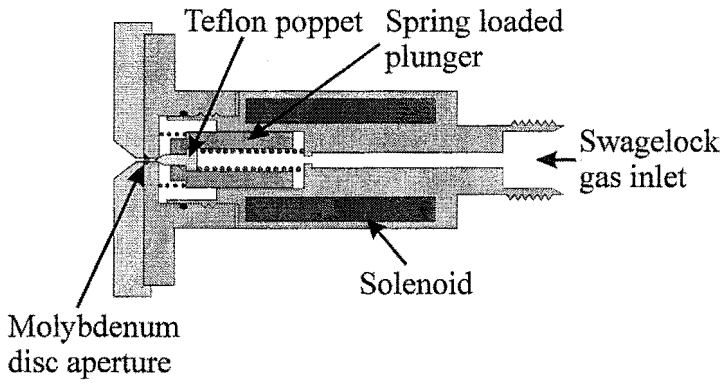

(b) Piezoelectric valve (scale 1:1)

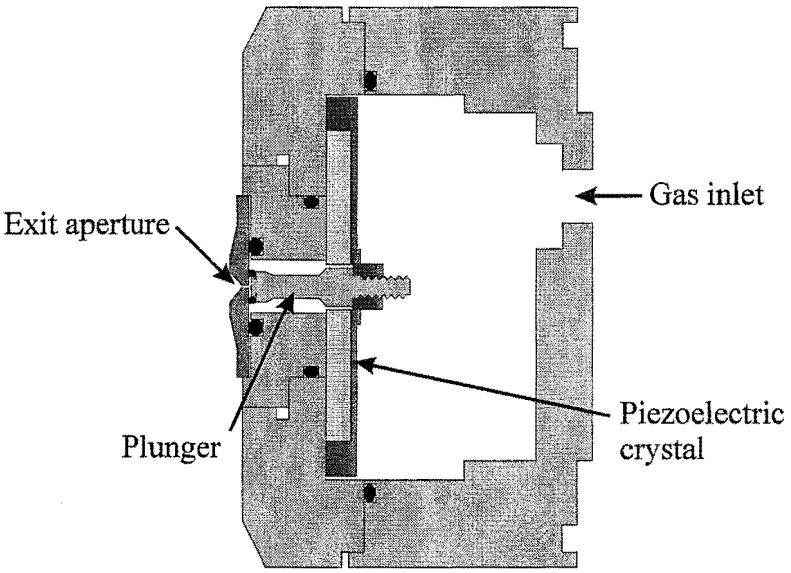

(c) Continuous nozzle (scale 1:1)

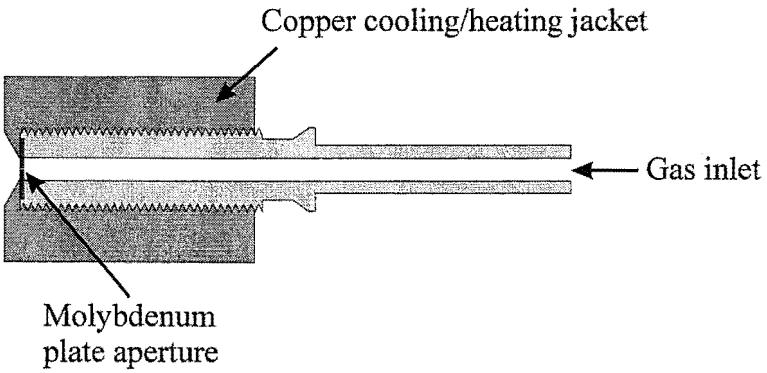

Figure 3.2.1 Cross-sectional views of the three nozzles.

3.2.1.2 Piezoelectric valve

The solenoid valve described above has been replaced with a P-286.20 piezoelectric valve. As well as overcoming the problems with the solenoid, this valve offers better beam-velocity resolution because of its faster operating time. The size of nozzle orifice is determined by a laser-drilled channel in the stainless steel front plate, 70 μm, and is sealed by the Viton o-ring at the tip of the plunger. The plunger is driven by a piezoelectric crystal, which deforms when a voltage is applied to it. The voltage supply unit has been modified so that the piezoelectric valve can be operated in either pulsed or continuous mode. The power supply unit, which can be externally triggered, controls the pulse width, delay, and frequency of the beam. The internally generated beam pulse frequency ranges from above zero to 500 Hz, the pulse width, from 0.1 - 3 m s.

3.2.1.3 Continuous nozzle

The size of the aperture for the continuous nozzle (which is 70 μm in this research) is determined by an aperture drilled in the molybdenum plate held to the body of the nozzle by the copper cooling/heating jacket. A MKS 258 Mass flow-meter valve connected to a MKS type 250B controller monitors the gas flow through the nozzle. The flow-meter controller regulates the pressure to either an internal or an external set point. In this research, the gas pressure is monitored externally by interfacing the flow controller with the pressure reading from a PDR-C-1B controller, which reads the pressure measured by a MKS Baratron, type 221, 0-1000 Torr. The beam nozzle is closed by a Nupro B-4HK needle valve to the gas supply. The experimental arrangement for the continuous nozzle is shown in Figure 3.2.2.

3.2.2 Beam gas handling system

A gas line system has been assembled to prepare beam gas mixtures, and is shown in Figure 3.2.3. The gas handling system is constructed from ¼" stainless steel or copper pipes, which are connected by Swagelock fittings and brass Nupro JN and B-4HK valves. Several custom-made stainless steel cylinders have been fabricated as gas reservoirs for the preparation of seeded beam mixtures.

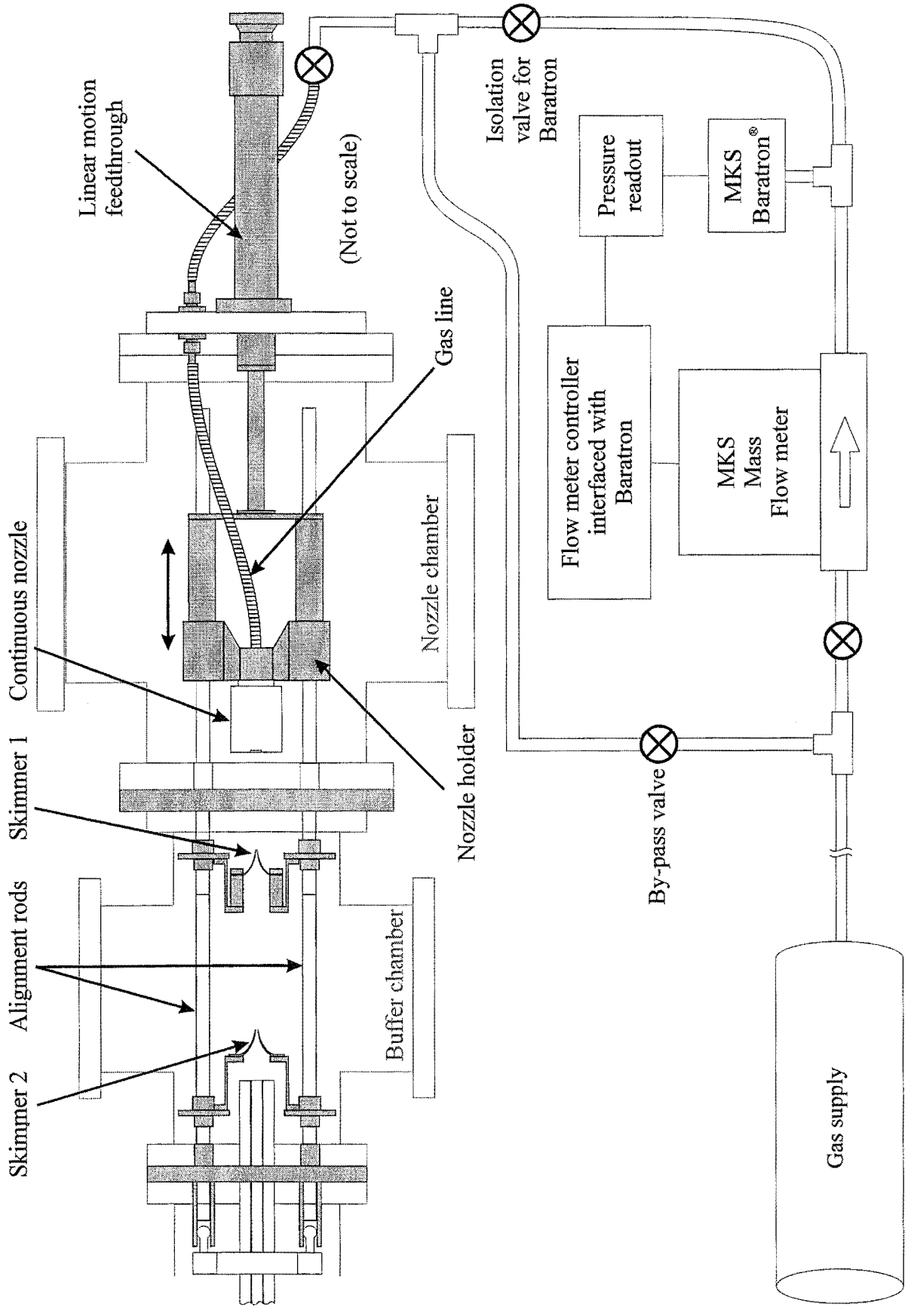

Figure 3.2.2 Configuration of the alignment system and supersonic molecular beam source.

The gas handling system can be isolated into two parts, which can be pumped separately by a 100 l min^{-1} Edwards Speedivac ES-100 mechanical pump. The first part of the gas line is used to supply gas to the molecular beam source, and is monitored by an MKS 122 5000 Torr Baratron, connected to an MKS PDR- C-1B controller. If the continuous nozzle is being used, this line is further regulated by the MKS Mass flow meter; otherwise, the flow meter can be bypassed. The other part of the gas handling system is used to supply either buffer gas when seeded mixtures are being prepared, or quencher gas for scattering experiments. In the latter case, a stepping motor controlled Leybold Heraeus variable leak valve is used to regulate the beam. A 130-psi dial gauge monitors the pressure in this part of the gas line.

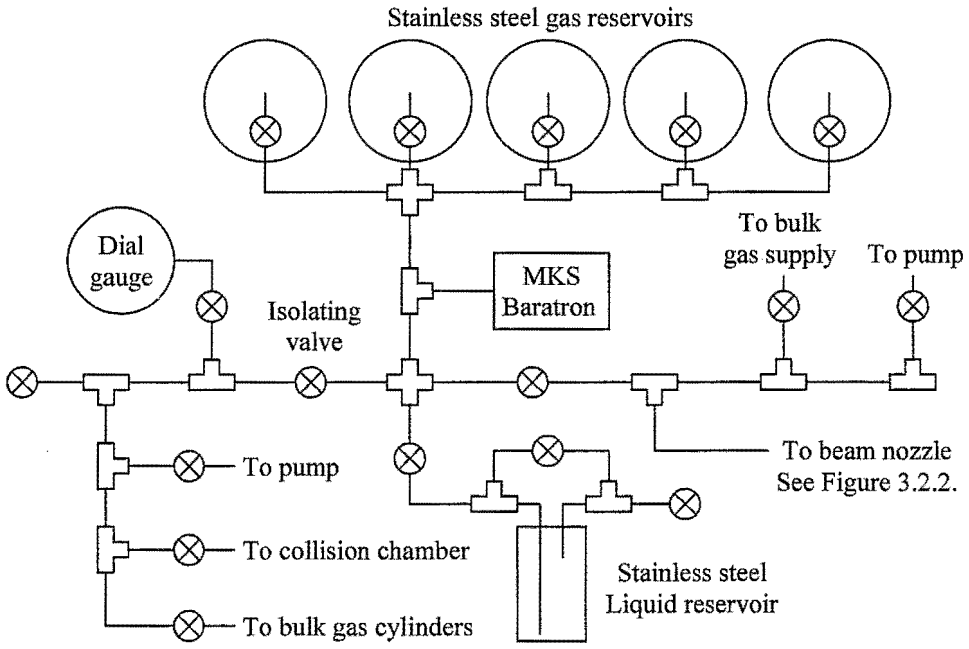

Figure 3.2.3. Gas handling system.

3.2.3 Beam collimation

Based on the principles discussed in Section 2.1, a supersonic molecular beam is extracted by a skimmer placed in the zone of silence of the supersonic expansion. In this experimental arrangement, this skimmer has a 1 mm diameter orifice. A second skimmer, which has a 1.5 mm diameter orifice, is used to further define the beam. Both skimmers are mounted on top hats, centred between the two alignment rods. The distance between

the nozzle and the tip of the first skimmer can be adjusted to optimise the beam conditions using the linear motion feed-through, on which the nozzle holder is mounted. The optimum nozzle-skimmer distance is dependent on the pressure of the beam gas used. This distance in our experiments has typically been 20 mm and the distance between the two skimmers is 140 mm.

A rotating beam chopper located between the two skimmers and clamped to the alignment rods was used to modulate a continuous beam. The blade of the rotating chopper can be modified depending on the desired width in relation to the frequency of the beam pulses. A custom-made chopper motor controller operates the chopper with a rotation frequency ranging from zero to 800 Hz.

3.3 Alignment system and Hexapole electric fields

3.3.1 Alignment system

Alignment of the physical components of the machine with the beam itself is critical to the success of these types of experiments. The alignment system can be separately described in two parts, the first is a permanent arrangement and the second is adjustable according to experimental requirements.

3.3.1.1 Part I

The first part is the alignment system is situated in the nozzle and buffer chambers. Here, at the point of production, the beam is aligned along the central axis of machine. This is achieved by a nozzle holder and the two skimmer-attached flanges, which are aligned by two ½" stainless steel alignment rods, as shown in Figure 3.2.2. The alignment rods are held in place inside the chambers by the two flanges highlighted in grey in Figure 3.2.2.

The nozzle holder is made of aluminium and is mounted on a linear motion feed-through, which is on an 8" flange at the front end of the molecular beam machine sealed with a Viton o-ring. All three types of nozzles can be mounted on the same nozzle holder with extra attachments to maintain the optimum nozzle-skimmer distance. The translator-mounted flange is supported by a separate *xyz*-translator on the rail system of the supporting frame, so the entire nozzle assembly can be removed for the aligning of the components inside the machine.

3.3.1.2 Part II

The second part of the alignment system extends from the hexapole chamber to the entrance of the detection chamber. Two configurations of the alignment system have been employed depending on the experimental arrangement. The configuration shown in Figure 3.2.2 is the original arrangement for single hexapole experiments; the hexapole is aligned with the beam by the ceramic hexapole mounts. The front hexapole mount is

fitted via ball joints into extension sleeves, which extend from the alignment rods in the buffer chamber. The hexapole mount at the far end is bolted to the entrance of the detection chamber, and can be adjusted according to the alignment requirement. Further details of the original hexapole mounts are discussed in Section 3.3.2.

The second alignment system configuration was designed for the tandem hexapole arrangement. Two ½" ground stainless steel rods with ball joints at one end are fitted into the sleeve extensions from the alignment rods in the buffer chamber. As shown in Figure 3.3.2 (c), the other end of the rods are held by a Perspex flange, which is again mounted at the entrance of the detection chamber and is adjustable for alignment purpose. This design provides easy access for the future addition or modification of experimental components. (See Figure 3.3.1.)

3.3.1.3 Alignment procedure

The nozzle assembly can be easily extracted from the chamber on the flange mounted rail assembly and supported on the rail for maintenance or testing. An alignment laser, which is a He-Ne laser (Applied Laser Systems, 670 nm 5 mW), is used to provide a virtual axis for the alignment of other experiment components with the beam axis. The alignment laser is mounted in place of the nozzle so that the laser beam goes through the on-axis apertures of two Perspex alignment blocks, which are mounted onto the alignment rods between the laser and the first skimmer. When the laser is perfectly aligned through the centre of the alignment rods, an evenly distributed laser spot can be seen on the first skimmer and a ring is observed around the tip of the second skimmer. The laser beam then defines the reference axis for the alignment of all other experimental components.

3.3.2 Original hexapole

The original hexapole is made of six 10 mm diameter centreless-ground stainless steel rods, all 833 mm in length. These rods are held in place by two ceramic mounts, as shown in Figure 3.3.1, and have an inscribed radius of 5.88 mm. The keyhole shaped slots in the ceramic mounts increase the surface distance between two rods in order to minimise electrical discharge across the surface of the hexapole mount when a high

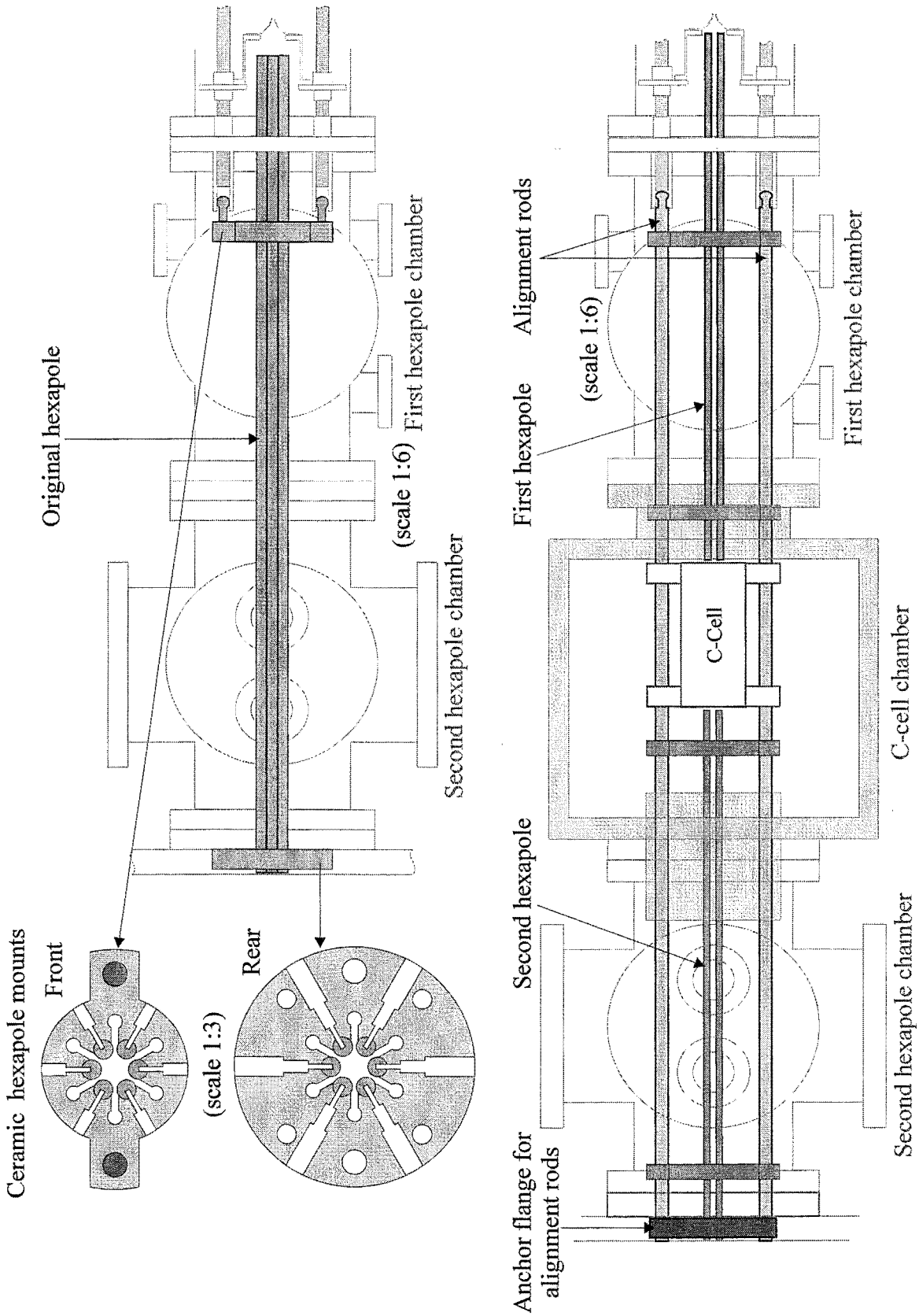

Figure 3.3.1 Configurations of the original single hexapole and the tandem hexapole arrangement. Details of the original ceramic hexapole mounts are shown with a scale of 1:3.

voltage is applied. The front ceramic mount has two ball joints, which can be pushed into the metal sleeves extending from the alignment rods in the buffer chamber. The rear ceramic mount is firmly bolted onto the inner wall of the detection/scattering chamber after the hexapole is aligned with the laser reference axis. An adjustable iris mounted on a can over the anchoring flange of the alignment rods is used as the exit aperture of the hexapole filter. It is usually set to a 2 mm diameter opening. The electrical connections to the hexapole rods are shown in Figure 3.3.2 (b). The two copper braids are soldered to high-voltage feed-throughs on the top flange of the second hexapole chamber. The required voltages for the hexapole filters are supplied by a pair of Glassman EH 0 – ±30 kV power supply units. In practice, only voltages up to ±7.5 kV are used as discharge across the rods will occur at applied voltages above ±12 kV.

3.3.3 Tandem hexapole arrangement

The tandem hexapole arrangement was proposed after the signal-hexapole experiments have been successfully carried out. The experimental advantages of such an arrangement are twofold. Firstly, increasing the length of the hexapole field would lead to an increase in the resolution of the hexapole filter in selecting molecules in specific quantum states. Secondly, by interposing a collision cell between the two hexapole-filters, it would allow the study of the rotational state of collision products. The first hexapole would be used to select the initial rotational states and the second hexapole to determine the resulting rotational states of the molecules after collisions. The tandem hexapole arrangement was eventually adopted as part of the Molecular Beam Electric Resonance spectrometer, by replacing the collision cell with an electric resonance cell, the C-cell.

The tandem hexapole arrangement is shown in Figure 3.3.1. Each hexapole is made of six ¼" diameter centreless-ground stainless steel rods, 530 mm in length. The rods are held by two Perspex hexapole mounts, as shown in Figure 3.3.2 (a), and have an inscribed radius of 4.74 mm. The Perspex mounts are designed to sit over the alignment rods, aligning the hexapole rods to the axis of the beam. The same power supply units can supply voltage to both hexapole filters. When different voltages for the hexapole filters are required, however, a pair of Glassman EH 0 – ±10 kV power supply units are used for the second hexapole filter.

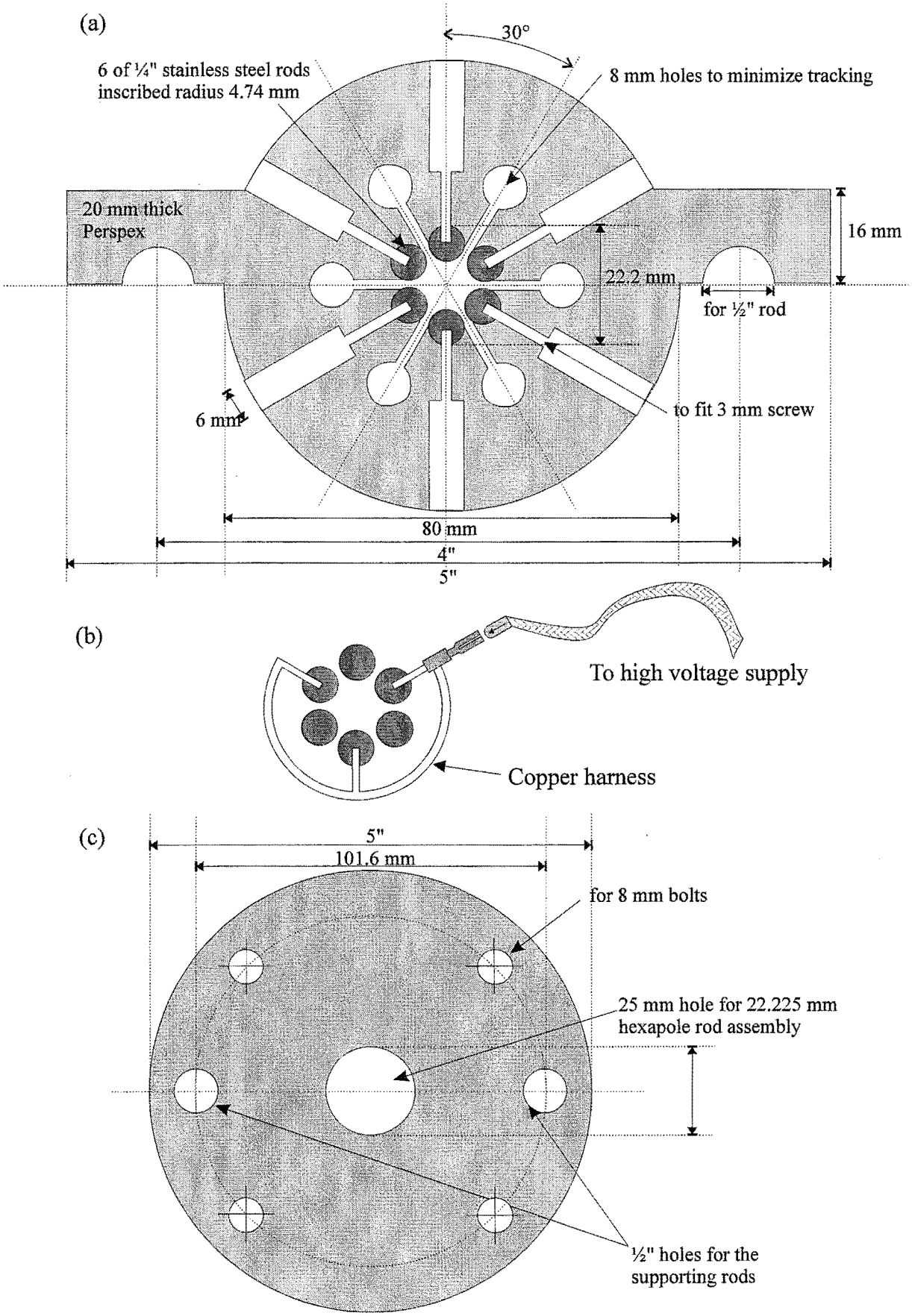

Figure 3.3.2 (a) New hexapole mount. (b) Electrical supply to the hexapole. (c) Perspex anchor flange for the alignment rods.

3.4 Resonance electric field

The resonance electric field, often referred to as the C-field, is an essential component in the Molecular Beam Electric Resonance spectrometer. As discussed in Section 2.4, the C-field must provide a uniform electric field, E, used to orient the molecules and a radio frequency (RF) field to induce the desired resonance transitions. Since, the transition dipole of a symmetric top molecule is orthogonal to its molecular axis, the RF field direction is required along the transition dipole of the molecule so the RF fields must have a component at right angles to the DC field, which is along the molecular axis. Two designs of the C-cell have been used to provide such electric fields. The C-cells are made of copper plates in order to obtain smoothly polished surfaces necessary to produce a uniform electric field. Both C-cells are 140 mm in length. The C-cell is enclosed in a Faraday cage to eliminate stray fields that might interfere with the resonance electric field.

3.4.1 First C-cell design

The first C-cell was designed and built with of a pair of parallel plates, each split into two sections as shown in Figure 3.4.1 (a). In order to maintain a uniform DC field, the RF plates must be kept at the same potential as the DC fields. The component of the RF field perpendicular to the DC field is obtained by making the size of the two facing RF plates different. The gaps between the RF and DC plates on each side are diagonally opposite with one above and one below the molecular beam path. To prevent any inhomogeneity in the electric fields, the vertical displacement of the gaps must be equal to the plate spacing, and the gaps should be less than 1 mm wide. [Muenter 1992] The details in the design of the first C-cell are shown in Figure 3.4.1 (a) and the 3-D view of the C-cell is shown in Figure 3.4.2 (b).

3.4.2 Second C-cell design

The second C-cell was design and built with of two sets of parallel plates. The RF field is directly perpendicular to the DC fields. It is a much simpler design, as shown in Figure 3.4.1 (b) with the 3-D view of the second C-cell shown in Figure 3.4.2 (c).

3.4.3 Faraday cage

The Faraday cage is designed to minimise interference from stray fields, and to support the plate assemblies of the C-cells. It is made of aluminium plates with a lid made of aluminium mesh, and is 146 mm in length. The cage is supported on and aligned to the alignment rods by Perspex mounts, which are attached to the cage. The C-cell itself is insulated from and aligned to the cage by Perspex holders at the base of the cage. The details in the design of the Faraday cage are shown in Figure 3.4.2 (a).

3.4.4 Electrical configuration

A Hewlett Packard 33120A waveform generator was used to generate the RF signal for the resonance electric field. The RF signal is usually fixed at a frequency between 1 and 3 MHz with amplitude of around 1.5 Vpp. The DC electric field strength was computer controlled using an ADDA14 computer I/O card, which has an output voltage range from 0 to 10 V. Two Spellman 0 – ±300 V voltage supplies, controlled by 0 - 10 V input voltages, have been used to provide the C-cell with voltages ranging from 0 to 600 V. (See circuit diagrams in Figure 3.4.3 (a) and (b).) More recently, two 0 – ±30 V power supplies have been used in place of the 0 - ±300 V power supplies to provide voltages with a more accurate voltage increment in the lower voltage range. The RF generating plates need to be kept at the same potential as the neighbouring DC plate. The circuit diagram for the custom designed distribution circuit of the RF and DC currents is shown in Figure 3.4.3 (c). Figure 3.4.3 (d) shows the electrical supplies for the first design of C-cell, and Figure 3.4.3 (e) shows a flow diagram of the C-cell electric field supplies. Several electric field configurations are possible for the second C-cell to provide the required electric field. A comparison of the C-cell performances is discussed in Section 4.1.5.

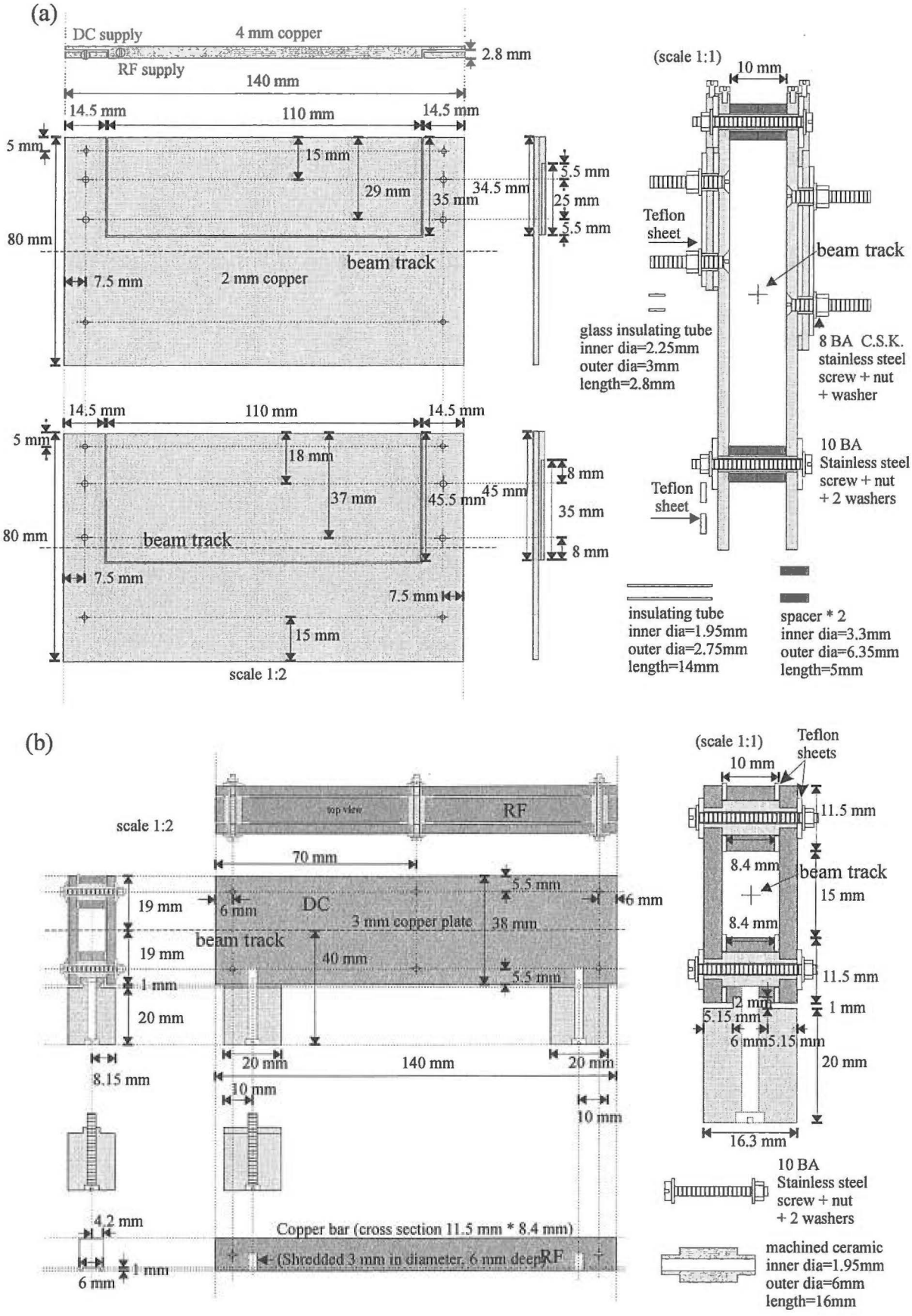

Figure 3.4.1 (a) First design of C-cell. (b) Second design of C-cell.

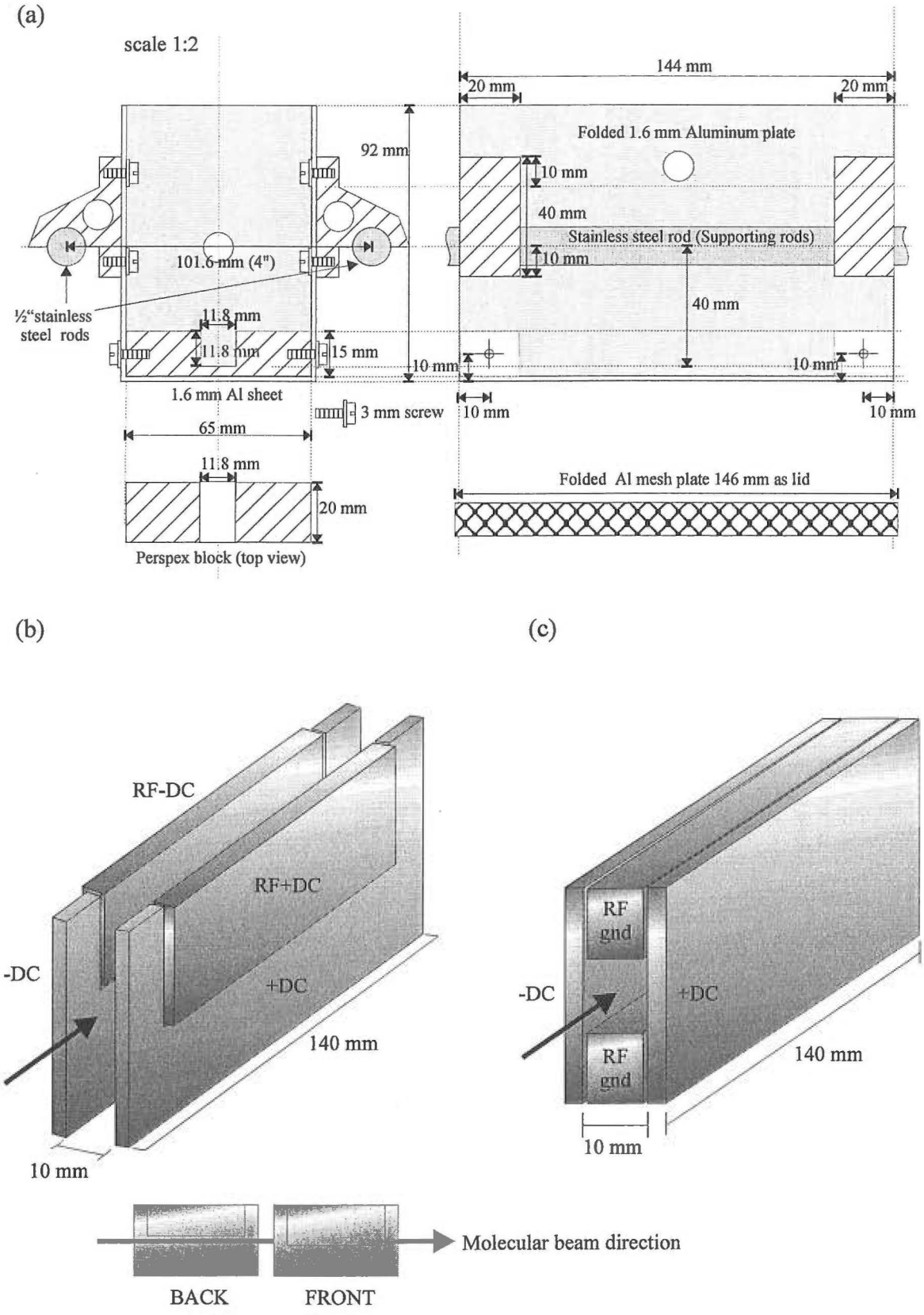

Figure 3.4.2 (a) Design of Faraday cage (b) 3-D view of the first C-cell. (c) 3-D view of the second C-cell.

(a) 0 - 10 V to 0 - +300 V supply

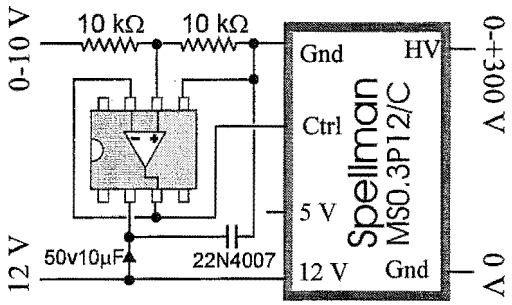

(b) 0 - 10 V to 0 - -300 V supply

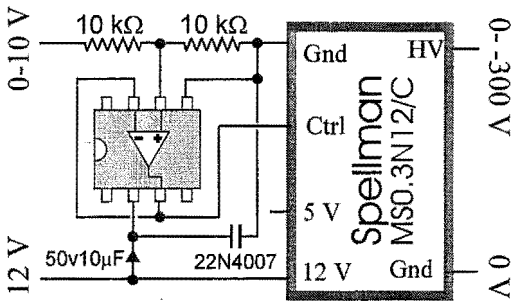

(c) RF & DC distribution circuit

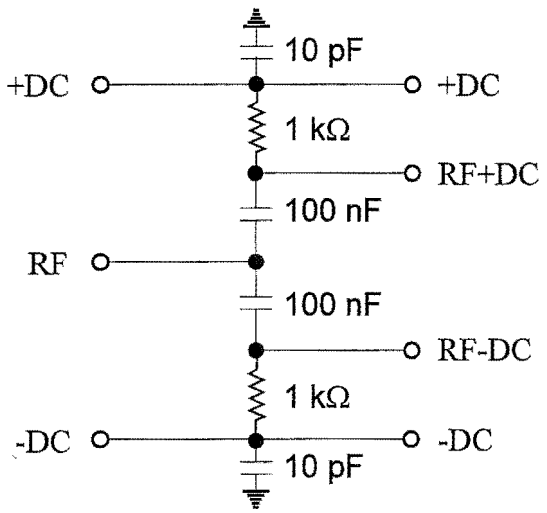

(d) Electrical supplies for C-cell

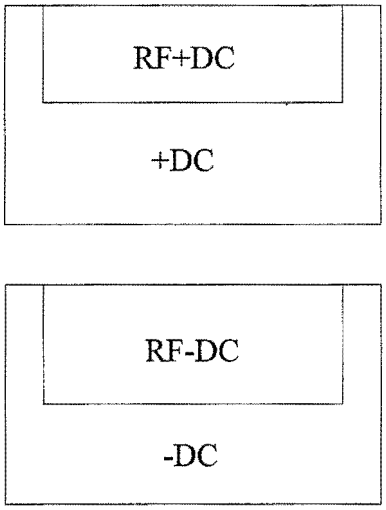

(e) Flow diagram of C-cell electric field supplies

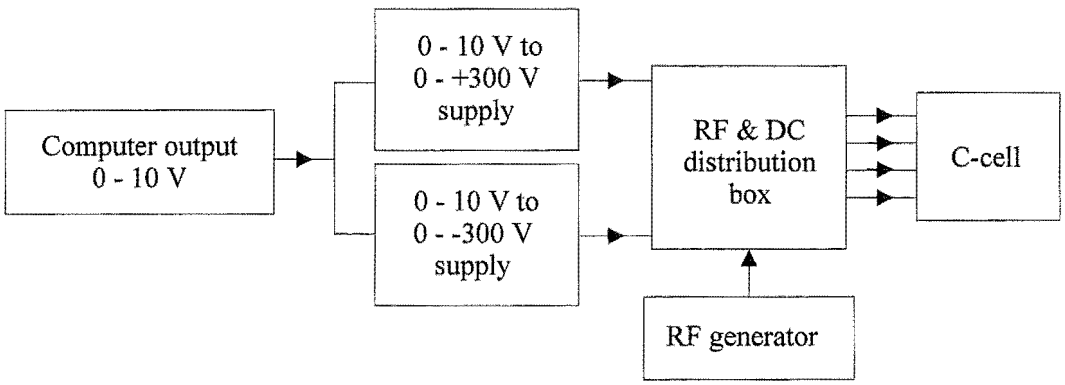

Figure 3.4.3 Configuration of C-cell electric field supplies.

3.5 Detection and signal processing

An Extranuclear 4-270-9 quadrupole mass spectrometer is used to detect the molecular beam. The beam signal could be processed in a variety of ways depending on the experimental arrangement and the required form of the results.

3.5.1 Mass spectrometer

Molecules arriving at the detector are ionised in the ion source, originally part of a Vacuum Generators SXP300 quadrupole mass spectrometer. The resulting ions are focused by three Einzel lenses, mounted directly behind the ion source, into an Extranuclear quadrupole mass filter. After passing the quadrupole rods, the mass selected positive ions are detected using a channeltron electron multiplier with a cone voltage between -1.5 – -2.5 kV. The channeltron electron multiplier converts individual ions into pulses of secondary electrons with amplification factor in the range of 10^5 to 10^7, depending on the cone voltage. The electron (current) pulses were observed directly using a sensitive Fluke PM3394B 200 MHz CombiScope. The current pulses could be amplified using instruments listed below:

- Extranuclear 032-3 pulse counting preamplifier/discriminator, which converts current pulses into TTL pulses; 5V, 250 ns wide. This was used for the pulse counting mode.

- SXP300 analog amplifier, which integrates and amplifies the current pulses into an analog voltage output. This output was processed by a Thurlby-DSA524 digital storage adapter, which was interfaced to the computer.

- Extranuclear 032-4 negative/positive ion preamplifier, which is used in conjunction with an Extranuclear 031-3 fast electrometer. The current pulses were integrated and converted to amplified voltage output of 0 – 10 V, depending on the sensitivity range and the readout option selected. The signal was directed to the computer through the ADDA14 interface.

- Stanford-Research-Systems-SR570 low-noise current preamplifier, which converts the current pulses into a voltage output. The sensitivity of the preamplifier ranges from 1 mA V^{-1} to 1 pA V^{-1}, and the maximum output is ±5V into a high impedance load (50 Ω output impedance). It was computer interfaced through an RS-232 port.

3.5.2 Signal processing

The mass spectrometer signal was processed according to experimental requirements. Two main types of signal were produced; voltage pulses or integrated analog voltage signals. These were processed in a variety of ways discussed below to obtain the optimum signal with the maximum signal-to-noise ratio.

3.5.2.1 Pulse counting mode

The pulse counting mode was used only for a pulsed or modulated beam signal. A signal in the form of voltage pulses was directed into a custom-built pulse counting control unit and subsequently into a computer through a PCL-8255 digital-digital lab card. The pulse counting unit operates by counting and accumulating pulse counts over a period of time, which defines a gate. The first gate was set to count signal pulses over the beam pulse and the second was set to count over the background. The difference in the counts between the two gates was taken to minimise the background signal.

3.5.2.2 Analog signal

The computer was used to process the analog signal from the selection of current amplifiers discussed in Section 3.5.1 through an ADDA-14 interface. The signal-to-noise ratio was improved by averaging over a large number of readings. The limit on the number of reading for averaging was imposed by the speed of the computer interfacing. Typical signals measured for upper Stark-state molecules focused by the hexapole filter were at least twice as large as the initial molecular beam signal.

3.5.2.3 Phase sensitive amplifier

The phase sensitive amplifier, which is also called a lock-in-amplifier, is essentially a filter tuned to the frequency of a low amplitude modulation, and is able to measure the amplitude of this modulation despite a very large background signal. In Molecular Beam Electric Resonance spectrometry, the desired signal, which is the depletion of total signal due to the resonance transitions, is very small compared to the total signal detected by the mass spectrometer and can only be extracted by such a phase sensitive amplifier. By modulating the amplitude of the RF electric field with a mark-space-ratio of one, the resonance field can be switched on and off with the RF amplitude modulation (AM) frequency. As a result, the total mass spectrometer signal modulates at the AM frequency, and the depletion in signal due to the resonance transitions can be measured by the lock-in-amplifier.

A Stanford Research Systems Model SR510 Analog Lock-in Amplifier was used to process the amplified signal from the quadrupole mass filter. A square waveform electric voltage was provided by a Goldstar Model OS-9020G oscilloscope as the AM frequency for the RF generator (Hewlett-Packard-33120A waveform generator), and as a reference frequency for the lock-in-amplifier. The output signal from the lock-in-amplifier, 0 - ±10 V, was processed by the computer through an ADDA-14 interface card. Figure 3.5.1 shows the mode of operation for the molecular beam electric resonance spectrometer.

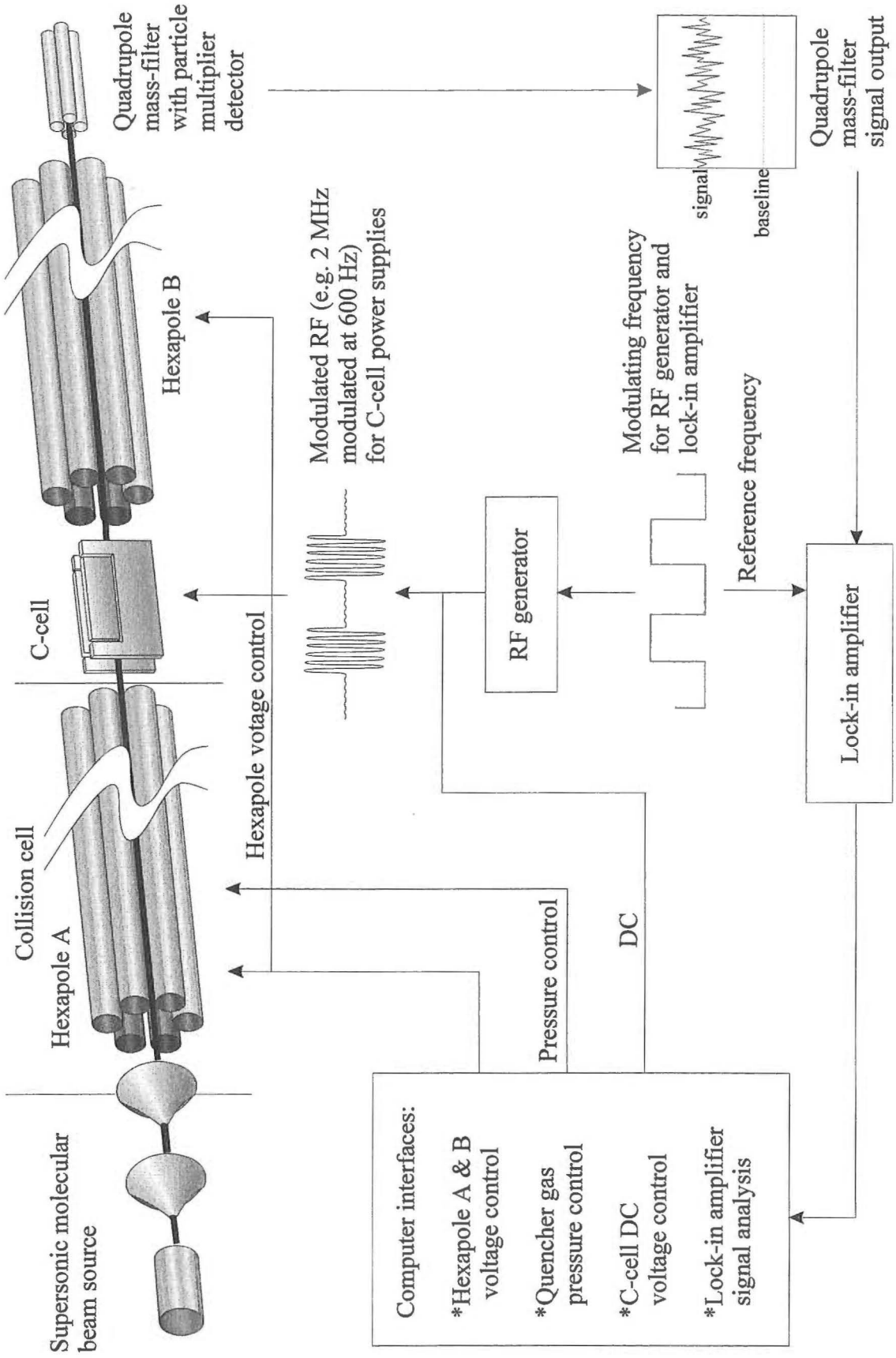

Figure 3.5.1 Schematic diagram of the experimental set up and the mode of operation for the electrical interfacing of the experiment using a computer.

3.6 Computer interfacing

All of the experimental data were processed using a computer, PC 486. This computer has also been used to control the hexapole voltages, regulate the quencher gas pressure in the collision chamber, read the pressure from an MKS Baratron transducer, provide the voltage output to the C-cell, and assign the settings for the lock-in-amplifier, etc. These tasks were performed using one or more of the following interface media: a PCL-7388 lab card, a PCL-8255 lab card, an ADDA-14 card, or an RS-232 port. A number of computer programs have been written to control experiments and for data acquisition and processing. The computer programs and/or subroutines used for controlling the equipment and reading data are included in Appendix C.

3.6.1 PCL-7388 lab card

This interface card is connected to a Crystalap-STD-206 driver unit, which operates a Howard-industries-1-19-4307 stepping motor used to control the Leybold-Heraeus variable leak valve that admits quencher gases into the collision cell.

3.6.2 PCL-8255 lab card

The PCL-8255 lab card is a programable digital-digital peripheral interface. It has programable input/output control functions up to 48 input/output lines and three independent 16 bit counters, and its port addresses are selectable.

It has been used to interface the computer with several 12-bit digital-to-analog converters to control the hexapole voltage supplies, the MKS 290 ion gauge controller (to read pressure measured by the ion gauge), and the pulse control unit (for signal acquisition and data processing).

3.6.3 ADDA-14 card

The ADDA-14 card is a 14-bit analog-to-digital and digital-to-analog conversion card, and is connected to an ADDA-14 converter, which has 16 analog-to-digital inputs, 2 digital-to-analog outputs, and 4 voltage outputs channels, ±5 V and ±12 V. All the channels are provided with BNC connectors through a homemade connector box.

The DC voltage for the C-cell was controlled by a digital to analog output, which has a range of 0 to 10 V. The voltage outputs from the mass spectrometer, voltage amplifiers and the lock-in-amplifier were connected to the analog-to-digital inputs. The pressure reading from an MKS HPS 919 Hot Cathode Controller was interfaced through one of the analog-to-digital input channels.

3.6.4 RS-232 port

Several commercial instruments used in the experiments are provided with computer interface capacity through RS-232 interfaces. These are the Thurlby-DSA-524 digital storage adapter, the Stanford Research Systems SR510 Lock-in amplifier, the Fluke PM3394B waveform generator, the 200 MHz CombiScope, and the MKS-670A Baratron controller.

3.7 Experimental methods

Several different experiments have been carried out in order to study the various characteristics of the molecular beam; such as the optimisation of beam signals, the determination of beam profiles, the measurement of $|JK\rangle$ ($\Delta M = \pm 1$) transition spectra, the measurement of the hexapole transmission curves, and the beam attenuation experiments. These are discussed in detail below.

3.7.1 Optimisation of beam signal

The first step in optimising the total beam signal was to make sure that the alignment of the machine is correct. The correct alignment would ensure that molecules focused on the axis of the beam by the hexapole field would be transmitted successfully to the detector. The increase in signal intensity with the hexapole energised was at least two-fold.

The second step in optimising the signal was to adjust the nozzle-skimmer distance to obtain the maximum supersonic beam signal. The signal was measured semi-automatically by adjusting the linear motion translator so that the nozzle position could be changed manually, and the beam signal was recorded automatically by the computer.

When the lock-in-amplifier was used, either the phase setting or the modulating frequency (that is also the reference frequency) must be adjusted to obtain the maximum signal. The latter adjustment was achieved by changing the frequency supplied from the Goldstar oscilloscope manually. The phase, however, could be adjusted manually or automatically using a computer program that reads and sets the phase in the lock-in-amplifier through the RS-232 interface.

3.7.2 Beam profile

The molecular beam profile was obtained by measuring the beam signal as a razor blade cuts across through the beam. The razor blade was mounted 45° to the beam axis on the *XYZ*-translator in the ion source chamber. The beam signal fell off as the razor blade was

moved across the beam stepwise. The fall-off between steps represents the density of the beam at that particular interval. The beam profile was reconstructed by numerically differentiating the beam signal with respect to the position of the razor blade.

3.7.3 $|JK\rangle$ spectra

As discussed in Section 2.4, the signal depletion due to $|JK\rangle$ ($\Delta M = \pm 1$) transitions could be measured using the lock-in-amplifier. A $|JK\rangle$ spectrum (as defined here) was obtained by measuring the signal from the lock-in-amplifier as a function of the DC electric field strength and keeping all other variables constant, in particular the hexapole field strength and the RF field strength and frequency. The range and the stepping increment of the DC electric field were selected by user-inputs into the computer program (see Appendix C.4).

3.7.4 Transmission curves

Transmission curves were obtained by monitoring the signal from a signal amplifier as a function of the voltage applied to the hexapole filters, keeping all other experimental variables constant. The voltage setting is determined by user inputs into a computer program. Hexapole transmission curves were obtained from the mass spectrometer signal, whereas rotational state dependent transmission curves were obtained from the lock-in-amplifier signal. The resolution of transmission curves is very much dependent on the size of the exit aperture and the beam alignment. This aspect is discussed further in Sections 4.1.3.2 and 4.1.5.3.

3.7.5 Attenuation experiment

Cross-sections were determined in quantum state specific molecular beam attenuation experiments using Beer's Law, see Section 2.5,

$$\ln \frac{I_0}{I} = n\sigma l = \frac{\sigma l P}{k_B T} \tag{3.7.1}$$

where I and I_0 are the transmitted and incident beam intensities, n is the particle number density in the collision cell, l is the path length through the collision cell, σ is the cross-

section, P is the pressure in the collision cell, k_B is Boltzmann's constant, and T is the temperature of the scattering species, that is, room temperature. Since the values of l, k_B, and T are constant, the attenuation experiments were carried out by measuring signals as a function of pressure.

The pressure in the collision cell was measured by an ion gauge, which was read by a computer program through the appropriate interfacing media. This pressure reading must be calibrated, because the sensitivity of the gauge varies depending on the quencher gas. The ion gauge pressure was calibrated against an MKS high sensitivity Model 670 0.1 Torr full scale absolute Baratron. During attenuation experiments, the pressure in the collision chamber was controlled by a Leybold Heraeus variable leak valve, which was opened by a computer interfaced stepping motor through the PCL-7388 lab card. The computer read the pressure every time the leak valve was opened or closed by the computer controlled stepping-motor until the pressure reading was within $\pm 5 \times 10^{-7}$ Torr of the target pressure.

3.7.6 Pressure measurement

Several pressure-measuring devices were used in this research. The choice of the device was dependent on the pressure range required. Thermocouple gauges (range atm – 10^{-3} mbar) were used to monitor the pressure at the outlet of the diffusion pumps and the turbo-molecular pumps. Ionisation gauges (range 10^{-3} – 10^{-10} mbar) and capacitance manometers, Baratrons (range atm – 10^{-6} mbar, depending on the manufacture specifications), were used to monitor the pressure in the main chambers of the molecular beam machine.

Ionisation gauges are very sensitive pressure-measuring devices. These gauges consist of a rhenium or tungsten filament, a grid, and a collector wire. Gas molecules are ionised by electrons emitted from the hot filament, at 75 eV. The resulting ions are accelerated by the grid (held at +150 V), and attracted to the collector (held at ground potential). The resulting current is measured through an external electrometer circuit. This current is proportional to the gas pressure in the gauge and is dependent on the electron impact ionisation cross-sections of the gas species.

Baratrons incorporate a thin metal diaphragm fixed between two electrodes. The pressure is measured electronically by the change in the capacitance between the two electrodes as the diaphragm deflects under the forces due to the pressure differential across the diaphragm. The reference side is either pumped or sealed under permanent vacuum, around 10^{-6} to 10^{-7} mbar. Baratrons measure absolute pressure, which is independent of gas species. Four Baratrons were used in this research, two of them were installed in the molecular beam machine (see Section 3.1.5 and 3.1.6), one in the gas handling line (see Section 3.2.2), and the last one in the flow-meter gas line (see Section 3.2.1.3). The flow-meter gas line can be bypassed so that the Baratron could be used to measure the pressure in the nozzle chamber.

3.7.6.1 Ion gauge calibration – Part I

Before a high accuracy Baratron was purchased specifically for this research, the pressure in the collision chamber was measured by an ionisation gauge and recorded by computer using a PCL-8255 lab card interfaced to the MKS-290 ion gauge controller.

The ion gauge and controller are factory calibrated with air, which has an electron impact ionisation cross-section of 2.81 $Å^2$ at 75 eV. The relationship between measured pressure, P_M, and true pressure, P_T, in terms of the ionisation cross-sections at 75 eV was determined by calibration against a differential MKS-310-CH Baratron (range 10 -10^{-5} Torr) in a separate vacuum system. [Blunt 1995] A series of pure gases with known 75 eV electron impact ionisation cross-sections were introduced into the vacuum chamber. The slopes from the pressure recorded by the ionisation gauge plotted against the Baratron reading gave the relationship between the measured pressure, P_M, and the true pressure, P_T.

$$P_T = \frac{P_M}{0.41\sigma_{EI} + 0.047} \tag{3.7.2}$$

where σ_{EI} is the electron impact ionisation cross-section. Table 3.7.1 summarises experimental electron impact ionisation cross-sections for some scattering gases. [Blunt 1995] Pressure measured by the ionisation gauges can be corrected using Equation (3.7.2) as long as the electron impact ionisation cross-section for the gas species are

known. Ion gauges are inherently less accurate than capacitance manometers and the readings do not exhibit the same degree of reproducibility on a day to day basis.

Table 3.7.1 Experimental 75 eV electron-impact ionisation cross-sections measured using an ion gauge. [Blunt 1995]

Species	σ_{EI} / Å^2	Species	σ_{EI} / Å^2
He	0.386	Xe	7.31
Ne	0.615	H_2	1.21
Ar	3.52	N_2	2.88
Kr	5.18	CH_3Cl	9.44

3.7.6.2 Ion gauge calibration – Part II

A high accuracy 690 MKS Baratron with a 0.1 Torr full-scale head was purchased and installed in the collision chamber, an MKS 670 Baratron controller was used to read and process the signal. An MKS HPS 919 computer readable Ion Gauge controller was also purchased to process signals from ionisation gauges interfaced through the ADDA-14 card, see Section 3.6.3. The Baratron readings were not used directly during an experiment for the following two reasons.

Firstly, the Baratron became unstable at very low pressures (10^{-6} - 10^{-7} range). Initially, to overcome this problem, the computer program operating the apparatus was modified to average over multiple readings from the MKS-670 controller. This mode of operation led to the discovery of a second problem. Interference between the control signal from the computer to the MKS-670 controller and the controller electronics resulted in a slight "anomalous" increase in the pressure reading. While this was not an issue for a single reading, when the controller was required to return a large number of pressure readings over a short time (100 readings per second) the offset in the pressure reading became considerable. During an attenuation experiment, the computer reads the pressure in the collision chamber every time the leak valve is opened or closed by the stepping-motor until the pressure reading was within $\pm 5 \times 10^{-7}$ Torr of the target pressure. For this

reason, the offset due to the interfacing interference could not be easily regulated because the number of the steps taken for each target pressure could not be pre-determined. It was therefore, better to calibrate an ion gauge using the Baratron and then to use the computer-readable controller to read the pressure during an experiment.

The ion gauge pressure reading from the MKS HPS 919 controller was calibrated against the Baratron pressure reading from the MKS 670 controller. A computer program (igcali.exe, see Appendix C.5) was written to take data for the calibration curves. After requesting a filename, the program waits for a user command to set the number steps for the stepping motor to open/close the leak valve, record an ion gauge pressure reading and a single Baratron pressure reading, or quit. Only a single reading from the MKS 670 controller is taken each time to minimise the electronic interference on the pressure reading. Therefore, it is necessary to wait until the pressure reading from the Baratron MKS 670 controller stabilises before the reading is taken at each pressure setting. Calibration curves are typically taken over the range of 10^{-7} to 10^{-4} Torr, depending on the quencher gas. An example of the ion gauge calibration curve is shown in Figure 3.7.1.

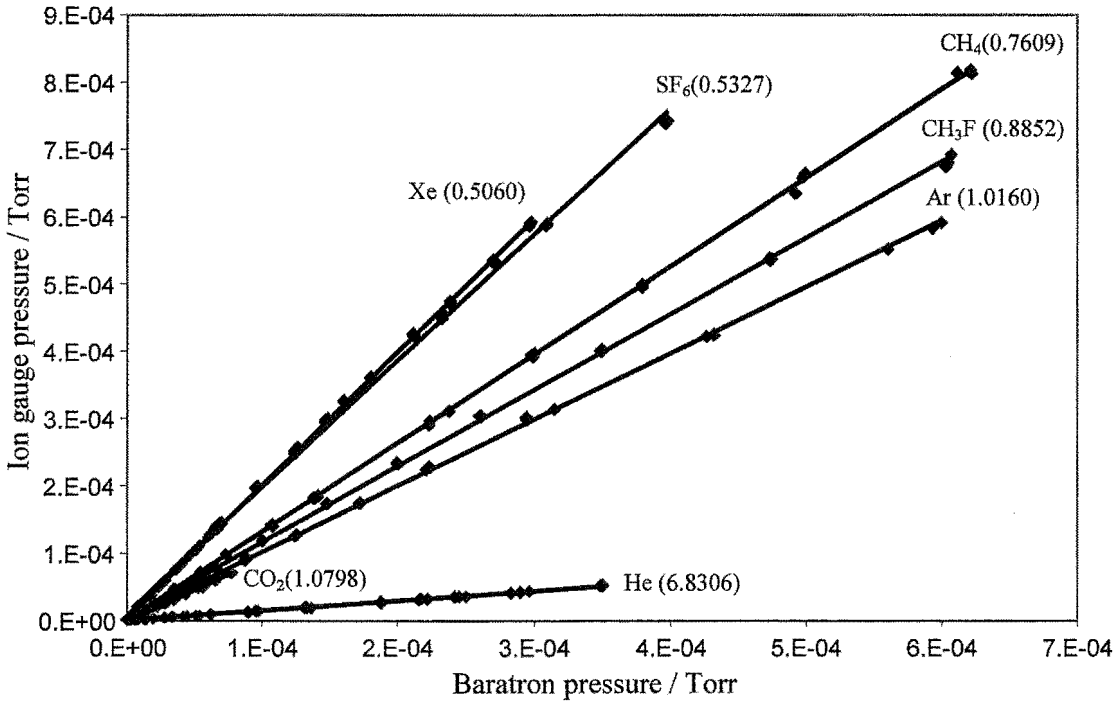

Figure 3.7.1 Ionisation gauge calibration curves for He, Ar, Xe, CO_2, CH_4, SF_6 and CH_3F. Ion gauge correction factors for each species are given in parentheses.

CHAPTER 4 RESULTS AND DISCUSSION

4.1 Beam characterisation

The characteristics of supersonic beams of symmetric top molecules in hexapole electric fields have been studied in single hexapole experiments and in tandem hexapole experiments. A Molecular Beam Electric Resonance spectrometer (MBER) was incorporated into the tandem hexapole for beam characterisation experiments. The interpretation of collision induced molecular beam attenuation experiments depends on our knowledge of beam characteristics, such as the profile, velocity and temperature of the beam. Collision cross-sections were determined from attenuation experiments of quantum state selected molecular beams with quencher gases. Hexapole electric filters have been used to select the upper Stark states in beams of symmetric top molecules. The rotational state distributions of the hexapole-selected beams are dependent on the applied hexapole potentials. In tandem hexapole experiments, the rotational state distributions of the resultant beams are also dependent on the potential of the uniform field region between the hexapole filters. The following sections discuss aspects of beam characterisation: the beam profile, the determination of beam temperature and velocity, the transmission of quantum state selected molecules in single hexapole experiments, tandem hexapole experiments, and in MBER experiments.

4.1.1 Beam profile

The experimental arrangement for measuring the molecular beam profile is described in Section 3.6.2.2. The beam signal falls off as the beam is progressively blocked by a razor blade, mounted 45° to the axis of the beam. The beam profile is obtained by plotting the differentiated signal over Δd, the stepping increment of the razor blade, against the position of the razor blade. Figure 4.1.1 shows beam profiles measured for CH_3F at hexapole potentials of 0 V and ±5 kV with an exit aperture of 2 mm diameter. The focusing effect of the hexapole filter is clearly illustrated by the increase of beam intensity when the hexapole is energised.

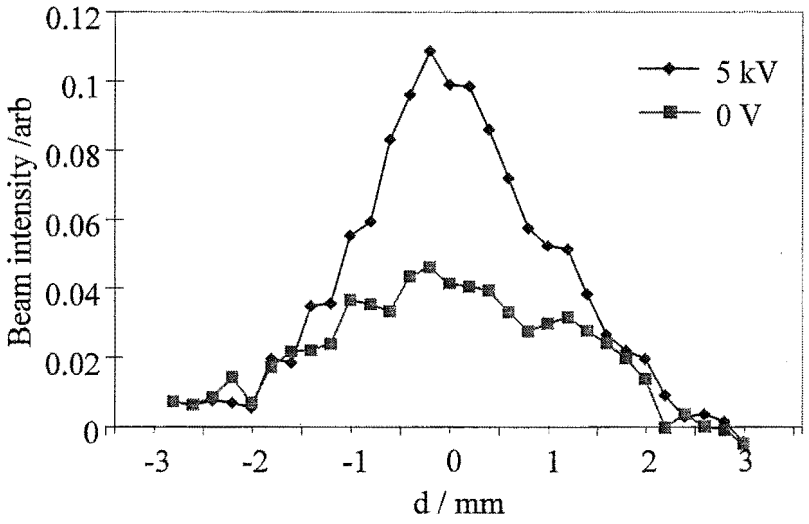

Figure 4.1.1 Beam profiles measured for a beam of CH_3F with hexapole potentials of 0 and ±5 kV.

4.1.2 Determination of beam temperature and velocity

For supersonic molecular beams, the temperature and velocity of the beam are dependent on the mass of the beam molecule, the position of the skimmer, and the stagnation pressure of the beam source, as discussed in Section 2.1. The position of the skimmer and the stagnation pressure are optimised, within the physical limitations of the experimental apparatus, in order to obtain a beam with maximum intensity and velocity, and minimum temperature. Therefore, the experimental beam temperature and velocity often fall short of the calculated value for the ideal case, see Section 2.1.2.3. Nevertheless, these calculations give good estimations of the experimental beam velocities for different neat and seeded beams. Accurate values for beam temperature and velocity must be determined experimentally.

4.1.2.1 Beam temperature

The temperature of the beam can be determined indirectly from the velocity distribution. The traditional method for measuring the beam velocity distribution uses a rotating disk with a narrow slit to extract a short pulse of the beam. The distribution, $f(t)$, of the flight time is measured and converted to a velocity distribution, $f(v) = f(l/t)$, where l is the path length from the rotating disk to the detector. In this experimental arrangement, the

rotating disk has been cut to modulate the beam with a mark-space-ratio of one. The trace of the falling edge of the time-of-flight (TOF) signal recorded by a fast digital storage oscilloscope contains the required velocity information. A computer program was developed by former colleague Dr C. Vallance using the Monte Carlo method to simulate the falling edge of the TOF signal, based on the velocity distributions described in Section 2.1.2.

$$f(v)dv = Av^2 e^{-m(v-u)^2/2k_B T_{//}}\, dv$$

where m is the mass of the molecular beam gas, u is the mean flow velocity of the beam, k_B is Boltzmann's constant, $T_{//}$ is the parallel translational temperature of the beam and A is a normalisation constant. Details of the Monte Carlo simulation program were discussed in the Ph.D. thesis of Dr C. Vallance. [Vallance 1999a] The beam velocity and temperature are estimated by fitting the simulated decay curve to the experimental decay curve. This proved to be an effective method of estimating the temperature of the molecular beam. The effect of the parallel translational temperature on the velocity distribution and signal decay of modulated beams are shown in Figure 4.1.2 for a mean flow velocity of 600 m s^{-1} for CH_3F.

Measurements of beam velocity profiles were made for neat continuous beams of CH_3F, CH_3Cl, CH_3Br, CF_3H, and $CHCl_3$ at beam stagnation pressures of around 100 – 150 Torr. Examples of the experimental and simulated decay curves are shown in Figure 4.1.3. The best-fitted values that are determined for the temperatures of these beams are 35K, 40K, 35K, 35K, and 35K, respectively. The beam temperatures and velocities determined for these molecules are summarised with values obtained using different methods and conditions in Table 4.1.1. Case 1 represents results using the method described above. Case 2 represents results measured from the arrival time distribution of a pulsed beam in a single hexapole experiment with a beam stagnation pressure of around 1000 Torr. The delay time for the beam pulse is determined from the maximum of the signal trace recorded by a fast oscilloscope. The beam temperatures were determined by fitting the experimental velocity distribution with calculated velocity distributions. These beam velocities are corrected relative to the velocity of an Ar beam, 552 m s^{-1}, taken from previously published results from this research group. [Cameron 1991] Case 3 represents results from fitting the calculated hexapole transmission curves to the experimental transmission curves. (See detailed discussion in Section 4.1.3.2.) The beam temperatures

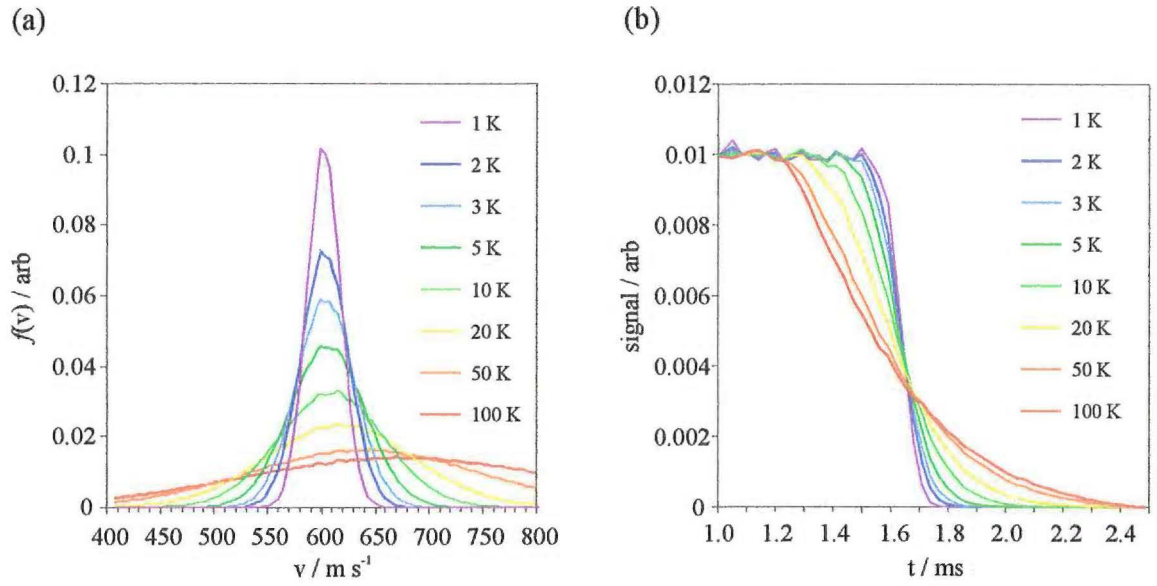

Figure 4.1.2. Effect of $T_{//}$ calculated for a supersonic beam of CH_3F with a mean flow velocity of 600 m s^{-1} on (a) the random velocity distribution and (b) the detected decay signal.

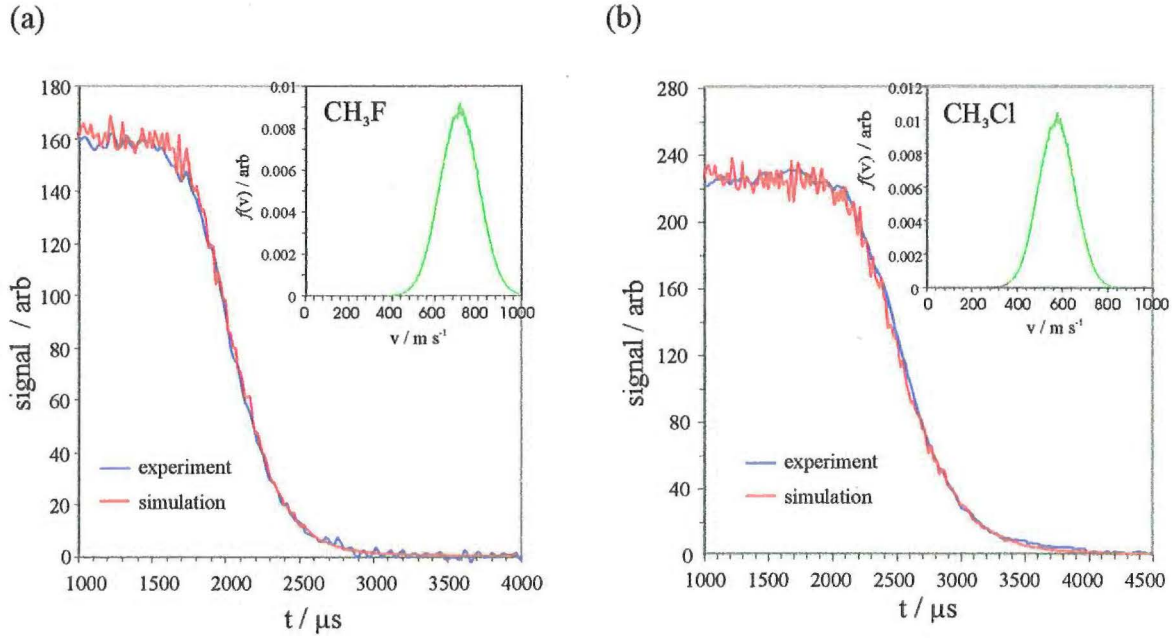

Figure 4.1.3 Experimental and simulated time of flight profiles and velocity distributions extracted from the decay curves for supersonic molecular beams of (a) CH_3F and (b) CH_3Cl.

were estimated assuming a beam temperature for Ar of 1.4 K. [Cameron 1994] Case 4 represents the previously published results using this experimental apparatus. [Cameron 1993 and 1994] In a supersonic expansion, the higher the beam stagnation pressure, the greater the number of collisions (as the particles exit the nozzle). Consequently, lower beam temperatures and higher beam flow velocities are achieved using higher beam stagnation pressures. The beam temperatures and velocities are not directly comparable between the cases in Table 4.1.1. This is due to a combination of factors associated with differences in the conditions for beam formations, such as, the nozzle type, the stagnation pressure of the beam source, and the nozzle-skimmer distance. The results in Case 4 are the most reliable of the four cases.

Table 4.1.1 Beam temperatures and velocities determined from the following methods. Case 1: Signal decay curves from a rotating disk and fitted to a Monte Carlo simulation. Case2: Arrival time distribution measured in a single hexapole experiment. Case 3: Determined from hexapole transmission curves measured in a single hexapole experiment. Case 4: Results from [Cameron 1993 and 1994] deconvoluted from time of flight measurements.

Beam species	Beam temperature / K and velocity / m s^{-1}			
	Case 1	Case2	Case 3	Case 4
CH_3F	35 - 690	14 - 675	10 - 686	-
CH_3Cl	40 - 553	18 - 579	10 - 575	29 – 543
CH_3Br	35 - 423	-	10 - 358	-
CF_3H	35 - 482	13 - 502	-	-
CCl_3H	35 - 410	-	-	21.4 – 397

4.1.2.2 Beam velocity

The mean flow velocity of the beam can be determined using a variety of methods. Some of the methods are described in the previous section; deconvolution of the falling edge of a chopped beam; the arrival time distribution from a pulsed beam source; fitting of the calculated hexapole transmission curves to the experimental results (discussed in detail in Section 4.1.3.2). Another method has been developed using a lock-in-amplifier with the Molecular Beam Electric Resonance spectrometer.

In the MBER experimental arrangement, the C-cell was positioned at a distance of 0.92 m from the mass spectrometer detector. The RF was modulated (amplitude modulation) in order that the small depletion in the signal due to resonance transitions could be detected using a phase sensitive (lock-in) amplifier. Due to the flight time of the beam molecule travelling from the resonance region to the detector, either the phase shift or the modulating frequency required adjustment in order to gain the maximum difference signal. Since the distance from the resonance region to the detector, D, was constant, then for a beam velocity of v, a linear relationship is found between the phase shift, PS, and the modulating frequency, MF, to be,

$$PS = -360\frac{D}{nv}MF + 360$$

where PS lies in the range 0° to 360°, and n is a positive integer. The most probable beam velocity can be determined from the above relationship when the phase shift or the modulating frequency is optimised for the beam. The accuracy of the beam velocities determined using this method is subjected to the experimental uncertainties. A better estimation of beam velocities could be determined when the modulating frequency was optimised while keeping the phase shift at zero.

4.1.3 Single hexapole experiment

The experimental arrangement is described in Section 3.3.2. Symmetric top molecules, such as the methyl halides, are quantised in the presence of an external electric field due to their permanent dipole moments, that is, the Stark effect. The three quantum numbers, J, K, and M_J describe the motion of such molecules in an electric field. J represents the total rotational angular momentum, K the projection of the total angular momentum vector J on the molecular axis, and M_J its projection on the laboratory axis defined by the electric field vector. (See details in Section 2.2) Rotational states can be selected in a beam of such molecules using a hexapole inhomogeneous electric filter. (See details in Section 2.3) Upper Stark states, where $KM_J < 0$, with their dipole aligned against the electric field, undergo sinusoidal trajectories in a hexapole inhomogeneous electric field. Thus the upper Stark states are focused toward the axis of the beam. The lower Stark states, $KM_J > 0$, with their dipole aligned with the electric field move toward high field (the hexapole rods) and are lost from the beam. The $KM_J = 0$ states are not affected by

the electric fields and follow linear trajectories defined by the nozzle and the skimmers. Upon exiting the hexapole electric field, the population inversion of the focused upper Stark states is maintained by uniform electric fields. As the beam passes adiabatically into a region of uniform electric field, the molecular dipole aligns with the new field and spatial orientation is achieved. This technique has been employed to study the effect of orientation on reactivity for symmetric top molecules. [Aitken 1994 and Brooks 1996]

4.1.3.1 Experimental hexapole transmission curves

Upper Stark-state molecules in a beam of symmetric top molecules are focused at the exit of the hexapole filter. Hexapole transmission curves show the focused beam signal (beam intensity) as a function of the hexapole voltage. The shapes of the hexapole transmission curves are dependent on the rotational state focusing characteristics and the experimental conditions. Table 4.1.2 lists some experimental parameters for the single hexapole experiments. Variable experimental parameters include the hexapole voltage, the exit aperture radius, and the beam gas mixture composition and its stagnation pressure, which alters the temperature and the velocity of the beam.

Hexapole transmission curves were measured for neat and seeded beams of symmetric top molecules. Hexapole transmission curves for beams of CH_3Cl, 5% CH_3Cl seeded in Ar, Kr, and Xe, 5% CH_3F seeded in Ar and Kr, CF_3H, and 5% CF_3H seeded in Kr, have been shown in the Ph.D. thesis of a former colleague, Dr S.A. Harris. [Harris 1997] Hexapole transmission curves for beams of 5% CH_3Br seeded in Kr, 5% CH_3F seeded in N_2, and 10% t-$C(CH_3)_3Br$ seeded in Kr, are shown in Figure 4.1.4.

Table 4.1.2 Constant experimental parameters for the single hexapole experiments.

Description	Dimension
Nozzle to 2nd skimmer distance	18.5 mm
2nd skimmer orifice radius	0.75 mm
Nozzle to hexapole distance	225 mm
Hexapole inscribed radius	5.88 mm
Hexapole filter length	833 mm

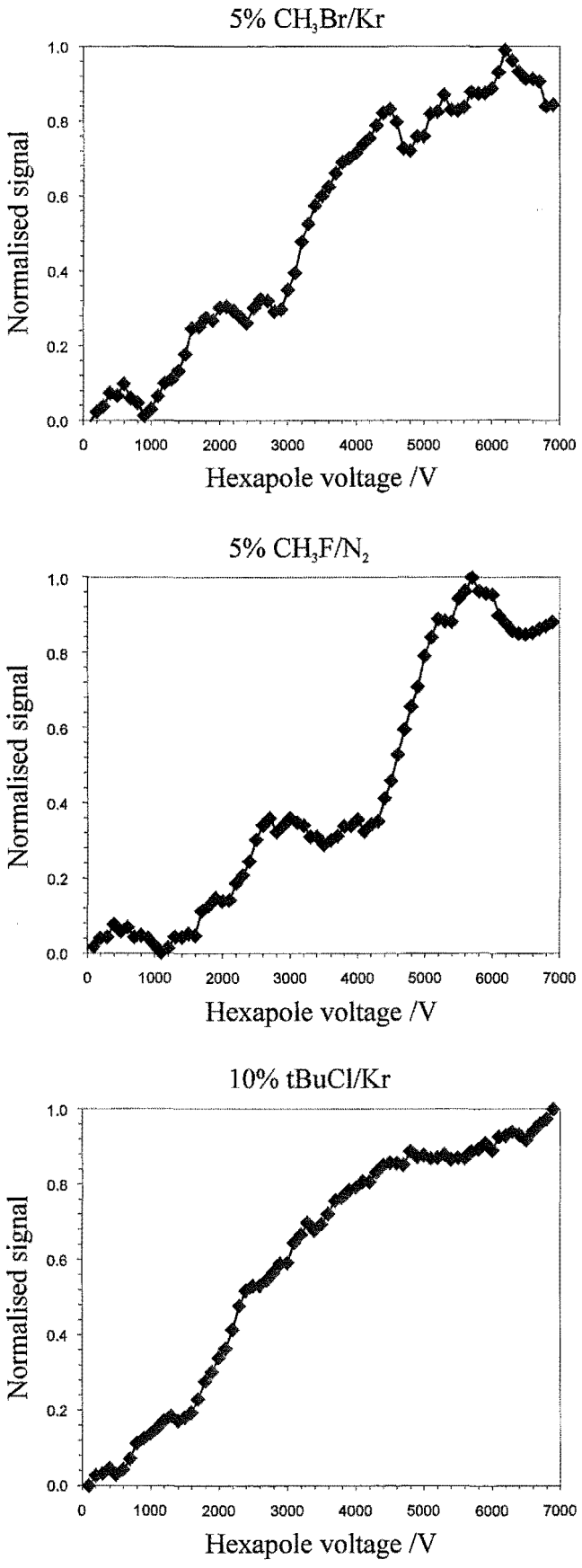

Figure 4.1.4 Experimental hexapole transmission curves.

4.1.3.2 Calculated hexapole transmission curves

Transmission curves are plots of intensities of molecules focused at the hexapole exit measured as a function of the hexapole voltage. Features in the transmission curves are due to the effect of electric field strength on the trajectories of individual rotational states as they pass through the hexapole filters. Molecules in $|JKM_J\rangle$ state are focused to the exit at their rotational state dependent hexapole focusing voltage, as described in Section 2.3.3. The identities of the quantum states corresponding to the features in the experimental transmission curves are verified by comparison with the calculated hexapole transmission curves.

The trajectories of symmetric top molecules in a hexapole filter are dependent upon the angle, θ, between the molecular dipole and the hexapole electric field direction, which can be described in terms of rotational quantum numbers J, K, and M_J from the values of $\cos\theta$. (See Appendix B.1 for details)

$$\langle\cos\theta\rangle = \frac{KM_J}{J(J+1)} = \rho \tag{4.1.1}$$

Beam molecules in lower Stark states are filtered out while those in upper Stark states are focused by the hexapole electric field. Transmission of upper Stark-state molecules in our experimental arrangements can be calculated using the equations for the state dependent trajectories of symmetric top molecules in a hexapole electric field, as described in Section 2.3. Based on Equation (2.3.35), the exit-focusing hexapole voltage for $|JKM_J\rangle$ state is given by

$$U_{JKM_J} = \frac{\pi^2 r_0^{\,2}}{6l_2^{\,2}} \frac{mv^2}{\mu} \frac{J(J+1)}{M_J K} \tag{4.1.2}$$

where r_0 and l_2 are the inscribed radius and the length of the hexapole filter, m, v, μ, are the mass, velocity, and the dipole moment of the beam molecule, respectively.

Under ideal condition (using very long hyperbolic hexapole rods), a well resolved transmission curve should show sharp peaks at the hexapole exit-focusing voltages of the corresponding $|JKM_J\rangle$ states. However, the resolution of the experimental transmission curves is restricted to the limits of our experimental apparatus (using relatively short

circular hexapole rods). The velocity spread of the beam and the finite entrance and exit conditions of the hexapole also reduce the resolution of the filter. The resolution is further reduced by the distribution in θ; the angle between the molecular dipole and the electric field, see Section 2.2. The value of θ determined in Equation (4.1.1) is an average value and is state dependent.

A computer program, transnew.exe, see Appendix C.2, has been written to simulate experimental transmission curves, for individual and/or a sum of individual focusing states transmissions. Professor P.R. Brooks originally developed this program (written in Fortran) and it was re-written in QuickBasic by Dr D.A. Blunt.

The transmission curve calculation is based on the determination of transmission probability (see Section 2.3.1.4) by solving Equation (2.3.30) at each hexapole voltage, beam velocity, and molecular orientation. The velocity distribution, $f(v)$, is described by Equation (2.1.16), and Simpson's rule is applied to the distribution for normalisation, thus the array of transmission probability can be reduced by integrating over the velocity distribution.

$$A(U_o, \rho) = \int_0^\infty A(U_o, v, \rho) f(v) dv \tag{4.1.3}$$

For an individual $|JKM_J\rangle$ state, the transmission probability is determined by finding the expected value of ρ and multiplying the appropriate probabilities $A(U_o, \rho)$ by the partition function, f_{JK}. The partition function is the fraction of molecules in rotational state $|JK\rangle$, which is described in Equation (2.3.33). The total transmission curve is found by the sum of all possible $|JKM_J\rangle$ states.

$$T(U_o) = \sum_{JKM_J} f_{JK} \int_0^\infty A(U_o, v, \rho) f(v) dv \tag{4.1.4}$$

Nearly all the necessary input parameters for the transmission curve calculations are known from the physical dimensions of the apparatus, which are partly listed in Table 4.1.2, and molecular properties, such as molecular dipole moments and rotational constants, which are listed in Table A.3 of Appendix A. Unknown parameters, such as

the beam velocity and translational and rotational temperatures of a given beam gas mixture, are determined experimentally or estimated to provide a good starting point for fitting the calculated results to the experimental data. Examples of calculated transmission curves for neat beams of CH_3Cl are shown in Figure 4.1.5.

The effect of beam temperature and the hexapole exit aperture on the transmission curves are shown in Figure 4.1.5. The top graph is calculated for a beam of CH_3Cl with a exit aperture of 2 mm in diameter and the bottom graph is calculated for a beam of CH_3Cl at a beam temperature of 5 K. Therefore, the dark green curves in both graphs are under identical conditions, which are the beam temperature of 5 K and exit aperture of 2 mm in diameter. The trade off between beam intensity and the resolution of the hexapole filter can be clearly seen in these graphs. The resolution of the hexapole filter can be drastically improved by reducing the beam temperature, and hence the beam velocity distribution. The lowering of the beam temperature can be achieved using seeded beams, as described in Section 2.1.3. For individual quantum state transmission curves, the variation in the beam temperature affects only the width of the "peaks", whereas the position of the "peak" is dependent on the mean flow velocity of the beam. Calculated transmission curves for an exit aperture of 2 mm diameter showed a reasonable intensity without losing too much of the resolution. Experimental measurements gave 2 mm diameter as the optimum exit aperture size for this work.

The mean flow velocity of a beam can be determined from the arrival time distribution measured using a pulsed source. Beam velocities and temperatures have been measured for inert gases and diatomic molecules using this experimental apparatus. [Cameron 1991] These results have been used to estimate the beam velocities and temperatures of seeded beams. Using these estimated conditions for the transmission curve calculations, the beam velocities and temperatures can be varied systematically, until the best match could be found between the calculated and the experimental transmission curves. The resulting beam velocities for the best fit and beam velocities measured or estimated using other methods are listed in Table 4.1.2 in Section 4.1.2.1. The differences between the values of the beam velocities are dependent on the experimental conditions and the accuracy of the simulated transmission curves as well as other calculations.

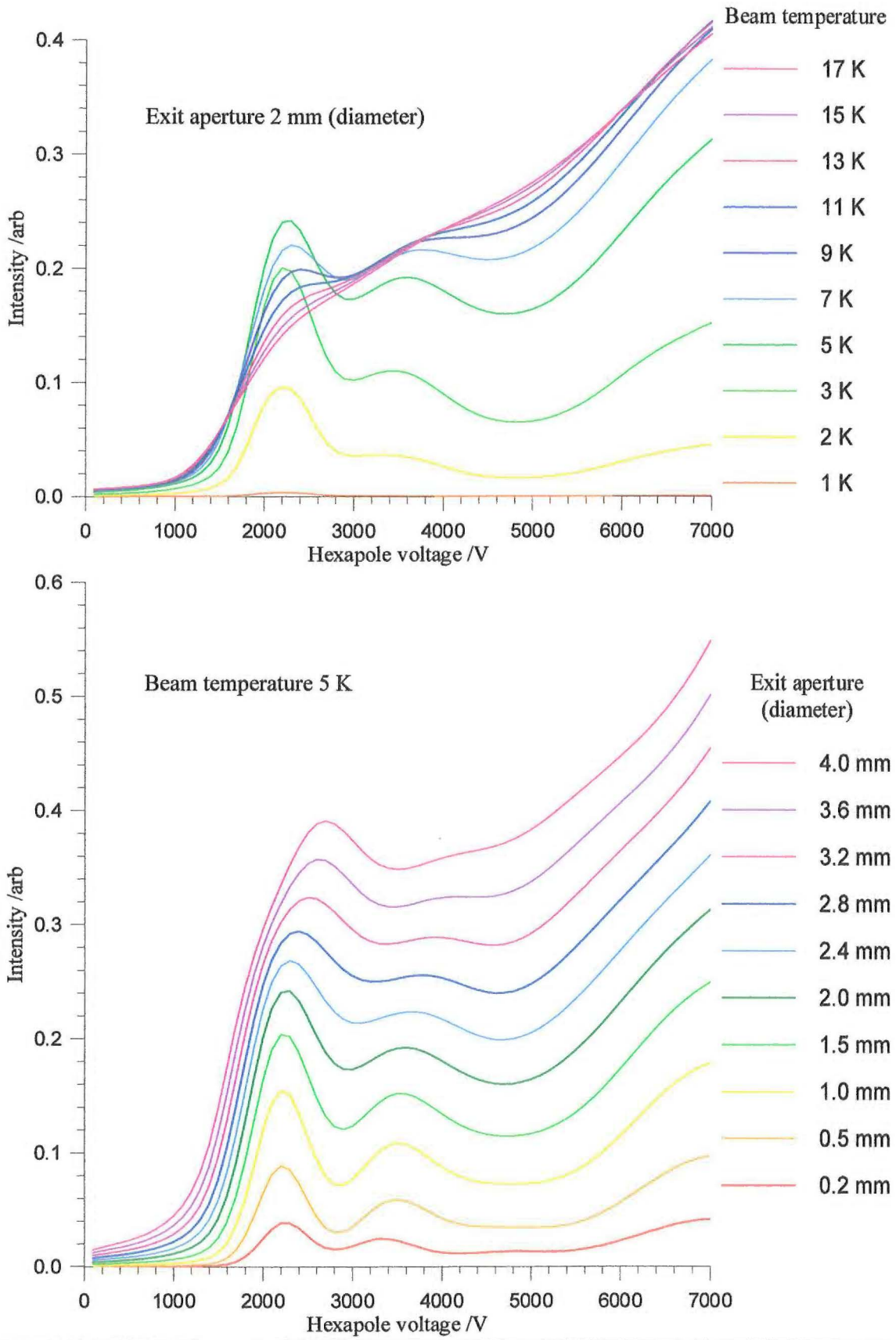

Figure 4.1.5 Calculated hexapole transmission curves for CH_3Cl.

4.1.4 Tandem hexapole experiment

The experimental arrangement for the tandem hexapole experiment is described in Section 3.3.3. The C-field is located between the two hexapole fields, A and B. The effect of the C-field on the beam of symmetric top molecules passing through the hexapole assemblies was investigated. The C-cell was designed for MBER. It was also used to study the lifetime for the scrambling of oriented molecules in a field free region.

4.1.4.1 Scrambling of the oriented molecules

In a beam of symmetric top molecules, the molecules in upper Stark states are focused by the first hexapole field, while those in the lower Stark states are lost from the beam. As the molecules enter the C-field region they are transmitted adiabatically and are spatially oriented with respect to the field direction. At the exit of the C-field, the molecules continue to be focused by the second hexapole field. However, if the beam enters a field free region (that is the C-field at ground potential), no external electric field vector is present, and the quantum number M_J becomes degenerate. The population inversion of upper Stark states acquired in the first hexapole field, A field, is then lost. As a result, molecules are said to be scrambled, they would then exhibit a randomised quantum state distribution as they enter the second hexapole field or B field.

The effect of spatial scrambling on the total beam signal was investigated by measuring hexapole transmission curves with and without an orienting field in the C-field region. Hexapole transmission curves have been measured with the C-field at ground potential and at a field strength of 20 V cm^{-1} for beams of four symmetric top molecules, CH_3F, CH_3Cl, CH_3Br, and CH_3I, as shown in Figure 4.1.6. The hexapole enhancement, which is the ratio of the beam signal with the hexapole field on to that with the hexapole field off, is lower when the C-field is switched off. At a hexapole potential of 5 kV, the hexapole enhancement is reduced by around 40% when the C-field potential is zero. This reduction in signal is due to the redistribution of the rotational states and has differential contributions from each rotational state present in the beam.

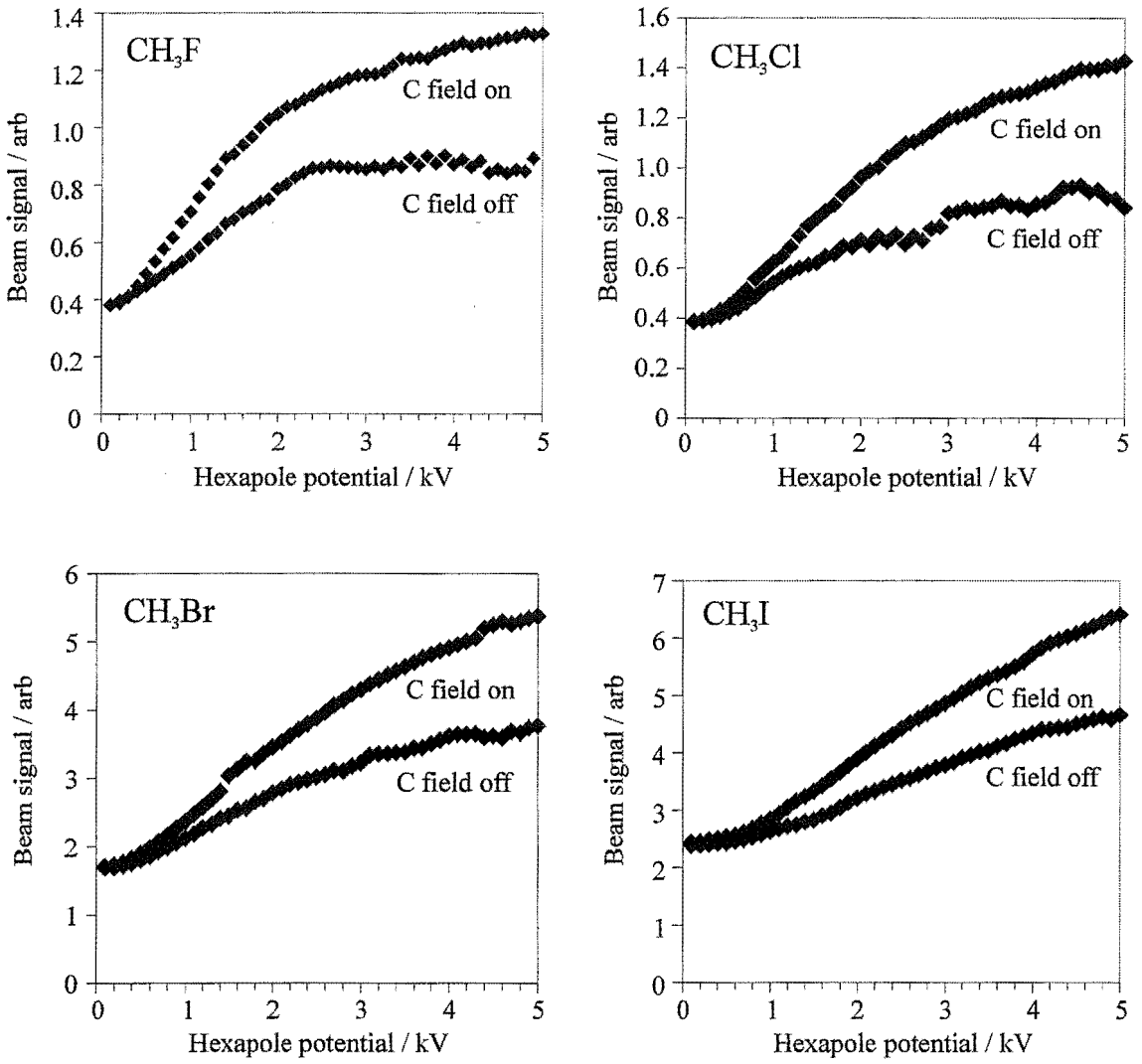

Figure 4.1.6 Hexapole transmission curves with zero and non-zero C-fields for methyl halides.

Table 4.1.3. Ratio of the beam enhancement with the C-field off to C-field on at a hexapole potential of 5000 V.

Beam	Enhancement ratio	
	Expt	Calc*
CH_3F	0.67	0.74
CH_3Cl	0.62	0.74
CH_3Br	0.69	0.69
CH_3I	0.73	0.68

*Calculated for beam rotational and translational temperatures of 30 K.

Assuming that after spatial scrambling has occurred in the C-field region, the molecules in a given $|JK\rangle$ state entering the second hexapole field are quantised in the strong inhomogeneous electric field to give equal populations of the possible M_J states. In such case, it may be expected that the reduction in signal for a given state should be roughly equal to $J/(2J+1)$, the fraction of beam molecules in the non-focusing lower Stark states. Monte Carlo simulations of molecular trajectories through the tandem hexapole arrangement were carried out to test this idea. The hexapole enhancements for the two cases, the C-field at non-zero and zero potential, were determined from the outcomes of 10,000 simulated trajectories through the hexapole filters. If the C-field potential is non-zero, molecules remain in the same rotational state for the entire trajectory calculation. If the C-field potential is zero, molecules are randomly assigned to a new M_J state in the second hexapole field. The simulations average the number of successful transmissions for the two cases over the rotational state distribution calculated using statistical thermodynamics. The resulting enhancement ratios for a hexapole potential of 5 kV for the two cases are compared in Table 4.1.3. The experimental and the calculated results are considered to be in good accord.

Bernstein and co-workers studied spatial orientation in a hexapole filter for a series of symmetric top molecules using the method of polarised laser photo-fragmentation. [Bernstein 1986-9, Gandhi 1987, 1988, and 1990] Results from those studies are compared with results from this work in the following sections.

4.1.4.2 Hyperfine coupling

The scrambling of the oriented molecules in a field free region could occur through the hyperfine interaction, which is the interaction between the nuclei and the dipole of the molecule. De-orientation by nuclear-spin coupling occurs when the electric field becomes very weak as the molecules enter a field free region. [Kaesdorf 1985] The angular momentum vector, J, is coupled to the total nuclear spin, I. The new total angular momentum is then given by the quantum number F, where $F = J + I, J + I - 1, \ldots, |J - I|$. The effect of hyperfine coupling on spatial orientation, which depends on the first order Stark effect, is dependent on the relative magnitudes of the Stark and hyperfine splitting.

The effect of hyperfine coupling is usually discussed under three types of conditions: weak field, strong field, and intermediate field. [Townes 1955]

In the weak field case, the Stark energy is considerably less than the hyperfine energy, and the hyperfine energy is almost undisturbed. The quantum numbers I, J, F, and M_F are required to describe the rotational state of the molecules. Molecules in the beam assume an ensemble of $|FJKIM_F\rangle$ states. The dipole of the molecule, μ, now lies along the axis of the molecule or angular momentum, K, which precesses around the total rotational angular momentum, J, in turn, J precesses around F, and F precesses around the direction of the electric field vector, E, represented by M_F. M_J is no longer a good quantum number since it is not a constant of the molecular motion. The Stark energy is dependent upon the angle, θ, between the dipole moment, μ, and the electric field vector, E. Averaged over time, the angle, θ, is given by

$$\cos\theta = \cos\theta_{KJ}\cos\theta_{JF}\cos\theta_{FE} \tag{4.1.1}$$

where

$$\begin{aligned} \cos\theta_{KJ} &= \frac{K}{J} \\ \cos\theta_{JF} &= \frac{J^2 + F^2 - I^2}{2JF} \\ \cos\theta_{FE} &= \frac{M_F}{F} \end{aligned} \tag{4.1.2}$$

The Stark energy is therefore,

$$\Delta W = -\frac{\mu K M_F (J^2 + F^2 - I^2) E}{2J^2F^2}$$

giving

$$\Delta W = -\frac{\mu K[J(J+1) + F(F+1) - I(I+1)]M_F E}{2J(J+1)F(F+1)} \tag{4.1.3}$$

This represents the case where the symmetric top molecules pass from the hexapole field into a field free region, hyperfine coupling occurs and the quantum states are redistributed. Gandhi *et al* demonstrated partial disorientation of CH_3I due to hyperfine coupling in a weak electric field in their study, that is, asymmetry of the polarised-laser-induced photo-fragmentation of oriented CH_3I molecules. [Gandhi 1987]

In the strong electric field case, the hyperfine energy becomes insignificant. The precession of J around E become so fast (MHz) compared to the hyperfine precessional frequency (kHz) that J and I are said to be de-coupled and the molecules assume $|JKM_J\rangle$ states as if there is no hyperfine coupling. This is the case as the molecules enter into the second hexapole field.

In the intermediate field case, the Stark energy and the hyperfine energies are comparable in magnitude. The solutions for the energy levels are a lot more complicated and are not considered in this discussion.

4.1.4.3 Minimum DC field requirement

The minimum field strength required to orient a beam of symmetric top molecules can be obtained directly by monitoring the beam signal as a function of the potential applied to the C-field region. As the field strength is increased, the beam signal increases. As the field is established in the C-cell, the upper Stark states focused by the first hexapole undergo adiabatic transitions into the C-field (remain oriented in the beam) and continue to be focused by the second hexapole field. Since the Stark energy is rotational state dependent, the minimum orienting field strength is also rotational state dependent. For a fully oriented beam, the minimum field strength is determined when no further increase in signal is observed with increasing field strength. Figure 4.1.7 shows the molecular beam signal measured as a function of the electric field strength with the hexapole voltages fixed at ±5000 V for beams of methyl halides. Measurements made for beams of CH_3F, CH_3Cl, CH_3Br, and CH_3I show that the beams are essentially fully oriented at a field strength of around 3 V cm^{-1}. The difference in the beam velocities and temperatures of the four symmetric top molecules studied in Figure 4.1.7 should account for the difference in the resulting curves.

There has been some confusion in the literature over the minimum field strength required in order to orient a quantum state selected beam of symmetric top molecules with estimations ranging from several hundred to less than 1 V cm^{-1}. Brooks *et al* determined the minimum orienting field requirement to be $\gtrsim$10 V cm^{-1} in an experimental arrangement similar to that used in this work. [Brooks 1969] The major difference

between their experimental arrangement and ours is the geometry of the hexapole filters and the C-field region. Brooks used two 8½" long hexapole filters, constructed of six 3/8" stainless steel circular rods with an inscribed radius of 9/32"; the hexapole regions were 235 mm each and the C-field region was 25 mm. This experimental arrangement has been modelled in this work using SIMION6.0 to simulate the resulting electric field, which showed that the Brooks arrangement suffered from significant field penetration from the hexapole rods into the C-field region. [Simion6.0 1995] The resulting electric field in the C-field region would have been highly non-uniform, even when the C-field was held at ground potential. The orientation of symmetric top molecules was therefore only observed when the applied field exceeded the penetrating field from the hexapole rods, resulting in an increased orienting field requirement. The present experimental arrangement included a Faraday cage to minimise the effects of field penetration from the hexapole rods, and the length of the C-field region is considerably longer than that used in Brooks' arrangement. The resulting electric field has been simulated by SIMION6.0, which showed minimal field penetration from the hexapole rods around the edge of the C-field region. This experimental arrangement should give a more reliable result in measuring the minimum orienting field strength.

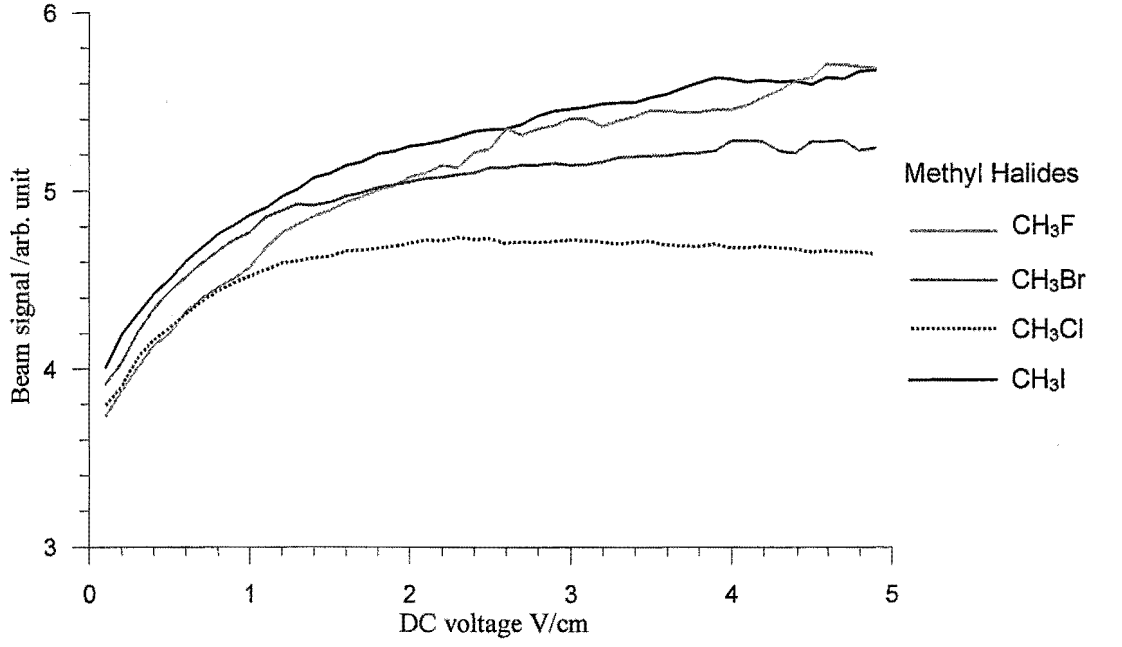

Figure 4.1.7 Beam signal measured at C-field strength 0 – 5 V cm^{-1} for beams of methyl halides.

Kaesdorf *et al* used a hexapole filter to study the angular-resolved photoelectron spectroscopy of free oriented CH_3I molecules. [Kaesdorf 1985] A guiding field, in which the electric field strength dropped gradually from 10 to 0.3 V cm^{-1}, was used to minimise the de-orientation effect. Since they did observe a small orientation effect they assumed that the molecules had remained orientated in the uniform field. It transpires from this work, see below, that the observation of only small orientation effect was more likely the result of randomisation in the weak field. The minimum orienting field strength of 0.3 V cm^{-1} is lower than our experimental observations. However, the conditions specific to their experiment are for a rotational temperature of about 200 K and the most probable value of J was about 16, where the effect of nuclear spin was reduced, i.e., $M_F \sim M_J$. According to the results in Figure 4.1.7, only a small fraction of molecules would have remained oriented at 0.3 V cm^{-1} contributing to the small effect of orientation reported by Kaesdorf *et al.*

Gandhi and Bernstein investigated the effect of the uniform orienting field on state selected CH_3I using the method of polarised laser-induced photo-fragmentation and a 3 m hexapole with hyperbolic rods. [Gandhi 1988 and 1990] Measurements were made of the degree of orientation of CH_3I for resolved rotational state selected beams with $|JKM_J\rangle$ = $|111\rangle$ and $|222\rangle$ using homogeneous orienting electric fields from 0 to 1 kV cm^{-1}. They found that the original degree of orientation of the symmetric top molecules could be recovered after they pass through a homogeneous weak-field region provided that the field strength exceeded some state dependent minimum values, sufficient to maintain an orientation axis. The minimum field strength required for the $|111\rangle$ state of CH_3I was found to be 0.32 V cm^{-1} and for the $|222\rangle$ state 0.24 V cm^{-1}.

Symmetric top molecules orient through an interaction between the molecular dipole and the electric field vector, that is, the Stark effect. The interaction energy is $\mu E\langle\cos\theta\rangle$, where θ is the angle between the two vectors and $\langle\cos\theta\rangle = M_J K\,[J(J+1)]^{-1}$. The orientation should occur when the interaction energy reaches some threshold value W_{th}, so that the required minimum orienting field for a given $|JKM_J\rangle$ state should be given by

$$E_{JKM_J} = \frac{W_{th}}{\mu}\frac{J(J+1)}{M_J K} \qquad (4.1.4)$$

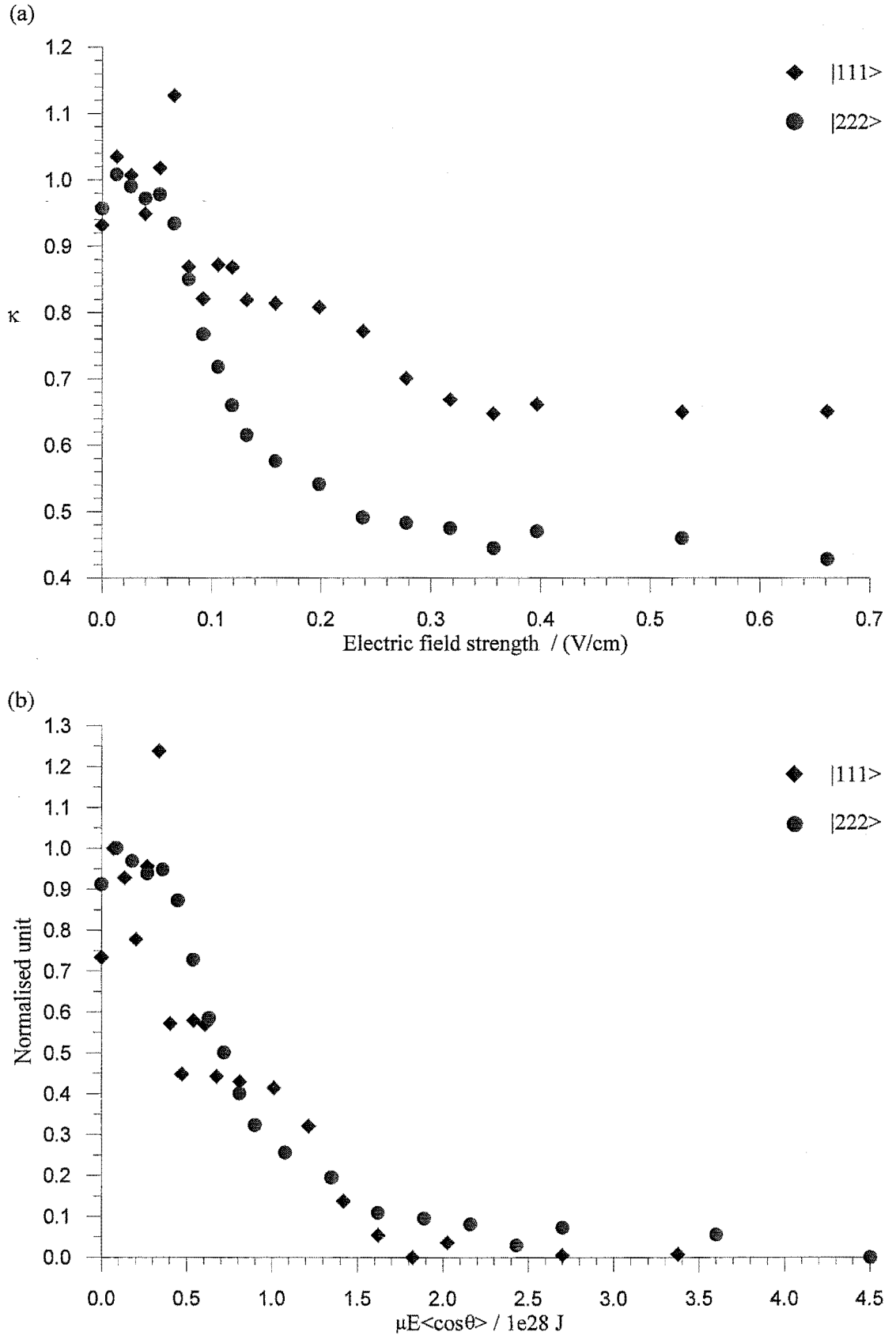

Figure 4.1.8 Ratio of orientation data taken from [Gandhi 1990] (a) plotted against electric field strength, (b) plotted against interaction energy with normalised units.

Accordingly, plotting the beam orientation data from single state experiments against $\mu E\langle\cos\theta\rangle$, rather than E used by Gandhi *et al*, should give similar curves for every rotational state. [Gandhi 1990] A plot is shown in Figure 4.1.8, (a) as a function of the electric field strength and (b) as a function of $\mu E\langle\cos\theta\rangle$. The agreement between the two sets of data for $|111\rangle$ and $|222\rangle$ states is clearly shown in Figure 4.1.8 (b). The value of W_{th} determined from Gandhi and Bernstein's data has been used to obtain an average value of E_{JKM_J} for CH_3I over the range of states up to $J = 7$, which cover the range of rotational states estimated for the beam conditions in this experimental arrangement. Complete orientation is predicted at field strength of 3.9 V cm^{-1}, which is in good agreement with our experimental result, as shown in Figure 4.1.7. Using the same method to estimate the value of E_{JKM_J} for the experimental conditions of Kaesdorf *et al*, where the most probable value of J was about 16, gives $E_{JKM_J} \gtrsim 10$ V cm^{-1}. Therefore, at the orientation field strength of 0.3 V cm^{-1} used in their work, only a small fraction of total rotational states would remain oriented in their experiment.

4.1.4.4 Estimation of de-orientation lifetime

A field at ground potential has been used previously as a scrambling field for oriented molecules. [Brook 1969] It is important to consider the mean lifetime for the spatial scrambling or de-orientation of oriented molecules in experiments, where the orienting electric field has to be switched off before collisions occur, for example, where charged particles are formed as a result of an electron or ion beam crossed with a beam of oriented molecules. Since the scrambling of the oriented molecules in a field free region most likely occurs through the hyperfine interaction, it might be expected that the lifetime for scrambling should be of the order of the hyperfine precessional period. The hyperfine frequencies corresponding to the methyl halides studied here are of the order of 6 kHz. [Bulthuis 1991] The lifetime of scrambling through the hyperfine interaction might then be predicted to be around 150 μs.

The initial attempt to determine the lifetime for the scrambling of the oriented molecules was made by comparing the resulted depletion in hexapole enhancement, described in Section 4.1.4.1, as a function of the beam velocities. Since the length of the C-field was

constant, if the flight time through the C-field was less than the average de-orientation lifetime for the beam, depletion in the beam signal due to the de-orientation at the C-field would be detected. The beam velocities were varied using the method of seeding. Experiments were conducted for beam mixtures of neat CH_3F, 80% CH_3F seeded in He, 60% CH_3F seeded in He, 40% CH_3F seeded in He, 20% CH_3F seeded in He, 10% CH_3F seeded in He, 10% CH_3F seeded in Ar, 10% CH_3F seeded in Kr, and 10% CH_3F seeded in H_2. The resulting depletions in hexapole enhancements are all around 33% except for 10% CH_3F seeded in H_2, which is slightly lower than the rest. These results indicated that the scrambling lifetime might be shorter than or around the detectable limits using this method. The highest beam velocity was 1583 m s^{-1} for a beam of 10% CH_3F seeded in H_2, and the flight time for these molecules to pass through the field free region is 0.000101 s. Therefore, the average lifetime for the scrambling effect should be less than or around 100μs neglecting the effects of the velocity distribution. The uncertainties associated with this method and the lack of experimental results for beams with higher velocities severely restricted the reliability of the conclusions.

In the second attempt, a chopper was used to regulate the beam. The fall-off in the signal trace was recorded by a fast oscilloscope and then simulated using a computer program. When the C-field was maintained as an orienting field, the trace of the falling edge recorded by the fast oscilloscope should reflect the velocity distribution of the beam. Therefore the temperature and velocity of the beam could be determined. (See Section 4.1.2.1.) The same trace recorded when the C-field was at ground potential should have been perturbed by the scrambling of the oriented molecules, enabling an estimation for the lifetime to be determined. However, the difference in the traces recorded for a range of C-field potentials and hexapole voltages were indistinguishable due to the spread in the beam velocity distribution. The broad velocity distribution resulted from the position of the chopper being approximately 2 metres away from the detector, and the frequency of the chopper would also influence the resulting shape of the trace.

Several attempts to improve the resolution of the measured velocity distribution were unsuccessful. The beam was pulsed using a piezo-electric nozzle to eliminate the influence due to the chopper frequency. When the C-field was switched off as the beam pulse was passing through the C-field region, a fast oscilloscope could record a fall-off of

the beam signal due to the deorientation effect. The influence of the beam velocity distribution could be subtracted by a comparison between the fall-off edge and the time-of-flight signal of the beam pulse. However, the width of the beam pulse was not long enough to show a more defined falling edge of the beam signal on the oscilloscope. The beam pulse width was later increased by altering the control unit, however due to the nature of the piezo-electric nozzle, it does not produce a beam pulse with a desirable pulse shape for measurements using this approach.

The final attempt, which was the best method used within the limitations of the current experimental arrangement, was to pulse the C-cell to ground potential using a pulse generator. By varying the pulse width, the signal depletion due to scrambling at ground potential could be measured as a function of time by recording the trace with a fast oscilloscope, as shown in Figure 4.1.9. Trace 1 is the time-of-flight signal detected by the mass spectrometer. It is delayed with respect to the field switching pulse, shown as Trace 2, by the flight time of the beam from C-cell to the mass spectrometer. Trace 1 shows the depletion in beam signal as a result of scrambling in the C-field when subjected to ground potential for 200 μs. The degree of the signal depletion should be directly proportional to the amount of de-orientation occurring during the zero-field interval.

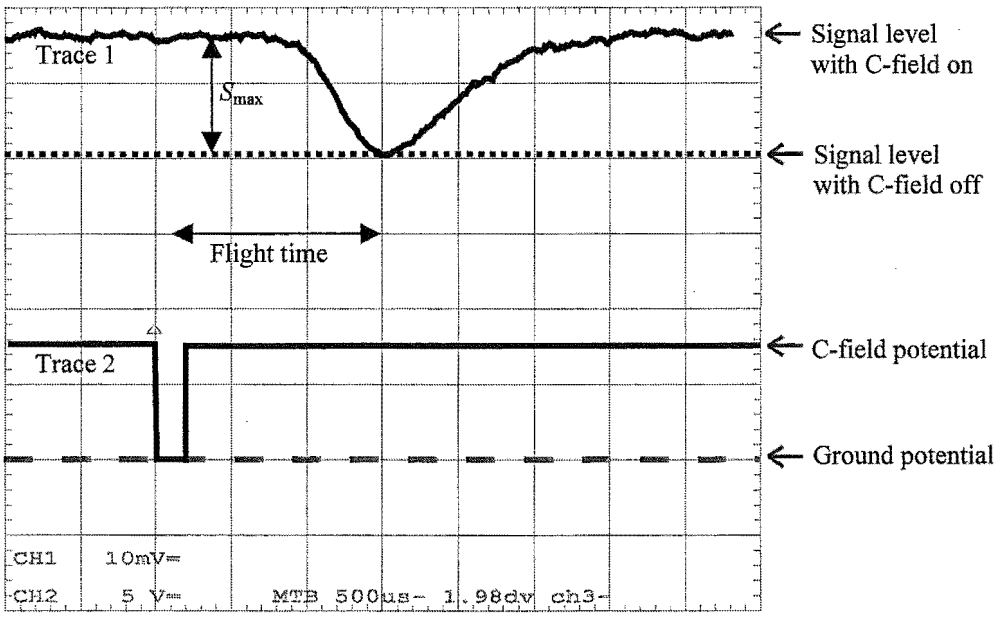

Figure 4.1.9 Traces recorded by a fast oscilloscope for a beam of CH_3F. Trace 1 is the beam signal and Trace 2 is the C-field plate potential.

Assuming that the scrambling of the oriented molecules follows first order kinetics, the depletion in the signal S(Δt), where Δt is the zero C-field pulse width, can be given by,

$$S(\Delta t) = S_{max}(1 - e^{-k\Delta t}) = S_{max}(1 - e^{-\Delta t/\tau}) \qquad (4.1.5)$$

where S_{max} is the maximum dip in the signal for C-cell at ground potential, k is the first-order rate constant, and τ is its reciprocal, the mean lifetime for scrambling.

A plot of the signal depletion against the zero C-field pulse width after the inversion of the exponential function could be fitted to determine the time constant for de-orientation. However, the signal depletion is extensively broadened by the beam velocity distribution, and these experimental conditions did not allow us to measure results reproducible enough to establish reliable values for the decay constant. The results indicated a lifetime in the range between 100 μs to 300 μs. This is consistent with the value of 150 μs deduced assuming the mechanism for scrambling to result from a smooth transition from rotational angular moment coupling to the electric field vector to coupling with the nuclear spin vector.

Two major problems are associated with this approach. The first is that the flight time for the molecule through the zero-field region is velocity dependent. For CH_3F, this is around 200 μs, which is roughly the same as the expected value for the lifetime estimation. This severely limits the range over which meaningful data can be collected. The second consideration is that many of the beam molecules will exit the C-field region before experiencing the entire width of the zero field pulse. Due to the broad time-of-flight distribution of the beam molecules arriving at the detector, the signal detected at a given instant will be consist of contributions from molecules, which have experienced zero field conditions for the entire range of times from 0 up to Δt. Consequently, the signal can not be strictly described by the first order rate equation given above, but is in fact some kind of integral over this function.

The velocity distribution within this experimental arrangement precludes the used of the tandem hexapole arrangement to measure accurate time dependent orientation properties. However, it should be possible to measure de-orientation lifetimes using a variant of the technique used by Gandhi and Bernstein. It is, in fact; possible to extract an approximate

orientation lifetime for CH_3I from the published results of Gandhi and Bernstein. [Gandhi 1990] Based on the degree of orientation measured under zero field conditions after the 640 μs flight time to the ionisation region for the |222> state, the de-orientation lifetime can be estimated to be around 220 μs. [Vallance 1999] In the experiment of Kaesdorf *et al*, a guiding field with reducing field strength from 10 V cm^{-1} to 0.3 V cm^{-1} was used with a flight time of around 530 μs for CH_3I. [Kaesdorf 1985] Based on a de-orientation lifetime of 220 μs determined from Gandhi and Bernstein's results, only 10% of the orientation integrity would have remained for the experiment of Kaesdorf *et al*. This most likely explains their success in obtaining only a small orientation effect.

4.1.5 Molecular beam electric resonance spectrometry

The technique of molecular beam electric resonance spectrometry has been employed to measure relative populations of the upper Stark-state molecules in beams of symmetric top molecules, Section 2.4. [Wiediger 1998 and Vallance 1999] The experimental arrangement is a variant of the tandem hexapole experiment, as described in Section 3.4. The two hexapole filters are referred as A-field and B-field, and the resonance field, C-field, is located between them. The C-cell provides a static DC field for defining the Stark energy and an RF field to affect transitions between ΔM_J states. Transitions between rotational states are excited by the RF oscillating field, which must be perpendicular to the DC field because the transition dipole is orthogonal to the molecular axis for M_J changing transitions of symmetric top molecules. When the beam of upper Stark-state symmetric top molecules (focused by the A-field) experiences the resonance radiation in the C-field region, transitions from upper Stark states into the lower Stark states (stimulated emission) or other non-focusing states may occur for a fraction of the total population in the beam. Molecules no longer in the upper Stark-states would not be focused by the B-field, resulting in a depletion of the total signal. The change in focused beam signal is related to the population of the initial state in the beam.

The first order Stark energy of a symmetric top molecule is given by

$$W = -\mu E \frac{KM_J}{J(J+1)}. \qquad (4.1.6)$$

The spectroscopic selection rules for rotational state transitions of symmetric top molecules are $\Delta J = 0, \pm 1$, $\Delta K = 0$, and $\Delta M_J = 0, \pm 1$, although Oka and Phillips have suggested that $\Delta M_J > \pm 1$ are possible under some circumstances. [Oka 1973, Johns 1975, and Phillips 1995] In the resonance region, the oscillating frequency used is in the radio frequency region, which induces $\Delta J = 0$, $\Delta M_J = \pm 1$ transitions only. The transition is tuned by the radio frequency so that $h\nu = \Delta W$.

$$h\nu = \Delta W = -\mu E \frac{K}{J(J+1)} [M_J - (M_J \pm 1)] = \pm \mu E \frac{K}{J(J+1)}. \tag{4.1.7}$$

For a $\Delta M_J = \pm 1$ transition of a given $|JK\rangle$ state of a symmetric top molecule, the DC field strength, E, and RF field, $h\nu$, must satisfy the relationship that

$$\frac{J(J+1)}{K} = \frac{\mu E}{h\nu}. \tag{4.1.8}$$

$|JK\rangle$ spectra, described in Section 3.6.2.3, have been measured as a function of the DC electric field strength with the RF field held constant.

4.1.5.1 Investigation of C-cell electrical configurations

Two C-cells, described in Section 3.4, have been constructed with geometries that ensure that a component of the RF field is perpendicular to the DC field in order to excite the resonant transitions. For the first C-cell design, a uniform RF field with a component perpendicular to the DC field is best provided when the RF field is supplied to the inner portions on both set of plates, as shown in Figure 3.4.2 (b). For the second C-cell, several electrical arrangements are capable of providing the required electric field configuration. Four different electrical wiring configurations have been investigated under the same experimental conditions.

The performances of the two designs are compared in Figure 4.1.10. While the first C-cell gave superior resolution, the second C-cell gave significantly higher signal amplitudes, and was therefore more suitable for attenuation experiments. Configuration (iv) and (v) gave relatively intense signals and comparable peak shape. The configuration in (v) with ±DC on the side plates and the RF at ground potential on the top and bottom plates was chosen for the attenuation experiments because of the less complicated

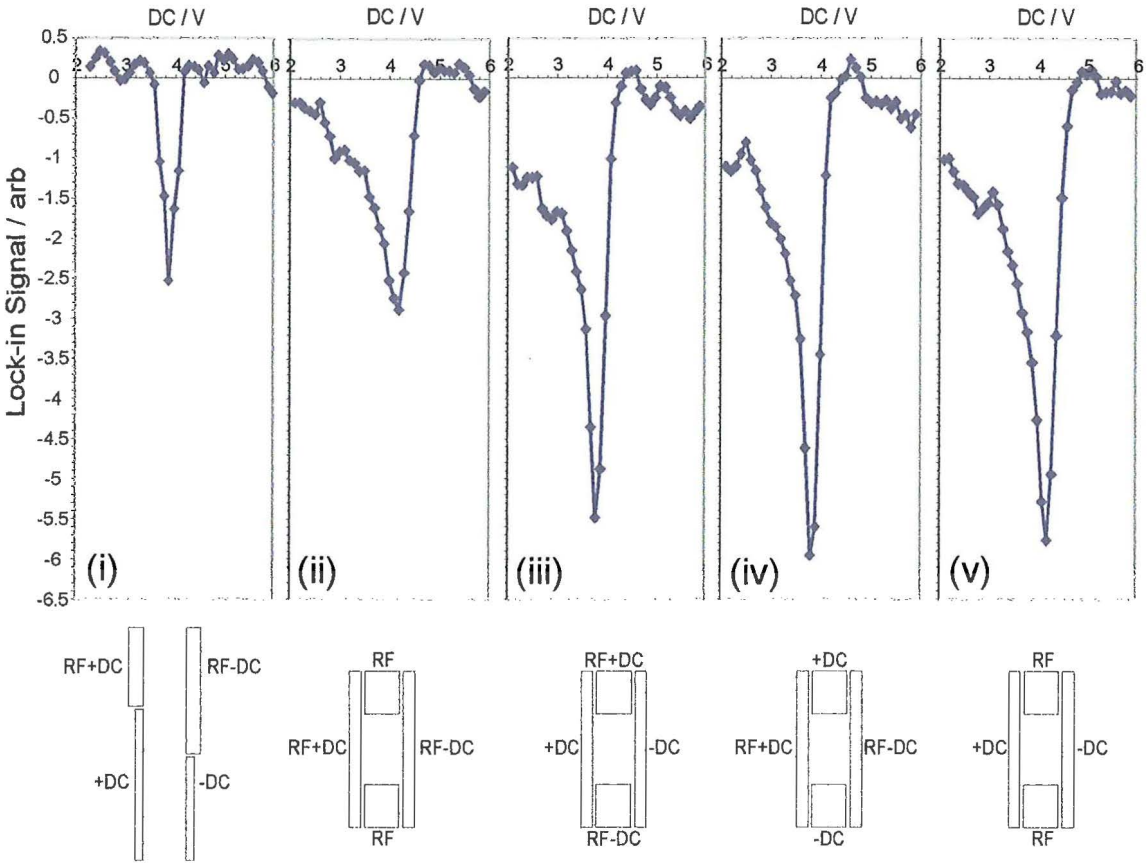

Figure 4.1.10 Comparison of spectra measured for the |11> rotational state in a beam of 10% CH_3F/Ar with five different electrical configurations of the first and second C-cell

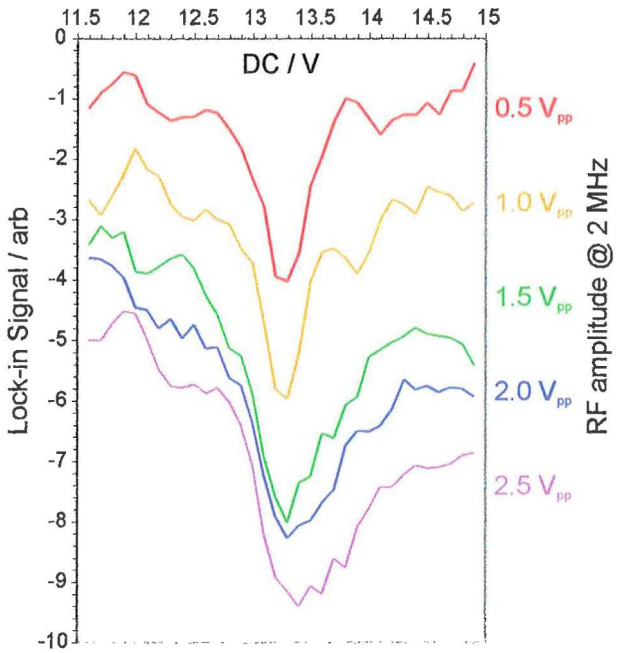

Figure 4.1.11 Effect of RF amplitude on the resonance signal measured for the |21⟩ peak of a 10% CH_3F/Ar beam at a hexapole voltage of 3 kV and RF frequency of 2 MHz.

electrical wiring required. The improved signal intensities from the second design are probably due to its relatively larger component of the RF field in the direction of the transition dipole moment of the beam molecule.

A Hewlett-Packard waveform generator was used for the RF field, see details in Section 3.4. The optimum signal was obtained with a frequency between 1 to 3 MHz. The DC field strength required for a ΔM_J transition depends on the RF frequency. From Equation (4.1.8), the DC field strength required to bring about a transition increases linearly with the fixed RF frequency used. An RF frequency of 2 MHz was used in all experiments. For RF frequencies above 3 MHz, it was found that the amplitude of the RF required exceed that available from Hewlett-Packard generator.

The amplitude of the RF field determines the number of transitions, low amplitudes result in a small signal due to the low number of transitions excited by the lower intensity of the radiation, while higher amplitudes lead to signal broadening. Figure 4.1.11 shows the effect of RF amplitude on the signal for the $|21\rangle$ spectra for a seeded CH_3F beam. The RF amplitude of 1.5 Vpp was used for these experiments. The decrease in the beam signal due to the depletion of upper Stark states by transitions is a small fraction of the total signal (~1 – 3%). In order to detect the small difference in signal with and without RF excited transitions; a lock-in-amplifier was used, see Section 3.5.2.3. The modulating frequency could be chosen such that the phase difference introduced by the flight time of the beam from the resonance region to the detector was minimised. Alternatively, the phase on the lock-in-amplifier could be adjusted to give the maximum signal. Since the optimum phase and modulating frequency were dependent on the flight time, the beam velocity could be estimated, as previously discussed in Section 4.1.2.2.

4.1.5.2 Experimental and calculated $|JK\rangle$ spectra

Examples of experimental and calculated $|JK\rangle$ spectra are shown in Figure 4.1.12. The experiment was carried out for a beam of 10% CH_3F seeded in Ar with the hexapole voltage at 4 kV and the RF frequency at 2 MHz. The calculation was performed under the same geometric conditions and both the rotational and translational temperatures of the beam were assumed to be 35 K, based on measurements discussed in Section 4.1.2.2.

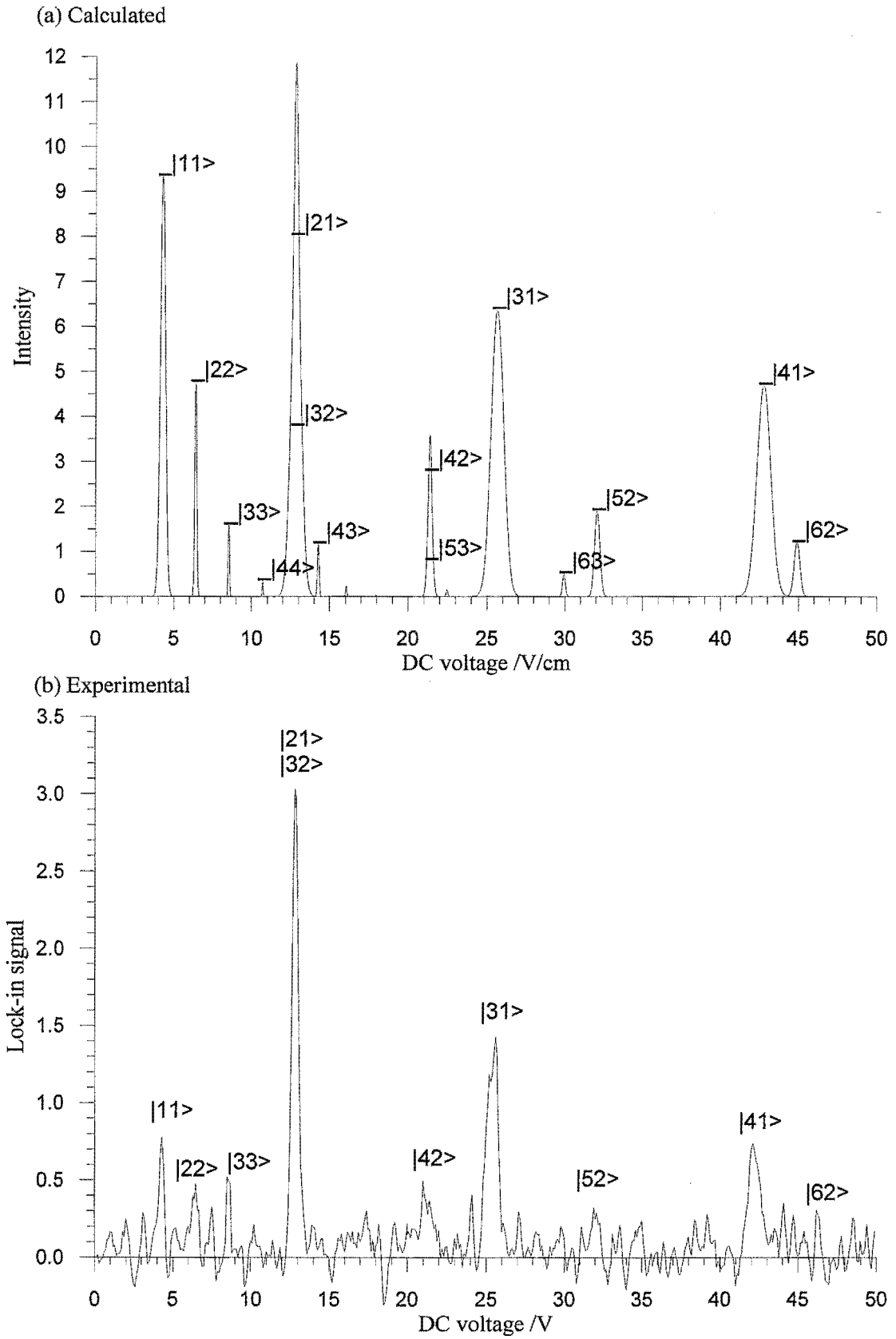

Figure 4.1.12 (a) Calculated |*JK*> spectra for CH_3F at RF of 2 MHz and beam temperature of 35 K. (b) Experimental result for a beam of 10% CH_3F/Ar at hexapole voltage of 4 kV and RF of 2 MHz.

Where peaks in the $|JK\rangle$ spectrum overlap in Figure 4.1.12 (a), the horizontal bars have been used to represent the relative contribution of that state to the total peak intensity. The identities of the $|JK\rangle$ states corresponding to peaks in the experimental results are confirmed by the calculated spectra. The discrepancies between the experimental and calculated spectra are due to measurement at a single hexapole voltage. As previously discussed in Section 4.1.3, molecules are focused to the exit of the hexapole field at rotational state dependent hexapole voltages. The calculated spectrum shows the intensities of the rotational states according to the temperature dependent population distribution, while the observed intensities are fractions of the total populations of the upper Stark-state molecules focused to the exit at that particular hexapole voltage. At any given hexapole voltage, molecules in all possible upper Stark states in the beam may be transmitted, but the transmission probabilities are rotational state dependent. Therefore, the relative intensities of the $|JK\rangle$ transitions depend not only on the rotational population distribution of the beam (beam temperature) but also on the focusing characteristic for each state.

The effects of the beam temperature and hexapole voltage can be distinguished from a comparison of spectra shown in Figure 4.1.13. All three spectra were obtained under identical conditions apart from those aspects mentioned for comparison. Details of the experimental conditions for each of the spectra are shown in the graphs. A comparison between Figure 4.1.13 (a) and (b) shows the effect of beam temperature on the population of the rotational states in the beam. The rotational temperature of the seeded beam, spectrum shown in (a), is clearly lower than the rotational temperature of the neat beam shown in (b). Spectrum (a) is dominated by three peaks, corresponding to the $|21\rangle$, $|31\rangle$, and $|41\rangle$ states, with decreasing intensities as expected from the trend shown in calculated spectra. Spectrum (b) is populated with many more peaks, corresponding to the higher $|JK\rangle$ states, indicating a higher rotational beam temperature.

A comparison between spectra (b) and (c) shows the effect of the hexapole voltage on the focusing of different rotational states. Spectra (b) and (c) are recorded under identical experimental conditions for a neat CH_3F beam apart from the hexapole voltages: (b) is recorded at 5 kV; (c) at 3 kV. The difference between the relative intensities of the peaks illustrates the effect of the focusing voltage on the corresponding states. For example, at

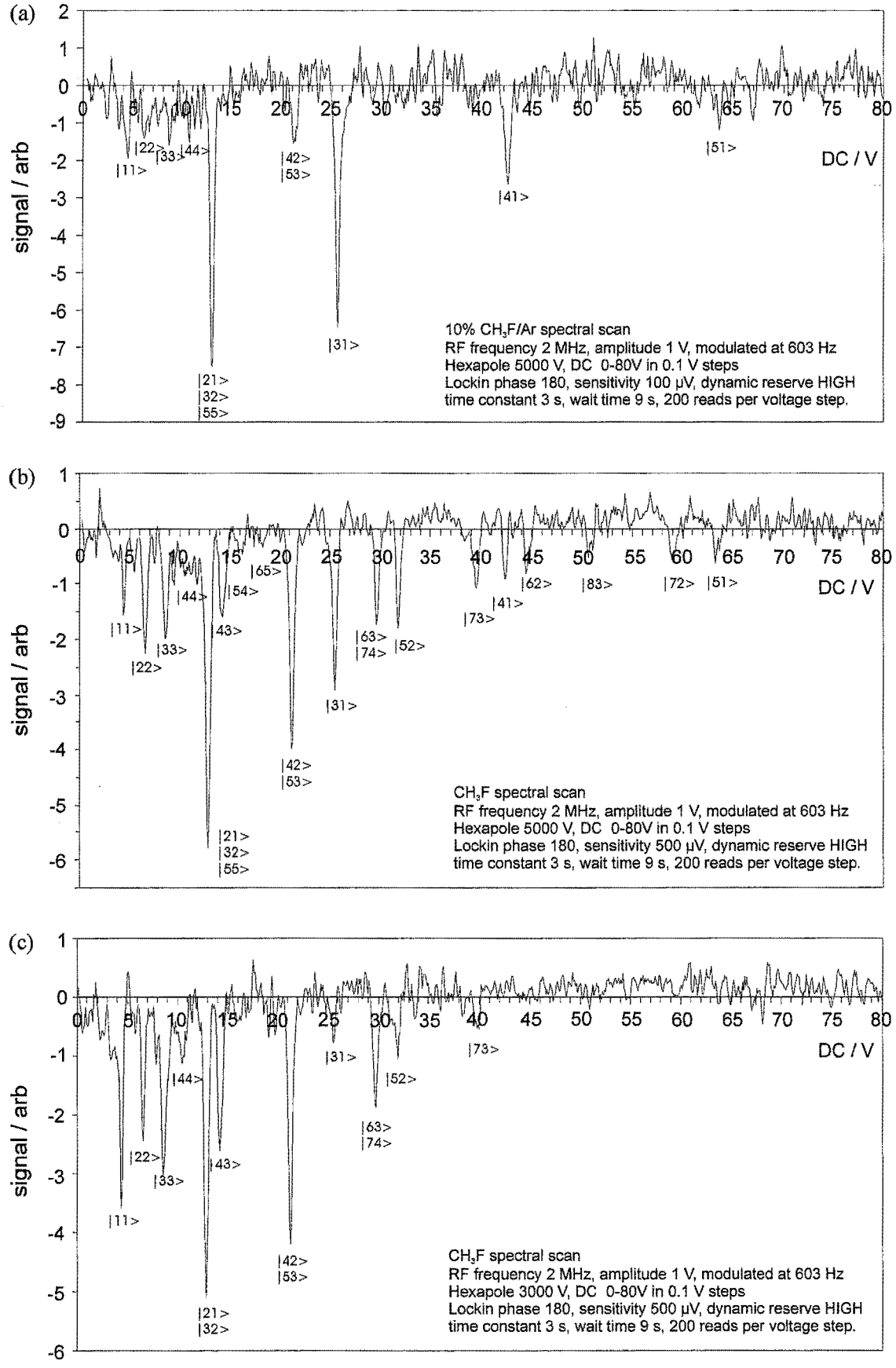

Figure 4.1.13 Effect of beam temperature and hexapole voltage on $|JK>$ spectra of CH_3F.
(a) 10% CH_3F/Ar at 5 kV. (b) neat CH_3F at 5 kV. (c) neat CH_3F at 3 kV.

3 kV, the peaks corresponding to the |11⟩, |33⟩, |43⟩, and |42⟩ states have higher intensities than they have at 5 kV, while the peaks corresponding to the |31⟩ and |52⟩ states have lower intensities and some other peaks have not appeared at all. The effect of the difference in the focusing voltage of different rotational states can be seen clearly in the three dimensional surface plot constructed from spectra measured at different hexapole voltages for a seeded beam of 10% CH_3F in Ar, as shown in Figure 4.1.14. The effect of the hexapole voltage on the signal intensity is discussed in detail in the following section on the transmission curves.

The 3-D surface plot of spectra measured over a range of hexapole voltages gives a more accurate view on the population of individual rotational states. In principle, if the rotational state distribution is known, the rotational temperature of the beam could be determined. Although, the population distribution of the rotational states may not be accurately determined from the intensities of the peaks in the spectra, the rotational states corresponding to the peaks can be identified correctly. The RF resonance technique shows promise as a good method for tagging individual rotational states of symmetric top molecules for investigations on the effect of individual quantum states in collision processes. Collisional relaxation of quantum state selected CH_3F has been studied using this technique. [Vallance 1999]

4.1.5.3 Hexapole transmission curves

A number of computer programs have been written to calculate the experimental transmission curves for individual rotational quantum states using several methods based on different assumptions. (See Appendix C.3 for an example in QuickBasic. Other transmission curve simulation programs are written in a graphical language, called LabVIEW.) Calculated and experimental results both showed that the physical alignment of the molecular beam - hexapole system is important. Several computer programs have been written in LabVIEW, Laboratory Virtual Instrument Engineering Workbench, which is a graphical programing language and an instrumentation and analysis software. [LabVIEW 1994] These programs calculate the trajectories for particular $|JKM_J\rangle$ states using equations described in Section 2.3.1 using the appropriate geometric parameters for the machine.

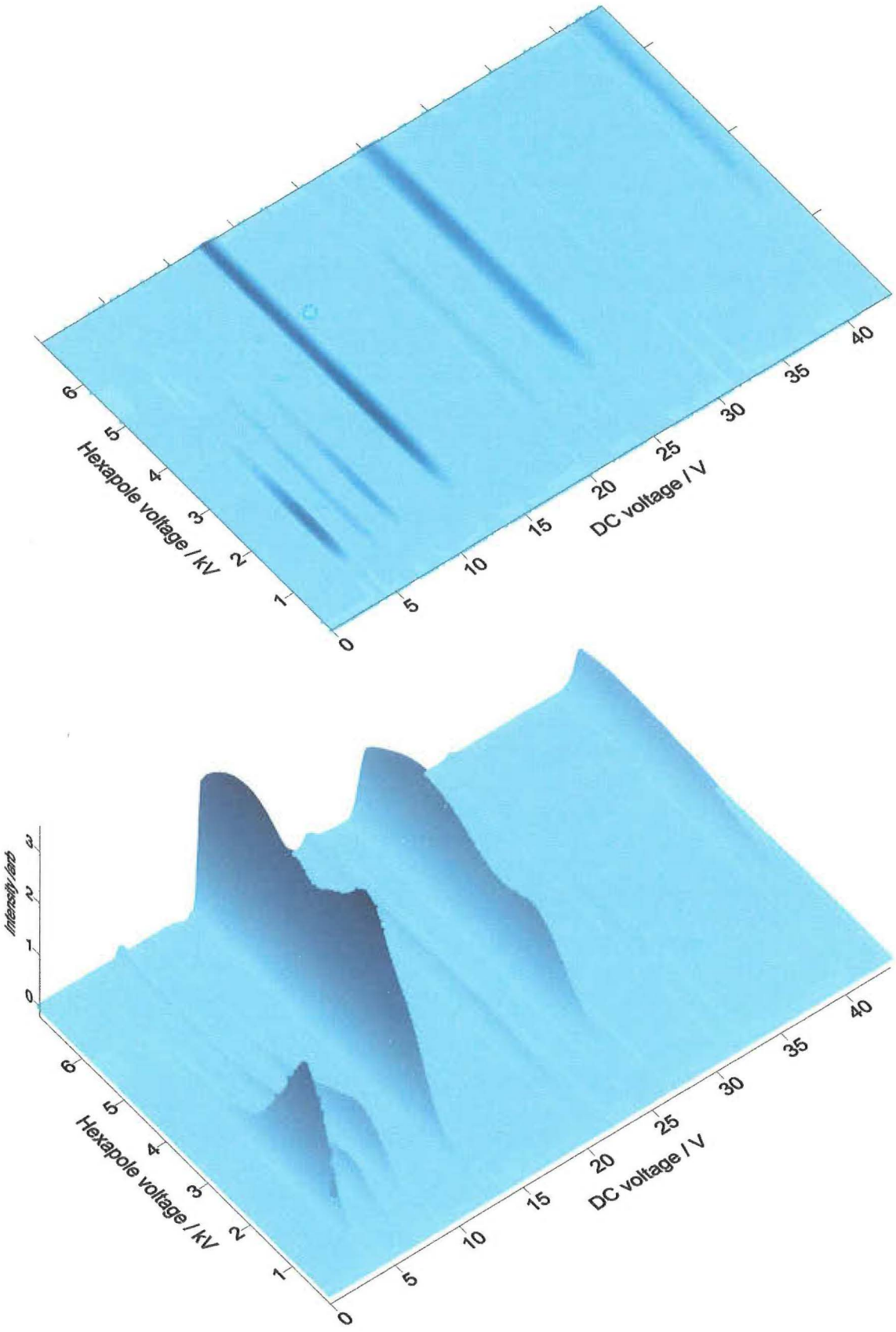

Figure 4.1.14 3-D plot of spectra measured at different hexapole voltages of transitions from M_J= -1 to M_J = 0 for individual |JK> states of CH_3F, in a beam of 10% CH_3F/Ar with RF = 2 MHz in the C-field.

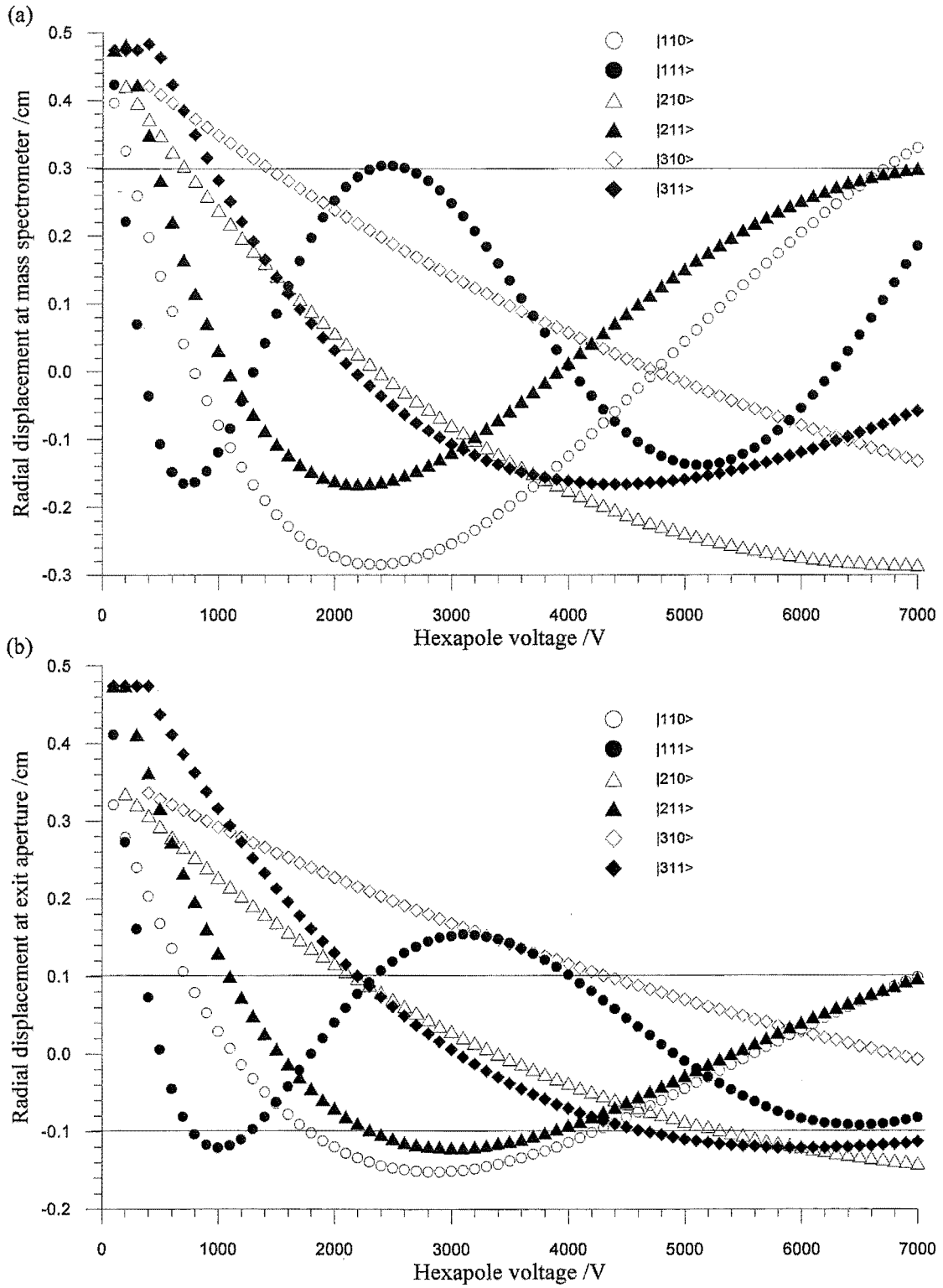

Figure 4.1.15 Calculated results of maximum radial displacement of molecules from the centre of the hexapole field at (a) the mass spectrometer and (b) the hexapole exit aperture. The M = 0 states represent molecules that have relaxed from M = -1 to M = 0 in the C-cell region. The M = 1 states represent upper Stark state molecules focused by the hexapole field.

The maximum radial displacement of the molecules in any azimuthal angle at the exit of the second hexapole filter and the mass spectrometer detector are shown as a function of hexapole voltages in Figure 4.1.15. In Figure 4.1.15 (a) the line at 0.3 cm on the y-axis represents the detection limit of the mass spectrometer, which shows that most of the molecules exiting the hexapole filter will be detected by the mass spectrometer. In Figure 4.1.15 (b) the two line at 0.1 cm and -0.1 cm represent the size of the exit aperture (2 mm in diameter). Points within the two lines means that all molecules of the indicated state will pass through the exit and be detected. Points outside this region mean that only fractions of the molecules in the represented state will pass through the exit. The $|JK0\rangle$ states represent molecules that underwent transitions from $M_J = -1$ to $M_J = 0$ in the C-cell region, and the $|JK1\rangle$ states represent molecules that remained in the same upper Stark state passing through all three fields. Therefore, depletion of signal due to resonance transitions are expected for $|JK\rangle$ states at the hexapole voltages where the difference between points marked by $|JK1\rangle$ and $|JK0\rangle$ are significant relative to the limits imposed by the exit aperture.

The outcome of this calculation also revealed the importance of the alignment of the experimental components. If the exit aperture was not in perfect alignment with the axis of the beam, the experimental results would not be able to be simulated by calculations with accuracy. This finding is confirmed by experimental transmission curves measured before and after alignment of the machine following an earth tremor. The effect of a slight change in the alignment of the machine is evident in the transmission curves, as shown in Figure 4.1.16.

For curves (i) and (ii), the difference in the shape of the curves resulting from the change in the machine alignment is significant. For curves (ii) and (iii), the positions of the peaks have moved slightly, the shapes of the transmission curves are relatively comparative. However, $|JK\rangle$ spectra measured under different alignment conditions showed little alterations. The trajectories of the upper Stark-state molecules in a hexapole field are sinusoidal, and molecules are focused to the axis at every half a period of the sine wave. It would therefore be reasonable to expect peaks in the transmission curves to occur at the hexapole voltages corresponding to the nodes of the sine wave molecular trajectories. Comparing curves (i) and (ii), a peak corresponding to one node only is evident for curve

(i), while in curve (ii) peaks corresponding to at least two nodes are observed. Comparing curves (ii) and (iii), peaks corresponding to the first two nodes are observed in different positions. This is due to the difference in the beam velocities, which are discussed in detail later.

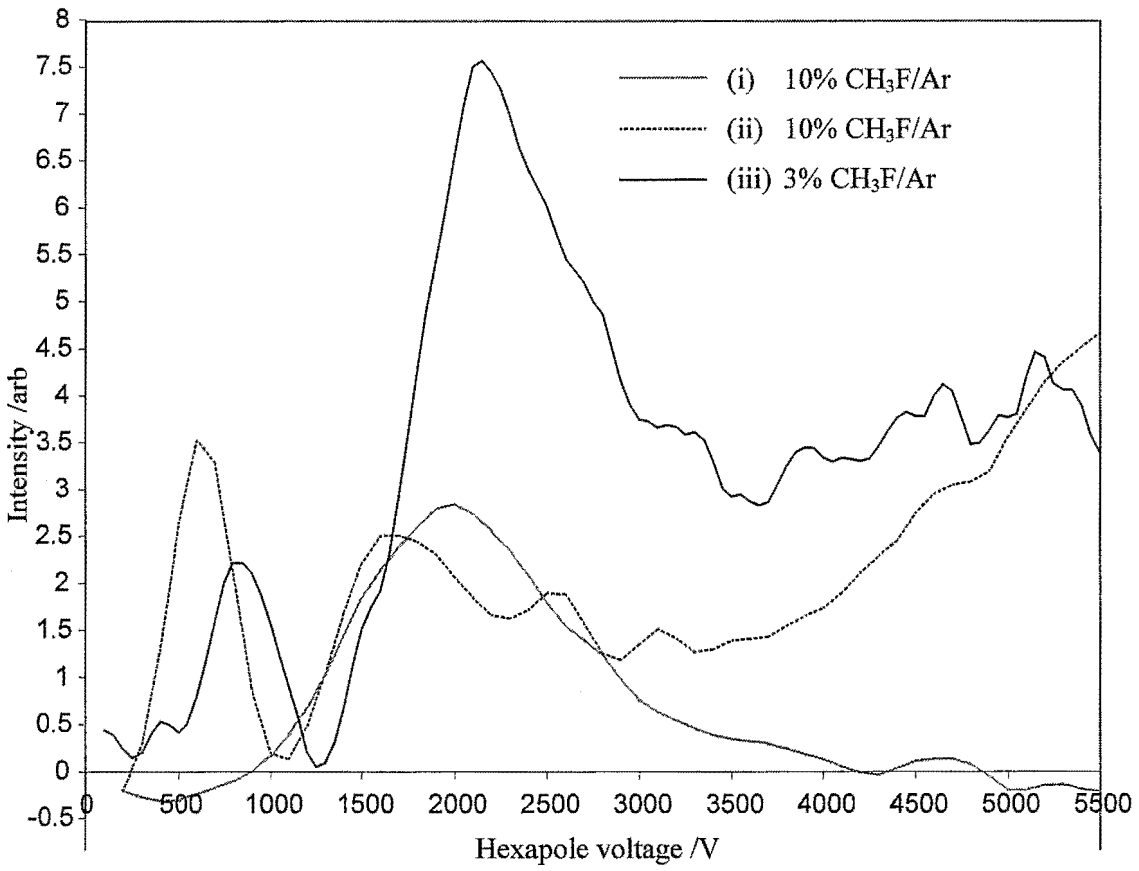

Figure 4.1.16 Transmission curve measured for the $|11\rangle$ rotational state in a beam of 10% CH_3F/Ar: i) before realignment; ii) after realignment, and iii) after realignment for a beam of 3% CH_3F/Ar.

The relationship between the hexapole voltage, $U_{o,f}(JKM_J,d_f)$, and the conditions for the focusing of specific states is given by the following equation, see Section 2.3.3 and units defined therein.

$$U_{o,f}(JKM_J, d_f) = \frac{\pi^2 v^2 m r_o^3}{6\, d_f^2 \mu} \frac{J(J+1)}{M_J K} \tag{4.1.9}$$

Plotting the mass spectrometer signal measured for transmission curves as a function of $U_o(M_JK)[J(J+1)]^{-1}$ instead of the hexapole voltage, U_o, should give curves with similar

peak positions for different rotational states under identical conditions. For convenience, plots of beam signal against $U_0(M_JK)[J(J+1)]^{-1}$ are called the state-independent transmission curves. Figure 4.1.17 shows good agreement between the state-independent transmission curves for different rotational states in (a) before and (b) after a realignment of the machine for a beam of 10% CH_3F seeded in Ar. Plot (c) shows state-independent transmission curves for a beam of 3% CH_3F seeded in Ar after realignment.

Wiediger *et al* used a similar approach to compare transmission curves measured for different beam mixtures taking the beam mass and velocity into account, and they have also found good agreements. [Wiediger 1998] They plotted beam signal against "reduced" voltage, $U_r = \mu U_0\langle m\rangle M_JK/[mJ(J+1)]$, where m and μ are the molecular mass and dipole moment, U_0 is the hexapole voltage, and $\langle m\rangle$ is the average mass in the seeded beam, since $v^2 \propto 1/\langle m\rangle$.

The state-independent focusing voltage is given as,

$$\frac{M_JK}{J(J+1)}U_{0,f}(JKM_J,d_f) = U_{0,f}(d_f) = \frac{\pi^2 v^2 m r_0^3}{6\, d_f^2 \mu} \qquad (4.1.10)$$

where r_0 is the inscribed radius of the hexapole filter, d_f is the focusing distance along the axis, m, μ, and v are molecular beam mass, dipole moment and velocity, respectively. The experimental results shown in Figure 4.1.17 are in good accord with the expectations based on Equation (4.1.10) that the peaks for in transmission curves overlap for different rotational states. According to Equation (4.1.10), the beam velocity is related to the state-independent focusing voltage, $U_{0,f}(d_f) \propto v^2$. A rough estimate of the beam velocity could be deduced from the state-independent transmission curves. A more detailed examination of the transmission curves shown in Figure 4.1.17 highlights the limitation in our ability to control beam conditions on a day to day basis.

The velocity of a supersonic beam depends on the experimental conditions, such as the nozzle-skimmer distance and the stagnation pressure of the beam source. The nozzle-skimmer distance is optimised for every new beam mixture. The stagnation pressure used is dependent on the type of nozzle and is limited by the pumping capacity in the nozzle chamber. For the pulsed mode solenoid and piezoelectric nozzles, the stagnation pressure was typically around 1000 Torr. For the continuous nozzle, it was around 100 Torr,

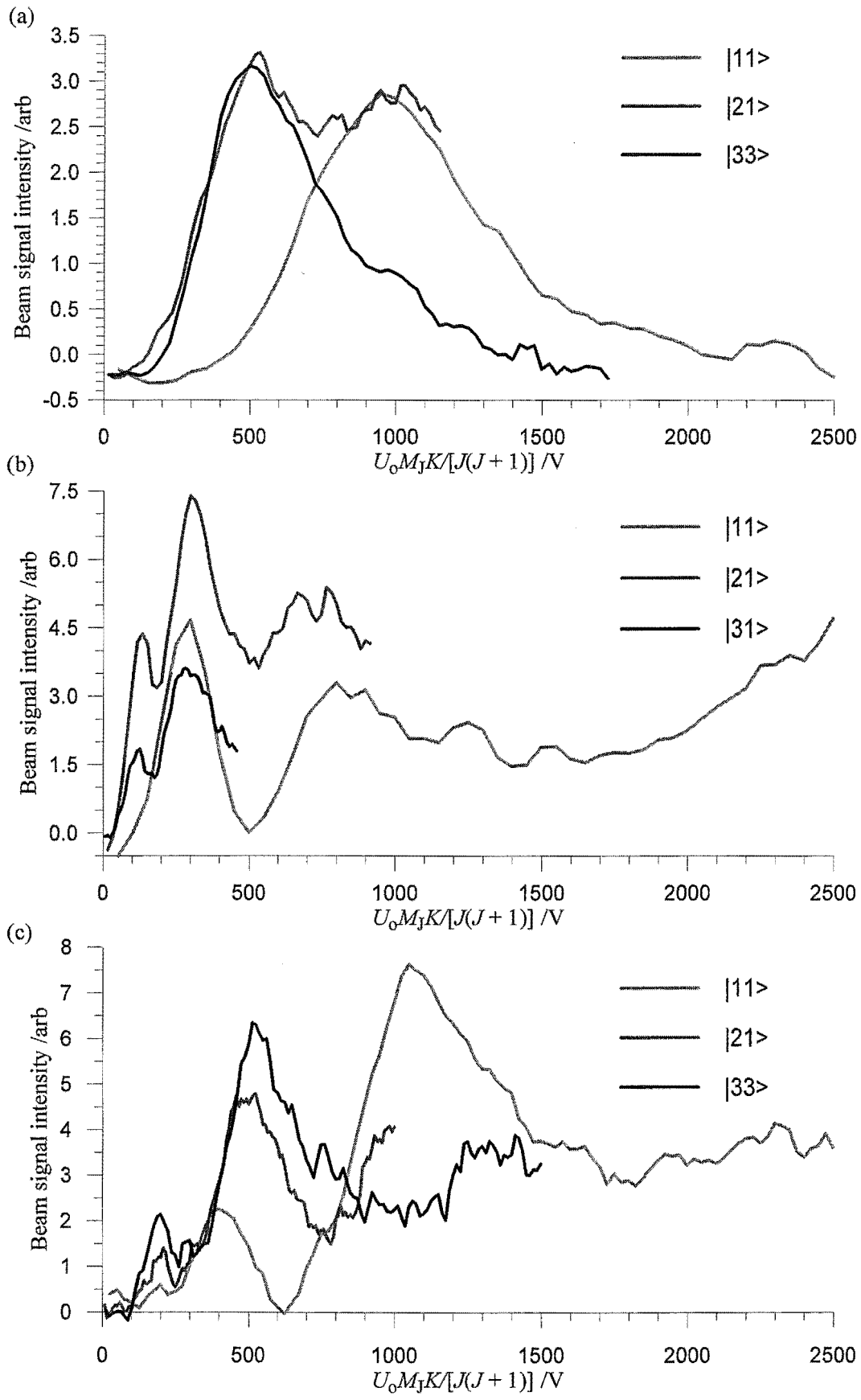

Figure 4.1.17 Beam signal plotted against $U_0M_JK/[J(J+1)]$ for a beam of 10% CH_3F/Ar (a) before and (b) after a realignment of the machine and (c) for a beam of 3% CH_3F/ Ar after realignment.

however, after the installation of the additional pumping station to the nozzle chamber, the stagnation pressure could be increased to about 200 Torr. The beam velocity could vary from day to day, even between experiments, especially if the running time of the experiment was long and gas reservoir pressure changed significantly. Even the small difference in beam velocities resulting from changes in nozzle stagnation pressure contributes to the difference in the hexapole focusing voltages, as shown in Figure 4.1.16 and 4.1.17.

Since the state-independent focusing voltage is proportional to v^2, a small change in the beam velocity has a large effect on the hexapole focusing voltage. Peaks in the state-independent transmission curves should appear at intervals of n^2, corresponding to the n^{th} node in focusing sinusoidal trajectories of the upper Stark-state molecules focused at the exit of the hexapole filter. Assuming an estimated beam velocity for 10% CH_3F seeded in Ar as 567 m s^{-1} and neglect the influence of the C-cell by treating the two hexapole filters as one long hexapole filter, 1210 mm in length, the value for the state-independent focusing voltage is 353 V. Using beam velocities estimated from the modulating frequency of the lock-in-amplifier, the approximate position of the peak corresponding to the first node in focusing molecular trajectory could be estimated. Positions of the peaks corresponding to higher nodes in the state-independent transmission curves could be predicted.

According to the relationship between the nodes of the trajectories and the corresponding state-independent focusing voltage, $U_o(M_J K)[J(J+1)]^{-1} \propto n^2$. The experimental results were found to agree with the theoretical predictions for the first node or two. Disagreements for larger values of n are likely due to the difficulty of achieving perfect alignment; this would result in peaks that would not necessarily appear exactly at the calculated positions in the transmission curves, and some peaks might not even appear at all, as seen in Figure 4.1.17.

Another factor contributing to the discrepancy between experimental results and theoretical estimation of the peak positions is the assumption that the effect of the C-cell on the trajectories of the focusing molecules was negligible. The length of the C-cell is short compared to the total length of the hexapole filter, and the C-cell is positioned on

axis between the hexapole filters. It would therefore be a reasonable assumption to overlook the effect of the C-cell in the case when the first node is at the exit of the hexapole filter, corresponding to the first expected peak in the state-independent transmission curve. However, the influence of the C-cell on the trajectories of the focusing molecules increases as the hexapole field increases; the discontinuity in the focusing trajectory due to the C-cell becomes more significant compared to the focal length of the hexapole filter. Therefore, disagreement between experimental and theoretical estimations of the peak positions in the state-independent transmission curves is to be expected at higher n values. This would not have been a problem for the comparison between the state-independent transmission curves of different states if the trajectories for all the molecules in different states were the same, since the length of the discontinuity, C-cell, in the molecular trajectory was constant. The extent of the disruption due to the C-cell on the focusing trajectories are state dependent, and the results can be seen clearly in Figure 4.1.17, particularly in (c). Nevertheless, the trends of the state-independent transmission curves are in accord with the theory discussed here.

Several computer programs have been written in LabVIEW using the Monte Carlo approach to simulate experimental transmission curves for the tandem hexapole-C-cell arrangement with limited success, although excellent agreement was found for a single hexapole. Some programs generate results that match transmission curves of some states but not for all the states. The relative intensities between the states can be obtained for a limited number of states from the state-independent transmission curves, as shown in Figure 4.1.17 (b) and (c). In summary, the limitation in our ability to control beam condition on a day to day basis and the disruption in the molecular trajectory due to the C-cell result in some difficulty in successfully simulating experimental transmission curves.

Experimental data are limited to a few low J value $|JK\rangle$ states. Higher $|JK\rangle$ states are focused at much higher hexapole voltages. Lower $|JK\rangle$ states are populated when the beam temperatures are very low. Under the current experimental conditions, transmitted intensities of the $|11\rangle$, $|21\rangle$, and possibly the $|31\rangle$ states are adequate to carry out investigations of state dependent collisional effects for seeded beams of methyl halides through resonance tuning of the C-cell.

4.2 *Collision cross-section*

Collision cross-sections are determined from attenuation of beams of symmetric top molecules scattered by bulk gases. Cross-sections are calculated using a modified expression of the Beer-Lambert law,

$$\sigma = \frac{1}{nl} \ln \frac{I_0}{I} \tag{4.2.1}$$

where n is the number density of the scattering gas species in the collision region, l is the length of the collision region, I_0 is the initial beam intensity in the absence of any scattering gas, and I is the measured beam intensity. Equation (4.2.1) can be rearranged to give,

$$\ln I = -nl\sigma + \ln I_0. \tag{4.2.2}$$

Cross-section, σ, can be deduced from the slope of $\ln I$ plotted against pressure, which is related to n through the ideal gas law.

$$n = \frac{N_A}{V_m} \frac{P}{760} \frac{273.15}{T} = \frac{133.3P}{k_B T} \tag{4.2.3}$$

where N_A is the Avogadro number, k_B is the Boltzmann constant, V_m is the molar volume at standard temperature and pressure of an ideal gas, units in m^3, P is the pressure in the scattering region in Torr, and T is the temperature of the scattering gas.

Attenuation experiments have been conducted using two experimental arrangements, the single hexapole-collision cell system and the tandem hexapole arrangement with the MBER spectrometer. Collision cross-sections have been determined from attenuation experiments for beams of methyl halides scattered by the inert gases, polar and non-polar molecules. Single hexapole experiments were carried out before the MBER spectrometer was developed. The data collected and the correlation drawn from those experiments are included here only for completeness.

4.2.1 Data analysis

Analysis of the results from the two experimental arrangements are discussed separately in the following sections.

4.2.1.1 Single hexapole experiment

The cross-sections determined are the defocusing cross-sections for the upper Stark-state molecules by the scattering gases in the hexapole-collision cell.

The length of the scattering region was from the tip of the second skimmer to the exit aperture of the hexapole filter, 0.884 m. Equation (4.2.2) becomes

$$\ln I = -2.865 \times 10^{22}\, \sigma P + \ln I_0 \qquad (4.2.4)$$

where P is expressed in Torr and σ will be in m^2. The slope of a $\ln I$ against P plot, then gives σ. Pressure in the scattering region was originally measured by a Bayard-Alpert type ionisation-gauge (Duniway stockroom, T-100-K) and recorded by the computer using the PCL-8255 lab card interfaced to the MKS 290 ion gauge controller. Measurements from the ion gauge are dependent on the ionisation cross-sections of the gas species, and ion gauge pressures were corrected through the relationship described in Equation (3.7.2), see Section 3.7.6.1. Equation (4.2.2) can be further expressed as

$$\ln I = \frac{-2.865 \times 10^{22} P_M}{0.41\, \sigma_{EI} + 0.047}\, \sigma + \ln I_0 \qquad (4.2.5)$$

where P_M is the measured ion gauge pressure in Torr and σ_{EI} is the ionisation cross-section at 75 eV.

The beam signal, I_P, for the defocusing of the upper Stark-state component of the beam for scattering gas pressure, P, at a given hexapole voltage, is obtained from the difference between the signal recorded with the hexapole voltage on, $I_{P,\,on}$ and that with the hexapole voltage off, $I_{P,\,off}$.

$$I_P = I_{P,\,on} - I_{P,\,off} \qquad (4.2.6)$$

Upper Stark-state molecules are focused when hexapole voltages are greater than the threshold upper Stark-state transmission voltages. The threshold voltage is given by: [Chakravorty 1982]

$$U_{th} = \frac{\pi^2 r_0^{\,3}}{6 l_1^{\,2}} \frac{m v^2}{\mu} \qquad (4.2.7)$$

where r_0 and l_1 are the inscribed radius and the length of the hexapole respectively and m, v, and μ are the mass, velocity and the dipole moment of the beam molecule in the hexapole field, respectively.

The beam signal with the hexapole voltage on, $I_{P,\ on}$, includes contributions from the focused upper Stark-state component as well as the much smaller non-focusing, $M_J K = 0$, component of the beam. Cross-sections that are calculated from the attenuation of the beam signal with the hexapole voltage off correspond to the elastic and inelastic scattering (changes in ΔJ only since ΔM_J is not defined in the absence of an electric field) of the non-focusing component of the beam. Cross-sections that are calculated from the difference signal correspond to the attenuation of the upper Stark-state components in the beam.

4.2.1.2 Molecular Beam Electric Resonance spectrometer

Attenuation cross-sections measured using the tandem hexapole arrangement are for the collisional relaxation of the upper Stark-state molecules measured using the MBER spectrometer.

The length of the collision cell is basically the length of the first hexapole enclosed as a collision cell, 0.548 m, from the tip of the second skimmer to the partition at the exit of the first hexapole field. Equation (4.2.2) becomes

$$\ln I = -1.776\times 10^{22}\,\sigma P + \ln I_0 \qquad (4.2.8)$$

The slope of $\ln I$ plotted against P, in Torr, gives σ in m^2. Pressure in the collision cell is measured by a calibrated ion gauge and recorded by the computer using the ADDA-14 interface card to the MKS HPS 919 Hot Cathode controller, see Section 3.7.6.3. An ion gauge calibration experiment was conducted for every new scattering gas used in attenuation experiments.

The lock-in-amplifier was used to measure the difference signal, I_L, which corresponds to the population of the selected upper Stark-state component in the beam after attenuation in the collision cell for the scattering gas pressure, P, at the hexapole voltage measured. Cross-sections determined correspond to ΔM_J changing collisions for the quantum states tuned by the MBER spectrometer.

4.2.2 Cross-section results – Single hexapole experiment

Table 4.2.1 lists cross-sections determined for a beam of CH_3F against quencher gases, He, Ar, Kr, Xe, N_2, N_2O, CO_2, CH_4, CH_3F, CH_3Cl and SF_6 for hexapole voltages of 0 V and 5 kV. Figure 4.2.1 shows a hexapole transmission curve for a CH_3F beam. Attenuation experiments were carried out at a hexapole voltage of 5 kV, because the focusing ability of the hexapole appeared to approach a maximum towards 5 kV.

Table 4.2.1 Cross-sections measured for beams of CH_3F with the collision partners shown.

Scattering gas	σ@ 0 kV /Å^2	σ@ 5 kV /Å^2
He	105 ± 24	152 ± 42
Ar	156 ± 21	220 ± 61
Kr	213 ± 57	259 ± 58
Xe	226 ± 33	320 ± 89
N_2	178 ± 30	249 ± 53
N_2O	193 ± 50	232 ± 86
CO_2	174 ± 12	204 ± 24
CH_4	234 ± 43	366 ± 84
CH_3F	266 ± 28	418 ± 43
CH_3Cl	363 ± 30	427 ± 38
SF_6	219 ± 59	225 ± 91

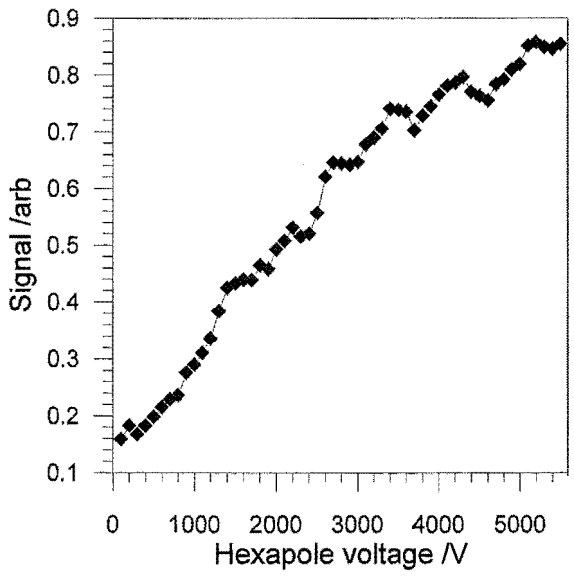

Figure 4.2.1 Hexapole transmission curve for a neat beam of CH_3F.

4.2.2.1 Variation with hexapole voltage

When the transmission curves of seeded beams were measured, features corresponding to specific rotational states were evident in the curves, as discussed in Section 4.1.3. Attenuation experiments were carried out for beams of symmetric top molecules against inert gases and nitrogen at a range of hexapole voltages from the threshold voltage to 6800 V, in 200 V step increments. Experimental cross-sections were found to vary with the hexapole voltages with cross-section maxima corresponding to specific M_J states. Most of the results have been published in the thesis of a former colleague, Dr S. A. Harris. [Harris 1997] Results for beams of 5% CH_3F seeded in Ar and in Kr are listed in Table D.1 and Table D.2 in Appendix D, for the purpose of comparison.

Figure 4.2.2 shows the experimental hexapole transmission curve for a beam of 5% CH_3F seeded in Ar and calculated transmission curves for the possible contributing rotational states, according to the calculations described in Section 4.1.3.2. Figure 4.2.3 shows plots of cross-sections against the measured hexapole voltages for a beam of 5% CH_3F seeded in Ar against a range of quencher gases.

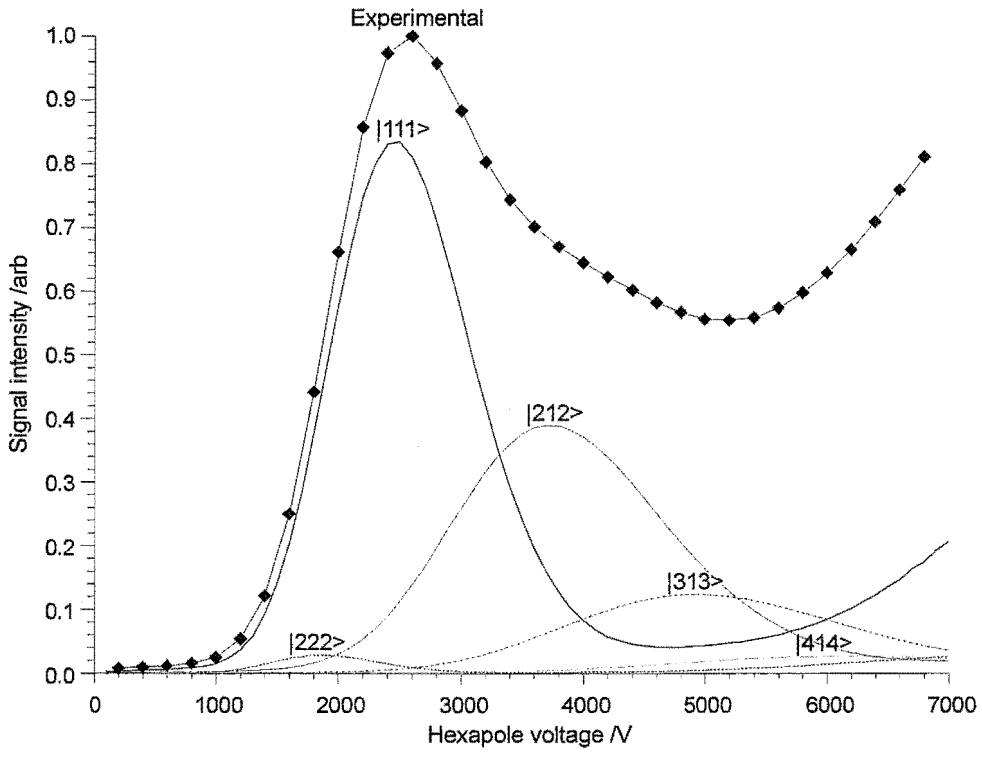

Figure 4.2.2 Experimental transmission curve for a beam of 5% CH_3F seeded in Ar and calculated hexapole transmission curves for possible contributing rotational states.

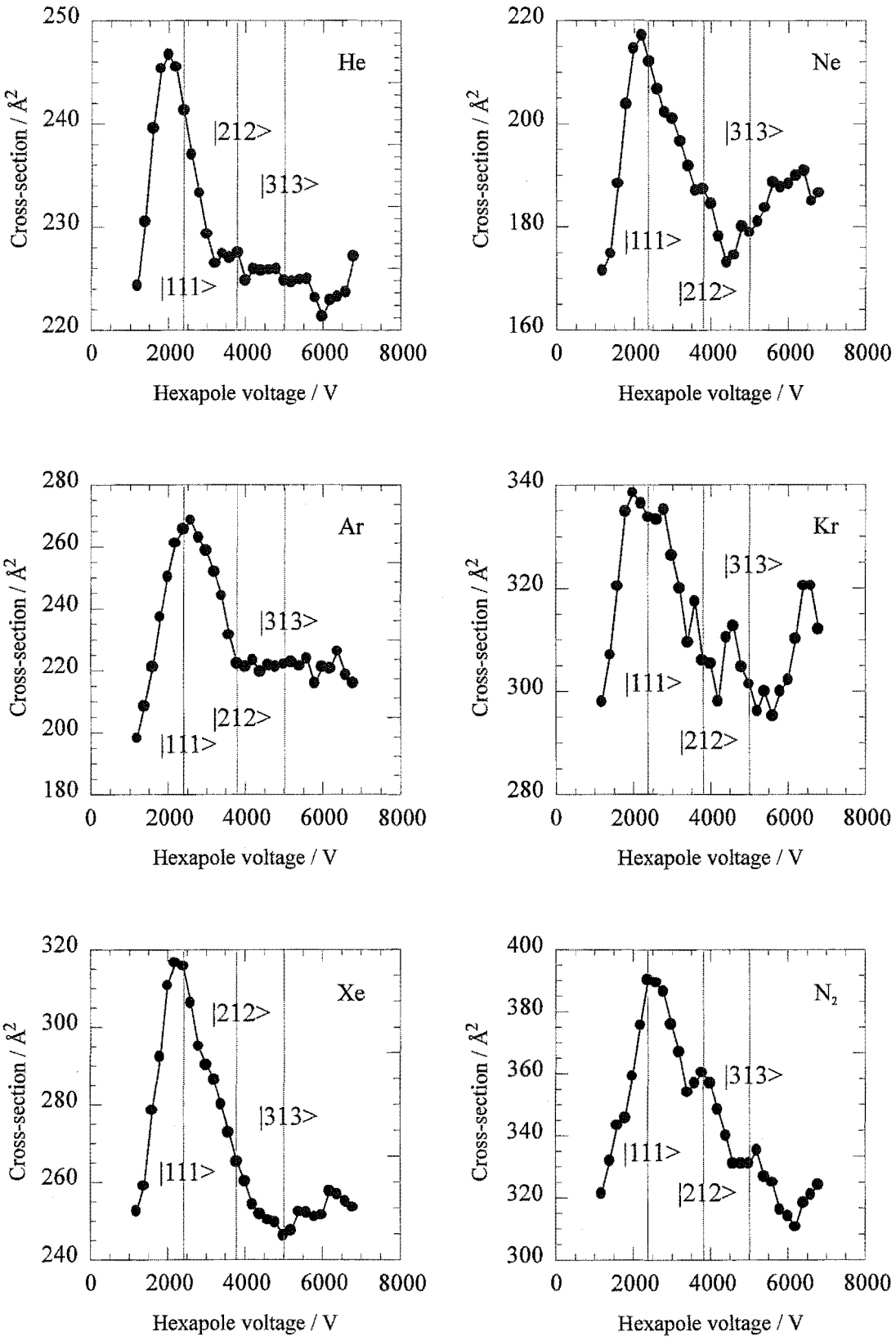

Figure 4.2.3. Cross-sections for beam of 5% CH_3F/Ar with scattering gases, He, Ne, Ar, Kr, Xe, and N_2, plotted against the hexapole voltages.

The major component of the beam focused below the hexapole voltage of 7 kV is the $|111\rangle$ upper Stark state. The upper Stark-state defocusing cross-sections, shown in Figure 4.2.3, follows a trend with the maximum value found at the hexapole voltage corresponding to the peak of the $|111\rangle$ state transmission curve, shown in Figure 4.2.2. This suggests that the defocusing cross-sections of the upper Stark-state molecules are rotational state dependent.

4.2.3 Cross-section results – MBER experiment

Cross-sections for specific rotational states could be determined from attenuation experiments conducted using the MBER technique described in Section 2.4. Table 4.2.2 lists cross-sections determined for specific quantum states in a beam of 10% CH_3F seeded in Ar scattered against Ar using the technique of MBER for hexapole voltages corresponding to transmission curve maxima. Cross-sections, determined for the same quantum state, showed a dependence on the hexapole voltages outside the standard deviation for the cross-sections measured at the peaks in the transmission curve. The data shown in Table 4.2.2 were measured after a careful alignment of the machine and correspond to the same conditions under which the transmission curves in Figure 4.1.17 (b) were collected. The dependence of the measured cross-sections on the hexapole voltage is discussed in the following section.

Table 4.2.2 Cross-sections measured for a beam of 10% CH_3F/Ar scattered against Ar using the technique of MBER at hexapole voltages corresponding to the peaks in the transmission curves shown in Figure 4.1.17 (b).

State	Hexapole voltage /V	Cross-section /Å^2	# points average
$\|11\rangle$	600	199 ± 10	11
$\|11\rangle$	1600	168 ± 16	10
$\|21\rangle$	800	210 ± 14	7
$\|21\rangle$	1800	197 ± 16	14
$\|21\rangle$	4500	148 ± 13	9
$\|31\rangle$	3400	180 ± 24	12

Table 4.2.3 Cross-sections and $\sigma v^{-0.4}$ determined for beams of seeded methyl halides against a range of quencher gases. For a beam of 10% CH_3F seeded in Ar, attenuation experiments for the $|11\rangle$ state were carried out at a hexapole voltage of 5200 V. For beams of 50% CH_3Cl seeded in Ar and 50% CH_3Br seeded in Kr attenuation experiments for the $|21\rangle$ state were carried out at a hexapole voltage of 3000 V.

Beam specie	Scattering gas	Cross-sections /Å^2	# pts aver	$\sigma v^{-0.4}$ /Å^2 (m s^{-1})$^{-0.4}$
10% CH_3F/Ar	He	138 ± 8	10	10.0
10% CH_3F/Ar	Ar	160 ± 9	10	12.7
10% CH_3F/Ar	Xe	179 ± 16	10	14.3
10% CH_3F/Ar	N_2	165 ± 11	10	13.1
10% CH_3F/Ar	CO_2	162 ± 15	10	12.9
10% CH_3F/Ar	CH_4	213 ± 31	10	16.7
10% CH_3F/Ar	CH_3F	367 ± 30	10	29.1
10% CH_3F/Ar	SF_6	177 ± 14	10	14.2
50% CH_3Cl/Ar	He	149 ± 24	9	11.0
50% CH_3Cl/Ar	Ar	184 ± 24	9	14.9
50% CH_3Cl/Ar	Kr	191 ± 7	9	15.6
50% CH_3Cl/Ar	Xe	201 ± 11	7	16.4
50% CH_3Cl/Ar	N_2	184 ± 15	6	14.8
50% CH_3Cl/Ar	CO	187 ± 12	9	15.1
50% CH_3Cl/Ar	CH_4	226 ± 21	9	17.9
50% CH_3Cl/Ar	CH_3F	318 ± 23	10	25.7
50% CH_3Cl/Ar	CH_3Cl	306 ± 22	11	24.9
50% CH_3Cl/Ar	SF_6	190 ± 16	8	15.5
50% CH_3Br/Kr	Kr	207 ± 20	9	17.6
50% CH_3Br/Kr	N_2	234 ± 17	10	19.6
50% CH_3Br/Kr	CO	219 ± 10	10	18.4
50% CH_3Br/Kr	CH_3Br	308 ± 27	10	26.2

In order to compare the effect of properties such as polarisability and dipole moment on cross-section, measurements were made for beams of methyl halides against several quencher gases under identical conditions. For CH_3F, a beam of 10% CH_3F seeded in Ar was used, and attenuation experiments have been conducted for the $|11\rangle$ state at a hexapole voltage of 5200 V, which gave the optimum signal for the beam. For CH_3Cl and CH_3Br, beams of 50% CH_3Cl seeded in Ar and 50% CH_3Br seeded in Kr were used.

Attenuation experiments conducted for both beams are for the $|21\rangle$ state at a hexapole voltage of 3000 V, which gave the optimum signal for both beams. Cross-section results are summarised in Table 4.2.3.

4.2.3.1 Hexapole voltage dependence

State specific attenuation cross-sections were found to depend on the hexapole voltage as a result of the varying electric field strength experienced by the molecules. This suggests that the cross-sections could be related to the Stark energy, which is dependent on the electric field strength as well as the rotational state. The interaction potential for this type of collision cross-section is dominated by the attractive van der Waals interaction, $V(r) = C/r^6$. The interaction energy, in this case, is assumed to be the Stark energy, $-\mu E\langle\cos\theta\rangle$. Therefore, the cross-section, σ, should be related to the Stark energy, that is, $V(r)$, so

$$\sigma = \pi r^2 = \pi\left(\frac{C}{V(r)}\right)^{\frac{1}{3}}$$

$$\sigma \propto V(r)^{-\frac{1}{3}} = (-\mu E\langle\cos\theta\rangle)^{-\frac{1}{3}} \propto \left(U_0\frac{M_J K}{J(J+1)}\right)^{-\frac{1}{3}} \qquad (4.2.9)$$

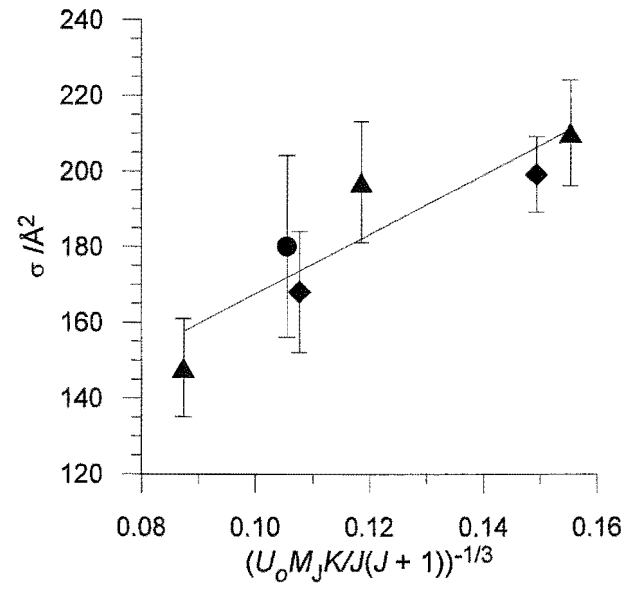

Figure 4.2.4 Plot of σ against $U_0M_JK/J(J+1)^{-1/3}$ for data in Table 4.2.2. The diamonds are for the $|11\rangle$ state, the triangles are for the $|21\rangle$ state and the circle is for the $|31\rangle$ state.

Figure 4.2.4 shows a plot of the cross-sections taken from Table 4.2.2 against the corresponding $[U_0 M_J K/J(J+1)]^{-1/3}$. The straight-line fit in the plot indicates that the experimental cross-sections are indeed related to the Stark energy. This supports the suggestion that ΔM_J transitions are involved in the attenuation process for the upper Stark-state molecules.

When a molecule in a higher quantum state undergoes a collision with a scattering gas particle, it could be relaxed into the monitored state, thus contributing to the signal. This would then partially compensate for the lost of signal intensity due to the attenuation process and effect the resulting cross-section. Figure 4.2.5 (a) shows the transmission curves of the three highest populated states in a beam of 3% CH_3F/Ar. At a hexapole voltage of 2100V, only a small fraction of the |21> state is focused, whereas at 3000V, all three states are focused. Figure 4.2.5 (b) shows the relative signal intensities for different $|JK\rangle$ states measured at the hexapole voltage of 3000V with and without Ar scattering gas in the collision region. This effect on the cross-section, due to the presence of a significant amount of a higher rotational state at the same hexapole voltage, is not significant enough to affect the good correlation shown in Figure 4.2.4. However, it does mean that the cross-sections measured are lower limits.

The effect on the cross-sections due to the collisional relaxation of higher rotational states is difficult to determine. However, this could be minimised in the following ways:

- By lowering the beam temperature, which decreases the population of the higher rotational states.
- By measuring at hexapole voltages where the signal detected for all other states are minimal.
- By measuring at hexapole voltages corresponding to the peaks of the transmission curves, i.e., the state-dependent hexapole focusing voltages, where maximum signal is observed.

(a) 3% CH_3F/Ar transmission curves

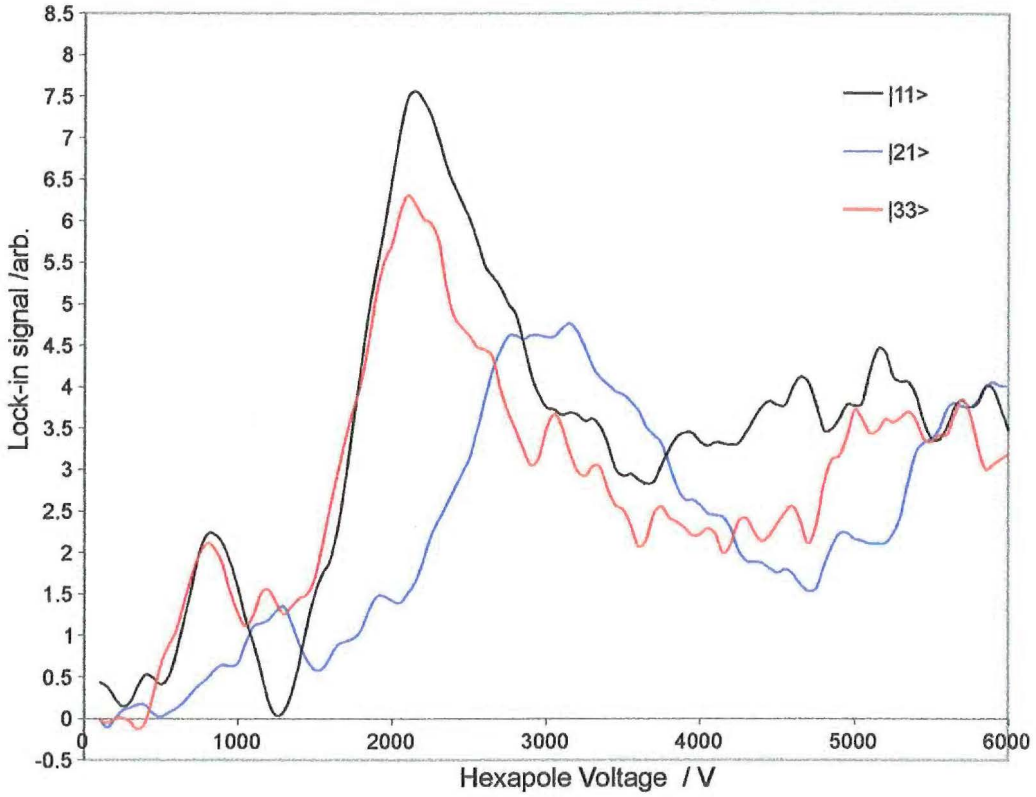

(b) 3% CH_3F/Ar spectra @ 3000 V

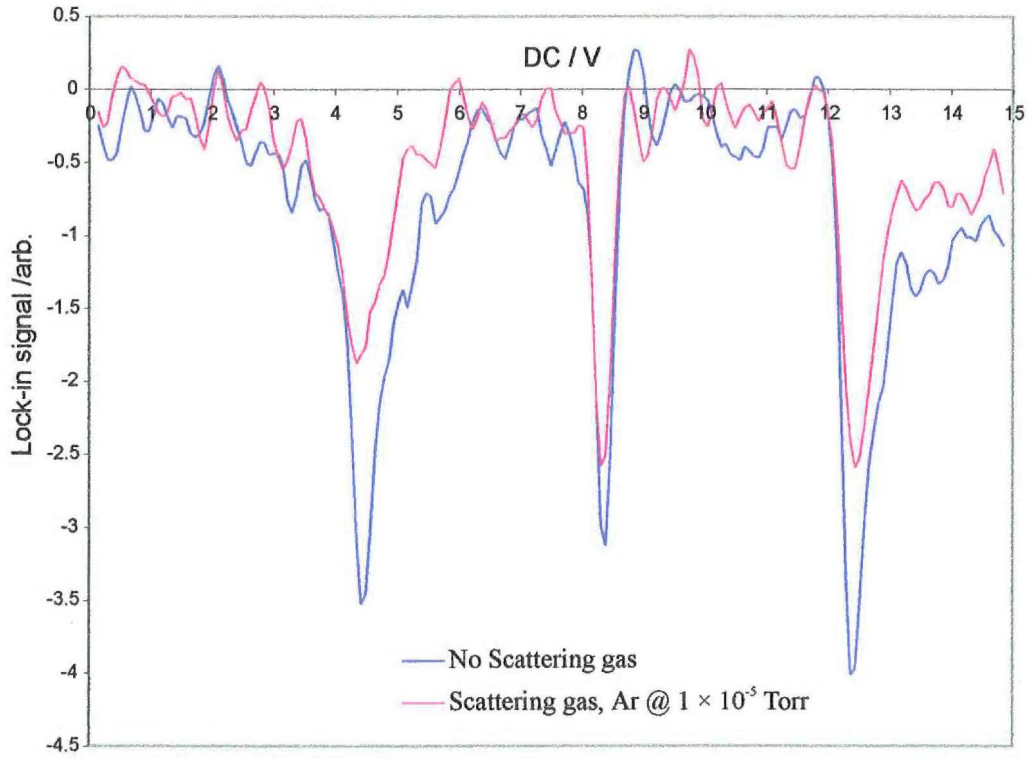

Figure 4.2.5 (a) Hexapole transmission curves for a beam of 3% CH_3F seeded in Ar. (b) Spectra of 3% CH_3F/Ar measured at a hexapole voltage of 3 kV with and without Ar scattering gas in the collision region.

4.2.4 Dependence of cross-section on relative velocity

Collisional relaxation of the upper Stark-state molecules in a hexapole filter has been attributed to the long-range van der Waals attractive interaction, see Section 2.5. Non-reactive scattering cross-sections are expected to show the following velocity dependence,

$$\sigma(v) \propto v^{-0.4} \tag{4.2.10}$$

where v is the relative velocity of the collision partner.

The relative velocities of the collision partners were estimated from Monte Carlo simulations using equations described in Section 2.1. A computer program using Monte Carlo simulations was written in LabVIEW. It takes the average of a large number of calculations for the relative velocities of the beam and scattering gas molecules. The velocities for each calculation are selected using random number generators, which are weighted to the velocity distributions of the beam and the scattering gases. The velocity distribution of the beam was calculated using experimentally determined mean flow velocities and the velocity distribution of the scattering gas was described by the Maxwell distribution at room temperature. Mean flow velocities for the beams were estimated from the modulating frequencies and the phases required for the optimum lock-in signal.

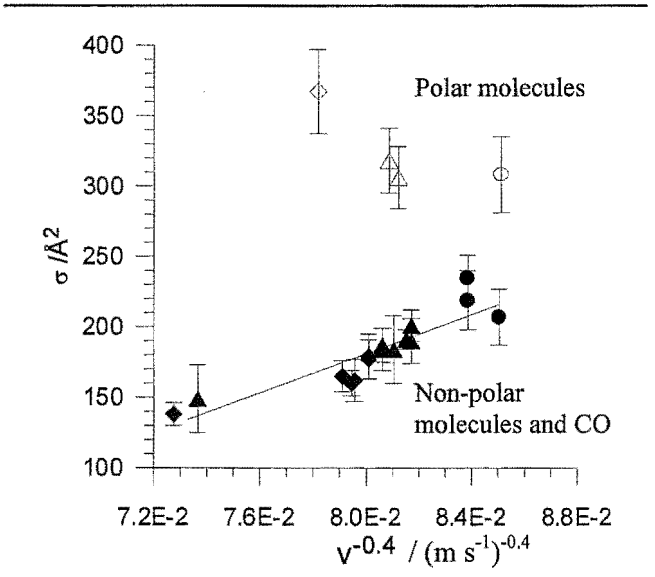

Figure 4.2.6 Cross-sections plotted against $v^{-0.4}$, where v is the relative velocity. Data taken from Table 4.2.3, diamonds are for a beam of 10% CH_3F/Ar, triangles are for a beam of 50% CH_3Cl/Ar, circles are for a beam of 50% CH_3Br/Kr, and the open symbols are for collisions with methyl halide scattering gases.

They are 508 m s^{-1} for a beam of 10% CH_3F seeded in Ar, 498 m s^{-1} for 50% CH_3Cl seeded in Ar, and 452 m s^{-1} for 50% CH_3Br seeded in Kr. Relative velocities for the collision partners in Table 4.2.3 were calculated, and are listed in Table D.3, in Appendix D. Figure 4.2.6 shows the cross-section results plotted against $v^{-0.4}$.

As shown in Figure 4.2.6, a linear relationship is observed for most of the collision pairs. The data represented by the open symbols are for cross-sections with both collision partners being methyl halides. These points do not fall in line with the rest, suggesting that the attractive interaction potential between the two permanent dipoles of the collision partners exerts significant influence on the collisional relaxation process of the symmetric top molecules, and must be taken into consideration.

According to Equation (2.5.14), the total **elastic** scattering cross-section is expressed as,

$$\sigma = \gamma_{MM}(s)\left(\frac{C}{\hbar v}\right)^{2/(s-1)} \tag{2.5.14}$$

where s = 6 and γ_{MM} = 7.547, taken from Table 2.5.1. Figure 4.2.8 shows the experimental cross-sections, as in Table 4.2.3, plotted against calculated cross-sections using Equation (2.5.14) for (a) a beam of 10% CH_3F seeded in Ar and (b) a beam of 50% CH_3Cl seeded in Ar. Linear relationships are found in both of the plots, however, the calculated cross-sections do not agree very well with the experimental results for inelastic

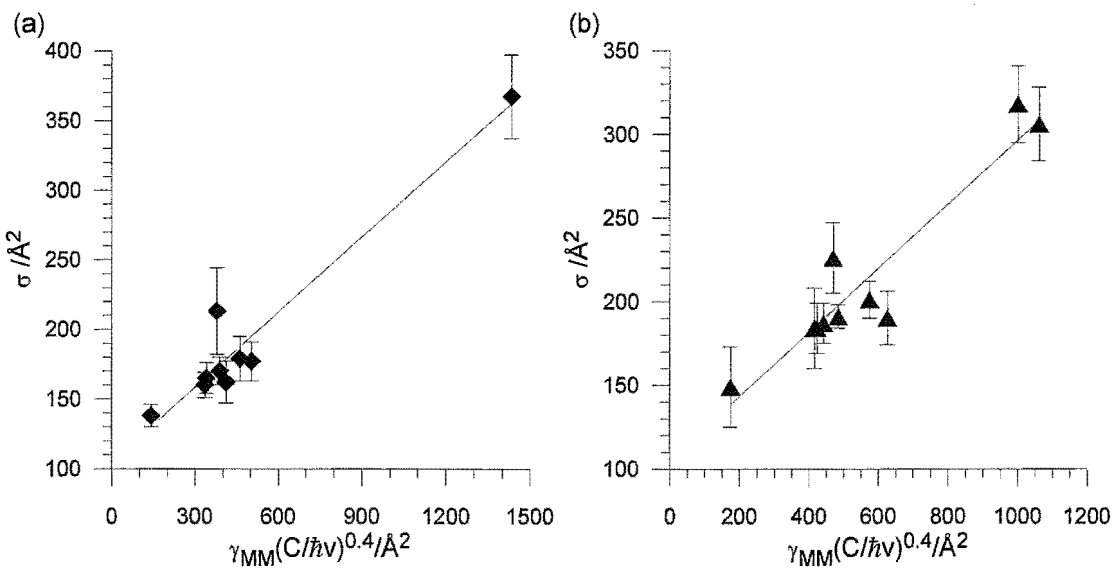

Figure 4.2.7 Experimental cross-sections plotted against calculated cross-sections, $\sigma = \gamma_{MM}(C/\hbar v)^{0.4}$, for (a) a beam of 10% CH_3F seeded in Ar and (b) a beam of 50% CH_3Cl seeded in Ar.

scattering. The trend lines in both plots intercept the experimental data at about 120 Å^2, and the slope for (a) is 0.13 and (b) is 0.15. It is expected that the forces involved in elastic and inelastic scattering processes would be similar and these plots do suggest this is the case. So, the relative velocity factor should be taken into consideration for the estimation of inelastic cross-sections. The intercept would correspond to a hard sphere cross-section and should be related to the physical "size" of the beam molecules.

4.2.5 Correlation with interaction potentials

The magnitudes of the experimental cross-sections and their correlation with the relative velocities, discussed above, imply that the interaction of the collision partners is dominated by the attractive van der Waals interaction, $V(r) = C/r^6$. For collisions between a polar molecule and an atom or a molecule (polar or non-polar), the polarisation interactions include an induced-dipole / induced-dipole interaction (that is the dispersion interaction), a dipole / induced-dipole interaction, and a dipole / dipole interaction when both the collision partners have permanent dipole moments.

$$C = C_{\text{disp}} + C_{\text{dip-ind dip}} + C_{\text{dip dip}}$$

Details of these terms are described by Equations (2.5.17) to (2.5.22) in Section 2.5. The parameters required for the calculation of C, polarisation volumes, ionisation potentials, and the dipole moments for some molecules, are listed in Table A.3 in Appendix A.

The cross-section can be expressed in terms of the van der Waals constant, C, and the interaction potential, $V(r)$,

$$\sigma = \pi r^2 = \pi \left(\frac{C}{V(r)} \right)^{\frac{1}{3}} \tag{4.2.11}$$

Cross-sections calculated using Equation (4.2.11) would be upper limits since they do not take into account the influence of collision velocity on the efficiency of energy transfer.

The cross-sections listed in Table 4.2.3 correspond to the relaxation of symmetric top molecules in specific rotational states by collisions with scattering gas molecules. Cross-sections for a specific rotational state measured for a fixed hexapole voltage should exhibit a linear relationship with $C^{1/3}$. Figure 4.2.7 shows plots of cross-sections against

$C^{1/3}$ calculated for, (a) the $|11\rangle$ state transition measured at 5200V for a beam of 10% CH_3F seeded in Ar, and (b) the $|21\rangle$ state transition measured at 3000V for a beam of 50% CH_3Cl seeded in Ar.

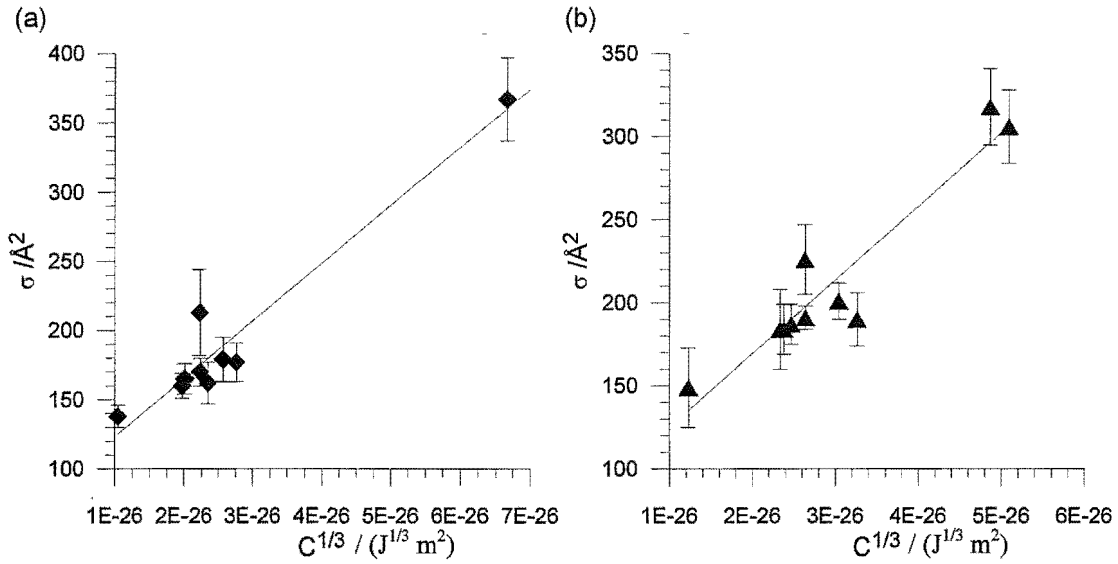

Figure 4.2.8 Cross-sections plotted against $C^{1/3}$ for data in Table 4.2.3: (a) the $|11\rangle$ state in a beam of 10% CH_3F seeded in Ar; (b) the $|21\rangle$ state in a beam of 50% CH_3Cl seeded in Ar.

Both plots in Figure 4.2.8 showed reasonably good correlation despite the neglect of relative velocity. Plots of cross-section against $C^{1/3}v^{-0.4}$ are shown in Figure 4.2.9.

The attenuation experiments carried out using the technique of MBER gave the relative population of the monitored rotational state in the beam. The beam signal was measured as a function of the pressure in the scattering region. The decrease in signal was due to the decrease in the population of the molecules in the monitored state. Elastic scattering results in small angle deviation from the molecular trajectory. Elastic collisions between a supersonic beam molecule in a specific rotational state and the scattering gas would most likely not result in failure to detect the molecule. The exit aperture in these experiments is very large compared to the tiny apertures used in experiments to measure elastic scattering cross-sections. The single hexapole experiments inherently compensate for elastic scattering by measurement of the beam signal difference with the hexapole on and the hexapole off. [Blunt 1998]

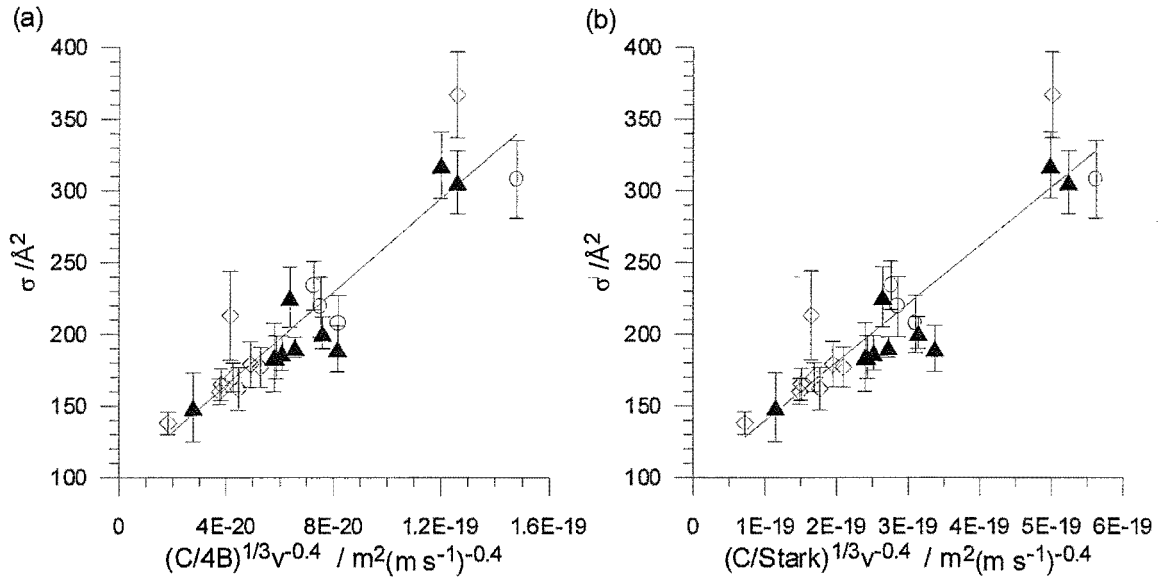

Figure 4.2.9 Cross-sections from Table 4.2.3 plotted against: (a) $(C/4B)^{1/3}v^{-0.4}$; (b) $(C/Stark)^{1/3}v^{-0.4}$. The symbolism: the diamonds are for a beam of 10% CH_3F seeded in Ar, the triangles are for a beam of 50% CH_3Cl seeded in Ar, and the circles are for a beam of 50% CH_3Br seeded in Kr.

According to the spectroscopic selection rules, both ΔJ changing and ΔM_J changing processes could occur, resulting in a decrease in the signal of the monitored rotational state. As previously mentioned in Section 2.5.3, the ΔJ changing transition energy is dependent on the molecule and the ΔM_J changing transition energy is the change in the Stark energy, which is dependent on the external electric field strength and the rotational state of the molecule. According to Equation (4.2.11), cross-section is related to $[C/V(r)]^{1/3}$, where $V(r)$ is the interaction potential. For a ΔJ changing process, where $|K| = 1$, $\Delta J = \pm 1$ and $\Delta M_J = 0$, the minimum transition energy corresponds to $J = 0 \leftrightarrow J = 1$ is equal to $4B$, where B is the rotational constant. Figure 4.2.9 (a) shows the experimental cross-sections plotted against $(C/4B)^{1/3}\ v^{-0.4}$ for all three types of beams. For a ΔM_J changing process, the interaction potential is the Stark energy, which is dependent on the molecular dipole moment, the rotational state and the hexapole electric field strength. The upper Stark-state molecules follow sinusoidal trajectories in a hexapole electric field; therefore, the electric field strength experienced by the molecule in the collision region is not constant. Molecular trajectories in the collision region, that is, the first hexapole filter, can be predicted using equations described in Section 2.3. The root mean square of the maximum displacement of the rotational state specific sinusoidal trajectory was used to

calculate the *average* electric field strength experienced by the molecules in the scattering region. Figure 4.2.9 (b) showed a plot of the experimental cross-sections against $(C/Stark)^{1/3} v^{-0.4}$, where Stark is the Stark energy for a specific rotational state at a specific hexapole field strength.

Both plots in Figure 4.2.9 showed good correlation, suggesting that either or both ΔJ and ΔM_J transition processes could contribute to the attenuation process. The trend lines in both plots intercept the experimental cross-sections at about 110 Å^2. Upper limits for the cross-sections have been estimated using Equation (4.2.4) for comparison with experimental values. For a beam of 10% CH_3F seeded in Ar the experimental cross-sections are ≥138 ± 8 Å^2 (He scattering gas) up to ≥179 ± 16 Å^2 (Xe scattering gas) and ≥367 ± 30 Å^2 (CH_3F scattering gas). For a ΔJ transition the calculated cross-sections are ≤78 Å^2 (He scattering gas) up to ≤192 Å^2 (Xe scattering gas) and ≤500 Å^2 (CH_3F scattering gas). For a ΔM_J transition the calculated cross-sections are ≤311 Å^2 (He scattering gas) up to ≤765 Å^2 (Xe scattering gas) and ≤1986 Å^2 (CH_3F scattering gas). Since the calculated cross-sections are upper limits, the experimental results, which are lower limits, are well within the range calculated for ΔM_J transitions for all collision partners. For ΔJ transitions, the experimental results are either larger or close to the calculated values, expect for the case of CH_3F beams with scattering gases SF_6 and CH_3F. Similar results have been found for CH_3Cl and CH_3Br on a variety of scattering gases. According to these calculations, the ΔM_J transition process appears to be the dominant process occurring in the attenuation experiments. In summary, because of the low energies involved in ΔM_J transitions the collisional relaxation event is inherently longer-range (larger cross-sections) than collisions that relax ΔJ states, which would occur at smaller intermolecular separations giving smaller cross-sections.

4.2.6 Comparison with Literature

Toennies first studied rotational quantum state specific inelastic scattering of molecules in the early 1960's. [Toennies 1960s] A rotationally state-selected beam of TlF prepared using a quadrupole electric field was focused into a gas-filled collision chamber. A second quadrupole filter placed slightly off axis was used to analyse the state distribution

of the scattered beam molecules. The cross-sections for ΔJ transitions were measured for a variety of scattering species; for the $|20\rangle \rightarrow |30\rangle$ transition a cross-section of 2 $Å^2$ was measured with He scattering gas and 375 $Å^2$ for collisions with NH_3. Total attenuation cross-sections for the $J = 2$ rotational state of TlF ranged from 152 $Å^2$, using He as scattering gas, to 2140 $Å^2$ using NH_3. For collisions involving inert gas atoms the dominant term in the interaction potential was the quadrupole induction potential, but for NH_3 the dipole-dipole interaction term was dominant and the large cross-sections were rationalised by the possibility of dipole locking of the TlF and NH_3 molecules. TlF, which exhibits a very high dipole moment (4.23 D) and a large polarisability volume (6.7 $Å^3$), was used in these experiments because of its desirable focusing properties in the quadrupole field. Because of the large dipole moment and small separation of adjacent J rotational levels in TlF, the energy for ΔJ transitions is approximately 8.05 J mol^{-1}, which is available through the quadrupole induction and dipole-dipole terms in the interaction potential at long-range, giving large collision cross-sections.

In a later study, the same group measured inelastic scattering cross-sections using crossed molecular beams for a supersonic beam of CsF seeded in Xe with a range of scattering species. [Borkenhagen 1970s] Again the CsF was chosen for its large dipole moment and focusing behaviour in the quadrupole fields used. The collision cell of the earlier experiments was replaced with a crossed beam of the scattering species in order to reduce the averaging effect of the broad velocity distribution of the scattering gas on the cross-sections. The scattering gases included the inert gases, N_2, CO_2, CH_4, SF_6, and symmetric top alkyl halides, such as CH_3Cl, CH_3Br, CF_3H, CF_3Cl and CF_3Br. The use of crossed beams greatly improved the resolution by narrowing the velocity distribution of the scattering gas relative to the beam-gas experiments. Cross-sections reported for (ΔJ = 1,2; ΔM_J = 0,1) transitions ranged from 0.5 $Å^2$ for the $|30\rangle \rightarrow |10\rangle$ transition with Kr quencher, up to 620 $Å^2$ for the $|20\rangle \rightarrow |30\rangle$ transition with CF_3H.

To assess the reliability of the cross-sections calculated using the van der Waals interaction potential, as shown in Equation (4.2.4), cross-sections were calculated for some of the TlF + inert gas collisions reported by Toennies. In all cases, calculated cross-sections are too high; for example, for a $\Delta J = 1$ transition calculated the cross-sections are

≤236 Å^2 for He scattering gas, ≤451 Å^2 for Ar, and ≤462 Å^2 for N_2, compared with the experimental values of 152, 388, and 343 Å^2 reported by Toennies. Accordingly, the cross-sections that are estimated for ΔJ transitions in this work should also be considered as upper limits. This reinforces the argument that the experimental cross-sections measured in this work correlates better with the cross-sections estimated for ΔM_J transitions.

Cross-sections measured in single hexapole experiments for the attenuation of neat and seeded beams of CH_3Cl with a range of scattering gases have been published. [Blunt 1998] Cross-section results reported here in Section 4.2.2 have also been published in a recent paper, discussing the collisional reorientation of symmetric top molecules in Stark fields. [Hu 1999] Experimental cross-sections are found to lie in the range from 200 Å^2 for a neat CH_3Cl beam on Ne to 670 Å^2 for a beam of 5% CH_3Cl seeded in Xe on N_2. Upper limits to cross-sections were calculated using a van der Waals interaction potential, Equation (4.2.11). For example, the defocusing cross-sections from the $|111\rangle$ state of CH_3Cl in collisions with Ar scattering gas were calculated to be:

- ≤670 Å^2 for a ($\Delta J = 0$; $\Delta M_J = \pm 1$) transition,
- ≤222 Å^2 for a ($\Delta J = +1$; $\Delta M_J = 0$) transition,
- ≤220 Å^2 for a ($\Delta J = +1$; $\Delta M_J = -1$) transition, and
- ≤226 Å^2 for a ($\Delta J = +1$; $\Delta M_J = +1$) transition.

The experimental cross-sections varied from 630 Å^2 at the lowest collision velocity (for a 5% CH_3Cl seeded in Xe beam) to 275 Å^2 at the highest collision velocity (for a neat CH_3Cl beam). For all other collision pairs, the same trend is found. The lowest experimental value is higher than the calculated values for a ($\Delta J + \Delta M_J$) transition and lower than the cross-section calculated for a $\Delta M_J = 1$ transition. Similarly, the highest experimental value is much closer to the value calculated for a $\Delta M_J = 1$ transition. These results support the conclusion that ΔM_J rather than ΔJ transitions are the dominating process for the attenuation of the focused upper Stark-state molecules in a hexapole filter. Calculations for the collision processes involving changes in J, K, M_J, as discussed in Hu *et al*, have also shown that the total collision cross-sections result predominately from ΔM_J transitions and collisions leading to changes in J and K are likely to be unimportant.

Oka *et al* investigated the selection rules, which apply during rotationally inelastic collisions, in NH_3, H_2CO and CH_3F using inverse Lamb dips in infrared laser Stark spectroscopy. [Oka 1973 and Johns 1975] They found very large collision-induced centre dips in laser Stark Lamb dip spectra for $J = K$ levels of CH_3F. These centre dips are the result of a four-level infrared-infrared double resonance effect and they provide information on rotational transitions during intermolecular collisions. Analysis of these large centre dip signals indicated that the rate of $\Delta M_J = \pm 1$ reorientation collisions relative to **all** inelastic collisions was in the order of 70%. It also noted that transitions for which $\Delta M_J > 1$ would increase the proportion of ΔM_J changing collisions.

Upper Stark-state collisional relaxation cross-sections for single rotational states of CH_3F measured in MBER experiments in this research have recently been published. [Vallance 1999] A computer transcription error was made in a conversion between units and the values in Table 1 in the paper should be scaled by a factor of 0.563, the corrected values are shown in Table 4.2.3. The cross-sections measured using this method are smaller compared to the values measured in single hexapole experiments for the same rotational state of CH_3F. This is the result of the difference in the electric field strength (hence ΔM_J transition energy) experienced by the upper Stark-state molecules in the beam. Table 4.2.4 shows the comparison of the *average* electric field strengths, the transition energies and the cross-sections calculated and measured in single hexapole experiments and in MBER experiments for the upper Stark $|111\rangle$ state in beams of seeded CH_3F with Ar scattering gas.

Table 4.2.4 Calculated and experimental cross-sections for the attenuation of the |11> upper Stark state in a beam of 5% CH_3F/Ar with Ar as scattering gas in a single hexapole experiment and in a beam of 10% CH_3F/Ar with Ar as scattering gas in MBER experiments.

Seeded beam mixture	Hexapole voltage / V	*Average* field strength / V m^{-1}	$E(\Delta M_J)$ J mol^{-1}	Calculated σ / Å^2	Experimental σ / Å^2
5% CH_3F/Ar	2600	39394	0.074	1255	270
10% CH_3F/Ar	5200	381468	0.712	589	160

Because the electric field strength experienced by upper Stark-state molecules is higher, the energy required for the rotational state transition is higher. The cross-section decreases as a result of the increased transition energy. As discussed in Section 4.2.3.1,

the cross-section for energy transfer due to the Stark energy is indeed related to the hexapole electric field. These results show the influence of the external electric field strength (Stark energy) on the cross-section and agree with the argument that the ΔM_J transition process is the dominant process in the collisional relaxation of the upper Stark-state molecules in a hexapole electric field.

Another powerful tool for the study of the interactions between molecules is the pressure-broadened linewidths of the rotational spectra of molecules. By measuring the width of microwave spectral lines, it is possible to identify the major types of intermolecular forces responsible for the broadening. [Anderson 1949] The broadening of CH_3F spectral lines in the presence of Stark fields has been well investigated by Lemaire *et al*, providing valuable insight into the collisional coupling effects between Stark components. [Lemaire 1997 and 1999] This method has been used to measure collision cross-sections for rotational transitions caused by dipole-quadrupole interactions between CHF_3 and non-polar molecules; showing that the first order dispersion interaction contributes largely to the collision cross-section. [Gierszal 1998]

Another useful tool for the study of collisional relaxation is the technique of double resonance experiments. [Freund 1973] Information on vibrational relaxation in CH_3F has been obtained from infrared-infrared double resonance experiments. [Preses 1972] Shoemaker *et al* have reported cross-sections for reorienting transitions of CH_3F for low-angular momentum states (J,K = 4,3 or 5,3) to be approximately 100 $Å^2$, and estimated the cross-section for a high-angular momentum state (J,K = 12,2) to be about 100 times smaller. [Shoemaker 1974] The cross-sections were derived from the intensity ratios of satellite resonance lines in four-level microwave optical-double-resonance spectra of CH_3F. However, the microwave experiments do not supply information on the relative velocities of the collision pairs, and the monitored satellite resonance line corresponds to a specific level-configuration where the collisionally coupled M_J states involve one or more quantum jumps. Shoemaker *et al* estimated the cross-section for reorienting CH_3F collisions from the intensity ratio of the satellite lines to the primary lines. They did not observe the satellite lines for spectra of high J and low K (J,K = 12,2) transitions, concluding that cross-sections for such states were about 100 times smaller than that for lower J states (J,K = 4,3 or 5,3).

Shoemaker *et al* have presented the argument that molecules with high J and low K states were not tipped easily, in conformity with the classical argument that more rapidly rotating objects were more difficult to reorient using an external force. Conversely, the cross-sections measured for the J,K = 1,1 state and other low level J states (reported in this thesis) would be greater than those found for the J,K = 4,3 or 5,3 states. In addition, the optical-optical-resonance spectra were recorded as a function of the Stark field strength with two cw lasers locked to a fixed frequency difference, and the Stark energies for the resonance transitions could be calculated from the positions of the satellite resonance lines in the spectra. The Stark energy corresponding to the (J,K = 4,3 or 5,3) spectrum is much smaller than the Stark energy corresponding to the (J,K = 12,2) spectrum reported by Shoemaker *et al*. According to Equation (4.2.4), the cross-section estimated for the (J,K = 12,2) spectrum (with a higher transition energy) is expected to be smaller than that for the (J,K = 4,3 or 5,3) spectrum. The finding in this research is, therefore, in agreement with shoemaker *et al*.

Silvers *et al* have studied the collisional depolarisation of state selected BaO $A\ ^1\Sigma^+$ (J, M_J) measured by optical-optical double resonance (OODR). [Silvers 1981] They have found a total M_J-changing cross-section of 8.4 ± 2.4 Å^2 for BaO ($A\ ^1\Sigma^+$) colliding with CO_2. They concluded that optical-optical double resonance spectroscopy was well suited for the investigation of elastic collisions and inelastic M_J-changing collisions. The extent of polarisation transfer by collisions could be characterised, and rules governing M_J changes determined. Their results have indicated the importance of long-range interactions in effecting molecular depolarisation. Snow *et al* reported a variation of the OODR technique using multi-photon ionisation, which can be used to study collisional disalignment of a large variety of electronic and rovibrational states of molecules. [Snow 1988] They have used this technique to study M_J-changing collisions of selected rovibrational levels of the $A\ ^2\Sigma^+$ states of NO with molecules possessing dipole and quadrupole moments. The cross-sections were not measurable (<1 Å^2) for molecules possessing no permanent moments and were up to 22 ± 5 Å^2 for collisions with CHF_3. They have proposed that disalignment (collisional redistribution of M_J levels) and quenching of electronically excited Rydberg states of NO (studied by Asscher and Haas [Asscher 1982]) were unrelated. The former is dominated by the multi-pole moments of the collision pair, whereas the ion-pair character of the collision intermediate dominates

the quenching cross-section. Such ion-pair reactions could take place at large inter-nuclear distances, accounting for large quenching cross-sections. This argument is not in disagreement with the finding in this research, since the cross-sections determined from the attenuation experiment are due to the change in the M_J rotational state, which is dominated by the attractive interaction potential (long-range interactions) and is dependent on the Stark energy. Although the signal intensity detected by the lock-in-amplifier is relative to the total signal measured by the mass spectrometer, the lock-in signal results from ΔM_J transitions of specific rotational states.

Recently, Hain *et al* following a suggestion made by Dr D.A. Blunt at a conference, studied the rotational-state-resolved collisional attenuation of hexapole focused hydroxyl radical beams by gas-phase target molecules using an instrument based on our single hexapole experiment. [Hain 1999] They have measured cross-sections for a beam of hydroxyl radicals rotationally state-selected by a hexapole filter using a range of scattering gases in the hexapole field. They have also found that molecules, which are elastically scattered, are still being successfully transmitted to the detector, causing a broadening in the velocity distribution of the beam signal. They have presented the argument that the apparent differences in cross-sections of different rotational states were an artifact of relying on peak heights to ascertain rotational state populations, which were perturbed by the elastic collision broadening in the velocity distribution of molecules. They have concluded that there was no evidence in their data for preferential scattering out of any of the states resolved in their focusing spectra, therefore, the dominant scattering mechanism was elastic scattering rather than M_J-changing collisions. The MBER experiments rely on the focusing of elastically scattered products and in addition features a large exit aperture in order to preclude an elastic scattering contribution to the attenuated lock-in signal. Hain *et al* confirmed that the elastically scattered products are focused even with their smaller exit aperture (2.5 mm). This supports our contention that the signal attenuation in the MBER experiments is dominated by inelastic scattering.

CHAPTER 5 CONCLUSION AND FUTURE DEVELOPMENTS

5.1 Conclusion

The technique of molecular beam electric resonance spectroscopy has proven to be a powerful tool for studying the rotational state-dependent properties of molecules with permanent dipole moments, such as symmetric top molecules. In the future, this technique could be very useful in monitoring selected rotational states in crossed beam experiments. The ability to easily record a spectrum of the rotational states in a supersonic beam of symmetric top molecules facilitates the process of signal optimisation through the control of the supersonic expansion, seeded beams, and the selection of hexapole voltage. It also provides information on the beam velocity and gives an estimation of the beam temperature.

The trajectories of the molecules in the hexapole fields are well characterised. Discrepancies between calculated and experimental transmission curves arise from elastic scattering broadening of the beam velocity distribution and the discontinuity of the focusing trajectory due to the presence of a uniform electric field in the C-cell. The rotational state population distribution of the molecular beam could be deduced from a comparison of the state-independent transmissions curves of all the observable rotational states in the beam.

Upper Stark-state defocusing cross-sections determined using the technique of MBER is largely contributed by ΔM_J transitions. Cross-sections for the relaxation of the $|111\rangle$ upper Stark state for CH_3F in a beam of 10% CH_3F seeded in Ar range from 138 $Å^2$ on He scattering gas to 367 $Å^2$ on CH_3F scattering gas. Cross-sections for the relaxation of $|211\rangle$ upper Stark state for CH_3Cl in a beam of 50% CH_3Cl seeded in Ar range from 149 $Å^2$ on He scattering gas to 318 $Å^2$ on CH_3F scattering gas. Cross-sections for the relaxation of $|211\rangle$ upper Stark state for CH_3Br in a beam of 50% CH_3Br seeded in Kr range from 207 $Å^2$ on Kr scattering gas to 308 $Å^2$ on CH_3Br scattering gas.

Contributions to the collision cross-section from changes in J, K rotational states are insignificant compared to changes in M_J. Experimental cross-sections have shown to be dependent on the relative velocities of the collision partners, hexapole electric field strength, and rotational quantum states of the beam molecules, that are characteristic to the ΔM_J transitions. Even though, the contribution from elastic scattering in the experimental cross-section is not determined, it is not likely to be significant enough to hinder the characteristics of the ΔM_J transitions.

Collisional relaxation through ΔM_J transition is dominated by attractive long-range interaction potential, including the dispersion, dipole / induced-dipole and dipole / dipole interactions. Under the MBER experiments, cross-sections are best measured for individual rotational states at the hexapole voltage corresponding to the first node of the sinusoidal trajectory at the exit of the second hexapole, where the elastic scattering would have the least influence on the transmission of the upper Stark-state molecules.

5.2 Future developments

In the future, the MBER arrangement will be used in the study of electron/ion collisions with rotational state selected molecules by crossed beam experiments. The molecular beam machine has been modified for the electron/ion-molecule crossed beam experiments. The ion source chamber can either accommodate a ion source, developed to produce an ion beam, or an electron gun, which produces an electron beam and was used in the crossed beam experiments investigating orientation effects in electron impact ionisation. [Vallance 1999a, Aitken 1995 and 1995a, and Blunt 1995] An ion imaging system has been installed in the detection chamber for the detection of product ions in the crossed beam experiment. (See Section 3.1.9.) Ion imaging detection is a fairly new technique and was originally developed for use in the study of photo-dissociation processes. [Compton 1993] The ion imaging technique allows the spatial distribution of a product species to be directed observed, and provides information for the entire three-dimensional angular and velocity distribution of a reaction product in essentially one single measurement. A detailed description of the ion imaging system has been reported in the Ph.D. thesis of a former colleague, Dr C. Vallance. [Vallance 1999a]

Electron/ion-molecule crossed beam experiments have been initiated, and ions produced in electron-molecule crossed beam experiment have been detected. However, a large amount of ions produced by the ionisation of the background particles have also been detected. Numerous attempts to eliminate the background signal and to improve the resolution of the detection system have been made with limited success. The molecular beam machine is currently under modification to improve the vacuum quality in the detection chamber. Several other experimental components are also under modification in order to improve the resolution of the detection system.

It is anticipated that the problems associated with the detection system should be resolved in the next six months, and the rotational state dependent properties will be studied in electron/ion-molecule crossed beam experiments, combining the ion imaging detection technique with the MBER technique.

REFERENCES

Aitken 1994 C.G. Aitken, D.A. Blunt, and P.W. Harland, *J. Chem. Phys*, 101, p. 11074–6, **1994**.

Aitken 1995 C.G. Aitken, Ph. D. thesis – Electron impact ionisation of molecular clusters and spatially oriented molecules, University of Canterbury, Christchurch, New Zealand, **1995**.

Aitken 1995a C.G. Aitken, D.A. Blunt, and P.W. Harland, *Int. J. Mass Spectrom. Ion Procs.*, 149/150, p. 279-86, **1995**.

Anderson 1949 P.W. Anderson, *Phys. Rev.*, 76, p. 647-661, **1949**.

Anderson 1966 J.B. Anderson, R.P. Andres, and J.B. Fenn, Supersonic nozzle beams, *Chpt 8* in Molecular beams *edited by J. Ross*, Advances in Chemical Physics volume X, John Wiley & Sons, Inc., **1966**.

Anderson 1997 R.W. Anderson, *J. Phys. chem. A*, 101, p. 7664-7673, **1997**.

Anton 1988 H. Anton, Calculus with analytic geometry, John Wiley & Sons, Inc. **1988**.

Asscher 1982 M. Asscher and Y. Haas, *J. Chem. Phys.*, 76, p. 2115-2126, **1982**.

Atkins 1998 P.W. Atkins, Physical Chemistry 6th edition, Oxford university press, **1998**.

Bernstein 1982 R.B. Bernstein, Chemical dynamics via molecular beam and laser techniques, Clarendon Press, Oxford, **1982**.

Bernstein 1986-9 (i) S.E. Choi and R.B. Bernstein, *J. Chem. Phys.*, 85, p. 150-161, **1986**. (ii) S.R. Gandhi and R.B. Bernstein, *J Chem. Phys.*, 88, p. 1472-3, **1988**. (iii) Q. Xu, K. Jung, and R.B. Bernstein, *J. Chem. Phys.*, 89, p. 2099-2106, **1988**. (iv) Q. Xu, M.A. Quesada, K. Jung, R. Scott Mackay and R.B. Bernstein, *J. Chem. Phys.*, 91, p. 3477-

3482, **1989**. (v) R.B. Bernstein, S.E. Choi, and S. Stolte, *J. Chem. Soc., Faraday Trans. 2*, 85, p. 1097-1113, **1989**.

Beuhler 1966 R.J. Beuhler, R.B. Bernstein, and K.H Kramer, *J. Am. Chem. Soc.*, 88, 5331, **1966**.

Biesen 1988 J.J.H. van den Biesen, Elastic Scattering I: Interal Cross Sections, *Chpt 19* in Atomic and Molecular Beam Methods Volume 1: Part II, *edited by G. Scoles*, Oxford University press, **1988**.

Blunt 1995 D.A. Blunt, Ph. D. thesis – Studies of state-selected and spatially oriented molecules, University of Canterbury, Christchurch, New Zealand, **1995**.

Blunt 1998 D.A. Blunt, S.A. Harris, W.P. Hu, and P.W. Harland, *J. Phys. Chem. A*, 102, p.1482, **1998**.

Borkenhagen 1970s (i) U. Borkenhagen, H. Malthan, and J.P. Toennies, *Chem, Phys. Lett.*, 41, p. 222, **1976**. (ii) U. Borkenhagen, H. Malthan, and J.P. Toennies, *J. Chem. Phys.*, 71, p. 1722, **1979**.

Brooks 1966 P.R. Brooks, and E.M. Jones, *J. Chem. Phys.*, 45, p. 3449-3450, **1966**.

Brooks 1969 P.R. Brooks, E.M. Jones, and K. Smith, *J. Chem. Phys.*, 51, p. 3073-3081, **1969**.

Brooks 1996 P.R. Brooks, P.W. Harland, Effect of Spatial Orientation on Electron Transfer and Electron Impact Ionisation in the Gas Phase, Advances in Gas Phase Ion Chemistry Volume 2, *edited by N.G. Adams and L.M. Babcock*, JAI Press Inc., London, **1996**.

Buck 1988 U. Buck, General Principles and Methods, *Chpt 18* in Atomic and Molecular Beam Methods Volume 1: Part II – Molecular Scattering, *edited by G. Scoles*, Oxford University press, **1988**.

Budenholzer 1975 F.E. Budenholzer, J.J. Galante, E.A. Gislanson, and A.D. Jorgensen, *Chem. Phys. Lett.*, 33, p. 245, **1975**.

Bulthuis 1991 J. Bulthuis, J.B. Milan, M.H.M. Janssen, and S. Stolte, *J. Chem. Phys.*, 94, p. 7181, **1991**.

Busch 1966 F. von Busch, *Z. Physik*, 193, p. 412, **1966**.

Cameron 1991 B.R. Cameron, and P.W. Harland, *J. Chem. Soc. Faraday. Trans.* 87, p.1069, **1991**.

Cameron 1993 B.R. Cameron, Ph. D. thesis – Investigations of the flow dynamics of supersonic molecular beams and the ionisation of molecular clusters by electron impact, University of Canterbury, Christchurch, New Zealand, **1993**.

Cameron 1994 B.R. Cameron, and P.W. Harland, *Rev. Sci. Instrum.*, 65, p.108, **1994**.

Cameron 1994a B.R. Cameron, C.G. Aitken, and P.W. Harland, *J. Chem. Soc. Faraday Trans.*, 90, p.935, **1994**.

Campargue 1984 R. Campargue, *J. Phys. Chem.*, 88, p. 4466-4474, **1984**.

Chakravorty 1982 K.K. Chakravorty, D.H. Parker and R.B. Bernstein, *J. Chem. Phys.*, 68, p. 1, **1982**.

Compton 1993 R.G. Compton and G. Hancock (editors), Research in Chemical Kinetics, Volume 1, Elsevier Science Publishers, **1993**.

Fluendy 1973 M.A.D. Fluendy and K.P. Lawley, Chemical Applications of Molecular Beams Scattering, Chapman and Hall, London, **1973**.

Freund 1973 S.M. Freund, J.W.C. Johns, A.R.W. McKellar, and T. Oka, *J. Chem. Phys.*, 59, p. 3445-3453, **1973**.

Gandhi 1987 S.R. Gandhi. T.J. Curtiss, and R.B. Bernstein, *Phys. Rev. Lett.*, 59, p. 2951-4, **1987**.

Gandhi 1988 S.R. Gandhi and R.B. Bernstein, *Z. Phys. D*, 10, p. 179-85, **1988**.

Gandhi 1990 S.R. Gandhi and R.B. Bernstein, *J. Chem. Phys.*, 93, p. 4024-4032, **1990**.

Gentry 1974 W.R. Gentry and C.F. Giese, *Rev. Sci. Instrum.*, 46, p. 104, **1974**.

Gierszal 1998 S. Gierszal, J. Galica, and E. Mis-Kuzminska, *J. Chem. Phys.* 108, p. 8976-8982, **1998**.

Goldberger 1975 M.L. Goldberger and K.M. Watson, Collision theory, Robert E. Krieger Publishing Company, Huntington, New York, **1975**.

Hain 1999 T.D. Hain, L. Baars-Hibbe, and T.J. Curtiss, *Chem. Phys. Lett.*, 305, p. 348-352, **1999**.

Harris 1997 S.A. Harris, Ph. D. thesis – Studies of Ion Molecule Reactive Processes, Electron Impact Ionisation, and Inelastic Collisions in State Selected Molecular Beams, University of Canterbury, Christchurch, New Zealand, **1997**.

Hu 1999 W.P. Hu, S.A. Harris, P.W. Harland, and L.F. Phillips, *Int. J. Quantum Chem.*, 71, p. 75-82, **1999**.

Johns 1975 J.M. Johns, A.R.W. McKellar, T. Oka, and M. Römheld, *J. Chem. Phys.*, 62, p. 1488, **1975**.

Kaesdorf 1985 S. Kaesdorf, G. Schönhense, and U. Heinzmann, *Phys. Rev. Lett.*, 54, p. 885-8, **1985**.

Kantrowitz 1951 A. Kantrowitz and J. Grey, Rev. Sci. Instrum., 22, p. 328, **1951**.

Kemble 1958 E. C. Kemble, The Fundamental Principles of Quantum Mechanics, Dover Publications, Inc., **1958**.

Kennard 1938 E.H. Kennard, Kinetic Theory of Gases with an Introduction to Statistical Mechanics, M^{c}Graw-Hill Book Company, Inc., **1938**.

Kramer 1965 K.H. Kramer and R.B. Bernstein, *J. Chem. Phys.*, 42, p. 767-770, **1965**.

LabVIEW 1994 LabVIEW graphical programing for instrumentation Student Edition Version 3.1, National instruments, Austin, TX, **1994**.

Landau 1959 L.D. Landau and E.M. Lifshitz, Quantum mechanics - non-relativistic theory, *translated from Russian by J.B. Sykes and J.S. Bell*, Pergamon Press, **1959**.

Lemaire 1997 V. Lemaire, L. Dore, G. Cazzoli; G. Buffa, O, Tarrini, and S. Belli, J. Chem. Phys., 106, p. 8995-9003, **1997**.

Lemaire 1999 V. Lemaire, L. Dore, G. Cazzoli; G. Buffa, O, Tarrini, and S. Belli, J. Chem. Phys., 110, p. 9418-9425, **1999**.

Levine 1970a I.N. Levine, Quantum Chemistry Volume I: Quantum Mechanics and Molecular Electronic Structure, Allyn and Bacon, Inc., **1970**.

Levine 1970b I.N. Levine, Quantum Chemistry Volume II: Molecular Spectroscopy, Allyn and Bacon, Inc., **1970**.

Lide 1998 D.R. Lide (Editor-in-chief), *CRC Handbook of Chemistry and Physics*, 79th edition, CRC Press LLC, **1998**.

Massey 1933 H.S.W. Massey and C.B.O. Mohr, *Roy. Soc. Proc.*, 141, p. 434-453, **1933**.

Massey 1934 H.S.W. Massey and C.B.O. Mohr, *Roy. Soc. Proc.*, 144, p. 188-205, **1934**.

Massey 1969 H. S. W. Massey, and E. H. S. Burhop, Electronic and Ionic impact phenomena Volume I, Oxford University Press: Oxford at the Clarendon press, **1969**.

Massey 1971 H. S. W. Massey, E. H. S. Burhop, and H. B. Gilbody, Electronic and Ionic impact phenomena Volume III, Oxford University Press: Oxford at the Clarendon press, **1971**.

Margenau 1971 H. Margenau and N. R. Kestner, Theory of intermolecular forces 2nd edition, Pergamon press, **1971**.

Miller 1988 D. R. Miller, Free Jet Sources, *Chpt 2* in Atomic and Molecular Beam Methods Volume 1, *edited by G. Scoles*, Oxford University press, **1988**.

Mott 1949 N.F. Mott and H.S.W. Massey, The theory of atomic collisions, Clarendon Press, Oxford, **1949**.

Muenter 1992 J.S. Muenter, Magnetic and Electric Resonance Spectroscopy, *Chpt 2* in Atomic and Molecular Beam Methods Volume 2, *edited by G. Scoles*, Oxford University Press, **1992**.

Oka 1973 T. Oka, *Adv. Atomic Mol. Phys.*, 9, p. 127, **1973**.

Pauly 1988 H. Pauly, Other Low-Energy Beam Sources, *Chpt 3* in Atomic and Molecular Beam Methods Volume 1, *edited by G. Scoles*, Oxford University press, **1988**.

Phillips 1995 L.F. Phillips, *J. Chem. Soc. Faraday Trans.*, 91, p. 4363, **1991**.

Present 1958 R.D. Present, Kinetic Theory of Gases, M^{c}Graw-Hill Book Company, Inc., **1958**.

Preses 1972 J.M. Preses and G.W. Flynn, *Bull. Am. Phys. Soc.*, 17, p. 573, **1972**.

Shirley 1963 J.H. Shirley, *J. Chem. Phys.*, 38, p. 2896-2913, **1963**.

Shoemaker 1974 R.L. Shoemaker, S. Stenholm, and R.G. Brewer, *Phys. Rev. A*, 10, P. 2047-2050, **1974**.

Silvers 1981 S.J. Silvers, R.A. Gottscho, and R.W. Field, *J. Chem. Phys.*, 74, p. 6000-6008, **1981**.

Simion6.0 1995 I. N. E. L. Lockheed Martin Idaho Technologies, Simion6.0, **1995**.

Snow 1988 L.D. Snow, R.N. Compton, and J.C. Miller, *J. Chem. Phys.*, 88, p. 1652-1657, **1988**.

Toennies 1960s (i) J.P Toennies, *Faraday Discuss. Chem. Soc.*, 33, p. 96, **1962**. (ii) J.P. Toennies, *Z. Phys.*, 182, p. 257, **1965**. (iii) J.P. Toennies, *Z. Phys.*, 193, p. 76, **1966**. (iv) H.G. Bennewitz, K.H. Kramer, W. Paul, and J.P. Toennies, *Z. Phys.*, 177, p. 84, **1964**.

Townes 1955 C.H. Townes and A.L. Schawlow, Microwave Spectroscopy, M^{c}Graw-Hill Book Company, Inc., **1955**.

Vallance 1999 C. Vallance, W-P. Hu, and P.W. Harland, *J. Phys. Chem. A*, 103, p. 665-670, **1999**.

Vallance 1999a C. Vallance, Ph. D. thesis – Studies of Elementary Collision Processes Under Single Collision Conditions, University of Canterbury, Christchurch, New Zealand, **1999**.

Vargaftik 1994 N.B Vargaftik, *Handbook of thermal conductivity of liquid and gases*, CRC Press, **1994**.

Wiediger 1998 S.D. Wiediger, P.W. Harland, J.R. Holt, and P.R. Brooks, *J. Phys. Chem. A*, 102, p.1112-1118, **1998**.

Zare 1988 R.N. Zare, Angular Momentum: Understanding spatial aspects in Chemistry and Physics, John Wiley & Sons, Inc., **1988**.

APPENDIX A TABLES OF USEFUL FACTORS

Table A.1 Useful constants

Quantity	Symbol	Value
Speed of light	c	2.99792458 E+8 m s^{-1}
Atomic mass unit	u	1.66054 E-27 kg
Avogadro constant	N_A	6.02214 E+23 mol^{-1}
Gas constant	R	8.31451 J K^{-1} mol^{-1}
Boltzmann constant	k_B	1.38066 E-23 J K^{-1}
Planck constant	h	6.62608 E-34 J s
	$\hbar = h/2\pi$	1.05457 E-34 J s
Vacuum permittivity	$4\pi\varepsilon_0$	1.11265 E-10 J^{-1} C^2 m^{-1}

Table A.2 Unit conversions

Quantity	Unit	Conversion
Joule	J	1 J = 1 kg m^2 s^{-2}
Angstrom	Å	1 Å = 10^{-10} m
Volt	V	1 V = 1 J C^{-1}
Electronvolt	eV	1 eV = 1.60219 E-19 J
Elementary charge	e	1 e = 1.602177 E-19 C
Pascal	Pa	1 Pa = 1 J m^{-3}
Torr	Torr	1 Torr = 133.3222 J m^{-3}
Atmosphere	atm	1 atm = 760 Torr = 101.325 kJ m^{-3}
Debye	D	1 D = 3.33564 E-30 C m

Table A.3 Values of mass, rotational constants A & B, dipole moment (μ), polarisability (α), ionisation potential (I.P.), and ratio of heat capacities (γ) for a range of molecules. Values taken from [Lide 1998] unless otherwise noted.

Species	Mass ($g\ mol^{-1}$)	A (cm^{-1})	B (cm^{-1})	μ (D)	α ($Å^3$)	I.P. (eV)	γ (C_p/C_v)
He	4.00	-	-	-	0.205	24.59	1.66[1]
Ar	39.95	-	-	-	1.64	15.76	1.67[1]
Kr	83.80	-	-	-	2.48	14.0	1.68[1]
Xe	131.30	-	-	-	4.04	12.13	1.66[1]
N_2	28.01	-	-	-	1.74	15.58	1.40[1]
CO	28.01	-	-	0.110	1.95	14.01	1.40[1]
N_2O	44.01	-	-	-	3.03	12.89	1.31[1]
CO_2	44.01	-	-	-	2.911	13.77	1.31[1]
SF_6	146.05	-	-	-	6.54	15.32	-
CH_4	16.04	-	-	-	2.593	12.61	1.30[1]
CH_3F	34.03	5.1596	0.9291	1.858	2.97	12.47	1.36[2]
CH_3Cl	50.49	5.097	0.4434	1.89	4.72	11.22	1.37[2]
CH_3Br	94.94	5.082	0.3192	1.82	6.03	10.54	1.34[2]
TlF	223.37	-	-	4.228	-	10.80	-

[1] Taken from [Vargaftik 1994].
[2] Calculated from beam temperature estimated experimentally.

APPENDIX B SUPPLEMENTARY THEORIES

B.1 Symmetric top molecules

The symmetric top Hamiltonian based on Equation (2.2.4) is,

$$\hat{H} = \frac{\hat{J}^2}{2I_\perp} + \left(\frac{1}{2I_{//}} - \frac{1}{2I_\perp}\right)\hat{J}_z^2 \tag{B.1.1}$$

where $\hat{J} = \hat{J}_x + \hat{J}_y + \hat{J}_z$; which are angular momentum operators, and must be determined. The eigenvalues of $\hat{J}$ and $\hat{J}_z$ can be obtained using the Ladder-Operator method. [Levine 1970a]

$$\hat{J}^2\psi = J(J+1)\left(\frac{h}{2\pi}\right)^2\psi$$

$$\hat{J}_z\,\psi = K\frac{h}{2\pi}\psi \tag{B.1.2}$$

where J is the angular momentum quantum number and must be an integer, $J = 0, 1, 2, ..., J$, and K is the quantum number used to describe the component of J on the molecular axis, z. For a given value of J, there can be $2J + 1$ values of K, $K = 0, \pm1, \pm2, ..., \pm J$. Hence, the total rotational energy can be expressed as:

$$\hat{H}\psi = E\psi$$

$$\frac{\hat{J}^2}{2I_\perp}\psi + \left(\frac{1}{2I_{//}} - \frac{1}{2I_\perp}\right)\hat{J}_z^2\,\psi = E\psi$$

$$E = \frac{J(J+1)h^2}{8\pi^2 I_\perp} + \left(\frac{h^2}{8\pi^2 I_{//}} - \frac{h^2}{8\pi^2 I_\perp}\right)K^2 \tag{B.1.3}$$

or as the rotational term value $F(J,K)$ in wave number units: [Levine 1970b]

$$F(J,K) = \frac{E}{h} = BJ(J+1) + (A - B)K^2 \tag{B.1.4}$$

where $A = h/8\pi^2 I_{//}$ and $B = h/8\pi^2 I_\perp$. When $K = 0$, there is no component of angular momentum about the molecular axis and all energy levels depend only on $I_\perp$.

Again, when the molecule is placed in an external electric field, the Hamiltonian should now be considered in terms of Euler angles. Equation (B.1.1) becomes:

$$\hat{H}=\frac{-h^2}{8\pi^2 I_\perp}\left[\frac{1}{\sin\theta}\frac{\partial}{\partial\theta}\left(\sin\theta\frac{\partial}{\partial\theta}\right)+\frac{1}{\sin^2\theta}\frac{\partial^2}{\partial\phi^2}+\left(\frac{I_\perp}{I_{//}}+\frac{\cos^2\theta}{\sin^2\theta}\right)\frac{\partial^2}{\partial\chi^2}-\frac{2\cos\theta}{\sin^2\theta}\frac{\partial^2}{\partial\phi\partial\chi}\right] \quad \text{(B.1.5)}$$

Where $\hat{J}^2$ and $\hat{J}_z^2$ are as follow: [Kemble 1958]

$$\hat{J}^2=\frac{-h^2}{4\pi^2}\left[\frac{\partial^2}{\partial\theta^2}+\frac{\cos\theta}{\sin\theta}\frac{\partial}{\partial\theta}+\frac{1}{\sin^2\theta}\left(\frac{\partial^2}{\partial\phi^2}+\frac{\partial^2}{\partial\chi^2}-2\cos\theta\frac{\partial^2}{\partial\phi\partial\chi}\right)\right]$$

$$\hat{J}_z^2=\frac{-h^2}{4\pi^2}\frac{\partial^2}{\partial\chi^2} \quad \text{(B.1.6)}$$

Solving the Schrödinger wave equation (see details in Section B.1.2):

$$\hat{H}\psi=E\psi$$

$$\frac{1}{\sin\theta}\frac{\partial}{\partial\theta}\left(\sin\theta\frac{\partial\psi}{\partial\theta}\right)+\frac{1}{\sin^2\theta}\frac{\partial^2\psi}{\partial\phi^2}+\left(\frac{I_\perp}{I_{//}}+\frac{\cos^2\theta}{\sin^2\theta}\right)\frac{\partial^2\psi}{\partial\chi^2}-\frac{2\cos\theta}{\sin^2\theta}\frac{\partial^2\psi}{\partial\phi\partial\chi}+\frac{8\pi^2 I_\perp E}{h^2}\psi=0$$

The energy E can be expressed as in Equation (B.1.4)

$$\frac{E}{h}=BJ(J+1)+(A-B)K^2$$

with

$$J=n_{max}+\tfrac{1}{2}|K+M_J|+\tfrac{1}{2}|K-M_J| \quad \text{(B.1.7)}$$

where J and K are as described in Equation (B.1.2) and M_J is the quantised component of J on a laboratory axis with permitted values, $M_J(h/2\pi)$, of $M_J = 0, \pm1, \pm2, ..., \pm J$ for a total of $2J+1$ values. The parameter n_{max} is defined in Section B.1.2.

A symmetric rotor is $2(2J+1)$-fold degenerate for $K \neq 0$ and $(2J+1)$-fold degenerate for $K = 0$. The M_J-degeneracy is removed when an electric field is applied to the molecule because in the presence of the field the energy of the molecule depends on its orientation in space. This splitting of states by an electric field is called the Stark effect. The Stark energy is given in Equation (2.2.5), $-\mu\varepsilon\cos\theta$. As shown in Figure 2.2.1, θ is the angle between J and the electric field E. Since the projection of J on the direction of E is expressed in terms of M_J, $\varepsilon\cos\theta$ might be expected to be $\varepsilon(M_J/J)$. Similarly, the component of μ along the J direction is $\mu(K/J)$, since K is an angular component of J on the molecular axis z. Therefore, the Stark energy might be expected simply to be [Townes 1955]‡

‡ When the vector model is used J^2 should be replaced with $J(J+1)$.

$$W_0 = -\mu\varepsilon\cos\theta = -\mu\varepsilon\frac{KM_J}{J^2} = -\mu\varepsilon\frac{KM_J}{J(J+1)} \qquad \text{(B.1.8)}$$

The Hamiltonian for the rotational motion of a symmetric top molecule in an electric field is,

$$\hat{H} = \frac{-h^2}{8\pi^2 I_\perp}\left[\frac{1}{\sin\theta}\frac{\partial}{\partial\theta}\left(\sin\theta\frac{\partial}{\partial\theta}\right) + \frac{1}{\sin^2\theta}\frac{\partial^2}{\partial\phi^2} + \left(\frac{I_\perp}{I_{//}} + \frac{\cos^2\theta}{\sin^2\theta}\right)\frac{\partial^2}{\partial\chi^2} - \frac{2\cos\theta}{\sin^2\theta}\frac{\partial^2}{\partial\phi\partial\chi}\right] - \mu\varepsilon\cos\theta$$

The Schrödinger equation $\hat{H}\psi = E\psi$ may be solved using the field-free wave function defined in Section B.1.2 as a basis. An infinite matrix may therefore represent the Hamiltonian with elements in Dirac notation: [Shirley 1963]

$$\langle J'K'M_J'|\hat{H}|JKM_J\rangle = \frac{\hbar^2}{2I_\perp}E_0\delta_{JJ'}\delta_{KK'}\delta_{MM_J'} - \mu\varepsilon\langle J'K'M_J'|\cos\theta|JKM_J\rangle \qquad \text{(B.1.9)}$$

where $E_0 = J(J+1) + [(I_\perp/I_{//}) - 1]K^2$. The eigenvalues for this matrix can be solved to give the Stark energy levels. The matrix elements of $\cos\theta$ have been determined and they can be found in [Townes 1955 p.96],

$$\langle J,K,M_J|\cos\theta|J,K,M_J\rangle = \frac{M_J K}{J(J+1)}$$

$$\langle J,K,M_J|\cos\theta|J\text{-}1,K,M_J\rangle = \left(\frac{[J^2 - M_J^2][J^2 - K^2]}{J^2(2J-1)(2J+1)}\right)^{1/2}$$

$$\langle J,K,M_J|\cos\theta|J+1,K,M_J\rangle = \left(\frac{[(J+1)^2 - M_J^2][(J+1)^2 - K^2]}{(J+1)^2(2J+1)(2J+3)}\right)^{1/2} \qquad \text{(B.1.10)}$$

B.1.1 Eulerian description of a symmetric top rotor

The Euler angles θ, ϕ, χ are described in Figure 2.2.1 with axes *x, y, z* fixed in the symmetric top rotor and axes *X, Y, Z* fixed in space (*Z* being the electric field axis). The rotational energy, $E = \frac{1}{2}(I\omega_2)$, can be described in the body-fixed axes as:

$$E = \frac{1}{2}(I_x\omega_x^2 + I_y\omega_y^2 + I_z\omega_z^2) \qquad \text{(B.1.11)}$$

where *I* is the moment of inertia and ω is the angular velocity. The motion of the rotor is described by the angular velocity *ω(t)*. The motion in axes *X, Y, Z* can be expressed in terms of θ, ϕ, χ and their rates of change. [Zare 1988]

The angular velocity $\dot{\theta}$ is along axis x' in Figure 2.2.1, its components are expressed as:

$$\begin{aligned} \dot{\theta}_x &= \dot{\theta}\cos\chi \\ \dot{\theta}_y &= \dot{\theta}\sin\chi \\ \dot{\theta}_z &= 0 \end{aligned} \tag{B.1.12}$$

The angular velocity $\dot{\phi}$ is along axis Z; its components can be expressed as:

$$\begin{aligned} \dot{\phi}_x &= \dot{\phi}\sin\theta\sin\chi \\ \dot{\phi}_y &= -\dot{\phi}\sin\theta\cos\chi \\ \dot{\phi}_z &= \dot{\phi}\cos\theta \end{aligned} \tag{B.1.13}$$

Finally, the angular velocity $\dot{\chi}$ is along axis z; its components can be expressed as:

$$\begin{aligned} \dot{\chi}_x &= 0 \\ \dot{\chi}_y &= 0 \\ \dot{\chi}_z &= \dot{\chi} \end{aligned} \tag{B.1.14}$$

Hence, ω along each axis can be described as:

$$\begin{aligned} \omega_x &= \dot{\phi}\sin\theta\sin\chi + \dot{\theta}\cos\chi \\ \omega_y &= -\dot{\phi}\sin\theta\cos\chi + \dot{\theta}\sin\chi \\ \omega_z &= \dot{\phi}\cos\theta + \dot{\chi} \end{aligned} \tag{B.1.15}$$

Given that for a symmetric top molecule $I_x = I_y \neq I_z$, $I_x = I_\perp$ *and* $I_z = I_{//}$, Equation (B.1.11) becomes:

$$E = \frac{I_\perp}{2}(\dot{\phi}^2\sin^2\theta + \dot{\theta}^2) + \frac{I_{//}}{2}(\dot{\phi}\cos\theta + \dot{\chi})^2 \tag{B.1.16}$$

Now the Z-axis of the space fixed frame is treated as the direction of the total angular momentum L of the molecule in space. The components of L in the body-fixed axes are: (according to Equation (B.1.15))

$$\begin{aligned} L_x &= I_x\omega_x = I_x(\dot{\phi}\sin\theta\sin\chi + \dot{\theta}\cos\chi) \\ L_y &= I_y\omega_y = I_y(-\dot{\phi}\sin\theta\cos\chi + \dot{\theta}\sin\chi) \\ L_z &= I_z\omega_z = I_z(\dot{\phi}\cos\theta + \dot{\chi}) \end{aligned} \tag{B.1.17}$$

However, they can also be written as:

$$\begin{aligned} L_x &= \Phi_{xZ} = L\sin\theta\sin\chi \\ L_y &= \Phi_{xZ} = L\text{ - }\sin\theta\cos\chi \\ L_z &= \Phi_{xZ} = L\cos\theta \end{aligned} \tag{B.1.18}$$

where Φ is called the *direction cosine matrix,* which transforms between the two axes described, e.g. Φ_{xZ}, via the three Euler angles. Combining the two sets of equations above:

$$\begin{aligned} I_x(\dot{\phi}\sin\theta\sin\chi + \dot{\theta}\cos\chi) &= L\sin\theta\sin\chi \\ I_y(-\dot{\phi}\sin\theta\cos\chi + \dot{\theta}\sin\chi) &= L\text{ - }\sin\theta\cos\chi \\ I_z(\dot{\phi}\cos\theta + \dot{\chi}) &= L\cos\theta \end{aligned} \tag{B.1.19}$$

Now, consider the component of L along the x' axis. It is perpendicular to the Z-axis, therefore, $L_{x'} = 0$. This component can be resolved into components along x and y as:

$$\begin{aligned} L_{x'} &= L_x\cos\chi + L_y\cos\left(\frac{\pi}{2}\text{-}\chi\right) \\ &= L_x\cos\chi + L_y\sin\chi \\ &= I_y\dot{\theta} \\ &= 0 \end{aligned} \tag{B.1.20}$$

where L_x and L_y are replaced by expressions given in Equation (B.1.17). If I_y is not equal to zero,

$$\dot{\theta} = 0\,.$$

This shows that the angle between the molecular axis of the symmetric top and the direction of L are constant. Equation (B.1.19) can be substituted. We find the conditions for the rate of change of ϕ with time,

$$\dot{\phi} = \frac{L}{I_y}$$

which shows that the molecular axis precesses about L at a constant angular velocity L/I_y. For the rate of change of χ with time,

$$\dot{\chi} = \left(\frac{L}{I_z}\text{-}\frac{L}{I_y}\right)\cos\theta$$

This shows that the symmetric top also rotates about its molecular axis at a constant angular velocity, $(L/I_z - L/I_y)\cos\theta$. The classical motion of a symmetric top molecule is illustrated in Figure 2.2.1.

B.1.2 Solution of Schrödinger wave equation in Eulerian description

The Schrödinger wave equation for a symmetric top molecule in Eulerian description is:

$$\hat{H}\psi = E\psi$$

$$\frac{1}{\sin\theta}\frac{\partial}{\partial\theta}\left(\sin\theta\frac{\partial\psi}{\partial\theta}\right)+\frac{1}{\sin^2\theta}\frac{\partial^2\psi}{\partial\phi^2}+\left(\frac{I_\perp}{I_{//}}+\frac{\cos^2\theta}{\sin^2\theta}\right)\frac{\partial^2\psi}{\partial\chi^2}-\frac{2\cos\theta}{\sin^2\theta}\frac{\partial^2\psi}{\partial\phi\partial\chi}+\frac{8\pi^2I_\perp E}{h^2}\psi=0$$

ψ can be written in the form:

$$\psi = \Theta(\theta)e^{iM_J\phi}e^{iK\chi} \tag{B.1.21}$$

where M_J and K must be integers 0, ±1, ±2, . . . in order to make the wave function ψ single valued. Θ must satisfy the following equation:

$$\frac{1}{\sin\theta}\frac{d}{d\theta}\left(\sin\theta\frac{d\Theta}{d\theta}\right)-\left[\frac{M_J^2}{\sin^2\theta}+\left(\frac{I_\perp}{I_{//}}+\frac{\cos^2\theta}{\sin^2\theta}\right)K^2-\frac{2\cos\theta}{\sin^2\theta}KM_J-\frac{8\pi^2I_\perp E}{h^2}\right]\Theta=0 \tag{B.1.22}$$

Introducing the following variables may solve this equation:

$$x=\tfrac{1}{2}(1-\cos\theta)$$

$$\Theta(\theta)=x^{\frac{1}{2}|K-M_J|}(1-x)^{\frac{1}{2}|K+M_J|}F(x) \tag{B.1.23}$$

Using the chain rule,

$$\frac{d\Theta}{d\theta}=\frac{d\Theta}{dx}\frac{dx}{d\theta},$$

and substituting the above variables, Equation (B.1.22) may be transformed into the form of the hypergeometic equation. [Townes 1955]

$$x(1-x)\frac{d^2F}{dx^2}+(\alpha-\beta x)\frac{dF}{dx}+\gamma F=0 \tag{B.1.24}$$

where

$$\alpha=|K-M_J|+1$$

$$\beta=|K+M_J|+|K-M_J|+2$$

$$\gamma=\frac{8\pi^2I_\perp E}{h^2}-\frac{I_\perp K^2}{I_{//}}+K^2-\left(\tfrac{1}{2}|K+M_J|+\tfrac{1}{2}|K-M_J|\right)\left(\tfrac{1}{2}|K+M_J|+\tfrac{1}{2}|K-M_J|+1\right) \tag{B.1.25}$$

Its solution can be obtained as a power series

$$F(x)=\sum_{n=0}^{\infty}a_nx^n$$

$$\frac{dF}{dx} = \sum_{n=0}^{\infty} n a_n x^{n-1}$$

$$\frac{d^2F}{dx^2} = \sum_{n=0}^{\infty} n(n-1) a_n x^{n-2} \qquad \text{(B.1.26)}$$

Substituting these into Equation (B.1.24) and after rearranging, [Vallance 1999a] the following relationship is obtained:

$$a_{n+1} = \frac{n(n-1) + \beta n - \gamma}{(n+1)(n+\alpha)} a_n \qquad \text{(B.1.27)}$$

The wave function in Equation (B.1.21) becomes:

$$\psi = e^{iM_J\phi} e^{iK\chi} \left(\frac{1}{2} - \frac{1}{2}\cos\theta\right)^{\frac{1}{2}|K-M_J|} \left(\frac{1}{2} + \frac{1}{2}\cos\theta\right)^{\frac{1}{2}|K+M_J|} \sum_{n=0}^{\infty} a_n \left(\frac{1}{2} - \frac{1}{2}\cos\theta\right)^n \qquad \text{(B.1.28)}$$

For ψ to be a satisfactory normalisable wave function, the series must terminate and become a polynomial, which requires the energy E in the form of Equation (B.1.4).

E can be rearranged from the definition of γ in equation (B.1.25),

$$\frac{8\pi^2 I_\perp E}{h^2} = \gamma + \frac{I_\perp}{I_{//}} K^2 - K^2 + \left(\frac{1}{2}|K+M_J| + \frac{1}{2}|K-M_J|\right)\left(\frac{1}{2}|K+M_J| + \frac{1}{2}|K-M_J| + 1\right)$$

in terms of A and $B.1$ as $h/8\pi^2 I_{//}$ and $h/8\pi^2 I_\perp$,

$$\frac{E}{h} = B\left[\gamma + \left(\frac{1}{2}|K+M_J| + \frac{1}{2}|K-M_J|\right)\left(\frac{1}{2}|K+M_J| + \frac{1}{2}|K-M_J| + 1\right)\right] + (A-B)K^2 \qquad \text{(B.1.29)}$$

Rearranging Equation (B.1.27), γ can be written as,

$$\gamma = n(n-1) + \beta n - (n+1)(n+\alpha)\frac{a_{n+1}}{a_n}$$

Assuming there is a finite sum corresponding to the final term in the summation that $a_{n+1} = 0$, i.e. there will be some value n_{max} of n. Let n_{max} as n,

$$\gamma = n_{max}(n_{max} - 1) + \beta n_{max} - 0$$

Substituting this into Equation (B.1.29) gives the result in Equation (B.1.7):

$$\frac{E}{h} = BJ(J+1) + (A-B)K^2$$

where $$J = n_{max} + \tfrac{1}{2}|K+M_J| + \tfrac{1}{2}|K-M_J| \qquad \text{(B.1.7)}$$

In order for ψ to be normalised and to give matrix elements with signs (or phases) consistent with Condon's and Shortley's convention, the first term of the series, a_0, must be taken as, [Townes 1955 p.62]

$$e^{\frac{i\pi}{2}|K-M_J|}\left[\frac{(2J+1)(J+\tfrac{1}{2}|K+M_J|+\tfrac{1}{2}|K-M_J|)!\,(J-\tfrac{1}{2}|K+M_J|+\tfrac{1}{2}|K-M_J|)^{\frac{1}{2}}}{8\pi^2(J-\tfrac{1}{2}|K+M_J|+\tfrac{1}{2}|K-M_J|)!\,|K-M_J|!\,(J+\tfrac{1}{2}|K+M_J|-\tfrac{1}{2}|K-M_J|)^{\frac{1}{2}}}\right]^{\frac{1}{2}}$$

From Equation (B.1.7) above, J must be a positive integer which is equal to or greater than $|K|$ or $|M_J|$, so that

$$\begin{aligned} J &= 0, 1, 2, . . \\ K &= 0, \pm1, \pm2, \ldots, \pm J \\ M_J &= 0, \pm1, \pm2, \ldots, \pm J \end{aligned} \qquad \text{(B.1.30)}$$

Referring to the illustration in Figure 2.2.1, $J(J+1)\hbar$ can be shown to be the square of the total angular momentum, **J**, $K\hbar$ is its projection on the molecular axis, J_z , and $M\hbar$ is its projection on the space fixed axis, J_Z.

B.2 Hexapole trajectories

Successful transmission of a symmetric top molecule in rotational state $|JKM_J\rangle$ through a hexapole filter must comply with the following experimental conditions.

B.2.1 Hexapole entrance condition

In this work, two skimmers are used to collimate the molecular beam. The maximum divergent angle, α_{sk}, may be defined by these skimmers, as shown in Figure 2.3.3. If a beam stop is used, the minimum divergent angle, α_{bs}, is defined by the beam stop. Hence the condition for a molecule to enter the hexapole is that the divergent angle α must be:

$$\alpha_{bs} < \alpha < \alpha_{sk} \qquad \text{(B.2.1)}$$

B.2.2 Hexapole field condition

For a focussing curve, the maximum radial displacement, $r(t_{max})$, occurs when the radial velocity $\dot{r}(t) = 0$. If $\dot{r}(t_{max}) = 0$, Equation (2.3.16) becomes:

$$\dot{r}(t_{max}) = -l_1\alpha\omega \sin(\omega t_{max}) + v\alpha \cos(\omega t_{max}) = 0$$

$$\frac{v\alpha}{l_1\alpha\omega} = \frac{\sin(\omega t_{max})}{\cos(\omega t_{max})} = \tan(\omega t_{max})$$

$$\omega t_{max} = \tan^{-1}\left(\frac{v}{l_1\omega}\right) \tag{B.2.2}$$

$$\left(\text{If } x = \tan^{-1}\left(\frac{a}{b}\right), \text{ then } \cos x = \frac{b}{\sqrt{a^2+b^2}} \text{ and } \sin x = \frac{a}{\sqrt{a^2+b^2}}\right) \quad \text{[Anton 1988]}$$

Substituting this into Equation (2.3.15), $r(t_{max})$ is:

$$r(t_{max}) = l_1\alpha_{max}\cos(\omega t_{max}) + \frac{v\alpha_{max}}{\omega}\sin(\omega t_{max})$$

$$= l_1\alpha_{max}\left(\frac{l_1\omega}{\sqrt{v^2+\omega^2 l_1^2}}\right) + \frac{v\alpha_{max}}{\omega}\left(\frac{v}{\sqrt{v^2+\omega^2 l_1^2}}\right)$$

$$r(t_{max}) = \frac{\alpha_{max}}{\omega}\left(\frac{\omega^2 l_1^2 + v^2}{\sqrt{v^2+\omega^2 l_1^2}}\right) = \frac{\alpha_{max}}{\omega}\sqrt{v^2+\omega^2 l_1^2}\left(\frac{v}{\sqrt{v^2}}\right)$$

$$= \frac{v\alpha_{max}}{\omega}\sqrt{1+\frac{\omega^2 l_1^2}{v^2}}, \text{ let } \beta_1 = \frac{l_1\omega}{v}$$

$$r(t_{max}) = \frac{v\alpha_{max}}{\omega}\sqrt{1+\beta_1^2} \tag{B.2.3}$$

$r(t_{max})$ is limited by the hexapole inscribed radius, r_o, where $r(t_{max}) < r_o$. Therefore,

$$r(t_{max}) = \frac{v\alpha_{max}}{\omega}\sqrt{1+\beta_1^2} < r_o$$

$$\alpha_{max} < \frac{r_o^2\omega^2}{v^2(1+\beta_1^2)} \tag{B.2.4}$$

B.2.3 Hexapole exit condition

Another limiting factor for the divergent angle α is the exit aperture, r_{ex}, at the hexapole field exit. Because the time required for the molecule to reach the exit is $t_{ex} = l_2 v^{-1}$, where l_2 is the length of the hexapole field. $r(t_{ex})$ can be expressed as follows,

$$r(t_{ex}) = l_1\alpha_{ex}\cosh(\omega\frac{l_2}{v}) + \frac{v\alpha_{ex}}{\omega}\sinh(\omega\frac{l_2}{v}), \text{ let } \beta_2 = \frac{l_2\omega}{v}$$

$$r(t_{ex}) = l_1\alpha_{ex}\cosh\beta_2 + \frac{v\alpha_{ex}}{\omega}\sinh\beta_2$$

Since $r(t_{ex}) < r_{ex}$,

$$\alpha_{ex}\left(l_1\cosh\beta_2 + \frac{v}{\omega}\sinh\beta_2\right) < r_{ex}$$

$$\alpha_{ex}\left(\beta_1\frac{v}{\omega}\cosh\beta_2 + \frac{v}{\omega}\sinh\beta_2\right) < r_{ex}$$

$$\alpha_{ex} < \frac{r_{ex}\omega}{v}(\beta_1\cosh\beta_2 + \sinh\beta_2)^{-1} \qquad \text{(B.2.5)}$$

In summary, the divergent angle α for focussing trajectories of a symmetric top molecule are physically limited by the skimmer, the nozzle-hexapole distance, l_1, the inscribed radius of the hexapole, r_o, the hexapole length, l_2, the exit aperture radius, r_{ex}, and the beam stop radius if it is present. The divergent angle must be greater than α_{bs} (if the beam stop is present) and less than α_{sk}. For the molecules to be successfully transmitted through the hexapole field α must also be less than α_{max} and α_{ex}.

B.3 Collision cross-section

B.3.1 Classical description

The differential cross-sections defined in Section 2.5.1 can be described in terms of spherical coordinates: [Massey 1933]

$$\frac{d\sigma}{d\omega} = \sigma(\theta), \text{ where } d\omega = 2\pi\sin\theta\, d\theta\, d\phi \qquad \text{(B.3.1)}$$

The total cross-section becomes:

$$\sigma = \int_0^{2\pi}\int_0^{\pi}\sigma(\theta)\sin\theta\, d\theta\, d\phi = 2\pi\int_0^{\pi}\sigma(\theta)\sin\theta\, d\theta \qquad \text{(B.3.2)}$$

These are simplified expression of the total cross-section that could be easily adopted into quantum theory and taking the mass, relative velocity, and the angular momentum of the collision system into account.

B.3.2 Quantum theory

The interaction potential for the type of collision cross-section, of interest, is dominated by the attractive van der Waals interaction V(r) in the form of

$$V(r) = -\frac{C}{r^s} \tag{B.3.3}$$

where C is a constant, the value of C depends on the types of interactions between the collision partners.

The total cross-section given in quantum terms for an interaction potential of this form is: [Massey 1969]

$$\begin{aligned}\sigma &= \frac{4\pi}{k^2}\sum(2n+1)\sin^2\eta_n \\ &= \frac{8\pi}{k^2}\int_0^\infty n\sin^2\eta_n\, dn\end{aligned} \tag{B.3.4}$$

where k is the wave number of relative motion, $k = \frac{1}{2} Mv_r\hbar^{-1}$ (M is the reduced mass and v_r is the relative velocity of the collision partners), and η_n is the phase shift produced in de Broglie waves for the relative motion associated with angular momentum $\{n(n+1)\}^{\frac{1}{2}}\hbar$.

The phases η_n are given by Jeffrey's approximation in the form: [Massey 1934]

$$\eta_n = \int^\infty \left(k^2 - \frac{n.n+1}{r^2}\right)^{\frac{1}{2}} dr - \int^\infty \left(k^2 - \alpha V - \frac{n.n+1}{r^2}\right)^{\frac{1}{2}} dr \tag{B.3.5}$$

where the lower limits of the integration are the zeros of the respective integrands and α is written as $2M\hbar^{-2}$. For large values of n:

$$\eta_n \cong \int \left(k^2 - \frac{n(n+1)}{r^2}\right)^{\frac{1}{2}} \left(1 - 1 + \frac{\frac{1}{2}\alpha V}{k^2 - \frac{n(n+1)}{r^2}}\right) dr = \int \frac{\frac{1}{2}\alpha V}{\left(k^2 - \frac{n(n+1)}{r^2}\right)^{\frac{1}{2}}} dr \tag{B.3.6}$$

This result is also given by Born's approximation. [Mott 1949, Goldberger 1975] Hence Jeffrey's approximation may be used for all values of n. Assuming $\alpha V = -Cr^s$, for large values of n,

$$\eta_n \cong \frac{1}{2} C \int_a^\infty \frac{1}{r^s \left(k^2 - \frac{n(n+1)}{r^2}\right)^{\frac{1}{2}}} dr = \frac{1}{2} \frac{C}{k} \int_a^\infty \frac{1}{r^{s-1}(r^2 - a^2)^{\frac{1}{2}}} dr \qquad \text{(B.3.7)}$$

where $a = (n + ½)k^{-1}$. Upon integration, the phases η_n can be expressed as:

$$\eta_n = \frac{C}{2ka^{s-1}} f(s) = \frac{Ck^{s-2}}{2(n+½)^{s-1}} f(s), \qquad \text{(B.3.8)}$$

where

$$f(s) = \frac{s-3}{s-2}\frac{s-5}{s-4} \cdots \frac{1}{2}\frac{\pi}{2} \text{ (for } s = \text{even)};$$

$$\frac{s-3}{s-2}\frac{s-5}{s-4} \cdots \frac{2}{3} \text{ (for } s = \text{odd)}; \qquad \text{(B.3.9)}$$

$$1 \text{ (for } s = 3); \frac{\pi}{2} \text{ (for } s = 2).$$

Using Massey and Mohr's method, the total cross-section may finally be written as:

$$\sigma = \gamma_{MM}(s)\left(\frac{C}{\hbar v}\right)^{2/(s-1)}$$

where η_n is taken to have the value of ½, and γ_{MM} is:

$$\gamma_{MM} = \pi\left(\frac{2s-3}{s-2}\right)(2f(s))^{2/(s-1)} \qquad \text{(B.3.10)}$$

A second method, derived by Landau and Lifshitz [Landau 1959], substitutes η_n with $\eta_n \cong A_s n^{2/(s-1)}$, where $A_s = Mf(s)C\hbar^{-2}k^{s-2}$. They found:

$$\sigma = \gamma_{LL}(s)\left(\frac{C}{\hbar v}\right)^{2/(s-1)}$$

where

$$\gamma_{LL} = \pi^2(2f(s)^{2/(s-1)}) \operatorname{cosec} \frac{\pi/(s-1)}{\Gamma[2/(s-1)]} \qquad \text{(B.3.11)}$$

Values of $\gamma_{MM}(s)$ and $\gamma_{LL}(s)$ for $s = 4, 6, 7, 8, 12$ are listed in Table 2.5.1. [Massey 1971]

Therefore, non-reactive scattering cross-sections are expected to show velocity dependence, where v as the relative velocity of the collision partners:

$$\sigma(v) \propto v^{-2/(s-1)} \qquad \text{(B.3.12)}$$

For attractive van der Waals interactions, s = 6 and C takes into account the dipole and polarisation interactions. According to Equation (2.5.16) the collision cross-sections should exhibit a $v^{-0.4}$ dependence.

APPENDIX C COMPUTER PROGRAMS

C.1 JK population for symmetric top molecules in RF field.

C:\orient\rfgaus.bas

```
' ************************************************************************
'
' Calculates the JK population for molecules at temperatures TJ and TK
' In a RF + Uniform electric field
' By Sunny Hu
' 25th October 1996
'
' ************************************************************************
C = 2.997925E+08
K = 1.38066E-23
H = 6.62618E-34
CLS
INPUT "Enter rotational constant, A in 1/cm: ", A
INPUT "Enter rotational constant, B in 1/cm: ", B
INPUT "Enter temperature of molecules, TJ in K: ", TJ
INPUT "Enter temperature of molecules, TK in K: ", TK
INPUT "Enter maximum J value to calculate: ", Jmax
INPUT "Enter radio frequency, in MHz: ", v
INPUT "Enter molecular dipole moment, in D (1D=3.33564e-30 Cm): ", D
D = D * 3.33564E-30
A = A * 100
B = B * 100
KT1 = K * TJ * -1
KT2 = K * TK * -1
HC = H * C
Hv = H * v * 1000000
AB = A - B
F$ = STR$(TJ) + "JKRF.DAT"
OPEN "C:\ORIENT\" + LTRIM$(F$) FOR OUTPUT AS #1
x$ = STR$(TJ) + "GAUS.DAT"
OPEN "C:\ORIENT\" + LTRIM$(x$) FOR OUTPUT AS #2
DIM F(5000), S(5000)
FOR E = 1 TO 5000
 S(E) = 0
NEXT E
FOR J = 1 TO Jmax
 PRINT ".";
 JPart = 0
 FOR K = 1 TO J
  E1 = HC * (B * J * (J + 1)) / KT1
  E2 = HC * (AB * K * K) / KT2
  Part = EXP(E1 + E2)
  EVcm = Hv * (J * (J + 1)) / (D * K) / 100
  Eng = E1 * KT1 + E2 * KT2
  DE = 10000 * Hv * EVcm / Eng
  FUD = 1
  PFUD = 1
  IF K <> 0 THEN PFUD = 2
  IF K <> 0 AND (3 * (K / 3)) = K THEN FUD = 12 ELSE FUD = 6
```

```
   JPart = JPart + Part * PFUD * FUD
   Part = Part * FUD
   FOR E = 1 TO 5000
      F(E) = Part * EXP(-((E / 100 - EVcm) ^ 2) / ((DE / 2) ^ 2))
      S(E) = S(E) + F(E)
   NEXT E
   PRINT #1, LTRIM$(STR$(J)); ","; LTRIM$(STR$(K)); ","; LTRIM$(STR$(Part)); ",";
LTRIM$(STR$(EVcm)); ","; LTRIM$(STR$(DE))
  NEXT K
NEXT J
FOR E = 1 TO 5000
  PRINT #2, LTRIM$(STR$(E / 100)); S(E)
NEXT E
CLOSE #1
CLOSE #2
```

C.2 Transmission curve calculation for single hexapole experiments

(transnew.exe)

```
DECLARE SUB SIMP (MM!, H!, Y(),
'
'□
' Calculates Transmission of JKM states through hexapole either
' individually or over all JKM states specified.
'
' Based on Phil Brooks, Rice University programs.
'
' ********************************************************************

' Read in parameter file

f$ = "c:\orient\mbd.dat"
t$ = "c:\orient\trns"
o$ = "c:\orient\tmit.dat"

OPEN f$ FOR INPUT AS #1
INPUT #1, YM, RM, XRG, XMU, L1, L2, RL, RS, R, VS, G, TS
INPUT #1, JINTEG, VOLT1, VOLT2, A5, B5, C5, TJ, TK, SPIN
CLOSE #1

' Declare arrays of appropriate sizes

CLS

INPUT "Calculate rho values for how many voltages: ", IVOLT
INPUT "What is the voltage increment: ", HVINC
INPUT "Calculate how many rho values at each voltage: ", JRHOM

DIM FV(JINTEG), HV(IVOLT), A(JINTEG), ABAR(IVOLT, JRHOM) AS SINGLE

' Determine some start-up variables

RLIN = .09537
AB = SQR(2 * 8.31E+07 * TS / YM)
A0 = RS / L1
ARL = RLIN / L1
```

```
VMIN = VS - 2 * AB
IF (VMIN < 0) THEN VMIN = 0
VINC = 4 * AB / JINTEG
WZ = 6 * XMU * 2010 / (YM * RL * RL * RL)

' Calculate velocity distribution and normalise

PRINT : PRINT "Calculating velocity distribution..."
FOR I = 1 TO JINTEG
 V = VMIN + VINC * (I - 1)
 DELV = V - VS
 V2 = DELV * DELV
 FV(I) = V * V * EXP(-V2 / (AB * AB))
NEXT I
NO = JINTEG
CALL SIMP(NO, VINC, FV(), FORM)
FOR I = 1 TO JINTEG
 FV(I) = FV(I) / FORM
NEXT I

' Calculate probability of transmission for each voltage and rho

PRINT "Calculating transmission probabilities..."
FOR IPHI = 1 TO IVOLT
 PHI = VOLT1 + HVINC * (IPHI - 1)
 HV(IPHI) = PHI
 PRINT IPHI;
 FOR JRHO = 1 TO JRHOM
  PRINT ".";
  RHO = JRHO / JRHOM
  W = SQR(WZ * RHO * PHI)
  V = VMIN
  FOR L = 1 TO JINTEG
   V = VMIN + VINC * (L - 1)
   IF (JINTEG = 1) THEN V = VS
   B1 = W * L1 / V
   B2 = W * L2 / V
   AV = (R / L1) / ABS((1 / B1) * SIN(B2) + COS(B2))
   AF = (W * RL / V) / SQR(1 + B1 * B1)
   IF AV < AF THEN A1 = AV ELSE A1 = AF
   IF A1 <= A0 THEN A1 = A0
   AL = (A1 * A1 - A0 * A0) / (ARL * ARL)
   A(L) = AL * FV(L)
   VL = A(L)
  NEXT L
  IF JINTEG <> 1 THEN CALL SIMP(NO, VINC, A(), VL)
  ABAR(IPHI, JRHO) = VL
 NEXT JRHO
 PRINT
NEXT IPHI

' Output transmission probability file

PRINT "Writing transmission probability file..."
OPEN o$ FOR OUTPUT AS #1
 PRINT #1, IVOLT, JRHOM
 FOR I = 1 TO IVOLT
  FOR JRHO = 1 TO JRHOM
   PRINT #1, ABAR(I, JRHO)
```

```
   NEXT JRHO
  NEXT I
CLOSE #1

' Calculate transmission curves for individual jkm states
A$ = ""

DO UNTIL A$ = "Q"
PRINT
PRINT "Press I for individual JKM transmission, T for total or Q to quit"
keyloop:
  A$ = UCASE$(INKEY$)
  IF A$ = "" THEN GOTO keyloop
  IF A$ = "I" THEN GOSUB indiv
  IF A$ = "T" THEN GOSUB tot
LOOP
END

indiv:
  PRINT
  J = 1
  DO WHILE J > 0
    INPUT "Enter J for transmission (-1 TO end): ", J
    IF J > 0 THEN
      INPUT "Enter K and M: ", K, M
      RHO = (M * K) / (J * J + J)
      JTRN = INT(RHO * JRHOM)
      f$ = t$ + LTRIM$(STR$(J)) + LTRIM$(STR$(K)) + LTRIM$(STR$(M))
      OPEN f$ FOR OUTPUT AS #2
      FOR I = 1 TO IVOLT
        PRINT #2, LTRIM$(STR$(HV(I))); ","; LTRIM$(STR$(ABAR(I, JTRN)))
      NEXT I
      CLOSE #2
    END IF
  LOOP
  RETURN

tot:
  PRINT
  INPUT "Enter maximum J to evaluate transmission for: ", Jmax
  PRINT
  PRINT "Calculating JK population of beam..."

  REDIM Part(Jmax, Jmax) AS SINGLE

  C = 2.997925E+08
  K = 1.38066E-23
  H = 6.62618E-34
  KT1 = K * TJ * -1
  KT2 = K * TK * -1
  HC = H * C
  AB = A5 - B5
  Q! = 0

  FOR J = 0 TO Jmax
    FOR K = 0 TO J
      E1 = HC * (B * J * (J + 1)) / KT1
      E2 = HC * AB * K * K / KT2
      Part(J, K) = EXP(E1 + E2)
```

```
    PFUD = 1
    FUD = 1
    IF K <> 0 THEN PFUD = 2
    IF K <> 0 AND (3 * (K / 3)) = K THEN FUD = 2
    Q! = Q! + PFUD * FUD * (2 * J + 1) * Part(J, K)
  NEXT K
 NEXT J

 FOR J = 0 TO Jmax
  FOR K = 0 TO J
    FUD = 1
    IF K <> 0 AND (3 * (K / 3)) = K THEN FUD = 2
    E1 = HC * (B * J * (J + 1)) / KT1
    E2 = HC * AB * K * K / KT2
    Part(J, K) = FUD * EXP(E1 + E2) / Q!
  NEXT K
 NEXT J

 PRINT "Calculating transmission curve..."

 OPEN t$ + "J" + LTRIM$(STR$(Jmax)) FOR OUTPUT AS #2

 FOR I = 1 TO IVOLT
  PRINT ".";
  temp = 0
  FOR J = 1 TO Jmax
   FOR K = 1 TO J
    Kdeg = (2 * K) + 1
    FOR M = 1 TO J
     RHO = (M * K) / (J * J + J)
     JTRN = INT(RHO * JRHOM)
     temp = temp + (Part(J, K) / Kdeg) * ABAR(I, JTRN)
    NEXT M
   NEXT K
  NEXT J
  PRINT #2, LTRIM$(STR$(HV(I))); ","; LTRIM$(STR$(temp))
 NEXT I
 CLOSE #2
 PRINT
 RETURN

SUB SIMP (MM, H, Y(), VL)
 M = MM
 VL = 0
 VODD = 0
 VEVEN = 0
 CORR = 0
 IF ((M - 2 * (M / 2)) <> 0) THEN
  CORR = (Y(M) + Y(M - 1)) * H / 2
  M = M - 1
 END IF
 FOR I = 1 TO M - 1 STEP 2
  VODD = VODD + Y(I)
 NEXT I
 FOR I = 2 TO M - 2 STEP 2
  VEVEN = VEVEN + Y(I)
 NEXT I
 VL = CORR + (Y(0) + Y(M) + 4 * VODD + 2 * VEVEN) * H / 3
END SUB
```

C.3 Transmission curve calculation for MBER experiments

```
DECLARE SUB SIMP (MM!, H!, Y(), VL!)
' ************************************************************************
'
' Calculates Transmission of JKM states through hexapoles and RF field
' either individually or over all JK states specified.
'
' Based on Phil Brooks, Rice University programs.
'
' Written 25 July 1997 by Sunny Hu
'
' ************************************************************************
DEF FNSINH (X) = (EXP(X) - EXP(-1 * X)) / 2
DEF FNCOSH (X) = (EXP(X) + EXP(-1 * X)) / 2

' Read in parameter file

f$ = "c:\orient\mbd.dat"
o$ = "c:\orient\RF.dat"

OPEN f$ FOR INPUT AS #1
INPUT #1, YM, RM, XRG, XMU, L1, L2, RL, RS, R, VS, G, TS
INPUT #1, JINTEG, VOLT1, VOLT2, A5, B5, C5, TJ, TK, SPIN
CLOSE #1

' Declare arrays of appropriate sizes
CLS
INPUT "Calculate rho values for how many voltages: ", IVOLT
INPUT "What is the voltage increment: ", HVINC
INPUT "Calculate how many rho values at each voltage: ", JRHOM
INPUT "number of entrance angles: (e.g. 10)", IALPHA
INPUT "fraction of molecules in shadow beam: (e.g. 0.33)", FRACS
INPUT "Radius of Mass spec in cm: (e.g. 0.3)", RMS

DIM FV(JINTEG), HV(IVOLT), A(JINTEG), ABAR(IVOLT, JRHOM) AS SINGLE
DIM FLX(9, IVOLT), FLX0(9, IVOLT), ALPHK(IALPHA), ALPHP(9, IALPHA) AS SINGLE
DIM FLOST(9, IALPHA), XRF(9, IALPHA), QRF(9, IALPHA), QRFV(IALPHA) AS SINGLE

' Determine some start-up variables

RLIN = .0909                    'was .09537 entrance radius in cm
AB = SQR(2 * 8.31E+07 * TS / YM)    'alpha (beam) for seed molecules
A0 = RS / L1                    'min incident angle to pass beam stop
ARL = RLIN / L1                 'max. incident angle
VMIN = VS - 2 * AB              'min speed for integration
IF (VMIN < 0) THEN VMIN = 0         'effusive beam
VINC = 4 * AB / JINTEG              'speed increment
WZ = 6 * XMU * 2010 / (YM * RL * RL * RL)   'partial calc for omega

' Calculate velocity distribution and normalise

PRINT : PRINT "Calculating velocity distribution..."
FOR I = 1 TO JINTEG
 V = VMIN + VINC * (I - 1)
 DELV = V - VS                  'difference between VS & V
 V2 = DELV * DELV
 FV(I) = V * V * EXP(-V2 / (AB * AB))
```

```
NEXT I
NO = JINTEG
CALL SIMP(NO, VINC, FV(), FORM)
FOR I = 1 TO JINTEG              'normalises FV
 FV(I) = FV(I) / FORM
NEXT I
IF JINTEG = 1 THEN FV(1) = 1
FOR J = 1 TO 9           'initialise matrix FLX and FLX0 with 0
 FOR IPHI = 1 TO IVOLT
 FLX(J, IPHI) = 0!
 FLX0(J, IPHI) = 0!
 NEXT IPHI
NEXT J

' Calculate probability of transmission for each voltage and rho

PRINT "Calculating transmission probabilities..."
FF = .5 * (1 - FRACS)'Fraction of beam in focusing (or defocusing) states
FOR IPHI = 1 TO IVOLT            'loop for various voltages
 PHI = VOLT1 + HVINC * (IPHI - 1)  'each voltage step
 HV(IPHI) = PHI
 PRINT IPHI;
 FOR JRHO = 1 TO JRHOM           'No. of calculation
  PRINT ".";
  RHO = JRHO / JRHOM
  IF (JRHOM = 1) THEN RHO = .5    'for RF aperture; only one JKM value
  W = SQR(WZ * RHO * PHI)        'calc omega
  V = VMIN                'L2=length of A+B+C field;
  LC = L2 / 2             'LC=distance to the middle of C field
  LMS = 10                'LMS=distance from end of field to MS detector
  FOR L = 1 TO JINTEG             'integration over speeds
   V = VMIN + VINC * (L - 1)
   IF (JINTEG = 1) THEN V = VS
   B1 = W * L1 / V
   B2 = W * L2 / V
   BC = W * LC / V
   AV = (R / L1) / ABS((1 / B1) * SIN(B2) + COS(B2))    'alpha of R(ex)
   AF = (W * RL / V) / SQR(1 + B1 * B1)              'alpha of R(max)
   IF AV < AF THEN A1 = AV ELSE A1 = AF       'A1=min of AF & AV
   A1S = R / L1           'angle at beginning of first section
   A0 = 0
IF A1 <= A0 THEN A1 = A0         'discards those blocked by beam stop
   AL = (A1 * A1 - A0 * A0) / (ARL * ARL)       'finds A(Vo,v,rho)
   A(L) = AL * FV(L)  'aperture * prob. of speed; finds Fjkm(Vo) at vel=v
   VL = A(L)
  NEXT L
  IF JINTEG <> 1 THEN CALL SIMP(NO, VINC, A(), VL)  'returns VL the final
  ABAR(IPHI, JRHO) = VL                    'normalised intensity
 NEXT JRHO                 'i.e. sums up the A(L) values found above

'**********Section to calculate trajectories*********
IF A1S < AF THEN A1S = A1S ELSE A1S = AF
DELAS = SQR(A1S * A1S) - SQR(A0 * A0)
INCAS = DELAS / IALPHA                    'stepping increment
FOR I = 1 TO IALPHA
  ALPHK(I) = A0 + INCAS * I          'array of integrated angles
NEXT I
JCMAX = 1
FOR J = 1 TO JCMAX                  'integrate over C field
```

```
LC = (L2 - 15) / 2 + 5 * J              'step of 5 cm in C field
LOB = L2 - LC                           'length of B field
BS = W * LOB / V
  FOR I = 1 TO IALPHA
'CONradial distance at the end of A field
  RCA = (L1 * COS(BC) + V / W * SIN(BC)) * ALPHK(I)
'CONradial speed at the end of A field
  RCADOT = ((V * COS(BC) - L1 * W * SIN(BC))) * ALPHK(I)
'DIVradial distance at the end of A field
  RDA = (L1 * FNCOSH(BC) + V / W * FNSINH(BC)) * ALPHK(I)
'DIVradial speed at the end of A field
  RDADOT = ((V * FNCOSH(BC) - L1 * W * SINh(BC))) * ALPHK(I)
'SHADradial distance at the end of A field
  RSA = (L1 + LC) * ALPHK(I)
'SHADradial speed at the end of A field
  RSADOT = V * ALPHK(I)
'(1) convergent trajectories in A field and convg in B field
'Radial distance at the end of B field
  RF(1) = RCA * COS(BS) + RCADOT / W * SIN(BS)
'Radial speed
  RFD(1) = RCADOT * COS(BS) - RCA * W * SIN(BS)
'(2) convergent trajectories in A field and div. in B field
  RF(2) = RCA * FNCOSH(BS) + RCADOT / W * FNSINH(BS)
  RFD(2) = RCADOT * FNCOSH(BS) - RCA * W * FNSINH(BS)
'(3) convergent trajectories in A field and undefl in B field
  RF(3) = RCA + RCADOT * LOB / V
  RFD(3) = RCADOT
'(4) Divergent trajectories in A field and convg in B field
  RF(4) = RDA * COS(BS) + RDADOT / W * SIN(BS)
  RFD(4) = RDADOT * COS(BS) - RDA * W * SIN(BS)
'(5) Divergent trajectories in A field and div. in B field
  RF(5) = RDA * FNCOSH(BS) + RDADOT / W * FNSINH(BS)
  RFD(5) = RDADOT * FNCOSH(BS) - RDA * W * FNSINH(BS)
'(6) Divergent trajectories in A field and undefl in B field
  RF(6) = RDA + RDADOT * LOB / V
  RFD(6) = RDADOT
'(7) Undeflected trajectories in A field and convg in B field
  RF(7) = RDA * COS(BS) + RDADOT / W * SIN(BS)
  RFD(7) = RSADOT * COS(BS) - RSA * W * SIN(BS)
'(8) Undeflected trajectories in A field and div. in B field
  RF(8) = RSA * FNCOSH(BS) + RSADOT / W * FNSINH(BS)
  RFD(8) = RSADOT * FNCOSH(BS) - RSA * W * FNSINH(BS)
'(9) Undeflected trajectories in A field and undefl in B field
  RF(9) = (L1 + L2) * ALPHK(I)
  RFD(9) = V * ALPHK(I)

    FOR K = 1 TO 9
    ALPHP(K, I) = -RFD(K) / V           'exit trajectory angle
    IF ALPHP(K, I) <> 0 THEN
    XRF(K, I) = RF(K) / ALPHP(K, I)     'downstream crossing distance
    END IF
    IF ABS(RF(K)) < R THEN FLOST(K, I) = 1 ELSE FLOST(K, I) = 0
    NEXT K  'molecules are inside field  'outside field, don't count
  NEXT I


'*****************************************************************
'     Now test to see if trajectories hit detector
```

```
'*****************************************************************
 FOR K = 1 TO 9
  QF = FF
  IF K = 3 * (K / 3) THEN QF = FRACS
  FOR I = 1 TO IALPHA
 IF ABS((LMS - XRF(K, I)) * ALPHP(K, I)) < RMS THEN
 PC = QF * FLOST(K, I)
 QRF(K, I) = ALPHK(I) * PC / (A1S * A1S / 2)
 ELSE
 PC = 0
 QRF(K, I) = 0
 END IF
  NEXT I
 NEXT K
 FOR K = 1 TO 9
  FOR I = 1 TO IALPHA
   QRFV(I) = QRF(K, I)            'converts QRF into vector for SIMP
   QRFV(0) = 0
  NEXT I
  CALL SIMP(IALPHA, INCAS, QRFV(), QQSC)
  IF K = 1 OR K = 5 OR K = 9 THEN FLX0(K, IPHI) = FLX0(K, IPHI) + QQSC * 3
  FLX(K, IPHI) = FLX(K, IPHI) + QQSC
 NEXT K    'flux when rf is off, factor of 3 to acct for non equilibration
NEXT J
'**********************End of RF section**************************************
PRINT
NEXT IPHI
' Output transmission probability file
PRINT "Writing transmission probability file..."
OPEN o$ FOR OUTPUT AS #1
 PRINT #1, "Voltage Conv-conv Conv-div  Conv-shad Div-conv  Div-div   Div-shad  Shad-conv
Shad-div  Shad-shad"
 FOR I = 1 TO IVOLT
 PRINT #1, USING "####### ##.##^^^^ ##.##^^^^ ##.##^^^^ ##.##^^^^ ##.##^^^^ ##.##^^^^
##.##^^^^ ##.##^^^^ ##.##^^^^"; HV(I); FLX(1, I); FLX(2, I); FLX(3, I); FLX(4, I); FLX(5, I);
FLX(6, I); FLX(7, I); FLX(8, I); FLX(9, I)
 NEXT I
CLOSE #1

SUB SIMP (MM, H, Y(), VL)
 M = MM
 VL = 0
 VODD = 0
 VEVEN = 0
 CORR = 0
 IF ((M - 2 * (M / 2)) <> 0) THEN
  CORR = (Y(M) + Y(M - 1)) * H / 2
  M = M - 1
 END IF
 FOR I = 1 TO M - 1 STEP 2
  VODD = VODD + Y(I)
 NEXT I
 FOR I = 2 TO M - 2 STEP 2
  VEVEN = VEVEN + Y(I)
 NEXT I
 VL = CORR + (Y(0) + Y(M) + 4 * VODD + 2 * VEVEN) * H / 3
END SUB
```

C.4 C-cell experiments

```
DECLARE SUB sethv2 (hexhv!, setv!)
DECLARE SUB sethv2 (hexhv!, setv)
DECLARE SUB msdata (mssig!, nreads%)
DECLARE SUB getdata3 (tscan%, nscan%, DIFF!)
DECLARE SUB sens (snum$, lsens$)
DECLARE SUB setdcrun ()
' NB - you must load the QB.QLB link library into QB to
' compile this program!!!
' to do this invoke the following command :
' qb ccell.bas /l qb

'Program to run the C-cell experiment:
'   RF frequency and modulation set manually using signal generator before
'   running program.  Program sets DC field.  Ramps from dcinit to dcfinal
'   in increments of dcinc.  Reads signal from mass spec collected via
'   lock-in-amplifier at each DC voltage to give difference spectrum.

REM $INCLUDE: 'qb.bi'

TYPE FunTable
        funNo         AS INTEGER     'function number
        channel       AS INTEGER     'high byte for direction
                                       'low byte for channel number
        bufferOff     AS INTEGER     'offset of buffer address
        bufferSeg     AS INTEGER     'segment of buffer address
        vi          AS INTEGER
        vf          AS INTEGER
        time        AS LONG
        steps       AS LONG
        datus       AS INTEGER
        returnValue   AS LONG
END TYPE

' declare the constants for channel number and directions
        CONST xCH2 = &H2

' function number definations
        CONST CMDxActive = 10
        CONST CMDxOutput = 30
        CONST CMDxInput = 31
        CONST CMDxDelay = 42
        CONST CMDxBase = 53
        CONST CMDxReset = 54
        CONST CMDxCwStep = 60
        CONST CMDxCcwStep = 61
        CONST CMDxStepSpd = 62
        CONST CMDxCwSpeed = 67
        CONST CMDxCcwSpeed = 68
        CONST CMDxBusy = 72
        CONST CMDxFirmware = 73

'DECLARE SUB lockin ()
DECLARE SUB setdc (dcvolts!, psmode$)
DECLARE SUB getdata (locksig, tcollect!, tconst!, nreads%)
DECLARE SUB getdata2 (inc!, totpoints%, npt%, ncycle%, locksig)
DECLARE SUB sethv (hexhv!)
```

```
DECLARE SUB setphase ()
DECLARE SUB setP (pressure!, meter, temp%)
DECLARE FUNCTION hexP! (meter)
DECLARE SUB stepsm (steps%)
DECLARE FUNCTION Cmd838% (cmdNo AS INTEGER, channel AS INTEGER, datus AS
INTEGER)
DECLARE FUNCTION InstallStatus! ()


'Set up com port for communication with lock-in-amplifier (com1 is used
'for the Baratron).
OPEN "COM1: 9600,N,8,2,CS,DS,CD" FOR RANDOM AS #1

10 CLS
PRINT , "1 - Change parameters for lock-in."
PRINT , "2 - Run experiment"
PRINT , "3 - Set DC potential"
PRINT , "4 - Set hexapole HV"
PRINT , "5 - Set phase on lock-in"
PRINT , "6 - Run externally controlled experiment"
PRINT , "7 - Manually set DC and collect data"
PRINT , "8 - Get trace from Combiscope"
PRINT , "9 - Quit"

val1$ = INPUT$(1)

SELECT CASE val1$

   CASE "1"
'Set up the lock-in-amplifier.
'     CALL lockin

   CASE "2"
    CLS
    INPUT "(1) Continuous or (2) pulsed beam or (3) pulse counting"; bmtype%
    IF bmtype% = 2 THEN
         INPUT "Number of cycles to read"; ncycle%
         INPUT "Number of points per cycle"; npt%
         totpoints% = npt% * ncycle%
    END IF
    IF bmtype% = 3 THEN
         INPUT "Time per scan (sec) "; tscan%
         INPUT "Number of scans "; nscan%
    END IF
    INPUT "Scattering gas in 1st Hexapole chamber? (1)"; gas%
    INPUT "Collect signal over a peak? (1) for yes"; peak%
    IF peak% = 1 THEN
         INPUT "Starting DC voltage:"; peakini!
         INPUT "Final DC voltage:"; peakfin!
         INPUT "Step increment:"; peakstep!
    END IF
    PRINT , "1 - Fix HV and RF and sweep DC"
    PRINT , "2 - Fix RF and DC and sweep HV"
    PRINT , "3 - Fix RF, DC and HV for attenuation expt"
    modec$ = INPUT$(1)
    mode% = VAL(modec$)
    GOTO 20

   CASE "3"
```

```
    CLS
    PRINT , "1 - 0-300V power supply"
    PRINT , "2 - Mike's amplifiers 0-60 V (Default option)"
    psmode$ = INPUT$(1)
15  IF psmode$ = "1" THEN
    INPUT "DC potential 0-300 V:"; voltage!
    ELSE INPUT "DC potential 0-60 V:"; voltage!
    END IF
    CALL setdc(voltage!, psmode$)
    PRINT "Actual voltage: " + STR$(voltage!)
    PRINT "Press M to return to main menu, N for a new voltage"
    pick$ = INPUT$(1)
    IF UCASE$(pick$) = "M" THEN GOTO 10 ELSE GOTO 15

  CASE "4"
PRINT "!!! Make sure Hexapole voltage supplies are connected correctly !!!"
19   PRINT "Both hexapole at the same potential (1)"
    INPUT "Hexapole at different potential (2)"; hex2%
  IF hex2% = 1 THEN
    INPUT "HV potential"; hexhv!
'    CALL sethv(hexhv!)
    CALL sethv2(hexhv!, 1)
    CALL sethv2(hexhv!, 2)
  ELSE
    INPUT "First HV potential"; hv1!
    INPUT "Second HV potential"; hv2!
    CALL sethv2(hv1!, 1)
    CALL sethv2(hv2!, 2)
  END IF
    PRINT "Press M to return to main menu, N for a new voltage"
    pick$ = INPUT$(1)
    IF UCASE$(pick$) = "M" THEN GOTO 10 ELSE GOTO 19

  CASE "5"
    CALL setphase
    GOTO 10



  CASE "6"
    INPUT "(1) Continuous or (2) pulsed beam"; bmtype%
    IF bmtype% = 2 THEN
        INPUT "Number of cycles to read"; totpoints%
        INPUT "Number of points per cycle"; npt%
    END IF

    PRINT "Variable parameter: 1 - Modulating frequency"
    INPUT "         (Default) 2 - others"; modf

    INPUT "HV potential"; hexhv!
    PRINT , "1 - 0-300V power supply"
    PRINT , "2 - Mike's amplifiers 0-60V (Default option)"
    PRINT , "3 - HP signal generator"
    psmode$ = INPUT$(1)

    IF psmode$ = "1" THEN
        INPUT "DC potential 0-300 V:"; voltage!
    ELSE INPUT "DC potential 0-60 V:"; voltage!
    END IF
```

```
'    IF modf <> 1 THEN INPUT "Phase"; phase

     INPUT "Wait time (sec)"; phtime!
     INPUT "Number of reads"; num
     INPUT "Output filename (xxxxxxxx.dat)"; name$

'    CALL sethv(hexhv!)
          CALL sethv2(hexhv!, 1)
          CALL sethv2(hexhv!, 2)
     CALL setdc(voltage!, psmode$)
     PRINT "Actual voltage: " + STR$(voltage!)

     OPEN "c:\ccell\data\" + name$ FOR OUTPUT AS #3

     PRINT #3, "HV potential ="; hexhv!; "V"
     PRINT #3, "DC potential ="; voltage!; "V"
     PRINT #3, "Wait time ="; phtime!; "sec"
     PRINT #3, "Number of reads ="; num; "reads"

     IF modf = 2 THEN
          PRINT #1, "F"
          INPUT #1, reffreq!
          PRINT #3, "Modulating frequency ="; reffreq!; "Hz"
          PRINT #3, "Signal"
     ELSE PRINT #3, "Mod-Freq., Signal"
     END IF

22   IF modf = 2 THEN INPUT "variable parameter"; xvalue
     IF psmode$ = "3" THEN INPUT "Frequency"; reffreq!
     totest! = 0

'Collecting data over time phtime!
     T = TIMER
     WHILE TIMER < T + phtime!
     WEND
     PORT = &H170
     FOR N = 1 TO num
          OUT PORT + 1, 0
          OUT PORT + 0, 0
          FOR I1 = 1 TO 8: a = INP(PORT + 8): NEXT I1
          FOR I2 = 1 TO 8: a = INP(PORT + 12): NEXT I2
          H6 = INP(PORT + 3)
          L8 = INP(PORT + 2)
          test! = (H6 - 64 * (INT(H6 / 64))) * 256 + L8 - 8192
          totest! = totest! + test!
     NEXT N

'Averaging signal and determining if this is the maximum so far.
     totest! = (totest! / num) * 10 / 8192

     IF psmode$ <> "3" OR bmtype% <> 3 THEN
          PRINT #1, "F"
          INPUT #1, reffreq!
     END IF

     IF modf = 2 THEN
          PRINT xvalue, totest!,
          PRINT #3, xvalue, totest!
```

```
        ELSE PRINT #3, reffreq!; ","; totest!
        PRINT reffreq!; ","; totest!,
    END IF
    PRINT "Press M to return to main menu, N for a new value"
    SOUND 783.99, 9.1
    pick$ = INPUT$(1)
    IF UCASE$(pick$) = "M" THEN CLOSE #3: GOTO 10 ELSE GOTO 22

  CASE "7"
    CALL setdcrun
    GOTO 10

  CASE "8"

' Retrieving data from the Fluke PM3394B Combiscope.

53 CLS
CLOSE
OPEN "COM1:19200,N,8,1, CS0, DS0, CD0" FOR RANDOM AS #1

' f$ = MID$(DATE$, 4, 2) + LEFT$(DATE$, 2) + LEFT$(TIME$, 2) + MID$(TIME$, 4, 2) + ".hpgl"
INPUT "Filename"; F$
OPEN "c:\ccell\data\" + F$ FOR OUTPUT AS #2

PRINT #1, "QP"; 1
Start! = TIMER
WHILE ((TIMER < Start! + 1) AND (LOC(1) = 0))
WEND
IF LOC(1) > 0 THEN
  PRINT "Response = ";
  DO
    Byte$ = INPUT$(LOC(1), #1)
    PRINT Byte$
    PRINT #2, Byte$;
    Start! = TIMER
    WHILE ((TIMER < Start! + 1) AND (LOC(1) = 0))
    WEND
 LOOP WHILE LOC(1) > 0
ELSE
 PRINT "No Response"
END IF
CLOSE #2

CLOSE

    PRINT "Press M to return to main menu, N for a new trace"
    pick$ = INPUT$(1)
    IF UCASE$(pick$) = "M" THEN GOTO 10 ELSE GOTO 53


  CASE "9"
    CALL setdc(0, psmode$)
    CALL sethv2(0, 2)
    CALL sethv2(0, 1)  'set spellman high voltage supply to zero
    END
END SELECT

'Set up DC voltage range, increment, and count times.
20 CLS
```

```
IF mode% = 3 OR gas% = 1 THEN
  IF InstallStatus <> 255 THEN
    PRINT "PCL-838.EXE was not installed"
    BEEP
    END
  END IF
  result = Cmd838(CMDxBase, 0, &H2E0)
  result = Cmd838(CMDxReset, 0, 0)
  result = Cmd838(CMDxActive, xCH2, 0)

END IF
INPUT "Beam gas"; name$
IF mode% = 3 OR gas% = 1 THEN INPUT "Scattering gas"; scatgas$
INPUT "RF frequency (MHz)"; rffreq!
rffreq! = 1000000 * rffreq!
INPUT "RF amplitude"; rfamp!
INPUT "Include Mass spect signal? Yes = 1, No = 2"; ms%
 PRINT "Both Hexapole at the same voltage (1)"
 INPUT "Separate 2nd Hexapole voltage (2)"; hex2%
  IF hex2% = 2 THEN
  INPUT "First hexapole voltage (V)"; hv1!
  PRINT "Second hexapole"
  END IF
' PRINT , "!!! Make sure that the HV supplies are connected correctly !!!"
IF mode% = 2 THEN
 INPUT "Initial hexapole voltage (V)"; hvinit!
 INPUT "Final hexapole voltage (V)"; hvfinal!
 INPUT "Step size (V)"; hvinc!
 INPUT "JKM state (xxx)"; jkm%
ELSE
 INPUT "Hexapole voltage"; hexhv!
END IF
IF mode% = 3 THEN
  INPUT "JKM state (xxx)"; jkm%
END IF

IF mode% = 1 THEN
 PRINT , "1 - 0-300V power supply"
 PRINT , "2 - 0-60V ADDA supply"
 psmode$ = INPUT$(1)
 INPUT "Initial DC voltage (V)"; dcinit!
 INPUT "Final DC voltage (V)"; dcfinal!
 INPUT "Step size (V)"; dcinc!


ELSE
IF peak% <> 1 THEN INPUT "DC voltage"; dcvolts!
 PRINT , "1 - 0-300V power supply"
 PRINT , "2 - 0-60V ADDA supply"
 psmode$ = INPUT$(1)
END IF

IF mode% <> 3 THEN
 INPUT "Wait time per voltage step in time constants"; tcollect!
 INPUT "Number of signal reads per step"; nreads%
END IF

IF mode% = 3 THEN
```

```
  INPUT "0.1 Torr Baratron (1), MKS290 ion gauge (2), 0.05 Torr Baratron (3), or HPS919 ion
gauge (4)"; meter
  INPUT "Pressure increment"; pinc!
  INPUT "Maximum pressure"; pfinal!
  INPUT "Number of steps before starting"; sstep%
  INPUT "Wait time per pressure step in time constants"; tcollect!
  INPUT "Number of signal reads per step"; nreads%
END IF
IF gas% = 1 THEN
  INPUT "0.1 Torr Baratron (1), MKS290 ion gauge (2), 0.05 Torr Baratron (3), or HPS919 ion
gauge (4)"; meter
  INPUT "Pressure increment"; pinc!
  INPUT "Number of steps before starting"; sstep%
END IF

PRINT "   "
COLOR 4, 0
PRINT , "Press S to start, M to return to main menu"
COLOR 7, 0

 choose$ = INPUT$(1)
 choose$ = UCASE$(choose$)
 SELECT CASE choose$
   CASE "S"
     Tstart = TIMER
     CLS
     PRINT , "Beginning experiment"
     PRINT , "Press 'k' to abort experiment"
     PRINT , "Press 't' for run time"
     GOTO 30
   CASE "M"
     GOTO 10
 END SELECT

IF bmtype% = 3 THEN GOTO 21 'bypass the lock-in
'Get modulation frequency from lock-in.
30  PRINT #1, "F"
 INPUT #1, reffreq!
 PRINT , reffreq!
 IF bmtype% = 2 THEN
    period! = 1 / reffreq!
    inc! = period! / npt%
 END IF

IF bmtype% = 1 THEN
'Get phase from lock-in.
  PRINT #1, "P"
  INPUT #1, refphase!
 END IF
'Get sensitivity setting from lock-in.
 PRINT #1, "G"
 INPUT #1, snum$
 CALL sens(snum$, lsens$)
'Get dynamic reserve setting from lock-in.
 PRINT #1, "D"
 INPUT #1, dynamic$
  SELECT CASE dynamic$
    CASE "0": dynres$ = "LOW"
    CASE "1": dynres$ = "NORM"
```

```
    CASE "2": dynres$ = "HIGH"
  END SELECT

 today$ = DATE$
 now$ = TIME$
 F$ = MID$(DATE$, 4, 2) + LEFT$(DATE$, 2) + LEFT$(TIME$, 2) + MID$(TIME$, 4, 2) + ".dat"
21 'OPEN "e:\ccell\" + f$ FOR OUTPUT AS #2
OPEN "c:\ccell\data\" + F$ FOR OUTPUT AS #2
35  SELECT CASE mode%
  CASE 1
    PRINT #2, F$
IF gas% = 1 THEN
PRINT #2, "Beam gas "; name$; " Scattering gas "; scatgas$
ELSE PRINT #2, name$
END IF
    PRINT #2, "Spectral scan - DC swept at constant RF and HV for " + name$
    PRINT #2, "Run at "; now$; " on "; today$
    PRINT #2, "RF frequency "; rffreq! / 1000000; " MHz, amplitude "; rfamp!; " V, modulated at ";
reffreq!; " Hz"
    PRINT #2, "Phase "; refphase!; " Sensitivity "; lsens$; " Dynamic reserve "; dynres$
   IF hex2 = 2 THEN PRINT #2, "First Hexapole at "; hv1!; " V"
   PRINT #2, "Hexapole HV "; hexhv!; " V"; "  Lockin phase set at "; refphase!
    PRINT #2, "DC voltage range "; dcinit!; "-"; dcfinal; " V in increments of "; dcinc!; "V"
 CASE 2
    PRINT #2, F$
IF gas% = 1 THEN
PRINT #2, "Beam gas "; name$; " Scattering gas "; scatgas$
ELSE PRINT #2, name$
END IF
    PRINT #2, jkm%; " transmission curve - HV swept at constant RF and DC"
    PRINT #2, "Run at"; now$; "on"; today$
    PRINT #2, "RF frequency "; rffreq! / 1000000; " MHz, amplitude "; rfamp!; "V, modulated at ";
reffreq!; " Hz"
    PRINT #2, "Phase"; refphase!; " Sensitivity "; lsens$; " Dynamic reserve "; dynres$
  IF peak% = 1 THEN
    PRINT #2, "DC over "; peakini!; " to "; peakfin!; " V in steps of "; peakstep!; " V"
  ELSE
    PRINT #2, "DC potential "; dcvolts!; " V ";
  END IF
    PRINT #2, "Lockin phase set at "; refphase!
    IF hex2% = 2 THEN PRINT #2, "First Hexapole voltage at "; hv1!
    PRINT #2, "Hexapole voltage range "; hvinit!; "-"; hvfinal; " V in increments of "; hvinc!; "V"
 CASE 3
    PRINT #2, F$
    PRINT #2, "Beam gas "; name$; " Scattering gas "; scatgas$
    PRINT #2, "Attenuation curve for "; jkm%; " state - fixed HV, DC and RF, sweep P"
    PRINT #2, "Run at"; now$; "on"; today$
    PRINT #2, "RF frequency "; rffreq! / 1000000; " MHz, amplitude"; rfamp!; " V modulated at ";
reffreq!; " Hz"
    PRINT #2, "Phase"; refphase!; " Sensitivity "; lsens$; " Dynamic reserve "; dynres$
  IF peak% = 1 THEN
    PRINT #2, "DC over "; peakini!; " to "; peakfin!; " V in steps of "; peakstep!; " V"
  ELSE
    PRINT #2, "DC potential "; dcvolts!; " V"
  END IF
  PRINT #2, "Hexapole HV "; hexhv!; " V"; "  Lockin phase set at "; refphase!
    PRINT #2, "Pressure increment "; pinc!; " to maximum of "; pfinal!
END SELECT
```

```
IF bmtype% = 3 THEN GOTO 23 'bypass the lock-in
'Get time constant from lock-in
  PRINT #1, "T 1"
  INPUT #1, tcon$
  SELECT CASE tcon$
    CASE "1"
      tconst! = .001
    CASE "2"
      tconst! = .003
    CASE "3"
      tconst! = .01
    CASE "4"
      tconst! = .03
    CASE "5"
      tconst! = .1
    CASE "6"
      tconst! = .3
    CASE "7"
      tconst! = 1
    CASE "8"
      tconst! = 3
    CASE "9"
      tconst! = 10
    CASE "10"
      tconst! = 30
    CASE "11"
      tconst! = 100
   END SELECT

  PRINT , "time constant ="; tconst!
  PRINT , "wait time (s) ="; tconst! * tcollect!
  PRINT #2, "Time constant"; tconst!; "s"
  PRINT #2, "Wait time (s)"; tconst! * tcollect!;
  PRINT #2, "Number of reads per voltage"; nreads%
  PRINT #2, "Entry, "; "Locksig,"; " Massig"
'idum is the number of points at which to collect data.
23
CALL setdc(0, psmode$)
'CALL sethv(0)
            CALL sethv2(0, 1)
            CALL sethv2(0, 2)

nstep% = 0
SELECT CASE mode%
  CASE 1
'    CALL sethv(hexhv!)    'Set HV if fixed throughout expt
IF hex2% = 2 THEN CALL sethv2(hv1!, 1) ELSE CALL sethv2(hexhv!, 1)
     CALL sethv2(hexhv!, 2)
    idum = INT((dcfinal! - dcinit!) / dcinc!)
IF gas% = 1 THEN
   PRINT , "Starting off valve ("; sstep%; "turns)"
   CALL stepsm(sstep%)
   nstep% = sstep%
   pinit! = hexP!(meter)
   IF pinit! < 0 THEN pinit! = 1E-09
END IF
  CASE 2
 IF peak% = 1 THEN
   dcvolts! = peakini!
```

```
   pdum = INT((peakfin! - peakini!) / peakstep!)
  END IF
    CALL setdc(dcvolts!, psmode$)
    idum = INT((hvfinal! - hvinit!) / hvinc!)
IF gas% = 1 THEN
   PRINT , "Starting off valve ("; sstep%; "turns)"
   CALL stepsm(sstep%)
   nstep% = sstep%
   pinit! = hexP!(meter)
   IF pinit! < 0 THEN pinit! = 1E-09
END IF
  CASE 3
'    CALL sethv(hexhv!)
IF hex2% = 2 THEN CALL sethv2(hv1!, 1) ELSE CALL sethv2(hexhv!, 1)
    CALL sethv2(hexhv!, 2)
 IF peak% = 1 THEN
   dcvolts! = peakini!
   pdum = INT((peakfin! - peakini!) / peakstep!)
 END IF
   CALL setdc(dcvolts!, psmode$)
   PRINT , "Starting off valve ("; sstep%; "turns)"
   CALL stepsm(sstep%)
   nstep% = sstep%
   pinit! = hexP!(meter)
   IF pinit! < 0 THEN pinit! = 1E-09
   idum = INT((pfinal! - pinit!) / pinc!)
   PRINT , "Number of pressure increments"; idum

END SELECT

'Looping through DC voltages and collecting signal from lock-in at each
'point.
COLOR 3

FOR i = 0 TO (idum + 1)
T1 = TIMER
 SELECT CASE mode%
   CASE 1
IF gas% = 1 THEN
     pressure! = pinit! + pinc!
     CALL setP(pressure!, meter, temp%)
    nstep% = nstep% + temp%
END IF
     dcvolts! = dcinit! + i * dcinc!
     CALL setdc(dcvolts!, psmode$)
     IF bmtype% = 1 THEN
          CALL getdata(locksig, tcollect!, tconst!, nreads%)
     ELSEIF bmtype% = 2 THEN
          CALL getdata2(inc!, totpoints%, npt%, ncycle%, locksig)
     ELSE
          CALL getdata3(tscan%, nscan%, locksig)
     END IF
    IF ms% = 1 THEN CALL msdata(mssig, nreads%)
         IF ms% = 1 THEN
          PRINT INT(dcvolts! * 1000) / 1000, locksig, mssig
          WRITE #2, dcvolts!, locksig, mssig
         ELSE
          PRINT INT(dcvolts! * 1000) / 1000, locksig,
          WRITE #2, dcvolts!, locksig
```

```
      END IF
    CASE 2
IF gas% = 1 THEN
      pressure! = pinit! + pinc!
      CALL setP(pressure!, meter, temp%)
     nstep% = nstep% + temp%
END IF
      hexhv! = hvinit! + i * hvinc!
           IF hex2% = 2 THEN
           CALL sethv2(hv1!, 1)          'set first hexapole voltage
           CALL sethv2(hexhv!, 2)        'set second hexapole voltage
           ELSE
         CALL sethv(hexhv!)            'set both hexapole voltage
            CALL sethv2(hexhv!, 1)
            CALL sethv2(hexhv!, 2)
           END IF
IF peak% = 1 THEN
peaksum! = 0
FOR j = 0 TO pdum + 1
   dcvolts! = peakini! + j * peakstep!
   CALL setdc(devolts!, psmode$)
     IF bmtype% = 1 THEN
          CALL getdata(locksig, tcollect!, tconst!, nreads%)
     ELSEIF bmtype% = 2 THEN
          CALL getdata2(inc!, totpoints%, npt%, ncycle%, locksig)
     ELSE
          CALL getdata3(tscan%, nscan%, locksig)
     END IF
    IF ms% = 1 THEN CALL msdata(mssig, nreads%)
         IF ms% = 1 THEN
          PRINT hexhv!, dcvolts!, locksig, mssig,
          WRITE #2, hexhv!, dcvolts!, locksig, mssig
         ELSE
          WRITE #2, hexhv!, dcvolts!, locksig
          PRINT hexhv!, dcvolts!, locksig,
         END IF
peaksum! = peaksum! + locksig
NEXT j
PRINT , "Peaksum = ", peaksum!
WRITE #2, "Peaksum,", peaksum!
ELSE
     IF bmtype% = 1 THEN
          CALL getdata(locksig, tcollect!, tconst!, nreads%)
     ELSEIF bmtype% = 2 THEN
          CALL getdata2(inc!, totpoints%, npt%, ncycle%, locksig)
     ELSE
          CALL getdata3(tscan%, nscan%, locksig)
     END IF
    IF ms% = 1 THEN CALL msdata(mssig, nreads%)
         IF ms% = 1 THEN
          PRINT hexhv!, locksig, mssig,
          WRITE #2, hexhv!, locksig, mssig
         ELSE
          WRITE #2, hexhv!, locksig
          PRINT hexhv!, locksig,
         END IF

END IF
   CASE 3
```

```
    pressure! = pinit! + i * pinc!
    IF idum = 0 THEN GOTO 234
    CALL setP(pressure!, meter, temp%)
        nstep% = nstep% + temp%
234   IF temp% = -32768 THEN EXIT FOR

IF peak% = 1 THEN
peaksum! = 0
FOR j = 0 TO pdum + 1
  dcvolts! = peakini! + j * peakstep!
  CALL setdc(devolts!, psmode$)
    IF bmtype% = 1 THEN
        CALL getdata(locksig, tcollect!, tconst!, nreads%)
    ELSEIF bmtype% = 2 THEN
        CALL getdata2(inc!, totpoints%, npt%, ncycle%, locksig)
    ELSE
        CALL getdata3(tscan%, nscan%, locksig)
    END IF
   preal! = hexP!(meter)
   IF ms% = 1 THEN CALL msdata(mssig, nreads%)
        IF ms% = 1 THEN
         PRINT preal!, dcvolts!, locksig, mssig,
         WRITE #2, preal!, dcvolts!, locksig, mssig
        ELSE
         PRINT preal!, dcvolts!, locksig,
         WRITE #2, preal!, dcvolts!, locksig
        END IF
    CALL setP(pressure!, meter, temp%)
        nstep% = nstep% + temp%
   PRINT nstep%
peaksum! = peaksum! + locksig
NEXT j
PRINT , "Peaksum = ", peaksum!
WRITE #2, "Peaksum,", peaksum!
ELSE
    IF bmtype% = 1 THEN
        CALL getdata(locksig, tcollect!, tconst!, nreads%)
    ELSEIF bmtype% = 2 THEN
        CALL getdata2(inc!, totpoints%, npt%, ncycle%, locksig)
    ELSE
        CALL getdata3(tscan%, nscan%, locksig)
    END IF
   preal! = hexP!(meter)
   IF ms% = 1 THEN CALL msdata(mssig, nreads%)
        IF ms% = 1 THEN
         PRINT preal!, locksig, mssig,
         WRITE #2, preal!, locksig, mssig
        ELSE
         PRINT preal!, locksig,
         WRITE #2, preal!, locksig
        END IF
  PRINT nstep%
END IF
  END SELECT

a$ = INKEY$
a$ = UCASE$(a$)
'Aborting run if program killed
  IF a$ = "K" THEN
```

```
    PRINT , "Run terminated.  Setting all potentials to zero."
    GOTO 40
  END IF

T2 = TIMER
Ttot = (T2 - T1) * (idum + 1 - i)
Thr = INT(Ttot / 3600): Tmin = INT(((Ttot - Thr * 3600)) / 60): Tsec = INT((Ttot - Thr * 3600))
MOD 60
PRINT "Time remaining: "; Thr; ":"; Tmin; ":"; Tsec

CLOSE #2
OPEN "c:\ccell\data\" + F$ FOR APPEND AS #2

NEXT i

40 PRINT "Closing valve and setting all voltages to zero"
  CALL stepsm(-1 * nstep%)
  CALL setdc(0, psmode$)
   CALL sethv(0)
   CALL sethv2(0, 1)
   CALL sethv2(0, 2)
  FOR i = 1 TO 3
    BEEP
    T = TIMER
    WHILE TIMER < T + .5
    WEND
  NEXT i
  PRINT #2, "Run time ="; TIMER - Tstart
  CLOSE #2


END


DEFINT A-Z
'execute PCL-838 command through interrupt 2f with AX=&hD202
'return error code, 0 for no error
'      This routine can handle all commands except
'        Set, SetSlow, Remain, In, Out, Read and Write
'
FUNCTION Cmd838 (cmdNo AS INTEGER, channel AS INTEGER, datus AS INTEGER)

          DIM InRegs AS RegType
          DIM Table  AS FunTable

          Table.funNo = cmdNo
          Table.channel = channel
          Table.datus = datus

      InRegs.ax = &HD202
          InRegs.bx = VARPTR(Table)
          InRegs.cx = VARSEG(Table)
          CALL INTERRUPT(&H2F, InRegs, InRegs)
          datus = Table.datus
          Cmd838 = InRegs.ax

END FUNCTION

DEFSNG A-Z
```

```
'-------------------------------------------
 SUB getdata (locksig, tcollect!, tconst!, nreads%)
'-------------------------------------------
 'Collects signal from lock-in-amplifier.  This is the difference signal
 'between the output of the mass spec with RF on and RF off.  Data is
 'collected over the time tcollect and averaged to be sent back to the
 'main program.

  T = TIMER

  WHILE TIMER < T + tcollect! * tconst!
  WEND
channel = 0
PORT = &H170
locktot = 0
FOR i = 1 TO nreads%
'  PRINT #1, "Q"          'read output from Lockin RS-232 DCE
'  INPUT #1, locksig
    OUT PORT + 1, 0
    OUT PORT + 0, channel
      FOR I1 = 1 TO 8: a = INP(PORT + 8): NEXT I1
      FOR I2 = 1 TO 8: a = INP(PORT + 12): NEXT I2
    H6 = INP(PORT + 3)
    L8 = INP(PORT + 2)
    locksigl = (H6 - 64 * (INT(H6 / 64))) * 256 + L8 - 8192
  locktot = locktot + locksigl
NEXT i
locksig = (locktot / nreads%) * 10 / 8192

END SUB

SUB getdata2 (inc!, totpoints%, npt%, ncycle%, locksig)

  DIM T(totpoints%), sig(totpoints%)
  channel = 0
  PORT = &H170
  locktot = 0

'Reading in data for set number of cycles from signal monitor output of
'lock-in.

tzero = TIMER
FOR i = 1 TO totpoints%
  T(i) = i * inc!
   WHILE TIMER < tzero + T(i)
   WEND

   OUT PORT + 1, 0
   OUT PORT + 0, channel
   FOR I1 = 1 TO 8: a = INP(PORT + 8): NEXT I1
   FOR I2 = 1 TO 8: a = INP(PORT + 12): NEXT I2
   H6 = INP(PORT + 3)
   L8 = INP(PORT + 2)
   sig(i) = (H6 - 64 * (INT(H6 / 64))) * 256 + L8 - 8192
   sig(i) = sig(i) * 10 / 8192
NEXT i

OPEN "c:\ccell\test.dat" FOR OUTPUT AS #7
```

```
PRINT #7, "Signal monitor output"
FOR i = 1 TO totpoints%
   PRINT #7, T(i), sig(i)
NEXT i

'Finding a minimum to start integrating signal from.
sigmin = 100000
FOR i = 1 TO npt% / 2
 IF sig(i) < smin THEN smin = sig(i)
 imin = i
NEXT i

'Changing origin in sig to first minimum.
FOR i = 1 TO totpoints% - imin
  sig(i) = sig(i + imin - 1)
NEXT i

PRINT #7, "First minimum found for point", T(imin), smin
PRINT #7, "shifted signal monitor signal"
FOR i = 1 TO totpoints% - imin
 PRINT #7, T(i), sig(i)
NEXT i


'Integrating peaks for RF on and RF off and taking the difference
sum1 = 0
sum2 = 0
FOR i = 1 TO ncycle% - 1
  FOR j = 1 TO npt% / 2
    k = (i - 1) * npt% + j
    sum1 = sum1 + sig(k)
  NEXT j
  FOR j = npt% / 2 + 1 TO npt%
    k = (i - 1) * npt% + j
    sum2 = sum2 + sig(k)
  NEXT j
NEXT i

locksig = ABS(sum2 - sum1)
PRINT #7, "Difference signal", locksig
CLOSE #7
END SUB

SUB getdata3 (tscan%, nscan%, DIFF)
DIFF = counter&(tscan%, nscan%)
END SUB

'------------
FUNCTION hexP! (meter)
'------------
'Reads the pressure in the hexapole from the Baratron or ion gauge.
'
SELECT CASE meter

CASE 1   'Pressure measured using 0.1 Torr Baratron (from 670 signal conditioner)

  bara! = 0
  OPEN "COM2: 9600,N,8,1,CS0,CD0,DS0,ASC" FOR RANDOM AS #4
```

```
  PRINT #4, "@020?"
  bara$ = " "
  LINE INPUT #4, bara$

  LOCATE 15, 10
  PRINT "Baratron pressure reading: - bara$ = "; bara$; "      "

  bara$ = RIGHT$(bara$, LEN(bara$) - 5)
  bara! = bara! + VAL(bara$)

  CLOSE #4

  hexP! = bara!

CASE 2              'Pressure read from ion gauge.
  PORT = &H1BC
  OUT PORT + 3, 191

  portA = INP(PORT)
  portB = INP(PORT + 1)
  theMSD = (NOT portA AND 240) / (2 ^ 4)
  theLSD = NOT portA AND 15
  theEXP = NOT portB AND 15

  theP! = (theMSD + (theLSD / 10)) * (10 ^ (theEXP * -1))
  hexP! = theP
  LOCATE 15, 10
  PRINT "Pressure=", theP

 CASE 3

' Reads from MKS627 50 mTorr Baratron through ADDA 14 card.  0-10V output
 ' of Baratron goes through Keithley voltmeter on 20mV scale to give a 0-2V
 ' analogue output.  This signal passes through an isolation amplifier with
 ' a gain of 5 to convert it to a 0-10 V signal for input into the ADDA14.
 ' The initial signal is therefore amplified by a factor of 500, and the pressure
 ' in Torr is given by P = 0.05*(V/500)/10, where V is the voltage into the ADDA card.
    CLS

 channel = 3
 PORT = &H170
 nreads = 100

 barasig = 0
 FOR i = 1 TO nreads
  OUT PORT + 1, 0
  OUT PORT + 0, channel
  FOR I1 = 1 TO 8: a = INP(PORT + 8): NEXT I1
  FOR I2 = 1 TO 8: a = INP(PORT + 12): NEXT I2
  H6 = INP(PORT + 3)
  L8 = INP(PORT + 2)
  bararead = (H6 - 64 * (INT(H6 / 64))) * 256 + L8 - 8192
  barasig = barasig + bararead
 NEXT i
  barasig = (barasig / nreads) * 10 / 8192   'amplified voltage signal received by ADDA
'Voltage output from Baratron (see calibration curve in c:\ccell\misc\\baracalib
 ' on P266)
  barasig = (barasig - .0688) / 427.87
  theP = .05 * (barasig / 10)  'Pressure in Torr.
```

```
  LOCATE 15, 10
  PRINT "Pressure=", theP
  hexP! = theP

CASE 4
' Pressure measured from analogue output of HPS919 ion gauge controller.

 channel = 3
 PORT = &H170
 nreads = 10

 voltage = 0
 FOR i = 1 TO nreads
  OUT PORT + 1, 0
  OUT PORT + 0, channel
  FOR I1 = 1 TO 8: a = INP(PORT + 8): NEXT I1
  FOR I2 = 1 TO 8: a = INP(PORT + 12): NEXT I2
  H6 = INP(PORT + 3)
  L8 = INP(PORT + 2)
  Vread = (H6 - 64 * (INT(H6 / 64))) * 256 + L8 - 8192
  voltage = voltage + Vread
 NEXT i

  voltage = (voltage / nreads) * 9.4 / 8192  'analogue output voltage from gauge controller
  '(9.4 volts full scale on ADDA14 corresponds to 8192 bits)

  theP = 10 ^ (voltage - 11!)

  LOCATE 15, 10
  PRINT "Pressure=", theP
  hexP! = theP

END SELECT

END FUNCTION

'--------------------
FUNCTION InstallStatus!
'--------------------
  DIM InRegs AS RegType
  InRegs.ax = &HD200
  CALL INTERRUPT(&H2F, InRegs, InRegs)
  InstallStatus = InRegs.ax

END FUNCTION

'---------
SUB Lockin
'---------
'Sets all the front panel operations for the lock-in-amplifier.
PRINT , "1 - Set auto offset"
PRINT , "2 - Set reference display (phase or frequency)"
PRINT , "3 - Set dynamic reserve"
PRINT , "4 - Turn output expand on/off"
PRINT , "5 - Get reference frequency"
PRINT , "6 - Set gain (sensitivity)"
PRINT , ""
PRINT , "0 - Return to main menu"
```

```
INPUT param%
  IF param% = 0 THEN RETURN

'SELECT CASE param%



END SUB

SUB msdata (mssig, nreads%)
'Get signal from mass-spec via 14 ADDA card use recorder 1000mV output

channel = 2
PORT = &H170
mstot = 0
FOR i = 1 TO nreads%
 OUT PORT + 1, 0
   OUT PORT + 0, channel
    FOR I1 = 1 TO 8: a = INP(PORT + 8): NEXT I1
    FOR I2 = 1 TO 8: a = INP(PORT + 12): NEXT I2
   H6 = INP(PORT + 3)
   L8 = INP(PORT + 2)
   mssigl = (H6 - 64 * (INT(H6 / 64))) * 256 + L8 - 8192
 mstot = mstot + mssigl
NEXT i
mssig = (mstot / nreads%) * 10 / 8192

END SUB


SUB sens (snum$, lsens$)
SELECT CASE snum$
CASE "1": lsens$ = "10 nV"
CASE "2": lsens$ = "20 nV"
CASE "3": lsens$ = "50 nV"
CASE "4": lsens$ = "100 nV"
CASE "5": lsens$ = "200 nV"
CASE "6": lsens$ = "500 nV"
CASE "7": lsens$ = "1 uV"
CASE "8": lsens$ = "2 uV"
CASE "9": lsens$ = "5 uV"
CASE "10": lsens$ = "10 uV"
CASE "11": lsens$ = "20 uV"
CASE "12": lsens$ = "50 uV"
CASE "13": lsens$ = "100 uV"
CASE "14": lsens$ = "200 uV"
CASE "15": lsens$ = "500 uV"
CASE "16": lsens$ = "1 mV"
CASE "17": lsens$ = "2 mV"
CASE "18": lsens$ = "5 mV"
CASE "19": lsens$ = "10 mV"
CASE "20": lsens$ = "20 mV"
CASE "21": lsens$ = "50 mV"
CASE "22": lsens$ = "100 mV"
CASE "23": lsens$ = "200 mV"
CASE "24": lsens$ = "500 mV"
END SELECT

END SUB
```

```
'-----------------
SUB setdc (dcvolts!, psmode$)
'-----------------

'Sets the DC voltage for the c-cell

 IF psmode$ = "1" THEN

' 300V power supplies
' ********************
' USE THESE TWO LINES IF USING A SINGLE DC SUPPLY (ONE SIDE OF C-CELL
GROUNDED)
'    message = INT((dcvolts! / 300!) * 16383)
'    dcvolts! = INT((message / 16383) * 300000) / 1000

'USE THESE TWO LINES IF USING 2 SUPPLIES
    message = .5 * INT((dcvolts! / 300!) * 16383)
    dcvolts! = 2 * INT((message / 16383) * 300000) / 1000

'Calibration correction to output voltage to achieve desired RF cell
' voltage (ADDA only puts out 9.5 V full scale instead of 10 V)

    message = message / .95

'Calibration correction (linear fit from input vs measured voltage)
   message = (message + .2292) / .9942

' Output straight from ADDA card (0-9.5 V)
' ****************************************
'USE THESE TWO LINES IF USING A SINGLE SUPPLY (ONE SIDE GROUNDED)
'  ELSE message = INT((dcvolts! / 27.6) * 16383)
'     dcvolts! = INT((message / 16383) * 27600) / 1000

'USE THESE TWO LINES IF USING DUAL +/- SUPPLIES  WITH OP-AMP BOARD (G=2)
ELSE message = .5 * INT((dcvolts! / 27.6) * 16383)
    dcvolts! = 2 * INT((message / 16383) * 27600) / 1000


END IF

'PORT = &H1A4
'OUT PORT + 3, 128:            REM Setting I/O card to mode 0
'OUT PORT, 0:                  REM zeroing ports A, B, C on card
'OUT PORT + 1, 0
'OUT PORT + 2, 0
'OUT PORT + 0, message MOD 256:    REM Output highest 4 bits
'OUT PORT + 1, INT(message / 256): REM Output lowest 8 bits

PORT = &H170
hi1 = INT(message / 256):    REM Set high bits
lo1 = (message AND 255):     REM Set low bits
OUT PORT + 4, 0: OUT PORT + 5, 0: OUT PORT + 6, 0: OUT PORT + 7, 0
OUT PORT + 4, lo1: OUT PORT + 6, lo1:    REM Output low bits
OUT PORT + 5, hi1: OUT PORT + 7, hi1:    REM Output high bits

END SUB

SUB setdcrun
```

```
CLS
'Setting phase on lock-in

    INPUT "phase"; phase!
    PRINT #1, "P"; phase!
    PRINT #1, "P"

'Scanning through range of DC voltages

67      INPUT "Minimum DC (0-60V)"; dcmin!
        INPUT "Maximum DC (0-60V)"; dcmax!
        INPUT "Increment"; dcinc!
        INPUT "High voltage"; hexhv!
        INPUT "Wait time (s)"; dctime!
        INPUT "Number of samples"; num
        PRINT "Data output as file dc.dat"
        PRINT , "Press K to kill scan"
OPEN "c:\ccell\dc.dat" FOR OUTPUT AS #3

         PRINT #3, "DC", "Signal"
      CALL sethv(hexhv!)
        CALL sethv2(hexhv!, 1)
        CALL sethv2(hexhv!, 2)
        j = INT((dcmax! - dcmin!) / dcinc!)

        FOR i = 0 TO j              'Stepping DC
         T1 = TIMER
         dc! = dcmin! + i * dcinc!
         CALL setdc(dc!, "2")
         T = TIMER
         N = 0
         totest! = 0              'Collecting data over time dctime!
         WHILE TIMER < T + dctime!
         WEND

         PORT = &H170
         FOR N = 1 TO num
          OUT PORT + 1, 0
          OUT PORT + 0, 0
          FOR I1 = 1 TO 8: a = INP(PORT + 8): NEXT I1
          FOR I2 = 1 TO 8: a = INP(PORT + 12): NEXT I2
          H6 = INP(PORT + 3)
          L8 = INP(PORT + 2)
          test! = (H6 - 64 * (INT(H6 / 64))) * 256 + L8 - 8192
          totest! = totest! + test!
         NEXT N

         totest! = (totest! / num) * 10 / 8192    'Averaging signal
         PRINT #3, dc!; ","; totest!
         PRINT , dc!; "    "; totest!
         b$ = INKEY$
         b$ = UCASE$(b$)
         IF b$ = "K" THEN GOTO 68

         T2 = TIMER
         Ttot = (T2 - T1) * (j - i)
         Thr = INT(Ttot / 3600): Tmin = INT(((Ttot - Thr * 3600)) / 60): Tsec = INT((Ttot - Thr *
3600)) MOD 60
```

```
            LOCATE 15, 50: PRINT "Time remaining: "; Thr; ":"; Tmin; ":"; Tsec

          NEXT i
          CLOSE #3
68      PRINT , "Enter N for new run, M to return to main menu"
          pick$ = INPUT$(1)
          IF UCASE$(pick$) = "M" THEN GOTO 69 ELSE GOTO 67

      CALL sethv(0)
         CALL sethv2(0, 1)
         CALL sethv2(0, 2)

69 END SUB

'----------------
SUB sethv (hexhv!)
'----------------
'Sets high voltage on hexapole

VALUE = INT((hexhv! / 30000) * 4095)
PORT = &H1AC
OUT PORT + 3, &H80
OUT PORT + 0, 0
OUT PORT + 1, 0
OUT PORT + 2, 0
OUT PORT + 0, VALUE MOD 256
OUT PORT + 1, INT(VALUE / 256)

END SUB

SUB sethv2 (hexhv!, setv)
'----------------
'Sets high voltage on hexapole

 IF setv = 1 THEN      'first hexapole Spellman high voltage supply
VALUE = INT((hexhv! / (10000 - 11.7) / .9319) * 4095)
   PORT = &H1A4
 ELSE                  'second hexapole Glassman high voltage supply
VALUE = INT((hexhv! / 30000) * 4095)
   PORT = &H1AC
 END IF
OUT PORT + 3, &H80
OUT PORT + 0, 0
OUT PORT + 1, 0
OUT PORT + 2, 0
OUT PORT + 0, VALUE MOD 256
OUT PORT + 1, INT(VALUE / 256)

END SUB

'------------------------
SUB setP (pressure!, meter, temp%)
'------------------------
  hPress! = .0001  'The upper limit for pressure
  stepAdj% = 0
  pExp% = INT(LOG(pressure!) / LOG(10))

  DO UNTIL ABS(hexP!(meter) - pressure!) < (10 ^ (pExp% - 1))
    IF hexP!(meter) < pressure! THEN sdir% = 1 ELSE sdir% = -1
```

```
    CALL stepsm(2 * sdir%)
    stepAdj% = stepAdj% + (2 * sdir%)
    theP! = hexP!(meter)

    IF theP! > hPress! OR theP! < 1E-09 THEN
     LOCATE 23, 3: COLOR 14: PRINT "Pressure reading abnormal, please rectify....";
     a$ = INKEY$
     DO UNTIL a$ <> ""
          a$ = INKEY$
          FOR x = 440 TO 1300 STEP 30     'sounds warning!!
            SOUND x, 1
          NEXT x
     LOOP
     IF UCASE$(a$) = "K" THEN temp% = -32768: EXIT SUB
     LOCATE 23, 3: COLOR 11: PRINT "Setting pressure now...";
     theP! = hexP!(meter)
    END IF

    IF ABS(theP! - pressure!) < (pressure! / 3) THEN
     T = TIMER
     DO UNTIL TIMER > T + .8
     LOOP
    END IF
  LOOP
  LOCATE 23, 3: PRINT SPACE$(30);
  temp% = stepAdj%
  pressure! = theP!

END SUB


SUB setphase
' Sets phase on lock-in-amplifier

    CLS

    PRINT , "1 - Set single value"
    PRINT , "2 - Scan through phases"
    phpick$ = INPUT$(1)
    SELECT CASE phpick$



'Input single phase to lock-in
         CASE "1"
           CLS
16       INPUT "Phase"; phase!
           PRINT #1, "P"; phase!
           PRINT #1, "P"
           PRINT , "Enter N for new phase, M to return to main menu"
           pick$ = INPUT$(1)
           IF UCASE$(pick$) = "M" THEN GOTO 666 ELSE GOTO 16
'Scans through a range of phases and records phase at which the signal was a
'maximum.
         CASE "2"
17       CLS
           INPUT "Minimum phase"; phmin!
           INPUT "Maximum phase"; phmax!
           INPUT "Increment"; phinc!
```

```
            INPUT "High voltage"; hexhv!
            INPUT "DC voltage (0-60 V)"; dcvolts!

          CALL sethv(hexhv!)
             CALL sethv2(hexhv!, 1)
             CALL sethv2(hexhv!, 2)
            CALL setdc(dcvolts!, "2")

            INPUT "Wait time (s)"; phtime!
            INPUT "Number of samples"; num
            INPUT "Filename (********.dat)"; phfile$
            PRINT , "Press K to kill scan"
OPEN "c:\ccell\data\" + phfile$ FOR OUTPUT AS #3
'Get modulation frequency from lock-in.
 PRINT #1, "F"
 INPUT #1, reffreq!
'Get sensitivity setting from lock-in.
 PRINT #1, "G"
 INPUT #1, snum$
 CALL sens(snum$, lsens$)
'Get dynamic reserve setting from lock-in.
 PRINT #1, "D"
 INPUT #1, dynamic$
   SELECT CASE dynamic$
     CASE "0": dynres$ = "LOW"
     CASE "1": dynres$ = "NORM"
     CASE "2": dynres$ = "HIGH"
   END SELECT
'Get time constant from lock-in
  PRINT #1, "T 1"
  INPUT #1, tcon$
  SELECT CASE tcon$
     CASE "1"
       tconst! = .001
     CASE "2"
       tconst! = .003
     CASE "3"
       tconst! = .01
     CASE "4"
       tconst! = .03
     CASE "5"
       tconst! = .1
     CASE "6"
       tconst! = .3
     CASE "7"
       tconst! = 1
     CASE "8"
       tconst! = 3
     CASE "9"
       tconst! = 10
     CASE "10"
       tconst! = 30
     CASE "11"
       tconst! = 100
   END SELECT

PRINT #3, "Frequency " + STR$(reffreq!) + "Hz"
PRINT #3, "Sensitivity " + lsens$ + " Time constant " + STR$(tconst!) + "s"
PRINT #3, "Dynamic reserve " + dynres$
```

```
PRINT #3, "Phase,", "Signal"
            j = INT((phmax! - phmin!) / phinc!)
            testmax! = 0
            maxph! = 0
            FOR i = 0 TO j
T1 = TIMER
'Stepping phase
              phase! = phmin! + i * phinc!
              PRINT #1, "P"; phase!
              T = TIMER
              N = 0
              totest! = 0
'Collecting data over time phtime!
              WHILE TIMER < T + phtime!
              WEND
'         PRINT #1, "Q"
'         INPUT #1, test!
PORT = &H170
FOR N = 1 TO num
   OUT PORT + 1, 0
   OUT PORT + 0, 0
     FOR I1 = 1 TO 8: a = INP(PORT + 8): NEXT I1
     FOR I2 = 1 TO 8: a = INP(PORT + 12): NEXT I2
    H6 = INP(PORT + 3)
    L8 = INP(PORT + 2)
    test! = (H6 - 64 * (INT(H6 / 64))) * 256 + L8 - 8192
              totest! = totest! + test!

NEXT N
'Averaging signal and determining if this is the maximum so far.
              totest! = (totest! / num) * 10 / 8192
              PRINT #3, phase!; ","; totest!
              PRINT , phase!; "     "; totest!
              IF ABS(totest!) > testmax! THEN
                testmax! = ABS(totest!)
                maxsign = SGN(totest!)
                maxph! = phase!
              END IF
              b$ = INKEY$
              b$ = UCASE$(b$)
              IF b$ = "K" THEN GOTO 18
T2 = TIMER
Ttot = (T2 - T1) * (j - i)
Thr = INT(Ttot / 3600): Tmin = INT(((Ttot - Thr * 3600)) / 60): Tsec = INT((Ttot - Thr * 3600))
MOD 60
LOCATE 15, 50: PRINT "Time remaining: "; Thr; ":"; Tmin; ":"; Tsec
            NEXT i
            CLOSE #3
            PRINT , "Maximum signal "; testmax!; " obtained when phase was "; maxph!
18        PRINT , "Enter N for new run, M to return to main menu"
            pick$ = INPUT$(1)
            IF UCASE$(pick$) = "M" THEN GOTO 666 ELSE GOTO 17
            PRINT , "Setting phase to "; phmax!
            IF maxsign = -1 THEN PRINT #1, "P"; maxph! ELSE PRINT #1, "P"; (maxph! + 180)
MOD 360
          END SELECT


666 END SUB
```

```
'---------------
SUB stepsm (steps%)
'---------------
 FOR x = 1 TO ABS(steps%)
   IF steps% > 0 THEN
        result = Cmd838(CMDxCwStep, xCH2, 0)
   ELSE
        result = Cmd838(CMDxCcwStep, xCH2, 0)
   END IF
 NEXT x
 FOR x = 1 TO 200: NEXT x

END SUB
```

C.5 Ion gauge calibration curve

```
' Program for calibrating ion gauge (read on HPS919) to MKS690 Baratron read
' on MKS670 signal conditioner. User sets pressure by opening leak valve
' via stepping motor. Pressure readings are then saved in a file.


DECLARE SUB setP (pressure!, meter!, temp%)
DECLARE FUNCTION hexP! (meter!)
DECLARE SUB stepsm (steps%)
REM $INCLUDE: 'qb.bi'
TYPE FunTable
        funNo         AS INTEGER     'function number
        channel       AS INTEGER     'high byte for direction
                                       'low byte for channel number
        bufferOff     AS INTEGER     'offset of buffer address
        bufferSeg     AS INTEGER     'segment of buffer address
        vi            AS INTEGER
        vf            AS INTEGER
        time          AS LONG
        steps         AS LONG
        datus         AS INTEGER
        returnValue   AS LONG
END TYPE
DECLARE FUNCTION Cmd838% (cmdNo AS INTEGER, channel AS INTEGER, datus AS
INTEGER)
DECLARE FUNCTION InstallStatus! ()

' declare the constants for channel number and directions
        CONST xCH2 = &H2

' function number definations
        CONST CMDxActive = 10
        CONST CMDxOutput = 30
        CONST CMDxInput = 31
        CONST CMDxDelay = 42
        CONST CMDxBase = 53
        CONST CMDxReset = 54
        CONST CMDxCwStep = 60
        CONST CMDxCcwStep = 61
        CONST CMDxStepSpd = 62
```

```
        CONST CMDxCwSpeed = 67
        CONST CMDxCcwSpeed = 68
        CONST CMDxBusy = 72
        CONST CMDxFirmware = 73

  IF InstallStatus! <> 255 THEN
    PRINT "PCL-838.EXE was not installed"
    BEEP
    END
  END IF
  result = Cmd838(CMDxBase, 0, &H2E0)
  result = Cmd838(CMDxReset, 0, 0)
  result = Cmd838(CMDxActive, xCH2, 0)

 CLS

   PRINT , "Ion Gauge Calibration program"
   INPUT "output filename: ", f$
   OPEN "c:\ccell\" + f$ FOR APPEND AS #1
   PRINT #1, "Baratron (MKS670)"; ","; "Ion gauge (HPS919)"


22  INPUT "Type Q to quit, S to start "; out$
   IF UCASE$(out$) = "Q" THEN END

' Controlling stepping motor to open leak valve.

   numSetps% = 0
33    INPUT "number of steps? ", temp%
   numSteps% = numSteps% + temp%
    CALL stepsm(temp%)
    PRINT "Press N for a new value, V to close valve, P for pressure"
    SOUND 783.99, 9.1
    pick$ = INPUT$(1)
    IF UCASE$(pick$) = "N" THEN
         GOTO 33
    ELSEIF UCASE$(pick$) = "V" THEN
         CALL stepsm(numSteps% * (-1))
         PRINT "Value closed"
         GOTO 22
    ELSEIF UCASE$(pick$) = "P" THEN
         Pbara = hexPI(1)
         PIonG = hexPI(4)
         PRINT #1, Pbara; ","; PIonG
         CLOSE #1
         OPEN "c:\ccell\" + f$ FOR APPEND AS #1
         GOTO 33
    ELSE
         BEEP
         GOTO 33
    END IF
```

Subroutines are the same as found in C.4

APPENDIX D DATA TABLES

Table D.1 Upper Stark-state defocusing cross-sections measured in single hexapole experiments for a beam of 5% CH_3F seeded in Ar against quencher gases, He, Ne, Ar, Kr, Xe, and N_2, at a range of hexapole voltages.

Hexapole / V	He	Ne	Ar	Kr	Xe	N_2
1200	224	171	198	298	252	321
1400	230	175	209	307	259	332
1600	239	188	221	320	278	343
1800	245	204	237	335	292	346
2000	247	215	250	339	311	359
2200	245	217	261	336	317	376
2400	241	212	266	334	316	390
2600	237	207	269	333	306	389
2800	233	202	263	335	295	386
3000	229	201	259	326	290	376
3200	226	196	252	320	286	367
3400	227	192	244	309	280	354
3600	227	187	232	317	273	357
3800	228	187	222	306	265	360
4000	225	184	221	305	260	357
4200	226	178	223	298	254	348
4400	226	173	220	310	252	340
4600	226	175	222	313	250	331
4800	226	180	221	305	250	331
5000	225	179	222	301	246	331
5200	225	181	223	296	247	335
5400	225	184	221	300	252	327
5600	225	189	224	295	252	325
5800	223	188	216	300	251	316
6000	221	188	221	302	251	314
6200	223	190	221	310	258	311
6400	223	191	226	320	257	318
6600	224	185	219	320	255	321
6800	227	186	216	312	254	324

Table D.2 Upper Stark-state defocusing cross-sections measured in single hexapole experiments for a beam of 5% CH_3F seeded in Kr against quencher gases, He, Ne, Ar, Kr, Xe, and N_2, at a range of hexapole voltages.

Hexapole / V	He	Ne	Ar	Kr	Xe	N_2
800	313	301	374	437	543	438
1000	316	312	394	449	555	448
1200	325	317	416	460	564	467
1400	327	328	423	460	571	478
1600	327	315	414	454	566	473
1800	322	310	403	450	560	471
2000	332	298	396	452	557	473
2200	321	296	389	445	551	467
2400	315	290	388	432	548	455
2600	300	286	379	424	541	446
2800	293	282	371	417	536	439
3000	285	277	357	416	529	444
3200	281	282	348	415	526	445
3400	288	284	348	419	533	443
3600	294	288	354	420	536	447
3800	301	286	367	418	529	472
4000	310	289	387	420	532	496
4200	318	300	398	434	536	498
4400	333	307	415	444	538	494
4600	348	314	429	451	540	489
4800	363	322	440	450	536	493
5000	363	321	442	451	536	494
5200	359	322	430	451	531	488
5400	349	316	425	447	525	478
5600	346	317	423	447	522	468
5800	339	315	430	440	513	466
6000	336	313	428	436	519	468
6200	335	305	418	427	513	463
6400	337	297	415	429	508	456
6600	336	295	414	433	493	448
6800	335	299	418	438	488	440

Table D.3 Relative velocities of the collision partners calculated using the Monte Carlo method, average of 10^6 calculations.

Beam specie	Scattering gas	Relative velocity /m s^{-1}
10% CH_3F/Ar	He	700
10% CH_3F/Ar	Ar	562
10% CH_3F/Ar	Xe	551
10% CH_3F/Ar	N_2	568
10% CH_3F/Ar	CO_2	560
10% CH_3F/Ar	CH_4	585
10% CH_3F/Ar	CH_3F	565
10% CH_3F/Ar	SF_6	551
50% CH_3Cl/Ar	He	679
50% CH_3Cl/Ar	Ar	535
50% CH_3Cl/Ar	Kr	527
50% CH_3Cl/Ar	Xe	524
50% CH_3Cl/Ar	N_2	542
50% CH_3Cl/Ar	CO	542
50% CH_3Cl/Ar	CH_4	565
50% CH_3Cl/Ar	CH_3F	538
50% CH_3Cl/Ar	CH_3Cl	532
50% CH_3Cl/Ar	SF_6	524
50% CH_3Br/Ar	Kr	474
50% CH_3Br/Ar	N_2	491
50% CH_3Br/Ar	CO	491
50% CH_3Br/Ar	CH_3Br	473